NASA TECHNICAL MEMORANDUM

NASA TM X-64561

NASA TM X-64561

CRYOGENIC RESEARCH AT MSFC

RESEARCH ACHIEVEMENTS REVIEW

VOLUME IV REPORT NO. 2

SCIENCE AND ENGINEERING DIRECTORATE
GEORGE C. MARSHALL SPACE FLIGHT CENTER
MARSHALL SPACE FLIGHT CENTER, ALABAMA

GEORGE C. MARSHALL SPACE FLIGHT CENTER

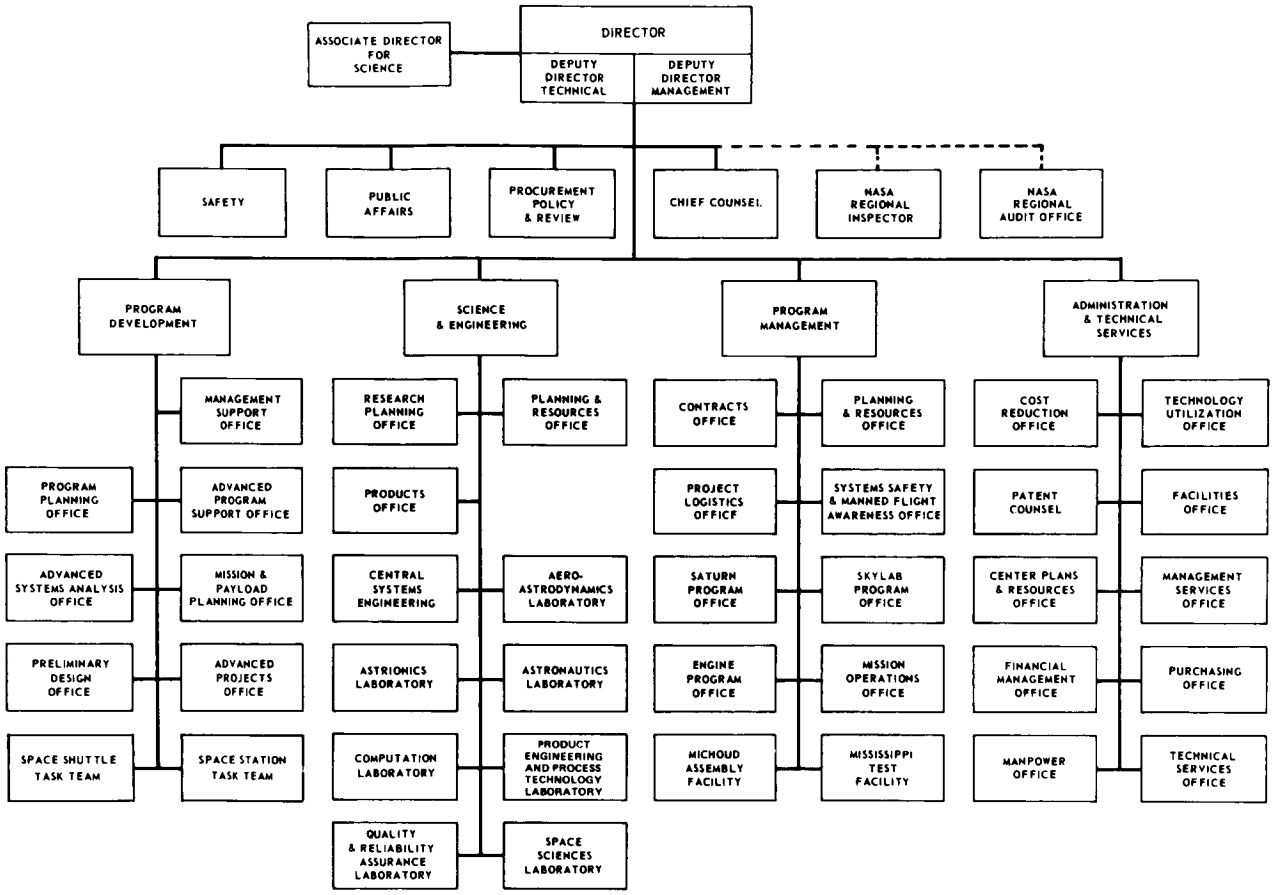

RESEARCH ACHIEVEMENTS REVIEWS COVER THE FOLLOWING FIELDS OF RESEARCH

- Radiation Physics
- Thermophysics
- Chemical Propulsion
- Cryogenic Technology
- Electronics
- Control Systems
- Materials
- Manufacturing
- Ground Testing
- Quality Assurance and Checkout
- Terrestrial and Space Environment
- Aerodynamics
- Instrumentation
- Power Systems
- Guidance Concepts
- Astrodynamics
- Advanced Tracking Systems
- Communication Systems
- Structures
- Mathematics and Computation
- Advanced Propulsion
- Lunar and Meteoroid Physics

PREFACE

The Research Achievement Reviews document research accomplished by the laboratories of Marshall Space Flight Center. Each review covers one or two fields of research and attempts to present the results in a form readily useable by specialists, system engineers, and program managers.

Reviews of this fourth series are designated Volume IV and will span the period from May 1970 through May 1972.

In accordance with NASA policy the International System of Units (SI Units), as defined in NASA SP-7012, are used in this publication.

The papers in this report were presented October 29, 1970.

William G. Johnson
Director
Research Planning Office

CONTENTS...

LIST OF TABLES

CONTENTS (Continued). . .

LIST OF ILLUSTRATIONS

CONTENTS (Continued) . . .

DESIGNS FOR ADVANCED INSULATION SYSTEMS

By J. M. Walters

LIST OF TABLES

LIST OF ILLUSTRATIONS

CONTENTS (Continued) . . .

MANUFACTURING DEVELOPMENTS IN INSULATION APPLICATION

By Iva C. Yates, Jr.

LIST OF TABLES

CONTENTS (Continued)...

LIST OF ILLUSTRATIONS

MULTILAYER HIGH PERFORMANCE INSULATION MATERIALS

By J. M. Stuckey

LIST OF TABLES

LIST OF ILLUSTRATIONS

SUPERCONDUCTING MAGNETS AND DEVICES FOR SPACE VEHICLES AND EXPERIMENTS

By Eugene W. Urban

CONTENTS (Continued)...

LIST OF TABLES

LIST OF ILLUSTRATIONS

CRYOGEN ACQUISITION IN ORBIT

By L. J. Hastings

CONTENTS (Continued)...

LIST OF TABLES

LIST OF ILLUSTRATIONS

LONG TERM CRYOGENIC STORAGE SYSTEM INTEGRATION

By R. E. Stonemetz, J. H. Pratt, and T. W. Winstead

CONTENTS (Continued)...

LIST OF TABLES

LIST OF ILLUSTRATIONS

ADVANTAGEOUS USE OF SLUSH AND GELLED SLUSH IN SPACE VEHICLES

By J. Z. Adamson

LIST OF TABLES

LIST OF ILLUSTRATIONS

PROPELLANT THERMAL STRATIFICATION

By T. W. Winstead

LIST OF ILLUSTRATIONS

MATERIALS FOR FOAM TYPE INSULATION

By W. E. Hill

LIST OF TABLES

LIST OF ILLUSTRATIONS

INTRODUCTION TO CRYOGENIC RESEARCH AT MARSHALL SPACE FLIGHT CENTER

By

J. E. Kingsbury

Cryogenic engineering is a vital part of the overall engineering effort at Marshall Space Flight Center (MSFC). During the last 15 years, the MSFC organization has been very successful in solving the problems of using cryogenic liquids in great bulk as propellants for the largest rocket motors in the world and in smaller amounts in auxiliary cooling and pneumatic systems. Within the last 10 years, a growing technology effort has led to an improved and broader knowledge of cryogens, which is necessary for the advanced hardware designs that will be needed for the long duration space missions of the future.

As can be seen from the papers in this report, the subject of cryogenics has many engineering ramifications. A many-sided matrix of problems results from large extremes of temperature, high volatility, troublesome fluidity, great metallurgical sensitivity, and hazardous chemical characteristics. When these conditions are cast in a space-mission framework of high acceleration in launch and flyback, unsettling lack-of-acceleration in orbit, long duration storage times, high density launch frequencies, large cryogen transfer requirements in space, and low cost, there results a wide array of problems involving many engineering disciplines, which exist to some extent in all major elements of MSFC. Many of the engineering disciplines are centered in the Astronautics Laboratory of MSFC, however, because of its role in the design of structural and propulsive systems, where the physical interface with cryogenic fluids is heaviest. A substantial proportion of the engineering problems that occur are related to cryogens. In fact, the number of engineers involved in solving cryogen problems is comparable, for example, to the number involved in solving propulsion problems.

The review papers presented in this report have subject matter that is of general application; whereas in several years, one may expect the subject matter to be more specific because of technology advances resulting from program application problems of the space shuttle and space station.

A PERSPECTIVE ON CRYOGENIC TECHNOLOGY FOR SPACE TRAVEL

By

David J. Miller

The history of cryogenic technology as it supports the space program is a good example of the benefits derived from research and technology activity well in advance of any firm ideas of mission applications. Beginning in the early sixties, studies directed by NASA, primarily by Marshall Space Flight Center, were aimed at feasibility determinations of manned planetary missions and lunar ferry missions. By 1964 the major cryogenic system components were sufficiently well known to permit reasonably good assessments of the usefulness and the interactions of these components. That is, by the mid-sixties studies and laboratory investigations had defined the range of performance and usefulness of multilayer high performance insulation, reliquefaction systems, propellant subcooling, and meteoroid and solar shielding, and had illustrated the difficult problem of zero gravity in connection with heat transfer and propellant flow and transfer.

In fact, activity in the field of cryogenic storage had burgeoned at such a rate that some degree of tidying-up was in order. Accordingly, in September 1964 a NASA Headquarters coordination group was established to examine the overall cryogenic storage supporting research and technology (SRT) program at NASA. This was primarily an Office of Advanced Research and Technology (OART) group, although the Office of Manned Space Flight (OMSF) and the Office of Space Science and Applications (OSSA) were represented. This coordination group found, as of 1964, that about 55 percent of NASA cryogenic storage research was in the OMSF program, about 35 percent was in the OART program, and the remainder was in the OSSA program. Many of the efforts in these programs were redundant and inadequately coordinated. By 1966 the SRT activity had been tightened up and project control had been rearranged. This resulted in curtailment of OMSF and OSSA support and some increase in OART support. In the process of reorienting the program, overall NASA funding for advanced cryogenic storage was reduced as a result of the elimination of unnecessary duplication. Also, by 1966, this coordination group working with Marshall Space Flight Center and Lewis Research Center personnel sufficiently ordered the relative priorities so that more emphasis was placed on achieving an adequate technology base to support genuinely long term cryogenic storage systems; i.e., approaching a lifetime of 1 year in space.

The previous Research Achievements Review on the subject of cryogenic technology research was held in the spring of 1967. At that time NASA's post-Apollo planning was still unresolved, and the primary justification for large scale cryogenic storage technology was still based on manned-planetary, nuclear-stage missions. In fact, any sort of launch dates based on the use of these stages for such missions was purely speculative. A great deal of progress was reported in the 1967 review, however. A quick scan of the papers presented indicates that there was a heavy emphasis on the solution of problems associated with use of high performance insulation.

In the 3.5 years since the previous review, the programmatic requirements have become more specific; manned planetary systems have virtually dropped out of the picture, and several other systems have appeared that were unknown in 1967 — the space shuttle, the space tug, orbital storage tanks, and the reusable nuclear stage.

Milestones that aim for the late seventies and early eighties have been established for development and operational systems. All of the components of the transportation system depend on hydrogen as at least one of the propellants. In any case, cryogenic systems are very much in the picture.

Various mission models are available for estimating propellant requirements and storage times. Based solely on the reusable nuclear stage (RNS) mission model, which encompasses six flights per year and a propellant loading of approximately 136 080 kg (300 000 lb) of liquid hydrogen,

816 480 kg (1.8 million lb) of hydrogen must be delivered to earth orbit. The total time for a typical earth-orbit-to-lunar-orbit mission and return is approximately 55 days, with multiple burns, the last being about 3 weeks after leaving earth orbit. Various models can be devised for shuttle refueling, but 2 weeks may be considered representative. In any case, it can be seen that extended storage times in earth, or lunar orbit, will be required. Comparable quantities of propellant may be required for space tug activities in support of lunar bases on other missions.

When considering only the hydrogen problem, it is evident that some form of propellant supply depot may be desirable. This is a departure from the earlier concepts involving cryogenic storage that were based on manned planetary models. Another departure is the likelihood of using smaller tanks. Smaller tank sizes are dictated by the space shuttle cargo volume; e.g., 4.572 m (15 ft) in diameter by 18.288 m (60 ft) long, rather than the 10.058-m (33-ft) diameter stage sizes used in earlier studies. To overcome situations where volume limitations are controlling, as high a density payload as possible is desirable; in the case of hydrogen, slush or even solid hydrogen would be preferred. The operational models being examined can impose some requirement for propellant transfer in low or zero gravity They also require reliable, simple fluid-line coupling and uncoupling devices. The reusability requirement, whether for nuclear or chemical transportation systems, imposes a long lifetime criterion (3 to 5 years), and this applies to the insulation and inert tankage as well as to the dynamic systems. Meteoroid protection and durable insulation are obvious requirements. A relatively new area of technology, gels, may result in some advances in minimizing boiloff or aiding the slosh problem.

The rather superficial analysis of cryogenics-related requirements presented here has generated some guidelines as to the type of technology that should be pushed in future years. Scanning the list of papers included in this report reveals a broadening of the technology areas, beyond those covered by the 1967 review, into topics that are vital to successful operational systems of the types under study. If one thing should be added, it is a flight test of a total cryogenic system. Hopefully, all of the previous planning for such a test may eventually lead to implementation, and the next cryogenic technology achievements review will contain some reports on the status of such an orbital experiment.

The overall cryogenic storage and handling technology activity is clearly well organized and focussed on solving recognized problems associated with stage design and operations. The current status is a good example of the vital part that a technology project plays in the NASA program.

MULTILAYER INSULATION THERMAL PROTECTION SYSTEMS TECHNOLOGY

By

E. H. Hyde

SUMMARY

This paper presents a summary of the work performed by Marshall Space Flight Center (MSFC) and industry during the past 9 years toward the development of flight-type multilayer insulation (MLI) systems. The MSFC MLI program is divided into three large categories: (1) the generation and compilation of MLI composite test data; (2) the analysis, design, and testing of heat flow through MLI applied to ducting, seams, electrical feedthroughs, structural supports, and the tank sidewall; and (3) the development, modification, and utilization of new testing procedures, tanks, and test facilities.

Numerous data have been generated, analyzed, and documented on different MLI composites. These data include the effects of temperature, layer density, bearing pressure, interstitial gas pressure, panel-joint application techniques, MLI material, and penetration thermal effects. Heat flow through penetrations has been studied with and without mass flow through or around the penetration.

Five insulated tanks have been tested with cryogens to obtain overall MLI system thermal performance, and comparisons of the applied thermal performance with the individual MLI material's ideal thermal conductivity shows thermal degradation between 300 and 1000 percent. Thermal degradation of MLI has occurred because of unexpected compression, blanket seams and gaps, high interstitial gas pressure, penetrations, attachment devices, structural support, ducting, and instrumentation heat leak into the stored cryogen.

Brief descriptions of these efforts are included in this paper. Since the 2.23 by 1.89 m (87.6 by 74.5 in.) diameter tank work is the latest MLI large tank application, it will be the only MLI system discussed in detail to show the typical areas that must be considered to develop a flightworthy MLI system. This description is typical of, but not necessarily identical to, the efforts involved in developing the other four MLI systems identified later. Thermal performance comparisons have been performed to show thermal improvements in MLI systems development and not for the purpose of making absolute systems comparison. Tank descriptions and MLI system design and thermal performance values can be obtained from the applicable references for the other four MLI systems.

Calorimeter data are presented for the double aluminized Mylar (DAM)/red foam and other MLI composites. Test results from a 50.8 cm (20 in.) diameter test tank are also presented. A 2.67-m (105-in.) calorimeter test tank has been insulated with DAM/red foam at MSFC and is in the process of being tested at high vacuum using liquid hydrogen as the test cryogen.

Other programs in progress or complete include the development of a flat-plate calorimeter standard; the design, test, and utilization of a new electrical calorimeter; and the acquisition and use by MSFC of a large hazardous-rated vacuum chamber together with improved instrumentation.

INTRODUCTION

MSFC has been engaged in the development of multilayer insulation systems for typical cryogenic and noncryogenic usage, as shown in Figure 1, for the past 8 years. The result of these efforts to date has been the development of MLI systems that are flightworthy and that provide thermal protection far superior to that of foams, powders, and other conventional insulation materials. The MLI systems developed earlier were basically derivatives of commercial techniques. This class of MLI systems did not represent a thermal-weight-optimized MLI system for space vehicles even though the thermal performance and system weight were adequate for short term missions of a few hours and for small vessels. Today, projected mission durations and vehicle tankage sizes have increased significantly,

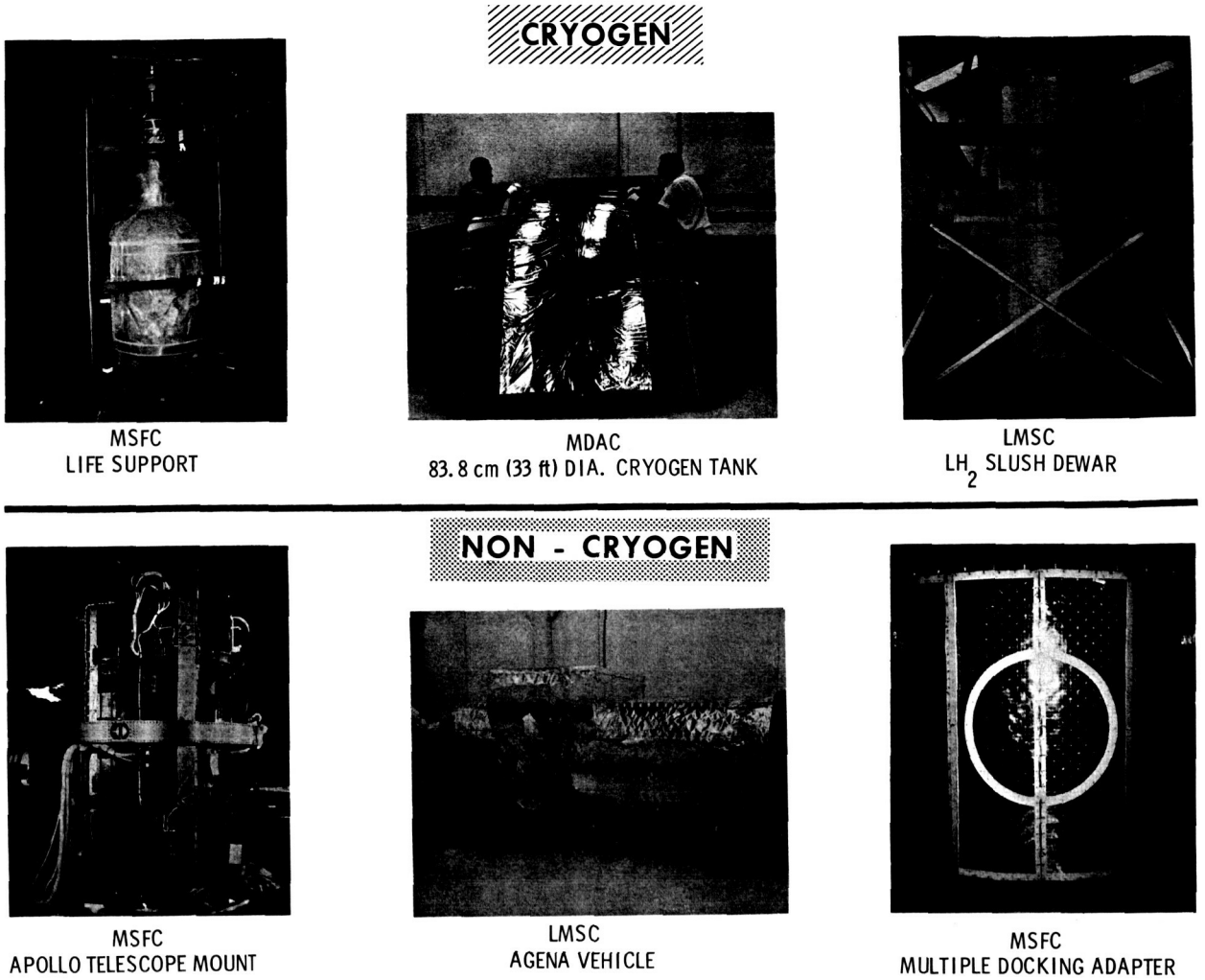

Figure 1. Multilayer insulation.

and the MLI systems developed earlier would impose an undesirable weight penalty on present and future vehicle application.

Since the development of the first MLI system at MSFC [1] (Table 1), MSFC and industry have attempted to reduce thermal degradation of applied MLI space systems in five fundamental ways: (1) by improving the basic MLI composite material; (2) by better definition of basic MLI material properties; (3) by accurate prediction of heat leaks through penetrations, seams, gaps and the basic MLI blankets; (4) by improving MLI tankage testing techniques; and (5) by developing and applying MLI systems to large size tank calorimeters. These factors are discussed in the following portions of this paper.

MLI REQUIREMENTS

Multilayer insulations with varying mission-duration and tank-size requirements have been studied. In 1964, mission durations of only 96 hr were common for tanks 2.44 to 3.05 m (8 to 10 ft) in diameter. Today, mission requirements have been extended to 1 year or more for tanks up to 10.1 m (33 ft) in diameter. For the short-duration missions, a large degradation in applied MLI thermal performance can be tolerated without excessive weight penalties or boiloff losses. However, as mission durations are extended and tank sizes become larger, reductions in applied MLI thermal

TABLE 1. COMPARISON OF DIFFERENT ATTACHMENT TECHNIQUES

Insulation Attachment Technique	Q_{DIST} for 2.67-m (105-in.) Tank W (Btu/hr)	k_{EQUIV} W/m °K (Btu/hr ft °R)	Average No. of Layers Due to Attachments	Q_{UNDIST} for 200 Layers W (Btu/hr)	Percent Increase in Q Due to Disturbance (%)	kN Factor W/m °K (Btu/hr ft °R)
A 	Aluminum Pin 16.8 (57.2)	11.93×10^{-5} (6.9×10^{-5})	277	10.7 (37.86)	57	3.30×10^{-2} (1.91×10^{-2})
	Nylon Pin 16.7 (57.0)	11.91×10^{-5} (6.89×10^{-5})	277	10.7 (37.86)	56	3.30×10^{-2} (1.91×10^{-2})
B 	Aluminum Pin 18.3 (62.5)	15.32×10^{-5} (8.86×10^{-5})	326	10.7 (37.86)	71	4.95×10^{-2} (2.86×10^{-2})
	Nylon Pin 18.2 (62.2)	15.27×10^{-5} (8.82×10^{-5})	326	10.7 (37.86)	70	4.95×10^{-2} (2.86×10^{-2})
C 	Aluminum Pin 20.7 (70.6)	9.70×10^{-5} (5.61×10^{-5})	190	10.7 (37.86)	93	1.85×10^{-2} (1.07×10^{-2})
	Nylon Pin 19.6 (66.9)	9.56×10^{-5} (5.53×10^{-5})	190	10.7 (37.86)	83	1.82×10^{-2} (1.05×10^{-2})
D 	Aluminum Pin 21.9 (74.8)	11.25×10^{-5} (6.5×10^{-5})	200	10.7 (37.86)	104	2.25×10^{-2} (1.30×10^{-2})
	Nylon Pin 19.8 (67.6)	10.13×10^{-5} (5.86×10^{-5})	200	10.7 (37.86)	85	2.02×10^{-2} (1.17×10^{-2})

General Assumptions
1. 0.635×10^{-3} cm (1/4 mil) single aluminized Mylar
2. 200 layers
3. 1.0×10^{-10} m (235 Å) aluminum coating
4. 52.4 layers/cm (133 layers/in.)
5. Surface temperature 295°K (530° R) and 20.6 °K (37° R)
6. Uncompressed areas

$K_{\perp} = 8.66 \times 10^{-5}$ W/m °K (5×10^{-5} Btu/hr ft °R)

$K_{\parallel} = 3.47 \times 10^{-2}$ W/m °K (2×10^{-2} Btu/hr ft °R)

Specific Assumptions (A, B, C)
1. Compressed areas

$K_{\perp} = 12.1 \times 10^{-2}$ W/m °K (7×10^{-2} Btu/hr ft °R)

$K_{\parallel} = 1.30 \times 10^{-2}$ W/m °K (7.5×10^{-2} Btu/hr ft °R)

2. Pin size
Length 1.01 cm (0.400 in.)
O. D. 0.634 cm (0.250 in.)
I. D. 0.217 cm (0.125 in.)

Specific Assumptions (D)
1. Pin area:

$K_{\perp}$ 3.47×10^{-3} W/m °K (2×10^{-3} Btu/hr ft °R)

$K_{\parallel} = 7.96 \times 10^{-2}$ W/m °K (4.6×10^{-2} Btu/hr ft °R)

2. Pin size
Length 3.71 cm (1.500 in.)
O. D. 0.634 cm (0.250 in.)
I. D. 0.217 cm (0.125 in.)

performance degradation and weight become increasingly important. The successful MLI applications to tankage by Government agencies and industry were not adequate for long mission durations without special cryogenic assists such as shadow shields, reliquefaction, or slush cryogens. Since shadow shields and reliquefaction devices would add weight to the flight systems, improvements in applied MLI thermal performance were desirable.

Short-term mission duration studies in 1965 and 1966 showed a requirement for less than 2.54 cm (1 in.) of applied MLI. However, storage of LH_2 for long-duration missions such as 1 year would require several centimeters of MLI, and this could not be accomplished with the MLI technology available in 1965 and 1966 on vehicles the size of the S-IVB without incurring significant thermal penalties. Consequently, MSFC established the objective of developing an adequate technology base suitable for the design of a passive thermal protection system with an insulation and boiloff propellant weight penalty on the order of 5 percent of the initial propellant weight for 1-year storage of liquid cryogens on large planetary propulsion stages.

To define exact thermal performance levels requires complex tradeoff studies for individual systems. These involve such factors as mission details, vehicle sizing, overall performance, and development, and cannot be effectively accomplished for general considerations. However, a useful

parameter for evaluating thermal performance is the thermal penalty that represents the weight of the propellant boiloff plus the weight of the insulation as a fraction of the initial propellant weight, $TP = (W_{BO} + W_{insul})/W_P$. Values for the thermal penalty can be determined for specific mission environmental conditions as a function of mission time. These values are strictly applicable only for the conditions assumed, but selection of reasonably typical conditions permits appropriate comparative evaluations to be made. Figure 2 shows thermal penalty versus mission time for LH_2 storage systems typical for launch vehicle insulation and for long-term insulation using existing and projected MLI thermal performance and density values. The environment assumed for Figure 2 approximates average earth orbital conditions and assumes that the tank is topped with LH_2 shortly before launch. The higher external temperatures during the brief transit through the atmosphere are neglected and the LH_2 undergoes no internal energy changes. The tank size, 10.1 m (33 ft) in diameter by 22.4 m (73.6 ft) in length, yields low thermal penalties; smaller diameter tanks would have somewhat higher weight penalties because of the correspondingly higher tank surface-area-to-volume ratios. It can be seen from the $k_e = 3.48 \times 10^{-2}$ W/m °K (2×10^{-2} Btu/hr ft °F) curve of Figure 2 that this class of thermal protection system would be ineffective for orbital storage times of more than 24 hr because of the substantial increase in thermal penalty above 0.2 just beyond 24 hr. To provide for long-term storage of LH_2, MLI's with much lower conductivities are required. MLI applied thermal conductivity values between 2.08×10^{-4} W/m °K (1.2×10^{-4} Btu/hr ft °F) and 3.470×10^{-4} W/m °K (2×10^{-5} Btu/hr ft °F) have been achieved in actual tank tests performed by industry and Government agencies.

Current research is primarily directed toward the development of design techniques to provide practical methods of achieving optimum reproducible performance. Particular attention is being

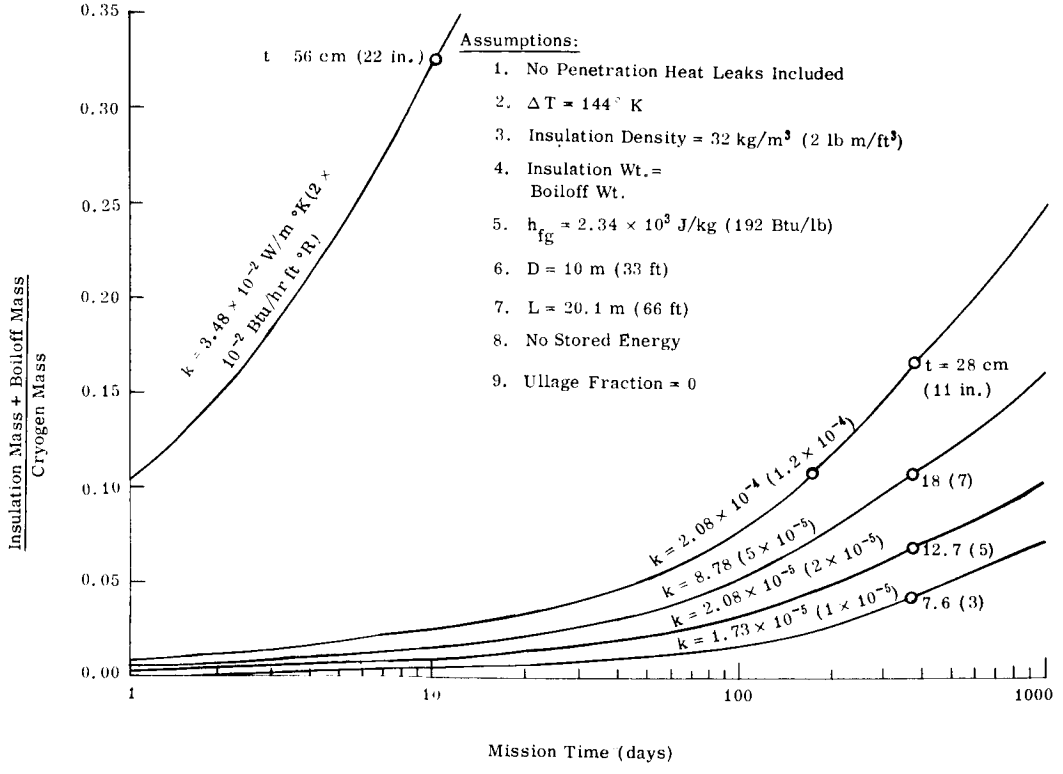

Figure 2. Insulation requirements for long duration storage.

given to insulation installation problems with low thermal conductivity tank supports and ducting.

MLI SYSTEM PERFORMANCE VARIABLES

The major component in the thermal protection system for a cryogenic tank is the MLI material used in the insulation blanket. For the system to be effective, two physical properties of the system need to be minimized; the thermal conductivity and the bulk density. The thermal conductivity of high performance insulation is a function of several variables, which are discussed individually in the following, while the bulk density is a function of the weight per unit area of one layer and the number of layers per unit thickness (layer density).

Temperature

The thermal conductivity of an MLI system is a function of temperature, which is shown in Figure 3 [2] for seven MLI configurations. Thermal conductivity data as a function of temperature are very important for accurate thermal analyses of insulated systems because of the large range of applicable boundary temperatures. The conductivity increases with temperature for all MLI materials, but the curves differ greatly for different systems. The temperature dependency is difficult to predict analytically because of the complexity of the conduction-radiation interaction and the contact resistance between layers. Therefore, temperature-dependent data must be acquired experimentally and are available only for a limited number of MLI materials. The data in Figure 3 were obtained using an electrical cylindrical calorimeter.

Layer Density

The thermal conductivity and weight density of an MLI composite are both strong functions of the layer density of the MLI blanket; i.e., the number of layers per unit thickness. In Figure 4 [3] the conductivities of eight MLI materials are shown as functions of layer density for a constant temperature differential [T_H = 300°K (540°R), T_c = 22.7°K (40°R)]. The appearance of a minimum point on most of the curves is a result of the conduction-radiation interaction. As the layer density increases, there is less contact between adjacent layers, and the conduction of heat through the material decreases. However, as the layer density decreases, there are fewer radiation shields per unit thickness and the radiation of heat through the unit thickness increases. Since the effective conductivity is proportional to the sum of the radiation and conduction modes of heat transfer, there is in general a layer density at which this sum is a minimum. This minimum point, however, will shift to a different layer density for different boundary temperatures. The bulk density of a material is a linear function of layer density, as shown in Figure 5 [3]. The degree of compaction of the various systems as additional layers are added is shown in Figure 6 [4]. The greater the divergence is from the straight line, the more the material compacts under its own weight. Since both conductivity and density are important parameters in comparing competetive systems, data of the type shown in Figures 4, 5, and 6 are essential.

Compression

As seen previously, both thermal conductivity (k) and bulk density (ρ) are functions of layer density for any MLI material. Layer density itself is a function of compaction and the compressive load applied. In Figure 7 [5], layer density is shown as a function of compressive load for several MLI composites. Layer density versus compression data can be combined with thermal conductivity versus layer density data to produce thermal conductivity versus compression as shown in Figure 8 [6].

As was shown in Figure 6, the compressive load resulting from the weight of each additional layer can compress the material to a much higher layer density. This higher layer density has been shown to cause an increase in the thermal conductivity and in the bulk density of the materials. This compression under very small loads is more pronounced for the more flexible materials; however, in the non-compressed state, these same materials are often superior in weight and conductivity to their less compressible counterparts.

At first evaluation some MLI composites might be eliminated from further consideration because of their acute compression sensitivities. However, recent developments in structural support design have proven that such evaluations can be incorrect. For example, the tendency of Superfloc[1] to compress was reduced through a structural innovation. The material was restrained at the desired layer density and a plastic pin coated with a frozen adhesive was inserted through the MLI blanket. As the adhesive thawed, it

1. General Dynamics/Convair trade name.

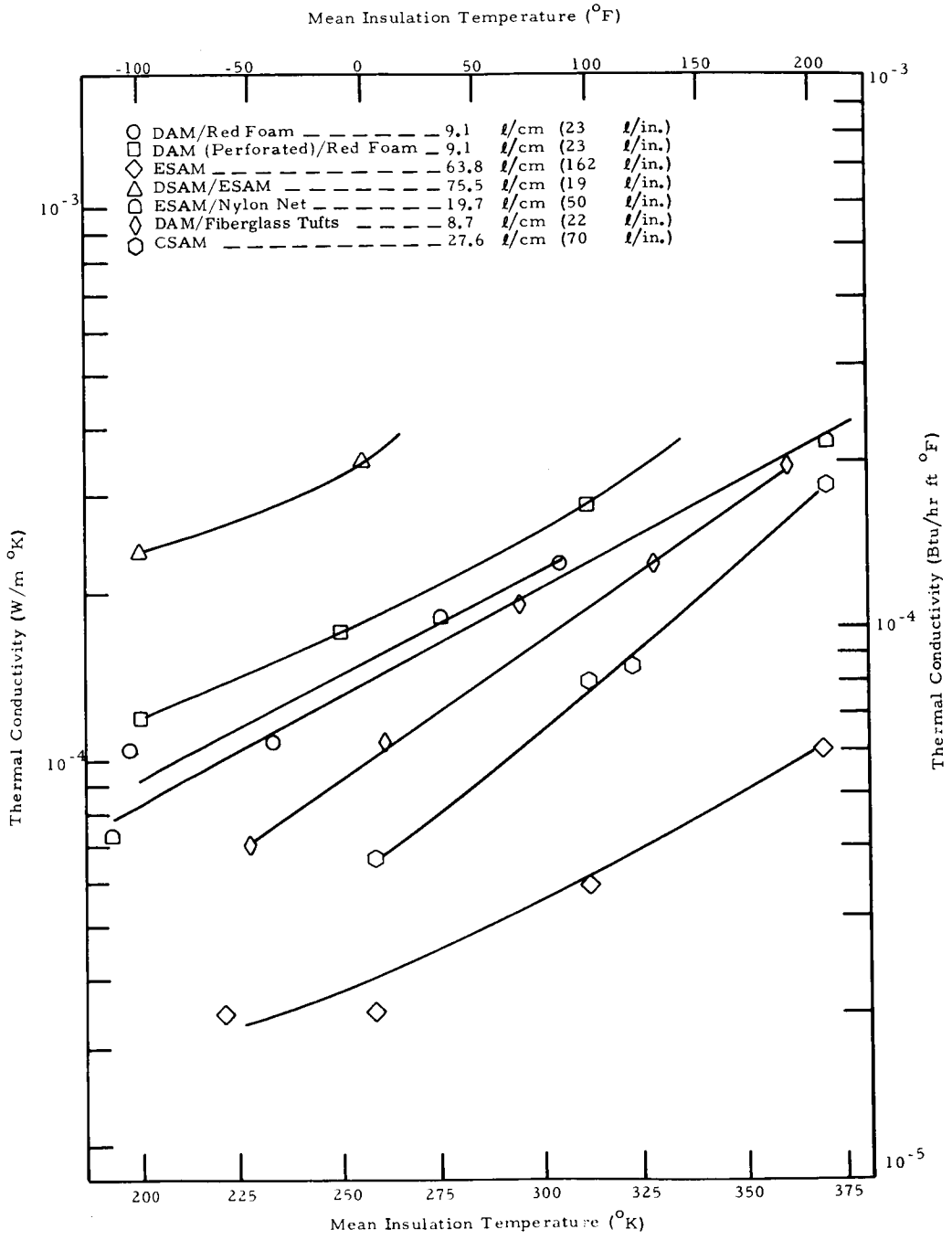

Figure 3. Temperature-dependent thermal conductivity data.

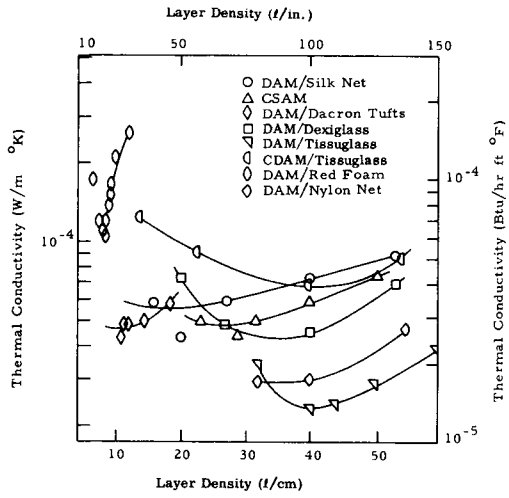

Figure 4. Layer-density-dependent thermal conductivity data [T_H = 299.9°K (540°R), T_c = 77.6°K (40°R)].

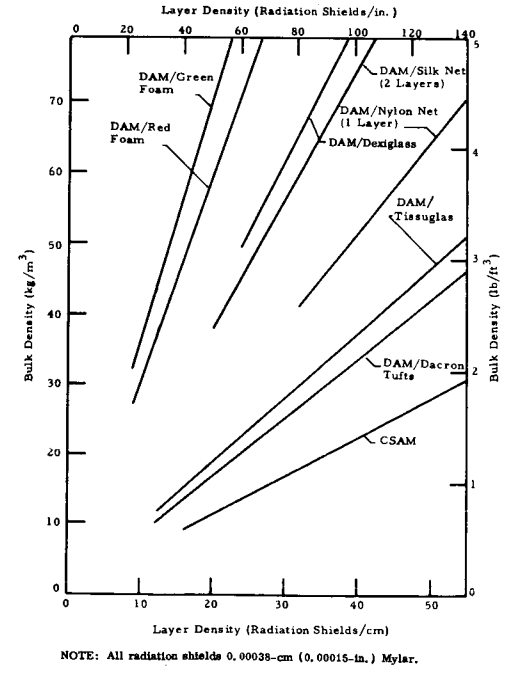

Figure 5. Bulk density versus radiation shield layer density for eight MLI composites.

attached to the individual layers, cured, and permanently bonded each layer to the pin. Thus, layer density control was achieved through design techniques rather than depending totally on MLI material characteristics. Consequently, while the compression dependence of an MLI composite is important, design considerations must be included in the overall evaluation of the system.

Another compression problem is often encountered with MLI materials when a few layers (10 to 30) are stacked with only self-loading. In this situation the layer density varies depending upon stacking methods, precompression, and the location of the point of thickness measurement. This variation is more apparent in the more flexible materials and becomes less significant as the number of layers is increased. However, flat plate calorimeter samples frequently contain between 10 and 30 layers. Because of the variations in thickness and contact resistance with this number of layers, large variations in reported thermal conductivities for seemingly identical specimens can be found in the literature. In an attempt to resolve this and other problems involved in obtaining reliable thermal conductivity data from flat plate calorimeters, MSFC is working with the National Bureau of Standards to establish standards for future flat plate calorimeter testing [7]. If successful, MSFC intends to utilize these standards for future MLI calorimeter testing for both in-house and contractor efforts.

Interstitial Gas Pressure

The conductivity data presented thus far were applicable only for evacuated insulation systems where the interstitial pressure is less than 1.33×10^{-3} N/m² [10^{-5} mm Hg ($P \leq 1 \times 10^{-5}$ mm Hg)]. However, if the insulation is used in the presence of gases, the introduction of gas molecules into the interstitial spaces within the blanket of insulation degrades the thermal performance of the MLI. The degradation results from heat conduction via the gas molecules; the extent of the degradation depends on the pressure and type of gas. Figure 9 [8] shows this pressure dependence for several MLI materials for helium interstitial gas.

Gaseous conduction causes the conductivity to rise several orders of magnitude at higher pressures. Ambient gases in the MLI can cause severe problems during the prelaunch period. Not only is the thermal performance poor, but the MLI blankets can become saturated with condensing water and frost. The approach taken to resolve the latter problem thus far has been to purge the MLI system

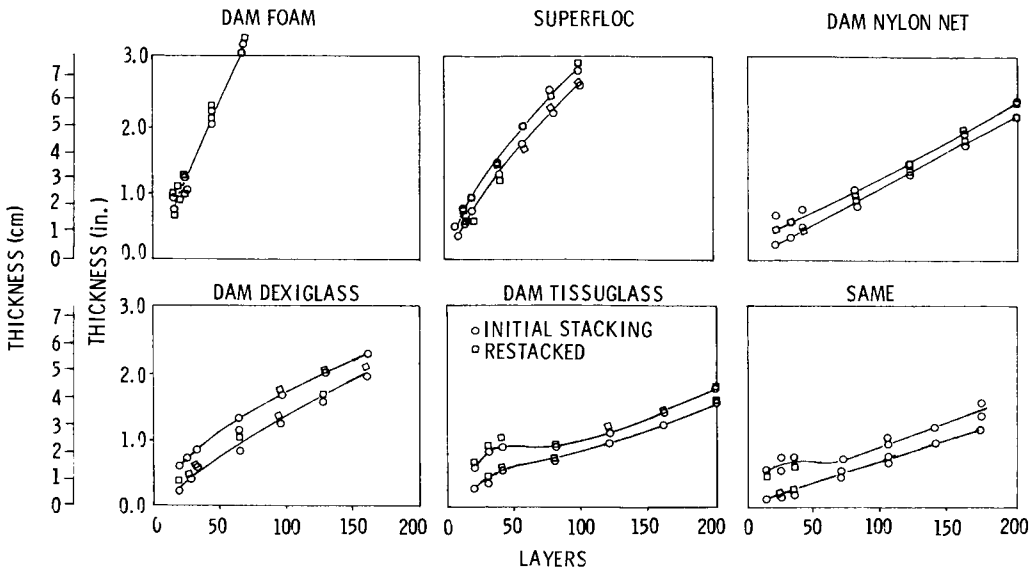

Figure 6. MLI layer density characteristics.

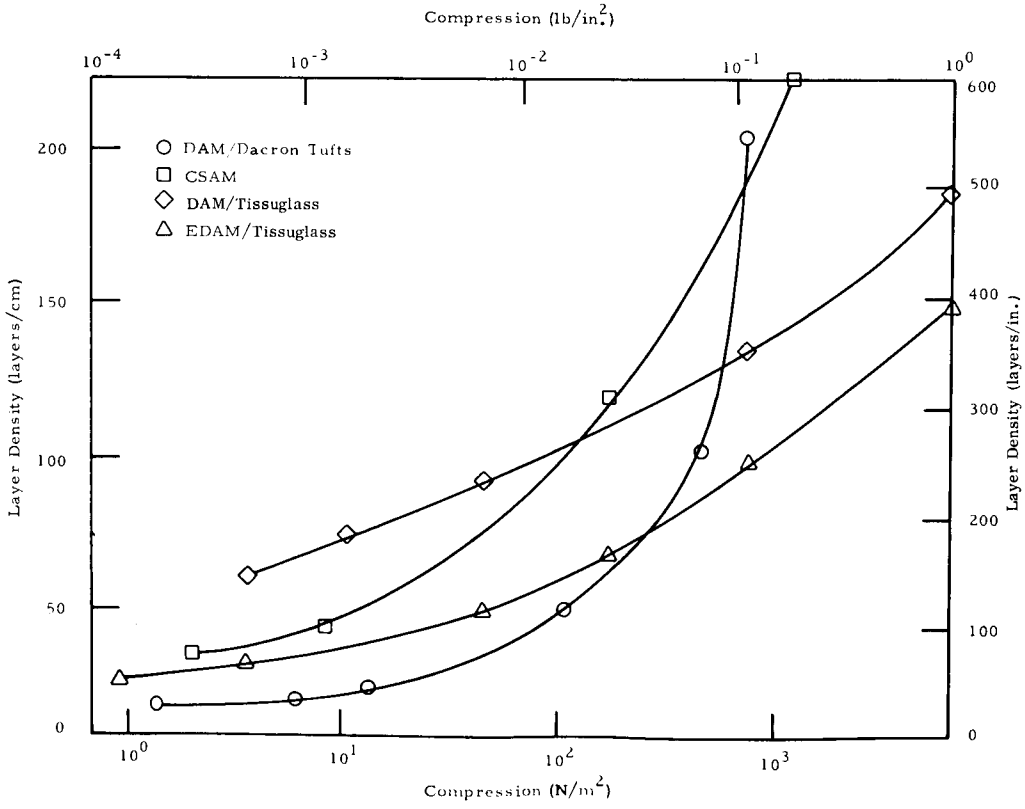

Figure 7. Layer density versus compression for four MLI systems.

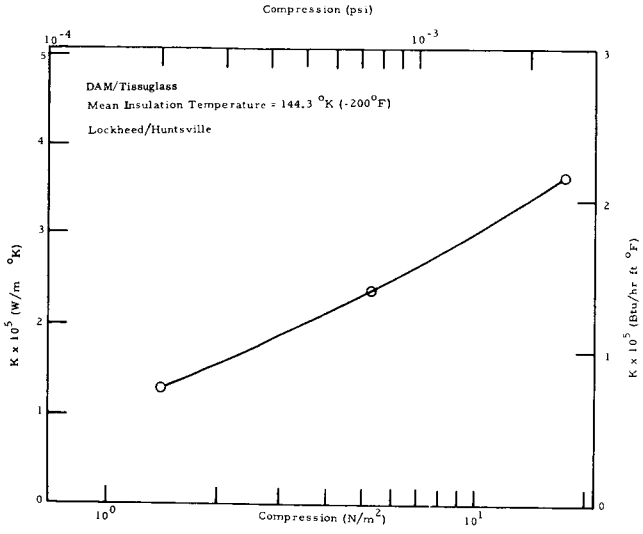

Figure 8. Thermal conductivity versus compression for DAM/tissuglass.

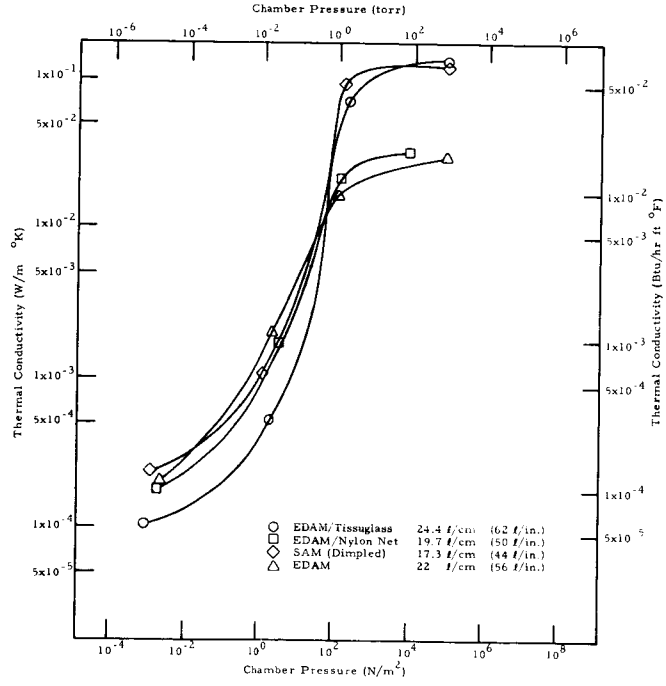

Figure 9. Pressure-dependent thermal conductivity data for four MLI systems.

continuously with helium gas until launch to prevent water accumulation and to accept the thermal degradation caused by the presence of the high-thermal-conductivity helium gas.

When the prelaunch MLI purge is utilized, natural outgassing and evacuation path restrictions frequently affect the MLI system's optimum evacuated thermal performance. Studies have been conducted to ascertain the time period involved, the effect of perforations, and the interstitial gas pressure during the period of gas evacuation. Results of two recent gas flow studies are presented in Figures 10 and 11.

Another aspect of interstitial gas pressure to be considered is the absorption, adsorption, or chemisorption tendency found in certain MLI materials, notably polyurethane foam. When such a material is evacuated, the absorbed gases are expelled into the interstitial spaces and gaseous conduction results. It has been found that heating the composite to an elevated temperature increases the energy of the absorbed molecules and expedites their desorption and evacuation as shown in Figure 12. When the material temperature is returned to its initial value, the conductivity is lower than it was before the heating cycle. These data imply that prebaking certain composites prior to their use in thermal protection systems could hasten the outgassing.

Blanket Joints

When the blanket application method is used (as opposed to a continuous wrap method), gaps or joints occur between adjacent MLI blankets on a cryogen tank. These gaps represent heat shorts that can seriously degrade the thermal performance of the insulation system. The effects of gaps in the MLI on overall thermal conductivity are presented in Figure 13 [9]. Testing of cryogen tanks has verified the degradation in thermal performance caused by gaps between MLI panels. The gap width must be traded off against blanket evacuation characteristics to arrive at the optimum configuration.

Tank Application

MLI thermal conductivity and bulk density are strong functions of several variables. When a tank is insulated with an MLI system, the application method used fixes or strongly affects the values of several of these variables; e.g., layer density, compressive load, area/length ratio for gaps, gap thickness, etc. The application method also introduces new peripheral materials into the blanket system; fasteners, tape, straps, supports, etc. These new materials also degrade the performance of the system. To develop an optimum application technique

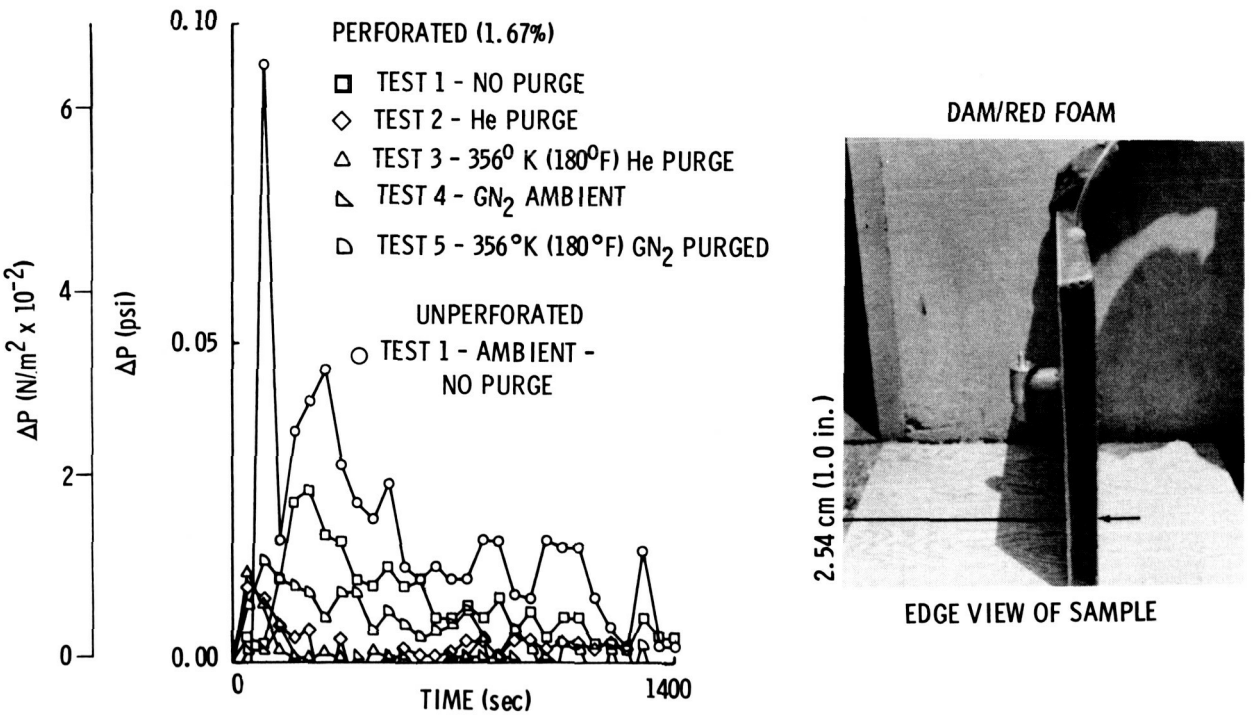

Figure 10. MLI differential pressure history.

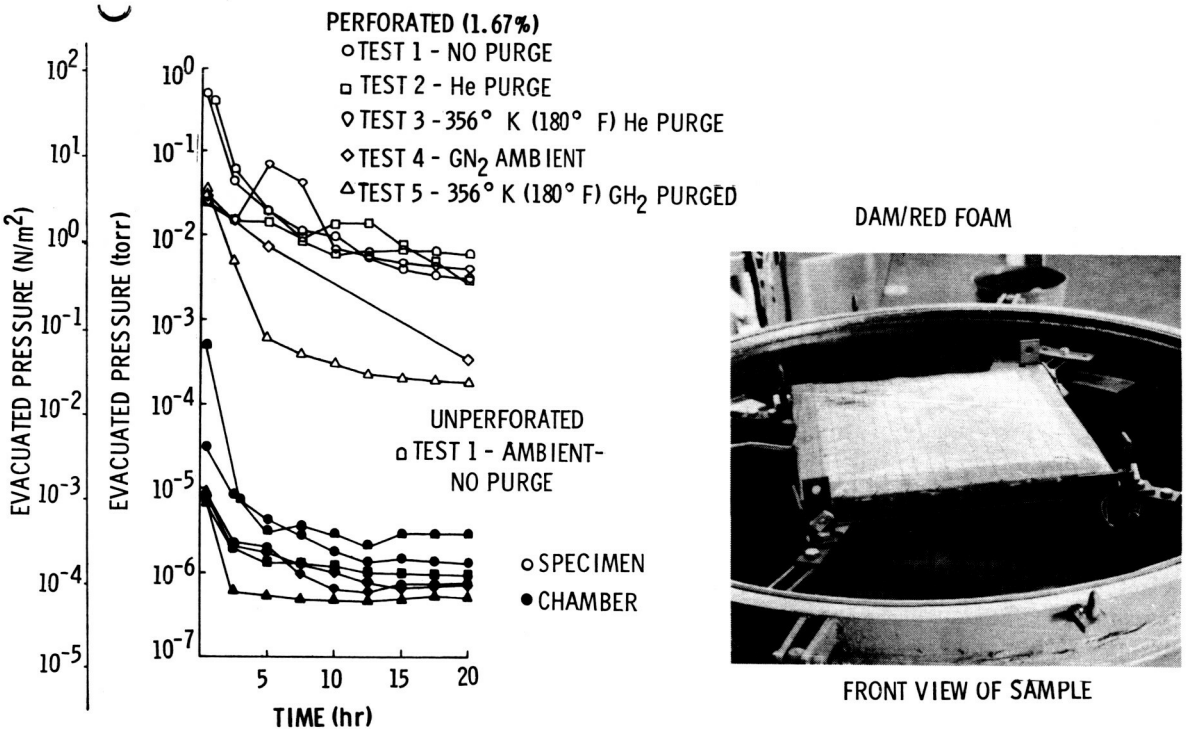

Figure 11. MLI evacuation characteristics.

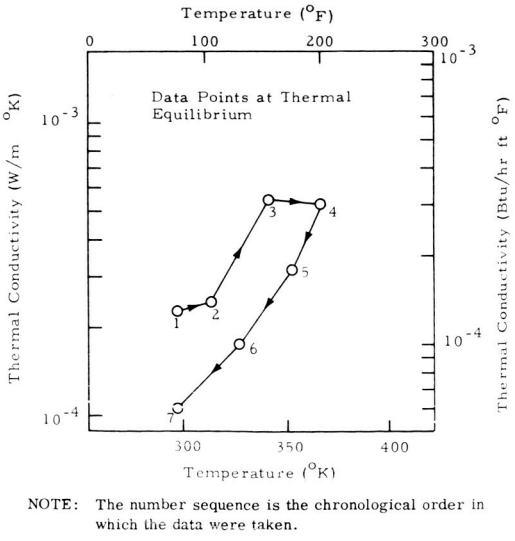

NOTE: The number sequence is the chronological order in which the data were taken.

Figure 12. Outgassing effect in DAM/red foam MLI composite.

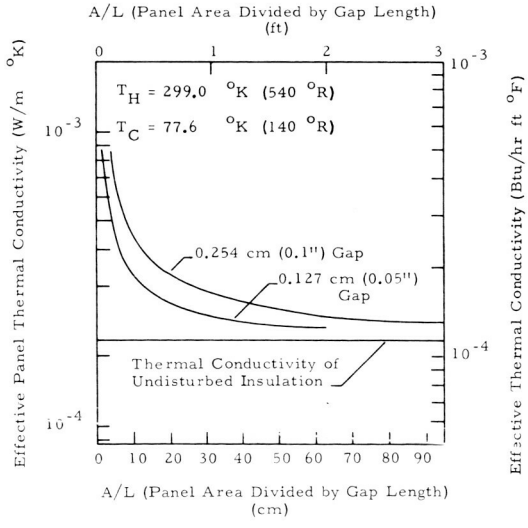

Figure 13. Effect of gaps on overall MLI panel conductivity.

for a particular MLI system, cryogen tank tests need to be conducted to compare different application techniques. By using a degradation factor, defined as $k_{\text{tank test}}{}^{2}/k_{\text{calorimeter}}$, the different application methods can be ranked according to degradation factor, as long as the same MLI material is used for both applications. The smaller the degradation factor is, the better the application method is. Sufficient data for comparison of various application techniques are not currently available.

MLI Material Configuration

There are numerous existing MLI material configurations, and new configurations are being developed continuously. Each type of MLI shows a particular dependency on each of the variables discussed previously. To define the performance dependency involves ranking the different candidate insulations as to their performance in relation to some chosen parameter. Since weight and conductivity are to be minimized, a logical parameter of comparison is the density-thermal conductivity product, ρk.

When ranking different composites for weight-limited applications, it is advantageous to present ρk data as a function of compression (or layer density) and temperature for different MLI materials. An example of this data is shown in Figure 14 [6]. When developing specific insulation systems, the effects of temperature and compressive load on density and thermal performance can be determined, and the MLI with the lowest ρk value can be selected from the curves. This will be the test MLI for the particular compression (or layer density) and temperature selected, and other MLI materials can be ranked accordingly. However, for a different compression and temperature, another MLI may be superior and the ranking will vary. After the MLI is chosen, the data for gaps penetrations, and attachment methods can be utilized to design an effective insulation system.

While several important parameters that affect the weight and conductivity of MLI materials have been discussed, there are other parameters that influence the choice of MLI materials for insulation systems. Fabricability, outgassing tendencies, reliability, strength, reusability, cost, and other characteristics of an MLI material must be considered before choosing a material for a particular application.

New MLI materials are continually being developed. Normally, the screening of these new materials requires expensive calorimeter testing to determine their potential as flightworthy insulation systems. A new, relatively inexpensive method of screening new materials has been developed recently to determine which of these materials should be considered for detailed calorimeter testing. This method is based on the analogy between thermal and electrical conduction. In this analogy, it is assumed that the radiation through an MLI composite is independent of spacer configuration. Therefore, the parameters of interest are solid conduction through the spacer material and contact conductance between the spacer and shield. If a family of spacers composed of the same material is to be screened to determine which is superior, the solid conduction parameter can be assumed to be virtually the same for each and the contact conductance will determine which of them is the best spacer candidate. The thermal contact conductance is a function of layer contact area. The same is true of electrical contact conductance. Therefore, by measuring the electrical conductance of the MLI composites under different compressive loads, one can obtain an indication of the thermal conductance at those compressive loads.

To test the theory behind the analogy, the dacron nets in Table 2 were electrically tested. The nets, manufactured by Apex Mills, N. Y., N. Y., differed in weight, thickness, and mesh count, but all were composed of dacron. It was concluded from the electrical tests that B-4A dacron net would perform better thermally than the others because it had the lowest electrical conductance [10]. Three of the dacron nets were then tested thermally on a flat plate calorimeter, and the results are presented in Table 3. The B-4A net did indeed have a very low thermal conductivity, as had been predicted.

The electrical analogy could be useful in the future for screening different spacer candidates, provided that the material composition of each is the same. If nets were compared to tissuglass, the assumptions behind the analogy would be violated, and the results would be invalid.

Semiempirical Correlation

In the previous topic, the advantage of having ρk data presented as a function of temperature and

2. The degradation factors for two different tank tests are described under the heading MLI Systems Development and Application.

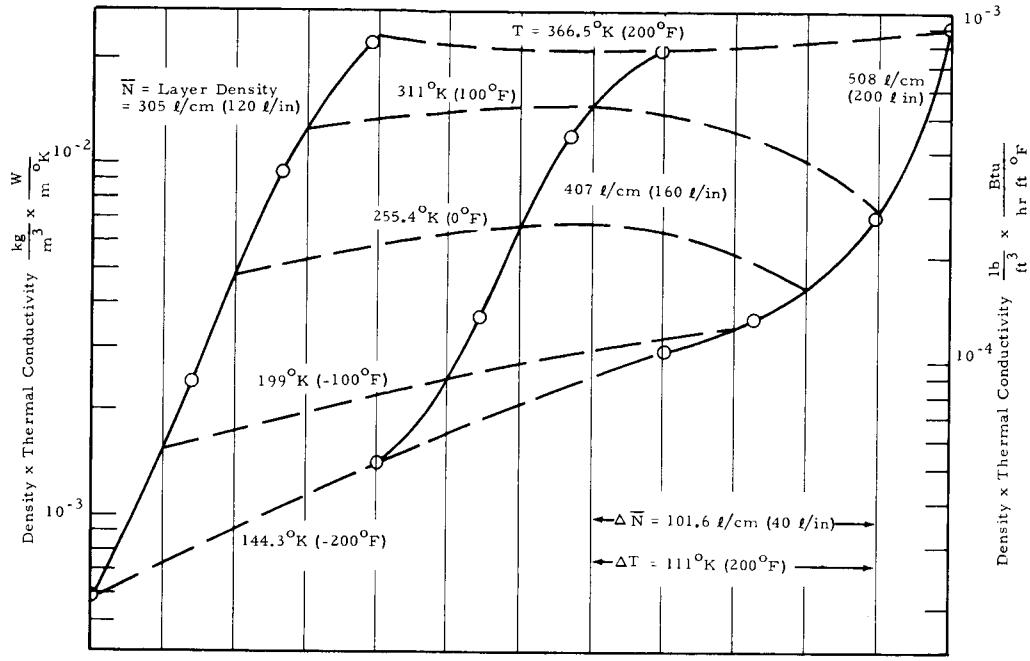

Figure 14. Density versus thermal conductivity carpet plot for DAM/tissuglass.

TABLE 2. PROPERTIES OF DACRON NET

Material	Weight kg/m^2 (lb/ft^2)	Thickness, cm × 10^3 (mil)	Mesh Count, meshes/cm^2 (meshes/$in.^2$)
Dacron Net B/1	0.0116 (0.0029)	16.2 (6.4)	40 (264)
Dacron Net B/2A	0.0096 (0.0024)	17.0 (6.7)	30 (198)
Dacron Net B/2B	0.0088 (0.0022)	16.2 (6.4)	25 (165)
Dacron Net B/3A	0.0068 (0.0017)	16.2 (6.4)	14 (94)
Dacron Net B/3B	0.0068 (0.0017)	17.0 (6.7)	14 (96)
Dacron Net B/4A	0.0052 (0.0013)	16.7 (6.6)	8 (53)
Dacron Net B/4B	0.0048 (0.0012)	16.0 (6.3)	7 (50)

layer density was discussed. When such data are not available, it is necessary to predict the dependency of ρk upon temperature and layer density. A semi-empirical correlation has been developed [3] for relating k to temperature and layer density for a general multilayer insulation system. The equation has the form

$$k = A\bar{N}^{B} T_m + C \frac{\sigma (T_H + T_C)(T_H^2 + T_C^2) t}{\left(\frac{1}{\epsilon_1} + \frac{1}{\epsilon_2} - 1\right) N},$$

TABLE 3. COMPARISON OF THERMAL AND ELECTRICAL TECHNIQUES

Material	Electrical Resistance @ 1.7 N/m^2 (2.5×10^{-4} psi), ohms	Optimum Thermal Conductivity ADL-12 Results, W/m °K (Btu/hr ft °F)	Optimum Layer Density, layer/cm (layer/in.)
Dacron Net			
B/4A	∞	10.4×10^{-6} (6.1×10^{-6})	20 (52)
B/3B	3.00×10^{14}	9.2×10^{-6} (5.3×10^{-6})	28 (72)
B/2A	6.50×10^{12}	2.69×10^{-5} (1.55×10^{-5})	30 (77)

where A, B, and C are constants; σ is the Stefan-Boltzmann constant; T_m, T_H, and T_C are the mean temperature, hot boundary temperature, and cold boundary temperature, respectively; t is the thickness; N is the number of radiation shields; $\overline{N}$ is the layer density; and ϵ_1 and ϵ_2 are the effective emittances of the sides of the radiation shields (corrected for metal to dielectric effects). The first term in the equation is an empirical expression for the contact conduction contribution. The coefficient A and the exponent B must be determined by thermal calorimetry. The second term in this polynomial is the analytical expression for the radiation contribution to the thermal conductivity between infinite parallel radiation shields, multiplied by a correction factor C and expressed as an equivalent conductance term. The factor C corrects for the interaction between the spacer and shield, relating to the optical properties of the spacer. The constants A, B, and C have been determined for most common MLI composites, and the effective emittances are likewise known for most MLI radiation shields. Therefore, these constants can be used in the semiempirical correlation to obtain a fair approximation of the conductivity for temperatures and layer densities for which no data are available.

An example of the usefulness of these correlations is shown in Table 4 [1, 11-14]. Five cryogen tank tests were conducted at different boundary temperatures and for different MLI materials. To compare their performance, the ρk products were adjusted to the same temperature boundaries by means of the semiempirical correlations for each material. The measured ρk value was multiplied by the ratio of the k obtained from the correlation for 286 to 22.2°K (515 to 40° R) boundaries to the k obtained from the correlation for the actual test temperatures to permit comparison of the test results as if all tests were conducted at 86 to 22.2°K (515 to 40° R). The comparisons are to be considered only approximate, since many assumptions were made in adjusting the temperatures and since the effects of seams, fasteners, penetrations, etc., were not treated in the adjustments.

PENETRATION THERMAL EFFECTS

Cryogen tanks for space applications will have penetrations through the MLI blankets in the form of vent lines, fill lines, structural supports, etc. These penetrations can constitute severe heat shorts to the cryogen. The heat leak through one poorly designed penetration can exceed the heat leak through the entire MLI blanket. Because of these potentially sizable penetration heat leaks, it is essential that they be predictable. This discussion presents a description of the penetration problem, the results accomplished, and the remaining work required.

Solid penetrations such as some support struts are the easiest to analyze. A knowledge of the dimensions, boundary temperatures, and thermal conductivity of such a penetration is generally adequate for accurate thermal analysis and prediction of the heat leak.

A schematic of an insulated cryogen tank showing an MLI pipe penetration is presented in Figure 15. The total heat leak to the cryogen is shown to be composed of two major components, the radial MLI heat leak and the penetration heat leak. The MLI heat leak was discussed in detail

TABLE 4. MULTILAYER INSULATION PERFORMANCE COMPARISON

Company	Tank Diameter, m (in.)	V Volume, m^3 (ft^3)	A_S Surface Area, m^2 (ft^2)	Insulation System, cm (mil)	Number of Layers	ΔX, cm (in.)	$\bar{N}$ layers/cm (layers/in.)	ΔT Test, °K (°R)	ρ System Density, kg/m^3 (lb/ft^3)	$k \times 10^4$ Measured Conductivity, W/m °K (Btu/hr ft °R)	$\rho k \times 10^3$ Test, W/m^4 °K (Btu × lb/hr ft^4 °R)	$\rho k \times 10^3$ Modified, W/m^4 °K (Btu × lb/hr ft^4 °R), 287/22.3 (515/40)
General Dynamics/ Convair	1.89 Dia. (74.5 Dia.) 2.21 Long (87.6 Long)	4.88 (172.6)	14.1 (152)	DAM[a] Dacron Needles Tank Mtg. 0.635×10^{-3} (1/4)	44 Radiation Shields 4 Face Sheets	3.81 (1.5)	11.8 (30)	293/22.3 (525/40)	With Attach 20.3 (1.27)	11.8 (6.8)	23.9 (8.6)	23.9 (8.6)
Lockheed	2.78 (109.7)	7.92 (280)	19.7 (212)	DAM Tissuglass 0.381×10^{-3} (0.15)	105 DAM 100 Tissuglass	1.78 (0.7)	58.1 (150)	116/22.3 (209/40)	No Attach 52.8 (3.3)	3.0 (1.74)	16.1 (5.8)	44.4 (16)
McDonnell-Douglas	1.83 Dia. (72 Dia.) 3.65 Long (144 Long)	8.00 (283)	42.0 (451)	DDAM[b] Shroud Mounted 1.27×10^{-3} (1/2)	11 Flat 10 Dimpled	3.81 (1.5)	5.5 (14)	284/164 (510/294)	No Attach 9.6 (0.6)	90.5 (52)	86.1 (31)	86.1 (31)
Lockheed	2.10 (82.6)	5.54 (196)	12.8 (138)	DAM Dexiglass Tank Mounted	30 DAM 27 Dexiglass	2.79 (1.1)	9.9 (25)	223/124 (400/123)	With Attach 30.9 (1.93)	2.6 (15)	80.6 (29)	144.0 (66)
MSFC	2.66 (105.0)	12.8 (454)	27.1 (292)	CSAM[c] 0.635×10^{-3} (1/4)	48	1.78 (0.70)	27.6 (70)	262/22.3 (470/40)	No Attach 24.0 (1.5)	27.8 (16)	66.6 (24.0)	83.1 (30)

a. DAM – Double Aluminized Mylar
b. DDAM – Dimpled Double Aluminized Mylar
c. CSAM – Crinkled Single Aluminized Mylar

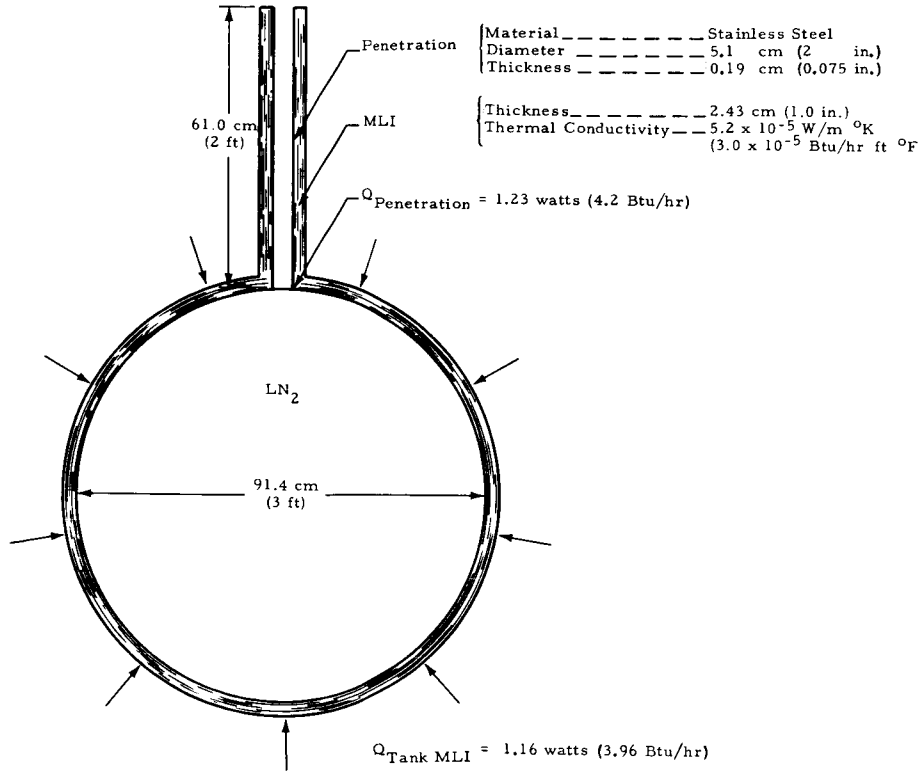

Figure 15. Penetrated spherical cryogen tank (LN_2).

earlier. The penetration heat leak represents another difficult heat transfer problem.

The different modes of heat transfer are shown pictorially in Figure 16. To accurately predict the penetration heat leak, the conduction, convection, and radiation must be considered. The significance of each of these modes of heat transfer on total heat leak, including the effects of both one- and two-dimensional conduction, is discussed below.

One-Dimensional Conduction

The simplest approach to the penetration heat leak problem is to consider the penetration to be perfectly insulated from lateral heat transmission (adiabatic wall), to neglect internal radiation and convection, and to solve the simple one-dimensional Fourier equation for the heat leak. The results of this form of analysis are presented in Figure 17 for a particular penetration for both stainless steel and fiberglass materials.

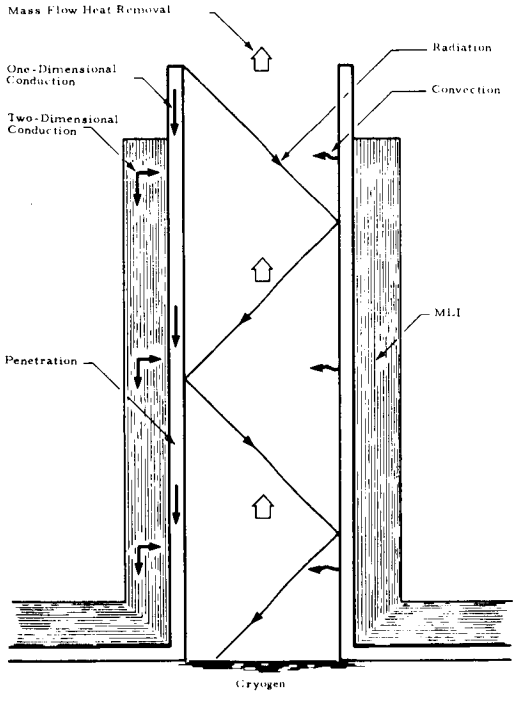

Figure 16. Complex heat transfer interactions in an insulated penetration.

Two-Dimensional Conduction

To improve the one-dimensional analysis, heat conduction perpendicular to the penetration is considered. The two-dimensional problem can be treated as a fin using a closed-form solution if the MLI conductivity is assumed constant and lateral conduction in the MLI is neglected. A more accurate solution can be obtained by computer thermal analysis. The results of a computer analysis are presented in Figure 17. The increase in calculated heat leak resulting from the nonadiabatic wall assumption is apparent.

Internal Radiation

Another improvement in the analysis can be realized by including the effects of radiation tunneling down the interior of the pipe. The results of the inclusion of radiation are presented in Figure 17 also. The importance of the radiation contribution is more obvious in the fiberglass example. Accurate treatment of this effect requires a computer thermal analysis.

Convection and Venting

When cryogenic gas is venting through the penetration, convection must also be considered in the penetration heat leak analysis. The effect of venting is shown in Figure 17. The decrease in total heat leak is a result of the convective cooling of the penetration wall by the cold venting gas. This convection effect is also treated most accurately by computer thermal analysis.

The importance and nonlinearity of the two-dimensional conduction effect, the radiation effect, and the convection effect are shown respectively in Figures 18, 19, and 20. Not only do these heat paths individually influence the penetration heat leak, but they also interact since each affects the longitudinal temperature distribution.

Computer Analysis Technique

In the computer thermal analysis of venting MLI penetrations, four modes of heat transfer must be considered:

1. Radial and longitudinal conduction within the penetration, the MLI, and the boiloff gas.

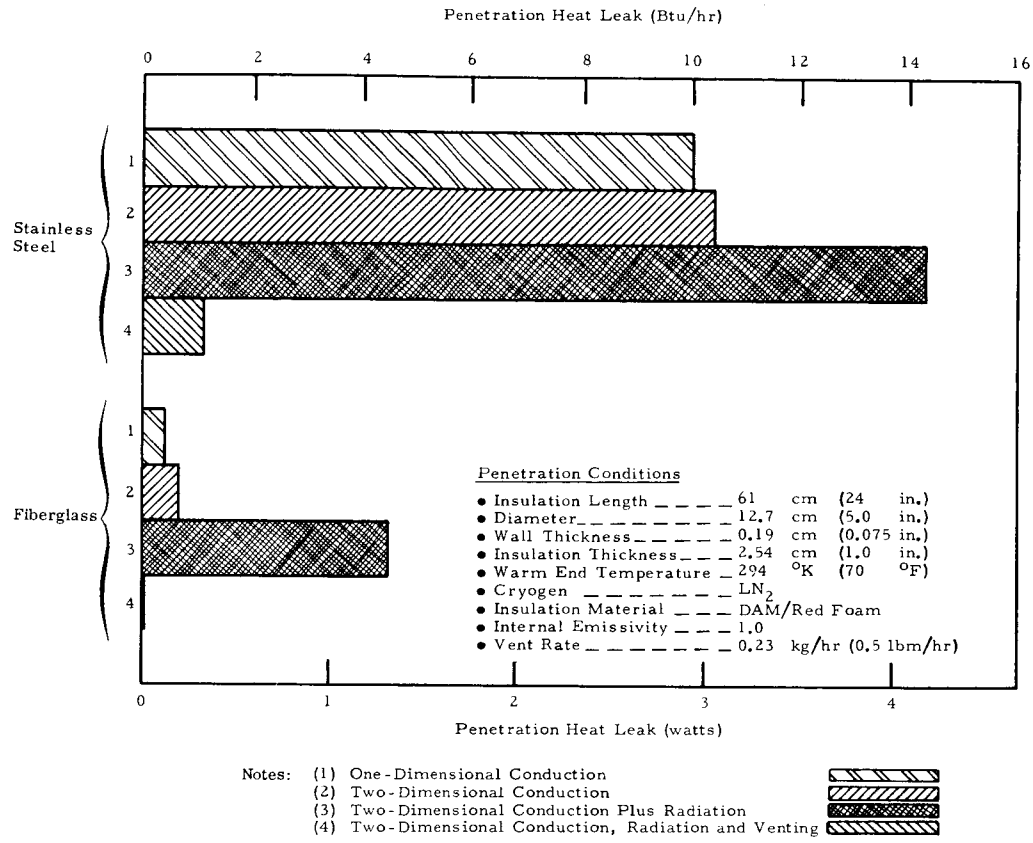

Figure 17. Penetration heat leak for various penetration conditions.

2. Radiation between the external surface of the MLI and the surrounding environment, and internal radiation within the cylindrical cavity of the penetration.

3. Convection between the inner pipe surface and the venting gas.

4. Enthalpy flow associated with the venting gas within the penetration.

The treatment of these heat transfer mechanisms is depicted in Figure 21. The penetration system is divided into finite size nodes connected by thermal resistance paths. Each node is assumed to be at a constant temperature throughout. For an exact treatment, each node would necessarily be infinitesimally small, but a judicious choice of node size and location allows an excellent approximation of the exact treatment.

The steady-state temperature of each node is desired, from which the heat transfer through each resistance path can be calculated. To obtain the solution, an energy balance is written for each node. For solid nodes within the network, the energy balance is:

$$\sum Q_{in} = \sum Q_{out} \quad ,$$

since each node represents a closed system under steady-state conditions.

For the gas nodes through which venting cryogen flows, the energy balance is:

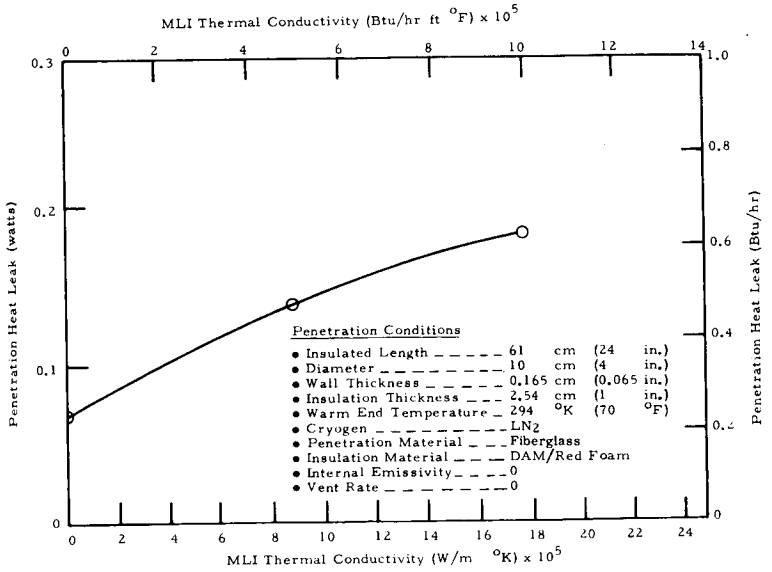

Figure 18. Effect of two-dimensional conduction on penetration heat leak.

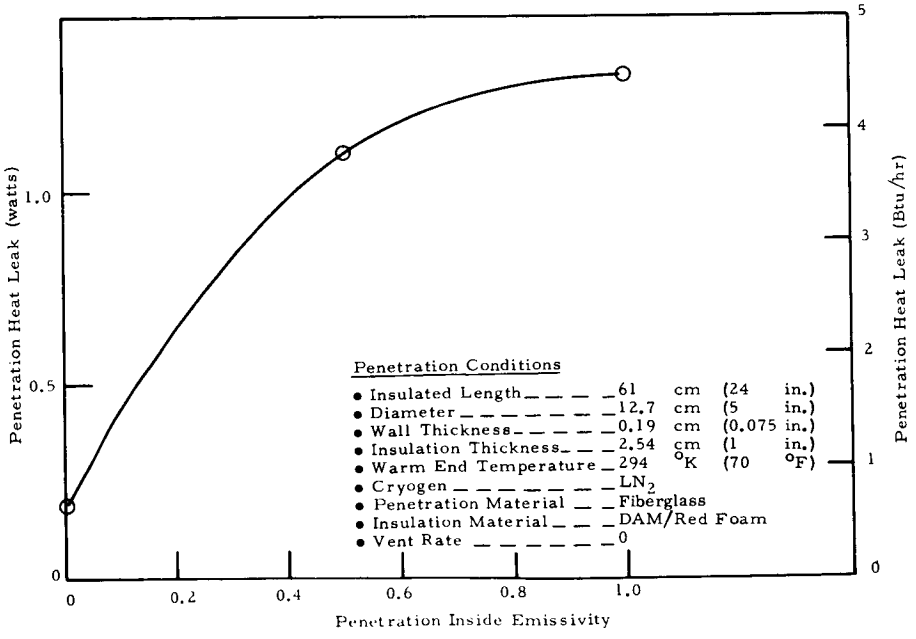

Figure 19. Effect of internal emissivity on penetration heat leak.

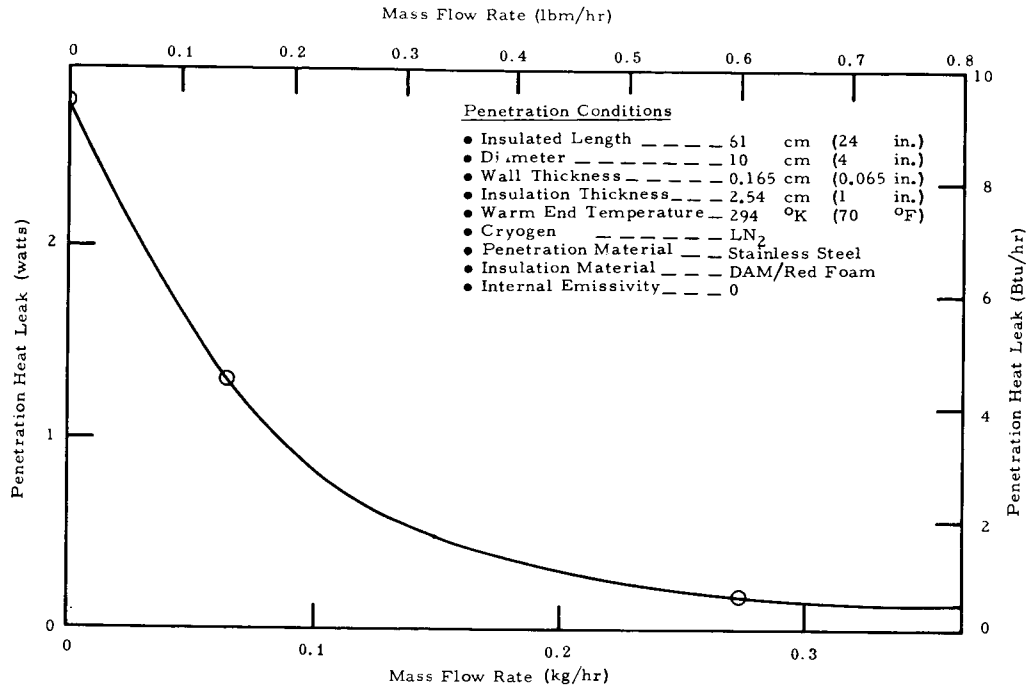

Figure 20. Effect of mass flow rate on penetration heat leak.

$$\sum Q_{in} = \dot{m}h_{in} = \sum Q_{out} + \dot{m}h_{out} \quad ,$$

since each of these nodes represents an open system under steady-state, steady-flow conditions.

Each Q can be replaced by the proper heat transfer expression as follows.

For conduction,

$$Q_{i-j} = \frac{KA(T_i - T_j)}{\Delta X} \quad ,$$

where K is the thermal conductivity evaluated at the mean temperature $(T_i + T_j/2)$.

For convection,

$$Q_{w-g} = HA\,(T_w - T_g)$$

where H is the film coefficient evaluated from the flow conditions, fluid properties, and geometrical considerations.

For radiation,

$$Q_{i-j} = \sigma A F_A \mathfrak{F}_e\,(T_i^4 - T_j^4) \quad ,$$

where F_A is the view factor and $\mathfrak{F}_e$ is the non-black-body correction factor that treats emission, reflection, and absorption characteristics of the surfaces.

For mass flow,

$$\dot{m}h_{ij} \approx mC_pT_i \quad ,$$

where h_{ij} is the specific enthalpy of the fluid evaluated at the interface temperature $(T_i + T_j/2)$ and C_pT_i is an approximation for h_{ij}.

For a network consisting of n nodes, there are n unknown temperatures to be determined. The energy balance equations represent n equations. Therefore, the equations can be solved simultaneously to yield the required node temperature and heat rates. A relaxation scheme is usually employed in solving these equations.

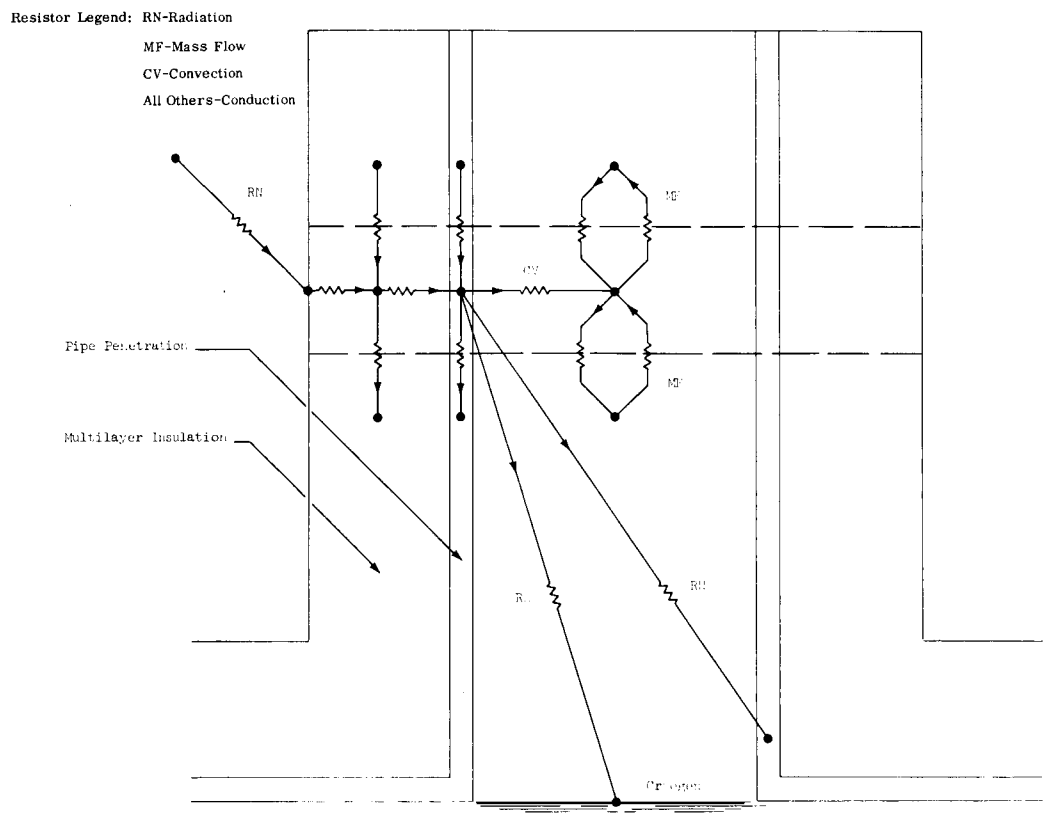

Figure 21. Nodal network representation of venting insulated penetration problem.

Comparison of Analytical and Experimental Results

It is apparent from the previous discussion that the interaction of the various modes of heat transfer for a penetration protected by MLI creates an extremely complex problem for analysis; a generalized, closed-form analytical solution has not been obtained, and the designer must resort to the use of a computer and/or experimental data. Experimental data are limited, however, both in numbers and in parametric variations of the variables. Table 5 represents the present state of information; a correlation of these data has not been conducted.

A comparison of computer results expected and actual experimental data has been conducted [15] in which a 0.508-m (20-in.) tank with known geometries, materials, etc., was evaluated for its penetration heat leak. Figure 21 represents the computer model in which the following parameters were considered: (1) lateral and perpendicular conduction in both the MLI and penetration, using temperature sensitive properties; (2) internal and external radiation; (3) vent gas flow rate and properties, and (4) temperature-sensitive convection mechanism from the penetration to the vent gas.

Experimentally, the vent gas flow rate was varied by placing electrical heaters inside the 0.508-m (20-in.) tank, thereby increasing the gross heat load by a known amount. The effectiveness of a neck cooling coil was also evaluated. Cooling of the top of the vent line did not completely eliminate the penetration heat leak. The cold temperature at the top of the vent line caused gas leakage through a teflon gasket located above the cooling coil. The chamber pressure and the tank sidewall heat flux increased. Since the sidewall heat flux changed, an accurate evaluation of this technique was impossible.

TABLE 5. COMPARISON OF MULTILAYER INSULATION PENETRATION STUDIES

Reference	Length Range, cm (in.)	Diameter Range, cm (in.)	Emissivity	End Temperature, °C (°R)	Penetration Materials	Insulation Description	Insulation Parallel Conductivity Considered	Internal Pipe Radiation Considered	Analytical or Experimental	Cryogen	Range of Heat Rates to Cryogen, W (Btu/hr)	Thickness Range, cm (in.)	Penetration Insulated	Date Documented
ADL[a]	43.1 (17)	15.25 (6)	0.35 0.025 (Partial)	78.4 (140) 223 (400) 300 (540) 418 (750)	304 Stainless	Aluminized Mylar and 2 Layers Silk Netting (7.8×10^{-3} m (7 mil) Thick	No	Yes	Experimental	Liquid Nitrogen	0 to 16.7 (0 to 57.3)	0.069 (0.027)	Yes	Jan., 1968
ADL[a]	43.1 (17)	15.25 (6)	0.35 0.035 0.86-0.94 0.41	78.4 (140) 223 (400) 300 (540) 418 (750) 116 (208)	304 Stainless Steel (85 to 151 W/m °K)	ϵ - 0.002 Essentially Adiabatic	No	Yes	Analytical	Liquid Nitrogen	0 to 10.2 (0 to 34.8)	0.069 (0.027) 0.025 (0.010) 0.002 (0.001) 0.083 (0.033)	Yes	Jan., 1968
LMSC/ HREC[b]	17.8 to 305 (7 to 120)	2.54 (1) 7.61 (3) 15.2 (6) 30.5 (12) 45.5 (18)	0	289 (520)	304 Stainless Titanium (Ti-6Al-4V) Fiberglass	Aluminized Mylar 70 Layers, 2.54 cm Thick. Temperature Dependent Value Input	Yes Temperature Dependent Value Input	No	Analytical	Liquid Hydrogen	0.06 to 24 (0.2 to ~2)	0.158 (0.0625) 0.318 (0.125) 0.625 (0.25)	Yes	Oct., 1967
NASA[c]	—	5.08 (2)	0	249 (520)	—	Aluminized Mylar 5 to 160 Shields, Nonconducting Spacers, Baffle Considered	Yes	No	Analytical	Liquid Hydrogen	—	—	No	Sept., 1968
DAC[d]	15.2 (6) 91.5 (36)	Not Given	0	295 (530)	Fiberglass Aluminum	NRC-2 50 Sheets	Unknown	No Curved, High L/D	Analytical and Experimental	Unknown	0.06 to 4.2 (0.2 to 14.33)	Cross Section 0.196 (0.31 $in.^2$)	Yes	Not Given
Martin[e]	416 (164) 91.5 (36) 175 (69)	15.2 (6) 25.4 (10)	0.15-1.0	223 (400)	Stainless Titanium Aluminum	Fixed Heat Flux Through HPL 0.315 W/m^2	No	Yes	Analytical	Liquid Hydrogen	~5.6 to 10.2 (~19 to 35)	0.198 (0.078) 0.477 (0.188)	Yes	Jan., 1969
ADL[f]	>2.54 (>1)	7.64 (3)	—	295 (530)	Copper	Aluminized Mylar, 5 Layers	Yes	—	Analytical and Experimental	Liquid Nitrogen	2.09 (7.17)	Solid Disc	No	Dec., 1964
LMSC/ Sunnyvale[g]	~5.08 (~2)	2.54 (1)	Not Given	295 (530)	Stainless Steel	50 Layers (~1.78 cm Thick)	Yes	No	Analytical and Experimental	Liquid Nitrogen	0.125 to 0.596 (0.427 to 2.034)	0.025 (0.01)	No	1967

a. Advanced Studies on Multi-Layer Insulation Systems. NASA CR-72368, Arthur D. Little, Inc., ADL 69913-00, Cambridge, Mass., January 13, 1968.
b. Hedden, R. O.: Superinsulation Thermal Conductivity Parametric Study. LMSC/HREC A784869, Lockheed Missiles & Space Company, Huntsville, Ala., October 1967.
c. Johnson, W. R.; and E. L. Sprague: Analytical Investigation of Thermal Degradation of High Performance Multilayer Insulation in the Vicinity of a Penetration. NASA TN D-4779, Lewis Research Center, Cleveland, Ohio, September 1968.
d. Price, J. W.; and T. G. Lee: Analysis, Design, and Testing of Heat-Short-Insulation Components for High Performance Insulation Systems. Cryogenic Engr. Conf. Paper D-6, Douglas Aircraft Co., Inc., Santa Monica, Calif.
e. Bowman, F. E., et al.: Development of Advanced Materials for Integrated Tank Insulation System for the Long Term Storage of Cryogens in Space. MCR-68-422, Second Quarterly Progress Report (October-December), Martin Marietta Corp., Denver, Colo., January 1969.
f. Design and Optimization of Space Thermal Protection for Cryogens – Analytical Techniques and Results. Topical Report 659 58-03-01, Arthur D. Little, Inc., Cambridge, Mass., December 18, 1964.
g. Coston, R. M.: A Study on High-Performance Insulation Thermal Design Criteria – Final Report. LMSC-A847882, Vol. I, Lockheed Missiles & Space Company, Sunnyvale, Calif., June 25, 1967.

Figure 22 shows the comparison between computer and experimental results. The good correlation has led to an expansion of the penetration analysis, both by computer and selected experiments, in which the following parameters will be varied:

1. Geometry
   a. Penetration length
   b. Penetration diameter
   c. Penetration wall thickness
   d. Penetration material
   e. Insulation thickness
2. Properties
   a. Penetration thermal conductivity
   b. Penetration emissivity
   c. Penetration material
   d. Insulation thermal conductivity
   e. Cryogen
3. Vent mass flow rate
4. Temperature levels

Results will be presented in a design handbook. Such a designer may then use the information directly.

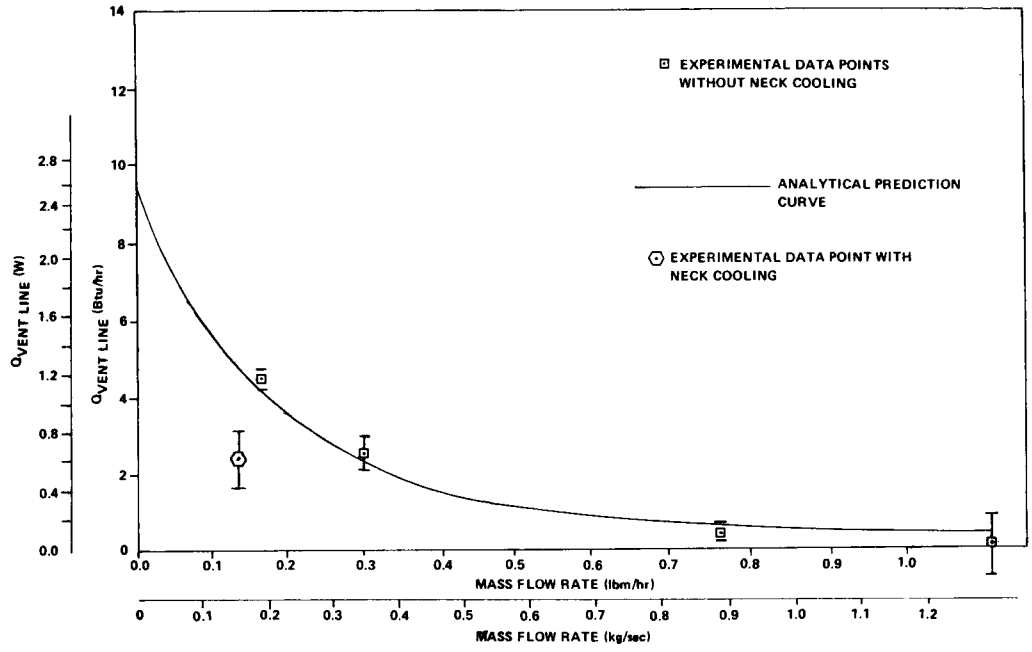

Figure 22. Comparison of analytical prediction curve with experimental data points.

MLI SYSTEMS DEVELOPMENT AND APPLICATION

Several MLI thermal protection systems have been designed and fabricated for subscale test tanks by MSFC and contractors. Some of these MLI test systems are shown in Figures 23 and 24. Different application techniques, different MLI systems, and different sizes and shapes of tanks were used in the tests. To compare results from the various tests, it is necessary to consider all the influencing parameters discussed in previous sections such as temperature extremes, gap geometry, layer density, ambient gas pressure, penetration heat leaks, MLI thickness, and MLI area. These tests have demonstrated the thermal performance of MLI systems under simulated flight conditions.

To clarify the considerations (data acquisition and reduction) that go into testing and evaluating an MLI system, an example is presented. The system to be considered is pictured in the right photograph of Figure 24. The test tank is 50.8 cm (20 in.) in diameter with ellipsoidal ends and a 10.2 cm (4 in.) diameter neck. The insulation system is double-aluminized Mylar/GAC-4 red foam. The boiloff rate at steady-state conditions was measured to be 1.76×10^{-5} kg/sec (0.142 lbm/hr), which corresponds to a total heat leak to the liquid hydrogen of 3.55 W (12.11 Btu/hr). Figure 25 presents the neckline heat leak as a function of boiloff rate along with a table of calculations. The curve was obtained by computer thermal analysis of the insulated tank and neck penetration. Since the boiloff rate was known, the neck heat leak was determined from the curve to be 1.31 W (4.48 Btu/hr). Since the total heat leak is the sum of the neck heat leak and the insulation heat leak, the insulation heat leak was found to be 2.23 W (7.63 Btu/hr). The Fourier equation was used to calculate a thermal conductivity of 20.9×10^{-5} W/m °K (12.05×10^{-5} Btu/hr ft °F). The density-thermal conductivity product is also presented in Figure 25. This applied thermal conductivity value of 20.9×10^{-5} W/m °K (12.05×10^{-5} Btu/hr ft °F) is twice the calorimeter value obtained for the same boundary conditions. This can be expressed as a degradation factor of 2.0 for this particular system as applied. The degradation is a

GENERAL DYNAMICS/CONVAIR
DAM DACRON NEEDLES

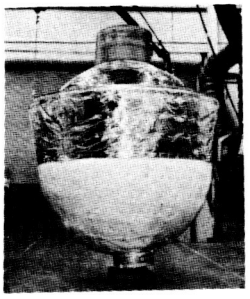

LOCKHEED MISSILES
AND SPACE CO.
DAM DEXIGLASS

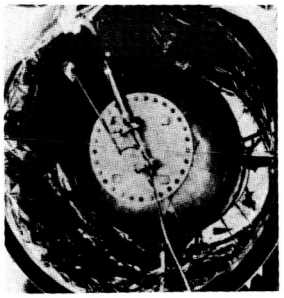

McDONNELL DOUGLAS
ASTRONAUTICS CO.
DAM DIMPLED

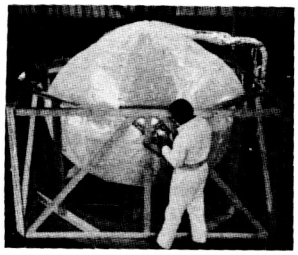

LOCKHEED MISSILES AND SPACE CO.
DAM TISSUGLASS

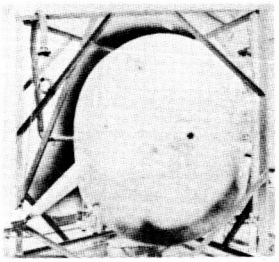

MARSHALL SPACE FLIGHT CENTER
CSAM

Figure 23. MLI systems development.

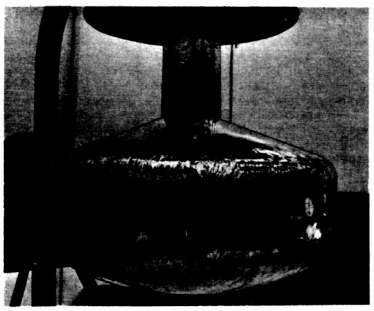

20 LAYERS DOUBLE
GOLDIZED MYLAR SILK NET

ADL TANK CALORIMETER

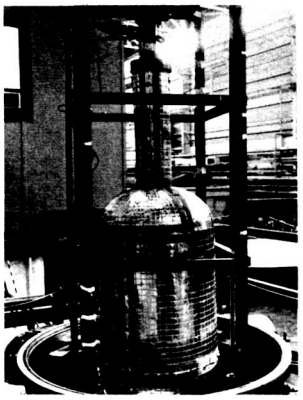

27 LAYER DOUBLE
ALUMINIZED MYLAR RED
FOAM

SCALE MODEL TANKS

CONSIDERATIONS:

- MATERIAL SELECTION
- SCALABLE APPLICATION
- THERMAL STABILITY
- MECHANICAL & TEMPERATURE EFFECTS
- INTERSTITIAL GAS FLOW
- ACCURATE TANK TESTING
- LARGE TANK TESTS
- VACUUM FACILITIES

Figure 24. Current MLI efforts.

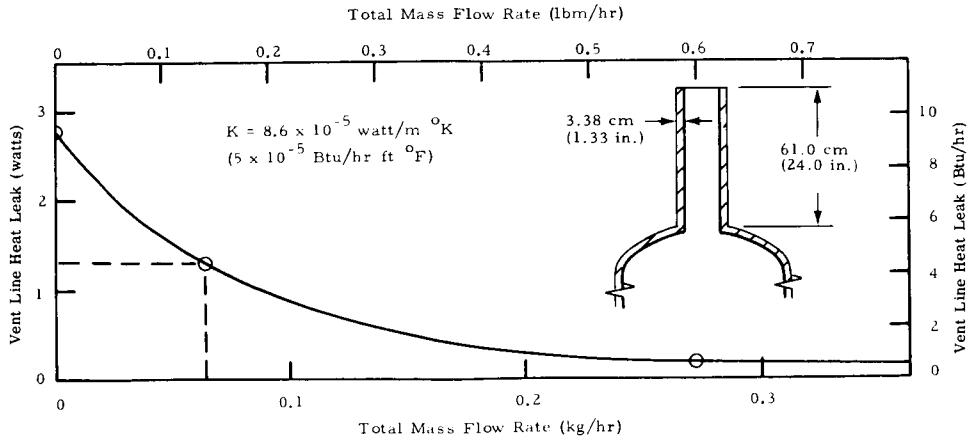

Insulation System	Composite Area Density	System Boiloff	Vent Line Heat Leak	Insulation Heat Leak	Applied Insulation Thermal Conductivity	Applied Heat Flux	Composite Area Density x Heat Flux
DAM/Red Foam	0.886 kg/m^2	3.547 watts	1.31 watts	2.23 watts	20.84×10^{-5} watt/m °K	1.40 $watt/m^2$	1.242 $\frac{watt}{m^2} \times \frac{kg}{m^2}$
27 Layers DAM 6.4×10^{-4} cm (0.25 mil) 26 Layers Red Foam 7.6×10^{-2} cm (30 mil)	0.1814 lbm/ft^2	12.11 Btu/hr	4.48 Btu/hr	7.63 Btu/hr	12.05×10^{-5} Btu/hr ft °F	0.445 Btu/hr ft^2	0.0807 $\frac{Btu}{hr\ ft^2} \times \frac{lbm}{ft^2}$

Figure 25. Reduction of DAM/red foam data — 50.8 cm (20 in.) diameter tank.

result of a combination of gaps, compression, layer density variations, the presence of structural materials, gas entrapment, etc. This degradation is analogous to degradations found in other engineering disciplines when actual systems are compared to ideal systems. The values of degradation factors will vary for different MLI materials and application techniques.

A comparison of the thermal performance of applied MLI systems is not straightforward. It is not correct, for instance, to compare systems applied to different size tanks with arbitrary application conditions. The best method of comparing MLI's for tank application is to establish and follow basic ground rules. For example, it is most desirable (although not absolutely essential) that the same tank and test facility be used for testing each MLI. This prevents errors that could be associated with different tank thermodynamics, different penetrations, different measuring equipment, etc. The temperature boundaries should be the same for each MLI. The criteria for system selection must be established; for example, in weight-limited situations, ρk should be minimum. In addition, each MLI should be applied at the layer density (or as near to it as possible) and with the attachment method that corresponds to the minimum ρk. Using these established ground rules, the superior MLI can then be chosen based on the test results.

The Convair Aerospace Combined Environments of Vacuum, Acceleration, and Temperature (CEVAT) test procedure is designed to determine the effects of the combined environments of vehicle launch on the structural and thermal performance of MLI systems. Subscale tanks are used in CEVAT testing, but the acceleration and evacuation rates are scaled upward to simulate the stresses experienced by an actual flight-size tank. The MLI thermal conductivity is measured before and after being subjected to the CEVAT test to determine whether gross

changes in thermal performance have occurred. The results of three CEVAT tests are presented in Table 6 [16, 17]. In Table 7 [17] the specific results of the CEVAT testing of a 63.5 cm (25 in.) diameter tank [insulated with 10.3 cm (4 in.) of Superfloc MLI using the bonded pin method of layer density control] are presented.

After completing the successful CEVAT testing of the Superfloc MLI system, a flightweight, 2.21 m (87 in.) diameter aluminum tank was developed for experimentally verifying the thermal performance of a complete cryogenic propellant storage system [18, 19]. A schematic of the complete system is shown in Figure 26. The aluminum tank is covered with a lightweight fiberglass fairing system and two MLI blankets. A total of six thermally efficient support struts are used to mount the tank inside an enclosure. The design, development, and testing of these system components are discussed in the paragraphs below.

Tank

The tank material selected was 2219 T62 aluminum alloy. The tank bulkheads were fabricated from a single piece of 2219 aluminum alloy plate by hot-spin-forming methods. The major and minor tank diameters are 2.23 m (87.6 in.) and 1.89 m (74.5 in.), respectively. Pressures used to determine the tank gages were 5.5×10^5 N/m^2 (80 psig) operating, 6.89×10^5 N/m^2 (100 psig) proof, and 9.35×10^5 N/m^2 (136 psig) burst. The tank was designed to be supported by 6 or 12 struts,

TABLE 6. CRYOGENIC INSULATION DEVELOPMENT

Objective: Evaluation of Thermal and Structural Performance of Insulations by Subjecting Scale Models to Combined Test Environments of Rapid Pressure Drop, Acceleration, and Low Temperature. Acoustic Noise Effects Evaluated Separately.
Test Requirements: Simulation of Saturn Trajectory.

		Insulation System	System Density kg/m^3 (lb/ft^3)	Test ΔT (°K) [Test ΔT (°R)]	Measured Conductivity (k_e), W/m °K (Btu/hr ft °F × 10^5) Initial	Measured Conductivity (k_e), W/m °K (Btu/hr ft °F × 10^5) Final	$\rho k_e \times 10^5$, W/m^4 °K (Btu/hr ft^4 °F) Final	$\rho k_e \times 10^5$, W/m^4 °K (Btu/hr ft^4 °F) Adjusted to ΔT = 293 - 22°C (525 - 40°R)	Structural Performance
73.6-cm (29-in.) Tank	NASA NRC-2 Design 	Shingle Concept 6 Battens 0.635 × 10^{-3} cm (1/4 mil) AM 1.93 cm (0.76 in.) Thick 25 Layer/cm (63 Layer/in.) Avg.	22.9 (1.43) (No Attachment Tapes)	284-21 (510-37)	9.7 (5.6)	No Test	No Test (8.0 Based on 'Initial')	No Test	Accel: 6.1 m/sec^2 (20 g) Vib: 7.2 g rms Response Evac: 6.66 × 10^2 N/m^2 (5 torr) in 120 sec Acoustics: 150 dB, 2 min. Appl. to 2.67 m (8.75 ft) Dia Tank (30% Tape), Length Not Crit., Failed at 30 X Evac.
73.6-cm (29-in.) Tank	Goodyear System 	AMA/Foam 2 Blankets 0.635 × 10^{-3} cm (1/4 mil) AMA 25 Layers Foam 26 Layers AMA 5.06 cm (2.00 in.) Thick	33.6 (2.1) (Including Face Sheets but No Lacing)	284-21 (510-37)	17.0 (9.8)	15.3 (8.8)	51.5 (18.5)	57.0 (20.5)	Accel: 5.95 m/sec^2 (19.5 g) Vib: 7.6 g rms Response Evac: 1.06 × 10^6 N/m^2 (80 torr) in 100 sec Acoustics: 150 dB, 2 min. Appl. to 2.67 m (8.75 ft) Dia Tank, Length Not Detrmd., Lack Info.
63.5-cm (25-in.) Tank	Convair System 	Superfloc 4 Blanket Layers 0.635 × 10^{-3} cm (1/4 mil) AMA 120 Layers 8 Face Sheets 10.2 cm (4 in.) Thick 11.8 Layers/cm (30 Layers/in.)	16.02 (1.8)	289-21 (520-37)	22.5 (13.0)	21.5 (12.4)	34.5 (12.4)	35.8 (12.9)	Accel: 5.25 m/sec^2 (17.2 g) Vib: 16 g rms Response Evac: 133 N/m^2 (1 torr) in 70 sec Acoustics: (No Test) Appl. to 2.67 m (8.75 ft) Dia Tank, Any Length

TABLE 7. SUMMARY OF THE 63.5-cm (25-in.) TEST TANK PROGRAM

Tank System Parameters

Tank Volume: 0.204 m^3 (7.2 ft^3)
Tank Surface Area: 1.67 m^2 (18.3 ft^2)
Fairing Area: 0 m^2 (0 ft^2)
Cryogen: LH_2
Penetrations Thermally Guarded

Insulation System Parameters

Insulation System: Superfloc
Nominal Thickness: 10.03 cm (4.0 in.)
System Density: 16 kg/m^3 (1.0 lb/ft^3)
Average Area: 2.21 m^2 (23.8 ft^2)
Configuration: Six 60-deg gores
Two hemispherical end caps
Number of Blankets: 4
Seam Length:
Blanket No. 1: 8.94 m (29.3 ft)
Blanket No. 2: 9.42 m (30.9 ft)
Blanket No. 3: 9.94 m (32.6 ft)
Blanket No. 4: 10.40 m (34.1 ft)
No. of Support Pins: 6
No. of Support Pin Grommets: 24
No. of Seam Pins With Grommets: 316
No. of Purge Pins: 0

Thermal Analysis

Ullage Pressure 10.1×10^4 N/m (14.7 psia)
Source Temperature: 298°K (535°R)
Sink Temperature: 22.3°K (40°R)
Performance:
Total Heat Flux: 0.583 W/m^2 (0.185 Btu/hr ft^2)
Insulation: 17 percent
Seams: 24 percent
Pins: 59 percent
Penetrations: 0 percent
Heat Flow Rate: 1.29 W (4.4 Btu/hr)
Mass Flow Rate: 2.9×10^{-6} kg/sec
(0.023 lbm/hr)

Thermal Test

Before Centrifuge Test
Duration: 38 hr
Cryogen Mass: 12.9 kg (28.5 lb)
Vacuum Pressure 3.61×10^{-4} N/m^2
(2.7×10^{-6} torr)

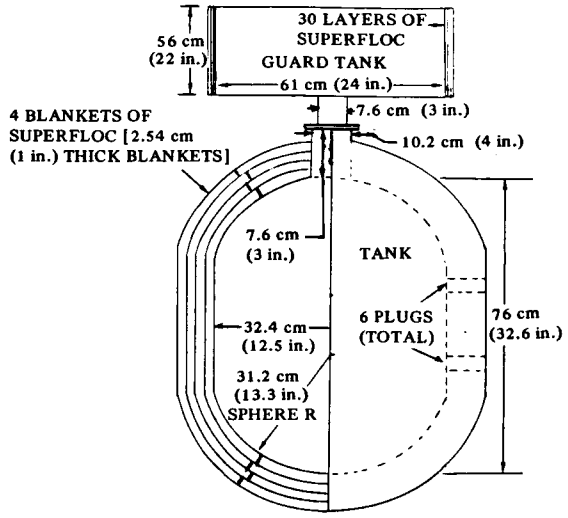

Ullage Pressure: 10.1×10^4 N/m^2 (14.7 psia)
Heat Flux: 0.597 W/m^2 (0.19 Btu/hr ft^2)
Heat Flow Rate: 1.35 W (4.6 Btu/hr)
Mass Flow Rate: 3.03×10^{-6} kg/sec
(0.024 lbm/hr)
After Centrifuge Test
Duration: 72 hr
Cryogen Mass: 12.95 kg (28.6 lb)
Vacuum Pressure: 3.76×10^{-4} N/m^2
(2.8×10^{-6} torr)
Ullage Pressure: 10.5×10^4 N/m^2 (15.3 psia)
Heat Flux: 0.565 W/m^2 (0.18 Btu/hr ft^2)
Heat Flow Rate: 1.26 W (4.3 Btu/hr)
Mass Flow Rate: 2.9×10^{-6} kg/sec
(0.023 lbm/hr)
Ground Hold Test
Cryogen Mass: 8.61 kg (19 lb)
Chamber Pressure: 10.1 N/m^2 (14.7 psia)
Ullage Pressure: 10.1 N/m^2 (14.7 psia)
Heat Flux: 157.5 W/m^2 (50 Btu/hr ft^2)
Mass Flow Rate: 7.56×10^{-4} kg/sec
(6.2 lb/hr)

Structural Test

Test Conditions:
Sink Temperature: 89°K (160°R)
Maximum "g" Load: 17.2 g's in 250 sec
Maximum Vibration Load: 16 g rms
Pumpdown: 133×10^2 N/m^2 (1 torr) in 70 sec
Signs of Structural Degradation: None

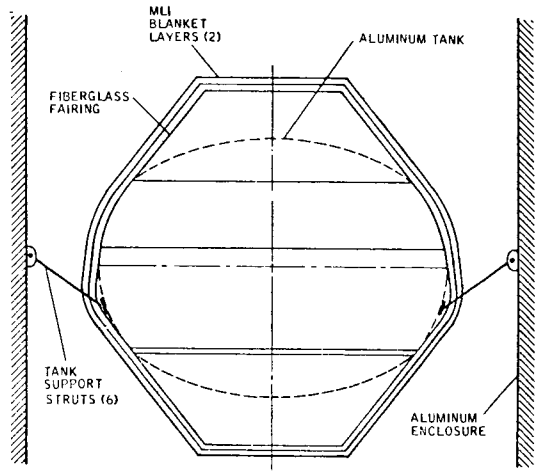

Figure 26. Schematic of 2.21 m (87 in.) diameter cryogenic storage system.

depending on the density of the cryogenic fluid to be stored. The access door diameter is 61.4 cm (24.5 in.). The door was equipped with ten 37-pin electrical pass-throughs for internal measurements, three 6.36 cm (2.5 in.) adapter plates, and one 6.36 cm (2.5 in.) vent opening. The adapter plates were used to pass through steel tubes for internal tank testing. The tank assembly including aft bulkhead, fill and drain line outlet, and door assembly, together with a special handling fixture and supporting struts, is shown in Figure 27. A series of acceptance tests was successfully completed to demonstrate conformance to tank design objectives. The acceptance test program included a hydrostatic proof pressure test at 6.89×10^5 N/m^2 (100 psig), a cryogenic chill test at 20.6°K (-423°F), and a helium leak test. Leak flow rates were found to be on the order of 2.83×10^{-10} m/sec (10^{-8} scc/sec) of helium.

Support Struts

The support system consists of the tank support struts and the tank enclosure that supports the total assembly. Six struts support the 2.21-m (87-in.) tank when liquid hydrogen is stored. The struts are tubular, fiberglass members with a diameter of 2.21 cm (0.83 in.), a 1.02 cm (0.040 in.) wall thickness, and a length of 54.0 cm (21.25 in.) between the bearing centers (Fig. 28). The end spools are made of titanium and equipped with spherical-ball-rod end fittings. The assembly is capable of length adjustment and incorporates locking features to prevent rotation. The tubular section is a multiply layup of 1448E fiberglass epoxy pregnated with the fiber orientation parallel to the strut centerline. The struts are arranged in pairs and spaced around the tank in 120-deg intervals. This arrangement provides axial, lateral, and rotational restraint while permitting tank geometry changes caused by pressurization and temperature gradients.

The struts were fabricated by casting a wash-away plaster mandrel around a 0.954 cm (0.375 in.) drill rod cone. The wash-away mandrel was made to the inside dimensions of the strut and included a depression for accepting a plastic split-ring assembly used for retaining 90 MLI disks. The disks reduced radiation tunneling through the hollow strut into the tank. The fiberglass application is shown in Figure 28 and is described in Reference 18.

Two of the support struts were subjected to the following test conditions:

1. Ambient temperature tension to 2260 kg (5000 lb).

2. Ambient temperature compression to 362 kg (800 lb).

3. No load cryogenic shock, 20.6°K (-423°F).

4. Cryogenic temperature tension to 2260 kg (5000 lb) at 20.6°K (-423°F).

5. Cryogenic temperature compression to 362 kg (800 lb) at 20.6°K (-423°F).

6. Cryogenic temperature tension test to failure at 20.6°K (-423°F).

The strut designed for a 2260-kg (5000-lb) tension load failed at a tension load of 4600 kg (10 175 lb). The primary failure was in interlaminar shear at the end fitting/tube shear plane.

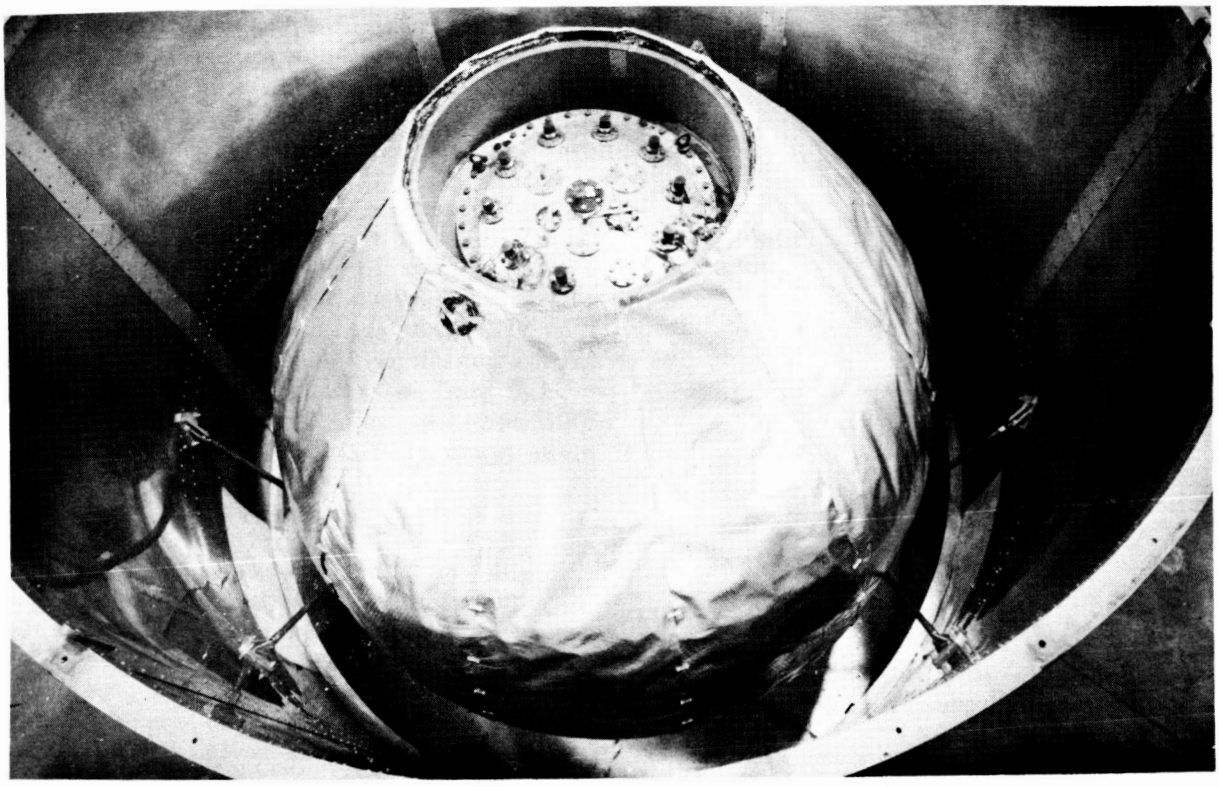

Figure 27. 2.21-m (87-in.) tank assembly.

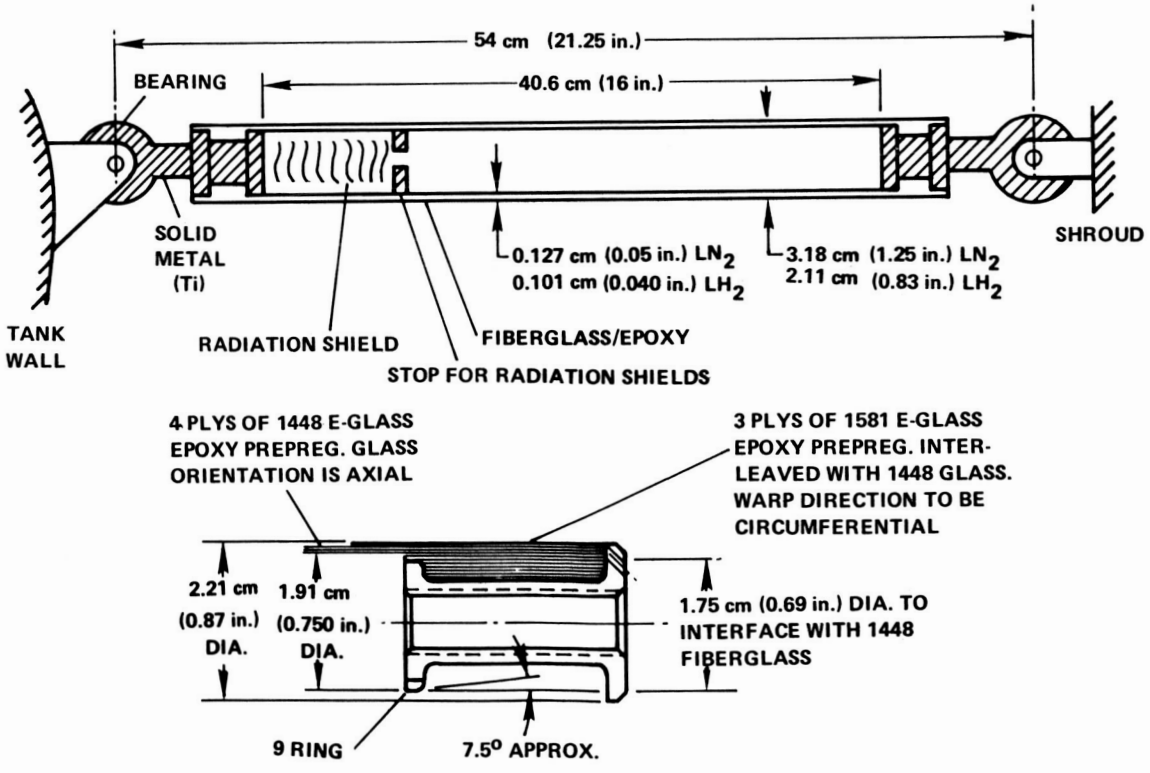

Figure 28. Fiberglass strut.

Enclosure

A structural enclosure was required to support the tank and to simulate the effect on a flight shroud when conducting cryogenic thermal tests. The enclosure was designed to support the tank when filled with the heaviest contemplated propellant (LF_2) in a 1-g field, and with an empty tank plus insulation and internal components during normal transportation conditions. The enclosure consists of the cylindrical, fore, and aft portions. The cylindrical section has an inside diameter of 280 cm (110 in.) and stands 287 cm (113 in.) high. The diameter provides sufficient propellant tank clearance for testing thick insulation systems, while still leaving access clearance between the outside of the enclosure and the interior wall of the 3.66 m (12 ft) diameter vacuum test chamber.

MLI Purge and Fairing Systems

The insulation system selected for this program [3] was Superfloc, which consisted of 0.636×10^{-3} cm (0.25 mil) double-aluminized Mylar radiation shields separated by small tufts of 0.102-cm (0.040-in.) dacron needles bonded to one side of each shield (Fig. 29). A performance comparison of various MLI materials showed Superfloc to have one of the lowest density-conductivity (ρk) factors [3], which is a measure of the insulation efficiency. In addition, Superfloc has high material strength, excellent gas purge and vent characteristics because of the discrete nature of the spacer tufts and the low system bulk density, and ease of application in that the spacer is integral with the shield and not handled separately.

To achieve a thermally and structurally efficient system, the Superfloc material was made into 1.91 cm (0.75 in.) thick gore and cap blanket sections, each containing 22 MLI core sheets [11]. The insulation system design called for two 22-sheet blanket layers, each layer consisting of twelve 30-deg gore sections and two circular cap sections. The seams of the two layers were staggered where possible to prohibit radiation tunneling directly to the tank. The insulation core sheets were bounded on both sides by structural face sheets of a scrim-reinforced Mylar material, Schjeldahl X-850. To minimize wrinkles and distortions in the material, blanket sections were hot formed on tools (Fig. 30) to fit a given area of the tank. To provide a smooth mounting surface for the MLI blankets, clearances for the tank door, pass-throughs, and support strut mounting brackets, and to provide a plenum for the helium gas purge system, a system of longitudinally axisymmetric fiberglass fairings were installed over the tank surface. Individual blanket sections were joined by twin pins and grommets as illustrated in Figure 31. This form of attachment was found to have the highest strength and the least degradation based on interlayer gas venting and blanket thermal performance characteristics. Additional strength was supplied by a freezing method of applying

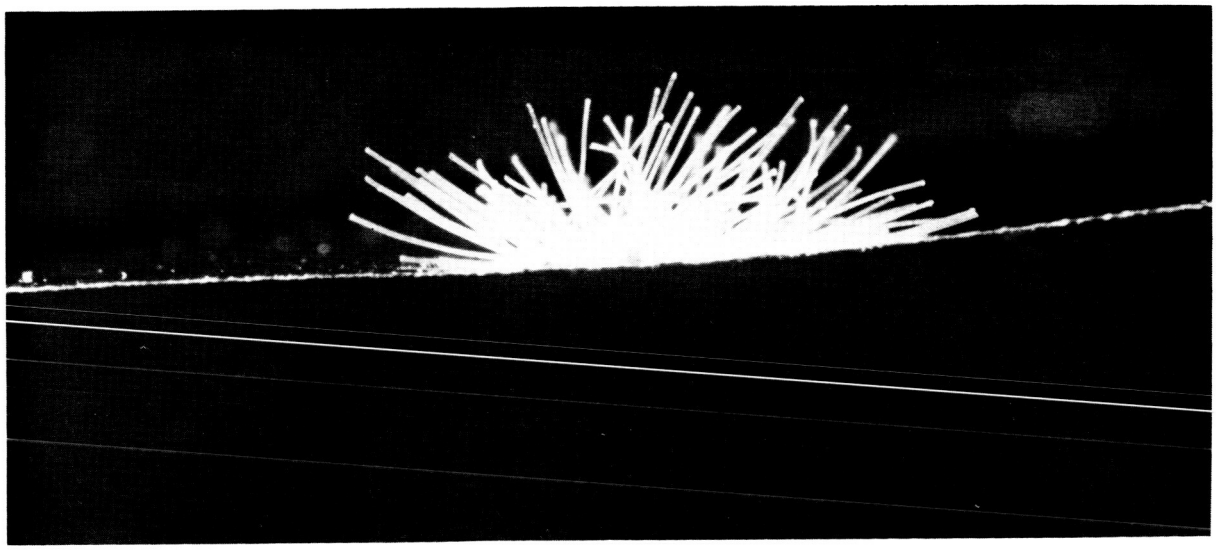

Figure 29. Dacron needles welded to one side of radiation shield.

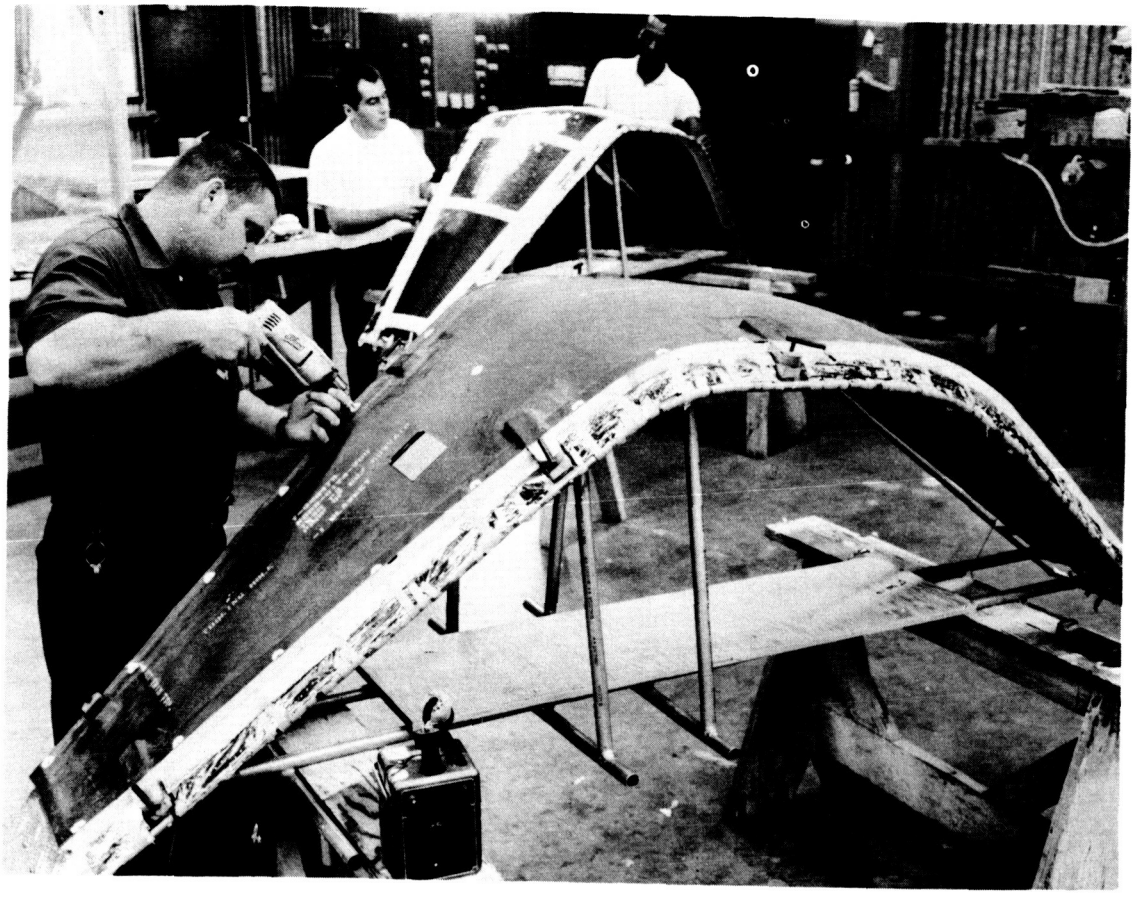

Figure 30. Blanket tool.

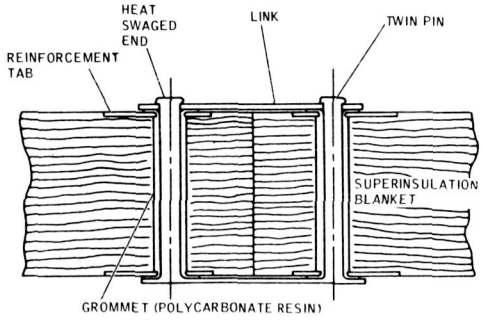

Figure 31. Twin pin fastener.

adhesive to grommets and by the procedure for bonding the Superfloc sheets to the grommets as described earlier. The blankets are held on the tank by fiberglass support pins that are mounted on the tank and penetrate each blanket layer.

The relatively large separation of 0.102 cm (0.040 in.) between the insulation layers provides a good path for evacuating the interstitial gases. For structural design purposes, the maximum pressure differential across the insulation blanket is the parameter of interest. Figure 32 presents these data as a function of evacuation length and pumpdown rates in multiples of the Saturn V pressure decay rate. At the nominal (1X) Saturn pressure decay rate, the maximum pressure differential is considerably less than 6.89×10 N/m^2 (0.01 psi) indicating that the stresses caused by the evacuation of the purge gases during launch are not expected to be critical for this type of insulation. The 2.21-m (87-in.) tank purge system was designed to inject helium into the interior of the insulation blankets to effectively remove the entrapped air. The purge system employed the existing fiberglass tank fairings as low pressure manifold systems to supply helium to 39 purge pins. Three purge pins were inserted through each of the interior 12 gore blankets, and the remaining 3 pins were used to purge the aft cap blanket. Purge pins were not provided for the forward cap blanket since the penetrations passing through this region gave adequate purging area.

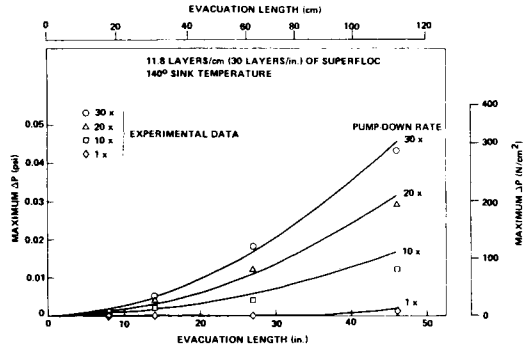

Figure 32. Variations of maximum pressure differential with evacuation length and pumpdown rate — Superfloc, 11.8 layers per cm.

The purge pins, made from the lexan grommets used for insulation blanket attachment are 0.318 cm (0.125 in.) inside diameter lexan tubes approximately 1.91 cm (0.75 in.) long that are slotted to provide helium flow to each layer of Superfloc making up the inner blanket. Purge gas was also fed to the purge opening in the outside blanket by a 0.0811-cm (0.032-in.) orifice in the nose of the purge pin. The helium gas injected into the center of the blankets by the purge pins traveled radially to the seams between the blankets and escaped from the insulation system via these joints.

Three fairings that were used as pin supply manifolds were sealed with Mylar tape to prevent excessive loss of helium through openings other than the purge pins, support strut penetrations, and tank door feed-throughs. The fairings were maintained at a positive pressure differential of approximately 3.43×10^2 N/m^2 (0.05 psi) to provide adequate flow through the purge pins while preventing excessive bulging of the thin fiberglass fairings.

Purge gas was provided to the three low pressure fiberglass manifolds by a relatively high pressure supply line. This 0.636 cm (0.25 in.) outside diameter by 0.07112 cm (0.028 in.) wall CRES tube was equipped with three sets of opposing 0.0811-cm (0.032-in.) orifices, two orifices for each fairing. This supply line was operated at approximately 13.79×10^5 N/m^2 (200 psi) to obtain a helium flow of 0.85 m^3/sec (0.3 ft^3/sec) into each fairing manifold. The total valume to be purged, fairing plus insulation, equaled 1.27 m^3 (45 ft^3). This is equivalent to one complete volume change every 150 sec. The system is assumed to be purged when a nominal 1 percent of air remains within the purged space.

The expression that describes the purge-gas process [20] is

$$\frac{N}{100} = \exp - \frac{(Q\theta)}{V} ,$$

where

Q = purge gas flow rate,

θ = time to purge,

V = purge volume,

and

N = percent of air acceptable at the end of the process.

The validity of this expression was demonstrated in Reference 20 in which experiments were conducted for aluminized Mylar and paper spacers, aluminum foil and paper, crinkled aluminum foil and paper, and crinkled aluminized Mylar. Using this relationship, a purge time of 690 sec would be required to reduce the remaining air concentration in the Superfloc blankets to 1 percent.

Another factor to be considered in the 2.21 m (87 in.) diameter tank experiment was the application of the Superfloc to the cryogenic test tank. MIL density control was one of the most important parameters to be considered. The initial step in designing the insulation blanket was to mock-up a series of geometric shapes that had been analytically selected as candidate configurations. A spare, single-piece bulkhead formed on the same mandrel as the final 2.21-m (87-in.) tank bulkheads was used for the insulation mockup. Full gore sections, conic sections, and combinations of the two were placed on the bulkhead for visual comparisons. The gores and conics were developed from projections of radial lines onto flat sheets tangent to the contour along their centerlines.

The basic blanket has structural face sheets (Schjeldahl X-850) with Superfloc as core sheets. Since the face sheets are more rigid than the Superfloc, the face-sheet material was used for configuration evaluation. Single sheets representing 20-, 30-, and 40-deg gore sections were mocked-up. The selected 30-deg gore configuration, shown in

Figure 33 [21], used 22 Superfloc core sheets sandwiched between two sheets of Schjeldahl X-850. The face sheets were crinkled and heat-formed to the required contour.

The blankets were laid up on contoured tooling forms. A preformed face sheet was applied first, followed by the 22 sheets of Superfloc, which were individually mounted and cut to oversize. Finally, the second preformed face sheet was added. Matching tooling was used to trim the blanket edges to a radial line and to locate all holes that required matched and coordinated hole patterns. After the blankets were trimmed and all holes were located, grommets were installed. The grommets were coated with adhesive, frozen, and then pressed into the blankets with a twisting motion. The attachment system includes reinforcement tabs [0.038-cm (0.015-in.) lexan deltas] for the face sheets, grommets, and twin pins. Tests have shown [17] that there is virtually no joint separation with a load of 13.6 kg (30 lb) per pin. Joint failure occurred at a loading of 23.0 kg (50.7 lb) per pin at room temperature and at 33.1 kg (73.3 lb) per pin at LN_2 temperature.

Fiberglass support pins were used to attach the blankets to the tank. The support system design was intended to minimize the number of pins required. This system had one fixed pin at each end of each gore blanket and a separate pin in the center of each gore, located just under the midfairing area. This center pin relieves approximately one-half the g-loading from the forward pin. However, its primary purpose is to absorb the weight of the lower half of the gore which would otherwise tend to compress the forward gore section and increase its density.

The weight of a gore blanket less pins is approximately 0.43 kg (0.95 lb). This load is transferred directly to the three support pins in each blanket. The insulation mounting arrangement and structural joint are shown schematically in Figure 34. The lexan delta on the blankets, during pump-down pressure load, is reacted by the pins. Assuming a maximum evacuation pressure differential of 6.89×10 N/m^2 (0.01 psi) across the Superfloc blanket for a Saturn V launch trajectory, it was found that the maximum pin load was 2.17 kg (4.8 lb). This value was obtained from a calculation performed for a grommet spacing of 21.6 cm (8.5 in.) in the midfairing area. The top blanket requires 30 pins and the inner blanket requires 18 pins.

The aft fairing cap has two cover blankets that were cut circular and trimmed to form a butt joint with the gore blankets. A fiberglass ring was used on top of the outer blanket to hold the edge firmly in place along the joint. Support pins, bonded to the aft conic fairing, pass through the grommets in the blankets and fix the ring in place.

The forward cap insulation blankets interface with the gore blankets, fill-and-drain-line insulation, and the thermocouple wiring insulation. They can be removed to obtain access to the tank door. The cap is made up of four blanket sections using left- and right-hand parts.

Thermal Testing

Thermal testing of the insulated 2.21-m (87-in.) tankage system was performed at the

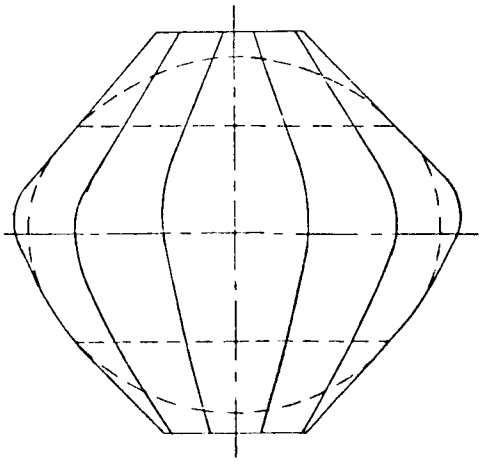

Figure 33. 2.21-m (87-in.) tank insulation, configuration III.

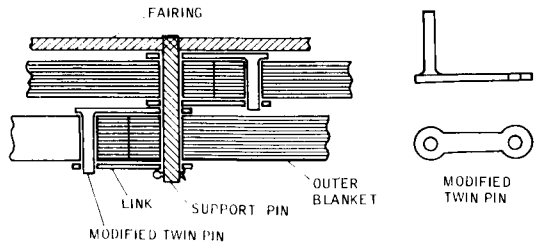

Figure 34. Insulation mounting arrangement and structural joint.

General Dynamics/Convair Sycamore Canyon Hydrogen Test Facility. The tank was mounted in an aluminum enclosure and placed in a 3.66 m (12 ft) diameter, double-walled space vacuum chamber. Two Kinney mechanical pumps and an 81.4-cm (32-in.) diameter oil diffusion pump provided the required pressure environment. The vacuum chamber was maintained at a constant temperature by circulating water between the two walls. The tank and insulation system were fully instrumented internally and externally. A total of 46 platinum temperature sensors, 40 carbon resistor liquid level sensors, and 7 strain gage pressure transducers were located within the tank. Externally, 60 Chromel-Constantan thermocouples measured tank, insulation, penetration, and enclosure temperatures. Boiloff gas flow rates were monitored by a Thermo-Systems hot film anemometer mass flowmeter and a Flow Technology turbine volume flowmeter.

The conditions that existed for each test were input into the computer program. Table 8 is a summary of the tank and insulation system parameters and presents the predicted and actual thermal performance of the total system.

MLI SYSTEM TEST FACILITIES

Thermal performance data for different MLI composites are obtained empirically using two principal methods of testing. The first method involves testing a small quantity of MLI material under rigidly controlled circumstances using a flat plate or cylindrical calorimeter. The second method involves applying an MLI system on a subscale cryogen tank and determining the performance of the applied system as discussed previously.

Pressure Control

Small differences in boiloff rates from these tanks cannot be detected unless the test tank ullage pressure is carefully and accurately controlled. A National Bureau of Standards (NBS) Barostat is used to control ullage pressure in MSFC test tanks. The NBS barostat was used during the neck tube penetration studies discussed in Penetration Thermal Effects. The pressure-time history of that test is shown in Figure 35. Information related to the design and operation of the NBS barostat has been documented in Reference 22. The barostat designed and used at the National Bureau of Standards is shown in cross section in Figure 36. Plates B and H are fixed in relative positions by four rods. Plates F and G are free to move between limit stops. Bellows E is sealed gas-tight to plates F and H and is evacuated. Bellows A is sealed by plates B and G and has three connections through plate B; one at P for an air intake, one at S for connection to a vacuum pump, and one at T that connects into the system to be controlled. The pressure control valve consists of a ball V attached to spring L. Spring-controlled plunger D operates the valve. The ball seats into a conical opening. The plates F and G are connected to a scale pan on which weights M can be placed.

In operation, weights that correspond to a pressure that is approximately the value desired are placed in the pan. If chamber A is originally at atmospheric pressure, the plates F and G remain against the upper stop and the valve KV is consequently wide open. With air entering tube P and being evacuated through tube S, the pressure in bellows A falls until the pressure therein balances the weights. At this pressure, the valve KV closes sufficiently so that the air flowing in through P equals that flowing out through S. Any deviation in flow changes the upward force on FG and either opens or closes valve KV, which changes the air flow through S until the pressure in A again balances the weights.

The performance of the barostat is dependent upon the flow of air into bellows A through P; for optimum pressure control, this airflow is about 1.66×10^{-5} m^3/sec (1 liter/min) secured by valve N and a suitable rotameter in line P, which is not shown in Figure 36. The bellows are copper-plated brass and are about 14.6 cm (5.75 in.) in diameter. The weight required to balance at 1 atm is nominally 149.5 kg (330 lb). The barostat controls the pressure to within 1.33 N/m^2 (0.01 mm of mercury) during the time needed to make readings, which is about 10 min. The barostat fails as an absolute pressure gage by a few tenths of a millimeter of mecury; i.e., the pressure obtained at various times by a given weight does not repeat by this amount. Perfection of the barostat in this respect has not been undertaken.

Calorimeter Test Facilities

Most thermal conductivity data obtained for MLI composites have been generated by flat plate calorimeters such as the A. D. Little Corporation Model 12 calorimeter shown in Figure 37. In an

TABLE 8. 2.21-m (87-in.) TANK PROGRAM SUMMARY

Tank System Parameters

Major Diameter: 2.67 m (87.6 in.)
Minor Diameter: 2.27 m (74.5 in.)
Tank Volume: 40.5 m^3 (175 ft^3)
Tank Surface Area: 1.41 m^2 (152 ft^2)
Fairing Area: 1.58 m^2 (170 ft^2)
Cryogen: LH_2
Penetrations Thermally Guarded

Insulation System Parameters

Insulation System: Superfloc
Nominal Thickness: 3.81 cm (1.5 in.)
System Density: ~20.5 kg/m^3 (~1.27 lb/ft^3)
Average Area: 1.63 m^2 (175 ft^2)
Configuration: Twelve 30-deg gores
Number of Blankets: 2
Seam Length
Blanket 1: 38.7 m (127 ft)
Blanket 2: 40.0 m (131 ft)
Number of Support Pins: 49
Number of Support Pin Grommets: 98
Number of Seam Pins with Grommets: 536
Number of Purge Pins: 39

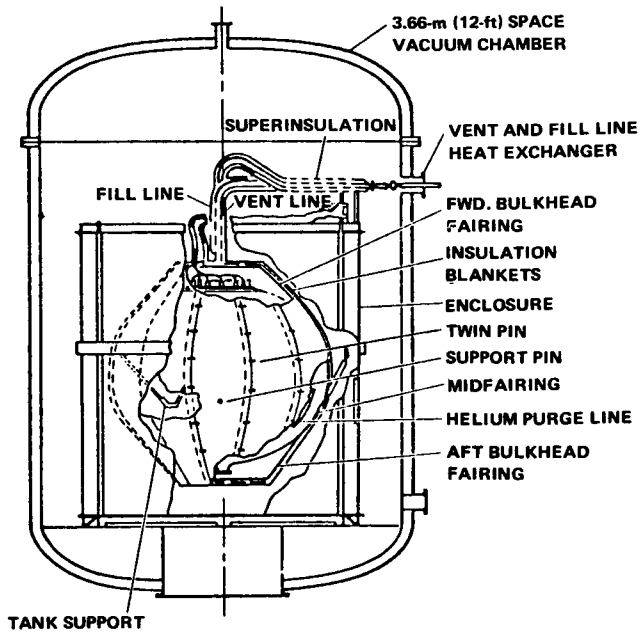

Predicted and Actual Thermal Performance

	Space Environment			Ground Hold	
	Thermal Analysis	Test 1	Test 2	Test 1	Test 2
Cryogen	LH_2	LH_2	LH_2	LH_2	LH_2
Chamber Pressure, N/m^2 (torr)	1.33×10^4 (1×10^6)	4.0×10^3 (3×10^{-5})	4.0×10^4 (3×10^{-6})	95.5×10^3 (29.55 in. Hg)	95.4×10^3 (29.5 in. Hg)
Tank Ullage Pressure, N/m^2 (psia)	10.1×10^4 (14.7)	10.31×10^4 (15.0 ±0.01)	10.2×10^4 (14.875 ±0.005)	9.98×10^4 (14.5 avg.)	9.98×10^4 (14.5 avg.)
Tank Percent Ullage	0	4	53	12	12
Sink Temperature, °K (°R)	22.3 (40)	20.6 (37)	20.6 (37)	20.6 (37)	20.6 (37)
Source Temperature, °K (°R)	299 (535	293 (525)	283 (508)	202 (363)	247 (440)
Heat Flux, Q', W/m^2 (Btu/hr ft^2)	0.816 (0.26)	0.850 (0.27)	0.911 (0.29)	303 (97)	308 (108)
Insulation, percent	34	30	28	—	—
Seams, percent	21	21	19	—	—
Pins, percent	41	39	35	—	—
Support Struts, percent	2	2	2	—	—
Line Penetrations, percent	2	8	16 (no guard)	—	—
Heat Flow Rate, Q_T, W/m^2 (Btu/hr)	13.4 (45.8)	13.9 (47.5)	15.1 (51.4)	4950 (17 000)	5560 (19 000)
Mass flow Rate, $\dot{m}$, kg/sec (lb/hr)	0.303×10^{-4} (0.24)	0.315×10^{-4} (0.25)	0.34×10^{-4} (0.27)	111×10^{-4} (88.5)	124×10^{-4} (99)

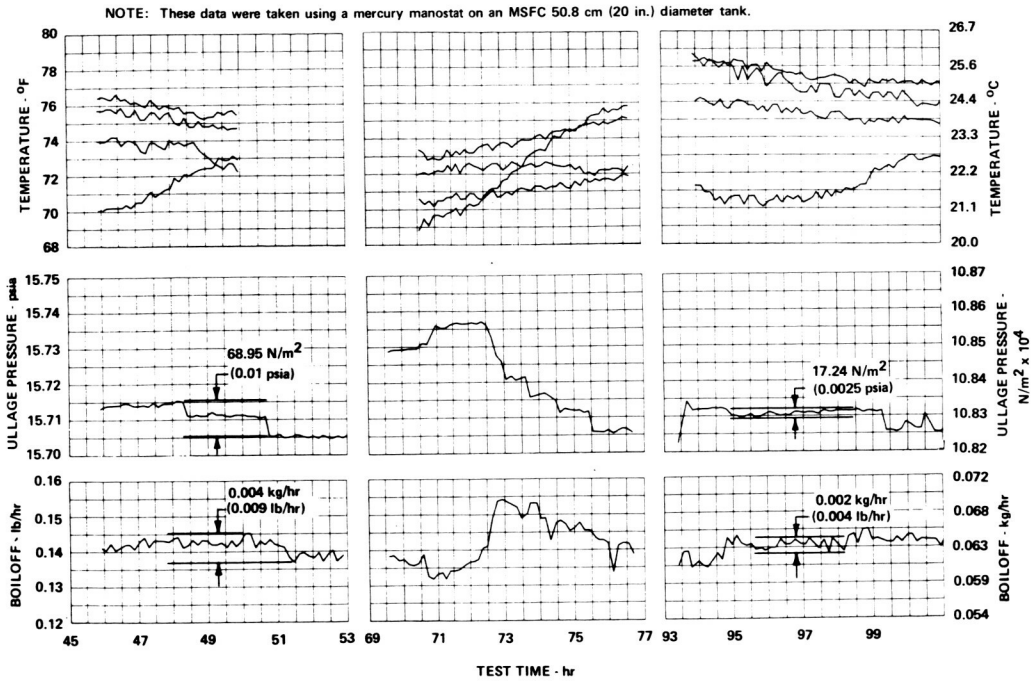

Figure 35. Pressure-time history of neck tube penetration test.

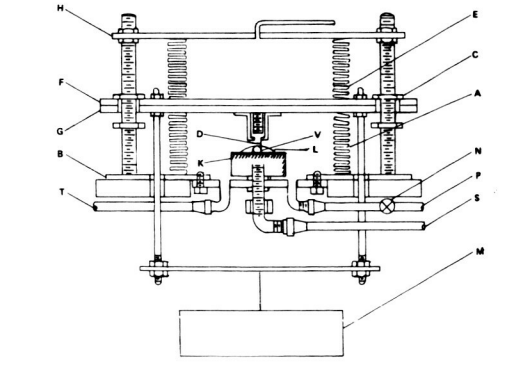

LEGEND

E – EVACUATED BELLOWS
A – BELLOWS MAINTAINED AT DESIRED PRESSURE
H AND B – FIXED MOUNTING PLATES
F AND G – FLOATING MOUNTING PLATES
M – WEIGHTS ATTACHED TO F AND G
D – SPRING CONTROLLED PLUNGER
V – BALL VALVE ATTACHED TO SPRING L
K – VALVE SEAT
P – PRESSURE LINE
S – SUCTION OR VACUUM LINE
N – A VALVE
T – LINE TO SYSTEM THE PRESSURE OF WHICH IS CONTROLLED BY THE BAROSTAT

Figure 36. NBS barostat.

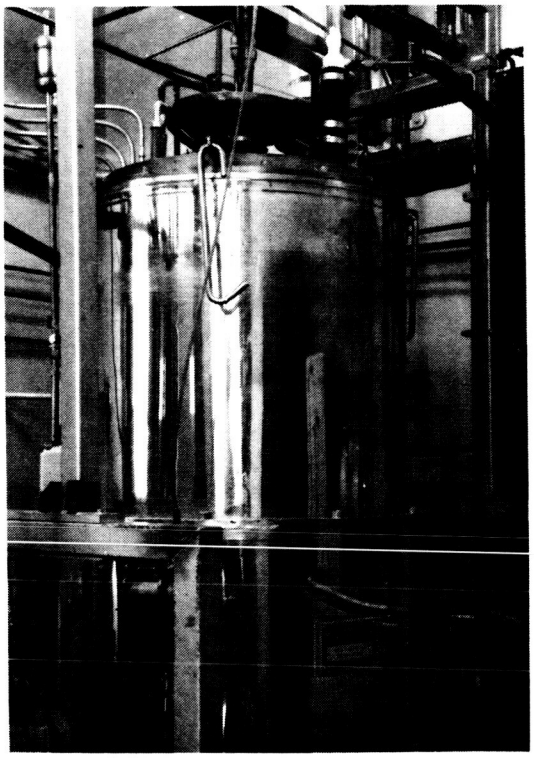

Figure 37. ADL-12 flat plate calorimeter.

actual test, the test specimen of MLI is placed between two flat plates; one of the plates is maintained at a cryogen temperature and the other is maintained at some elevated temperature, which is usually room temperature. The heat flux is measured by monitoring the cryogen boiloff rate. Since the area and thickness of the specimen are known, the effective conductivity for these temperature extremes can be determined.

Another type of MLI calorimeter was developed in 1967 by Lockheed-Huntsville. This is the electrical calorimeter shown in Figure 38. The operating principle of this calorimeter is described by the one-dimensional radial heat conduction equation. A specimen of insulation is wrapped circumferentially around a cylindrical heater that is maintained automatically at any desired temperature from cryogenic temperatures to 394°K (250° F). The outside surface of the MLI specimen is maintained at a slightly lower temperature, and the heat flux through the insulation is determined from the heater power input. This calorimeter has three desirable characteristics; it can be used to obtain temperature dependent conductivity data, it is inexpensive to construct, and it is very accurate [23]. Both types of calorimeters must be enclosed in vacuum chambers capable of simulating orbital pressures, and both are valuable to MLI technology.

Tank Test Facilities

The tank tests that have been conducted at MSFC were described previously. These tanks range in size from 50.8 cm (20 in.) to 2.67 m (105 in.) diameters and require large vacuum chamber facilities. In Figure 39 the NASA/MSFC 4.58-m (15-ft) vacuum chamber is shown schematically. The curve shown in this figure presents a nominal pressure history during evacuation. Figure 40 is a photograph of the MSFC 6.1-m (20-ft) vacuum chamber facility. A pressure history for a nominal pumpdown is also presented for this chamber.

CONCLUSIONS

Several conclusions can be drawn from the results of MSFC and contractor efforts in MLI

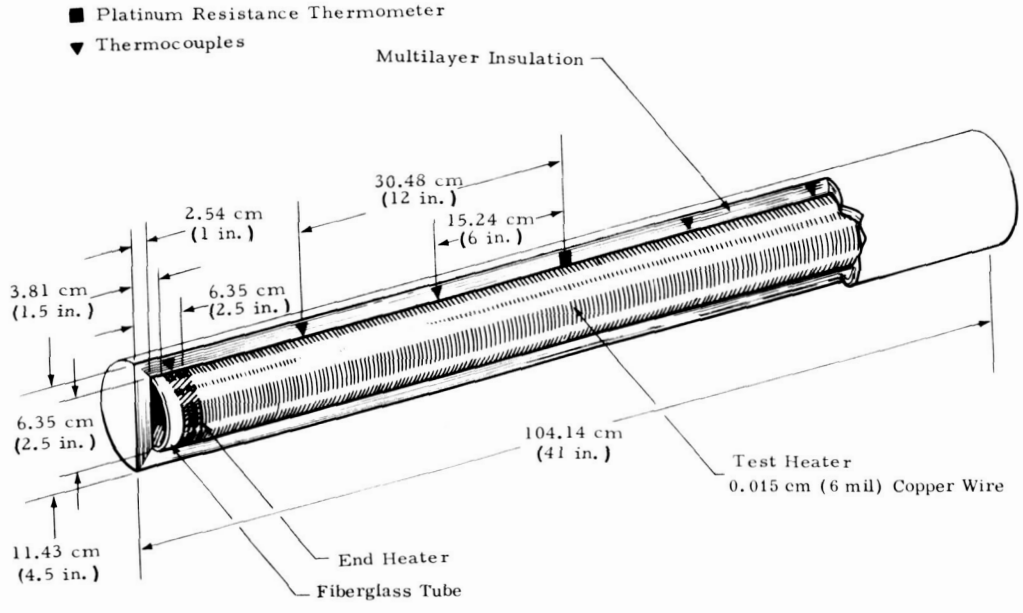

Figure 38. Lockheed-Huntsville automated electrical cylindrical calorimeter.

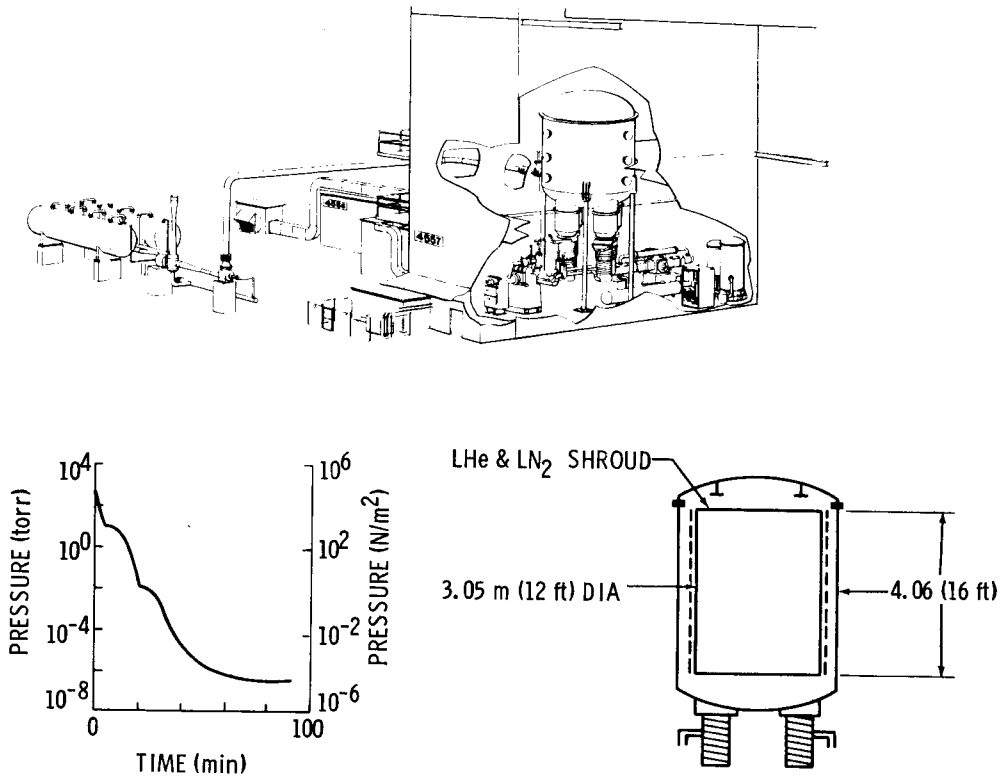

Figure 39. MSFC 4.58-m (15-ft) vacuum chamber.

technology development. They are presented under the appropriate headings below.

MLI System Performance

Two physical properties of an MLI system determine its performance in an insulation system; thermal conductivity and bulk density. These two properties have been found to be functions of the following variables:

1. Calorimetry has shown thermal conductivity to be a strong function of temperature for all MLI systems. Data have been generated for several systems showing this dependency.

2. Calorimeter and compression tests have shown, respectively, that thermal conductivity is a function of layer density and layer density is a function of mechanical compression. The dependencies have been measured for several MLI's. Careful consideration must be given to the compression inherent in several MLI attachment techniques.

3. Interstitial gas pressure has been shown to thermally degrade MLI performance; many studies have been conducted to define and resolve this problem.

4. Actual techniques have been developed for attaching MLI blankets to the curved sidewalls of different size tanks. Degradation factors associated with certain wrapping techniques have been empirically determined for certain MLI's on certain tanks.

5. New and improved MLI materials have resulted from the efforts expended. As shown in Figure 41, continued effort has resulted in a continued decrease in weight and thermal conductivity.

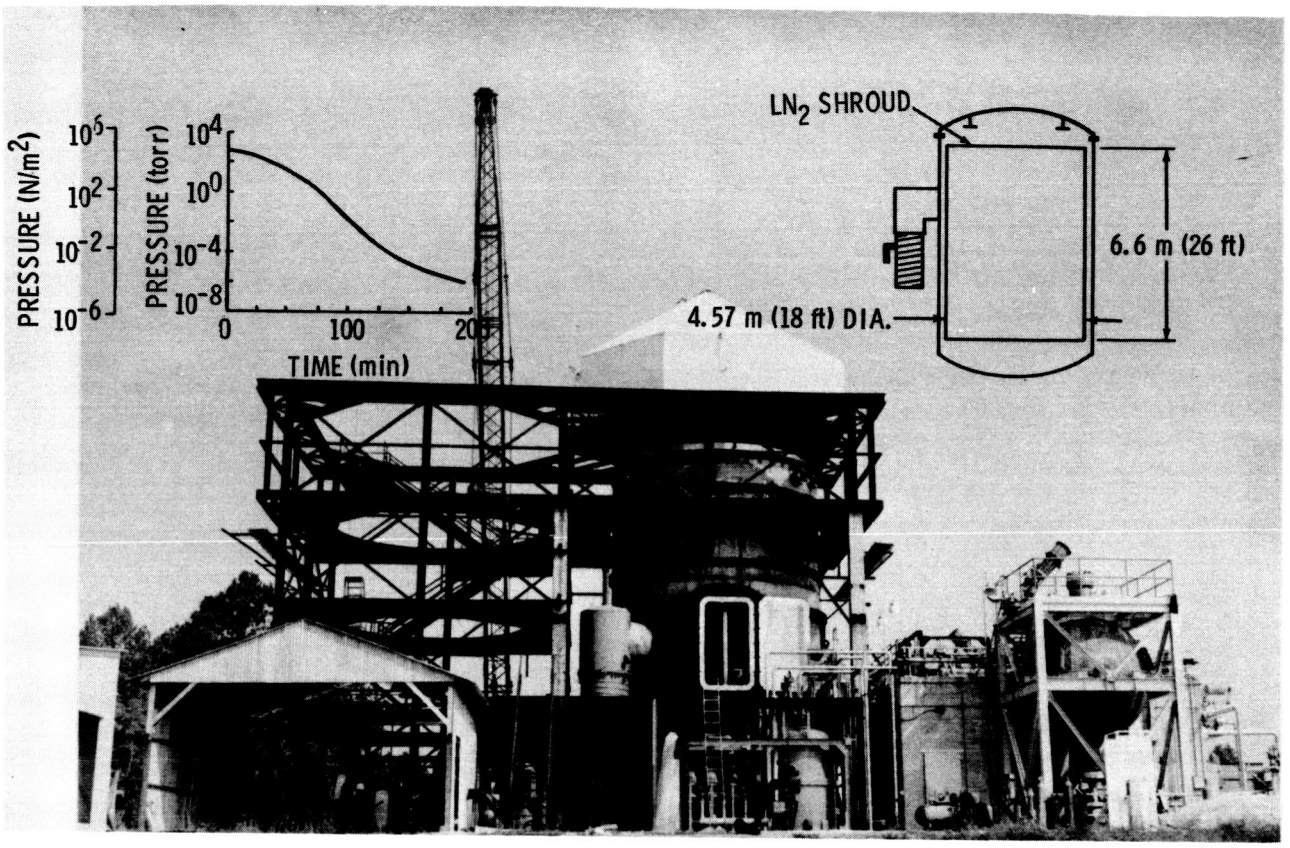

Figure 40. 6.1-m (20-ft) vacuum chamber.

Penetrations

It has been shown empirically and analytically that penetrations through the MLI blanket substantially degrade the performance of an MLI thermal protection system. Prediction of penetration heat leaks is therefore essential in designing effective insulation systems. Solid penetrations can be handled adequately with current techniques. However, hollow pipe penetrations represent an immediate obstacle to further insulation system development because of the complexity of the heat transfer mechanisms involved. The problem has been defined and methods of solution have been developed. Some data have been generated for penetration thermal performance as a function of thermal and physical variables. Such parametric data are required for optimum design of hollow pipe penetrations through the MLI blankets. Some empirical data have been obtained to verify the analytical results.

MLI Systems Development

Numerous cryogenic tank tests have been conducted to verify the performance of the total thermal protection system under simulated flight conditions. Important data have been acquired from these tests, and the MLI insulation systems have shown marked improvement with continuing effort. Numerous test facilities and equipment are now available for measuring ideal and applied values of thermal conductivity.

To obtain an indication of the progress made in MLI development, a thermal comparison of the Superfloc MLI performance to five other MLI test tank programs has been made (Fig. 41). The assumptions and inadequacies of the analytical adjustment were discussed previously. The purpose of the comparison is to demonstrate progress rather than to detail MLI system advantages.

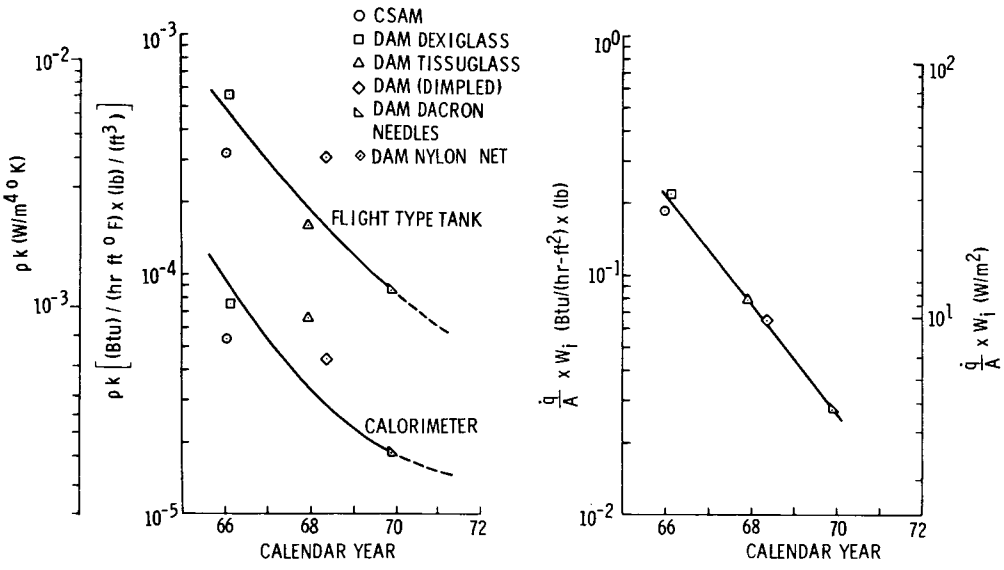

Figure 41. MLI thermal performance history.

Two basic performance indices are frequently used to express the efficiency of an MLI system. One index is the bulk density-apparent thermal conductivity product. The other is the heat flux-unit weight product (Qi × Wi). The thermal conductivity and density of an MLI system are both dependent on the MLI estimated installed thickness. The heat flux and unit weight, however, are dependent on the calculation of the tank surface area and the number of layers applied to the test tank. The surface area of a tank and the number of layers in an MLI composite can be determined more accurately than the thickness of an installed MLI composite. For this reason, the curve of the heat flux-unit weight product for different MLI systems contains less scatter than the thermal conductivity-density product curve.

However, the data used to plot these curves were originally obtained at different boundary temperatures. Thermal conductivity equations, described earlier, were used to adjust all thermal performance data to a common set of boundary temperatures 286°K (515°R) and 22°K (40°R). Obtaining the adjusted heat fluxes for each MLI composite required the use of a layer density value, or estimated thickness. The use of an MLI thickness value in each MLI system caused an error in both the adjusted thermal conductivity and the heat flux. The density calculation is thickness dependent but the unit weight is computed independent of thickness. The analytical adjustment does not account for thermal degradation caused by seams, gaps, and fasteners.

To further understand the progress in MLI efforts, a plot of expected mission times for different diameter tanks as a function of heat flux is presented in Figure 42. Each tank is assumed to be 95 percent filled with liquid hydrogen saturated at 1.03×10^5 N/m^2 (15 psia). The stored liquid remains at a constant temperature. The mission times for each tank diameter were computed as the time required to boiloff 5 percent of the initial LH_2 mass. For the same heat flux values, large diameter tanks have a much longer mission time capability than smaller diameter tanks. As the tank diameter increases, the area-to-volume ratio and consequently the heat rate per unit volume decrease. Therefore, from a thermal standpoint, propellants should always be stored in a container having the highest volume-to-surface-area ratio possible.

Although the analytical adjustments are not explicitly correct, they do permit a reasonable assessment of MLI thermal progress. As shown in Figure 41, applied MLI heat flux has been reduced about 800 percent for approximately the same MLI

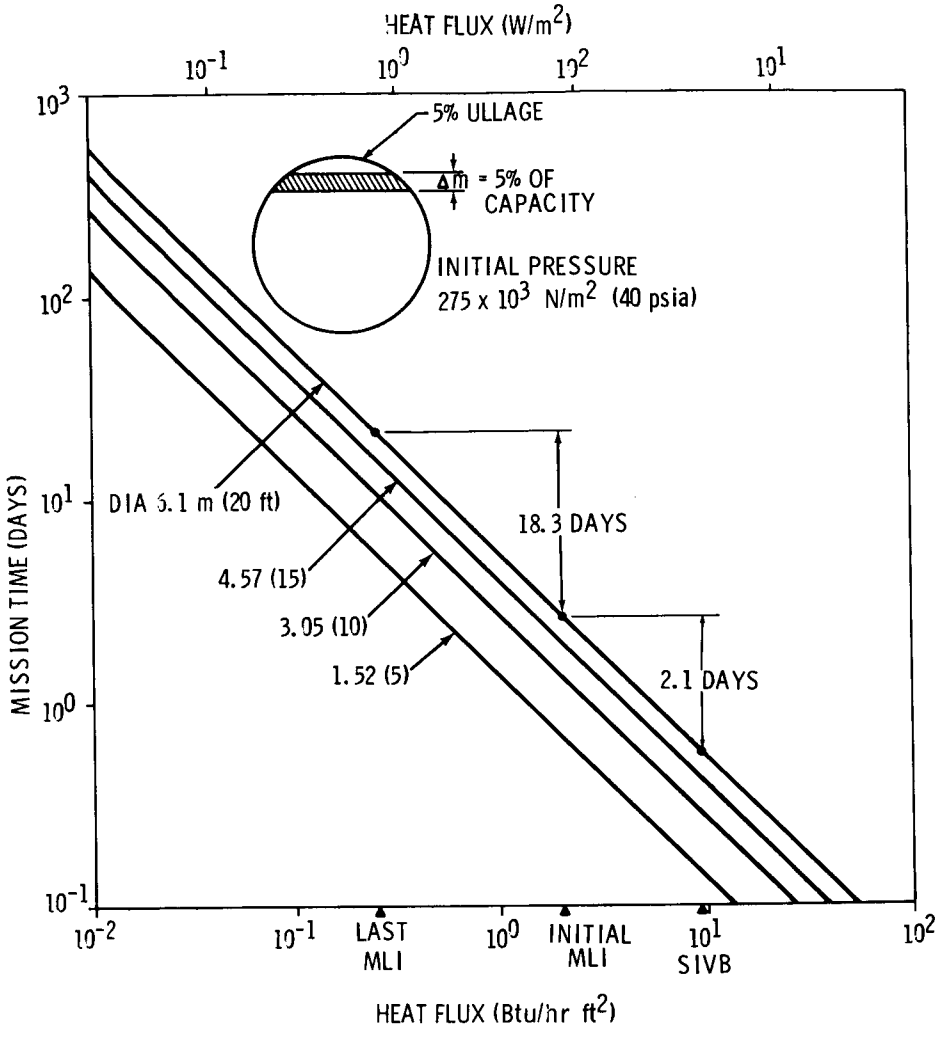

Figure 42. Thermal progress.

weight and boundary temperatures. However, a comparison of the Superfloc heat flux-unit weight factor with ideal thermal performance values shows a degradation of more than 300 percent. This implies that even better performance can be achieved from the same number of layers by reducing heat leaks through gaps, seams, and fasteners, and by reducing the weights of the various components.

FUTURE WORK

In earlier experiments MLI has been applied to cryogenic tanks and tested for one fundamental purpose: to demonstrate that multilayer insulation could withstand typical flight loads and that reasonable thermal performance could be achieved for short missions. The past discussion has verified that this

objective has been achieved. However, with long term missions becoming increasingly more important and inert vehicle weights more critical, a need exists to define the basic factors that influence MLI thermal performance more thoroughly. To achieve this new objective, MSFC has built three tank-type calorimeters. These tanks are 2.67 m (105 in.) in diameter. None of the tanks has a conventional structural support system. Instead, each tank is suspended by a concentric fill-and-drain line that acts as the structural support. Therefore, only one line penetrates the MLI applied to the test tank. As a result, MLI systems can be tested and the applied thermal performance can be evaluated without the combined effects of multiple extraneous heat leaks. Only one analytical adjustment to the test data is required; i.e., adjustment of the heat flow through the tube to the tank. A comparison of the applied thermal performance data with calorimeter data will establish the degradation factor for each MLI tested. Knowing this factor accurately will eliminate the requirement for unnecessary safety factors that add extra layers (weight) to an insulation system. However, this is only one part of the solution to defining overall thermal performance.

Once the basic MLI thermal performance has been established, the thermal effects of penetrations can be determined by measuring the increase in the boiloff rate compared with the boiloff from the clean tank test. Correlation of these results with analytical predictions will permit a better thermal evaluation. In the past, the temperature gradient along the penetration was used to correlate the test data with analytical predictions. With the new test tank calorimeter concept, the temperature gradient and the change in boiloff rate can be used to correlate with the analytical predictions. If necessary, the thermal math models can be adjusted to better represent the true thermal performance.

Other areas requiring continued efforts are outlined in the following.

MLI Performance

More data are needed for k and ρk as functions of temperature and layer density (or compression). These data should be generated for all competitive MLI systems over the full useful ranges of temperature and layer density. The results of this continuing development are shown in Figure 41 for the last several years. Future efforts could result in the dashed line extrapolation.

Efforts must be continued in solving the problem of interstitial gas pressure thermal degradation, especially during the ground-hold period of a mission.

The development of optimum application techniques for MLI blankets must be continued and data must be generated to accurately predict the degradation factors encountered for such techniques.

Penetrations

Hollow pipe penetrations require computer thermal analysis to accurately predict their performance because of the complex heat transfer mechanisms involved. Parametric data must be generated for the pipe penetration heat leaks associated with various thermal and physical variables. Testing will be required to verify the analytical results.

MLI Systems Performance

In addition to MLI calorimeter and penetration data, subscale cryogen tank test data are also needed to verify the performance of the total thermal protection system under simulated flight conditions. Tank tests must continued in the future to extend the performance improvements achieved in the past. Only such tests can demonstrate the flightworthiness of an MLI thermal protection system. Comparisons of separate tests of complete MLI systems on cryogenic tanks cannot be performed until guidelines and criteria are established for such tests.

APPENDIX
ASTRONAUTICS LABORATORY, TEST DIVISION CRYOGENIC FACILITIES

Introduction

The first cryogenic facilities at MSFC were constructed in the 1950's. Gradually these facilities were expanded, and today they comprise a combined lox storage capacity of 3187 m^3 (842 000 gal), a combined liquid hydrogen storage capacity of 1249 m^3 (330 000 gal) and a liquid nitrogen storage capacity of 530 m^3 (140 000 gal).

The existing cryogenic facility run tanks, which are only used during component, engine, or stage firings and which represent a variety of differently insulated and uninsulated tanks, are not included in the above capacities. The high pressure gas storage facilities at MSFC, which supply pressurants in the operation of cryogenics, include facilities for storage of 433.3 m^3 (15 300 ft^3) of gaseous hydrogen, 390.8 m^3 (13 800 ft^3) of gaseous nitrogen, and 164.3 m^3 (5800 ft^3) of gaseous helium. With the expansion of the cryogenic facilities, a wealth of experience and knowledge was and is being gathered in cryogenic instrumentation, handling, storage, transportation, cleanliness requirements, reliquefication, materials compatibility, etc. The facilities described in the following represent only a small portion of MSFC's facilities, but they represent the existing and planned unique facilities for cryogenic research.

Cryogenic Slosh Test Facilities (Fig. A-1)

The lox slosh facility has the equipment necessary to provide slosh motions within a 3.35 m (11 ft) diameter, 87.1-m^3 (23 000-gal) tank to study pressurization during draining cycles. The facility provides the capability to perform studies of tank pressurization, propellant geysering, lox stratification, sloshing, and tanking phenomena. The tank is equipped with viewing ports for still, motion picture, and television cameras to supplement the normal instrumentation system. The slosh tank can be oscillated at a frequency range of 0.0 to 0.7 Hz and has a maximum displacement of 20.3 cm (8 in.) (peak-to-peak) by use of a hydraulic drive mechanism. The facility is instrumented to give pressures, liquid levels, temperature, and flows in the pressurization and drain line systems.

The liquid hydrogen slosh facility provides the capability to perform research and development tests in the areas of tank pressurization, stratification, sloshing, tanking phenomena, and recirculation. The tank is an S-IV Battleship with a 121.1-m^3 (32 000-gal) liquid hydrogen vessel separated from the 35.9-m^3 (9500-gal) lox vessel by a common bulkhead. This facility utilizes the same drive mechanism and gas generator-heat exchanger system as does the lox slosh facility. It is instrumented to give pressures, liquid levels, temperatures, and flows similar to the lox slosh facility.

Low-Gravity Test Facility

This facility (Fig. A-2) is located in an east bay of the Saturn V Dynamic Test Stand. This facility has 90.2 m (296 ft) free-fall height providing 4.3 sec free-fall duration. The maximum drag shield drop weight is 1814 kg (4000 lb) and it is designed for a 25-g deceleration. The drag shield is capable of accepting test packages with a maximum envelope size of 0.91 m (3 ft) in diameter by 1.22 m (4 ft) in height and with a weight of 181.4 kg (400 lb). The facility is capable of achieving test environments ranging from 2.5×10^{-2} g to 1×10^{-5} g. The facility is primarily used in low-gravity fluid mechanics and thermodynamics phenomena studies, calibration of accelerometers, studies of subjecting flight instrumentation to low-gravity conditions, and exploratory studies for zero-g manufacturing.

Hydrogen Slush and Flowmeter Calibration Facility

This facility (Fig. A-3), which is presently being activated, consists of the following hardware: a 11.36-m^3 (3000-gal) liquid hydrogen weight tank and slush hydrogen generator, a 0.40-m^3 (14-ft^3) 241.3×10^5 N/m^2 (3500-psig) cold helium vessel, a 106-m^3 (28 000-gal) liquid hydrogen storage tank, an 87.1 m^3 (23 000-gal) slush hydrogen storage tank, and a 283.2-m^3/min (10 000-ft^3/min) vacuum pumping unit and an associated heat exchanger. The

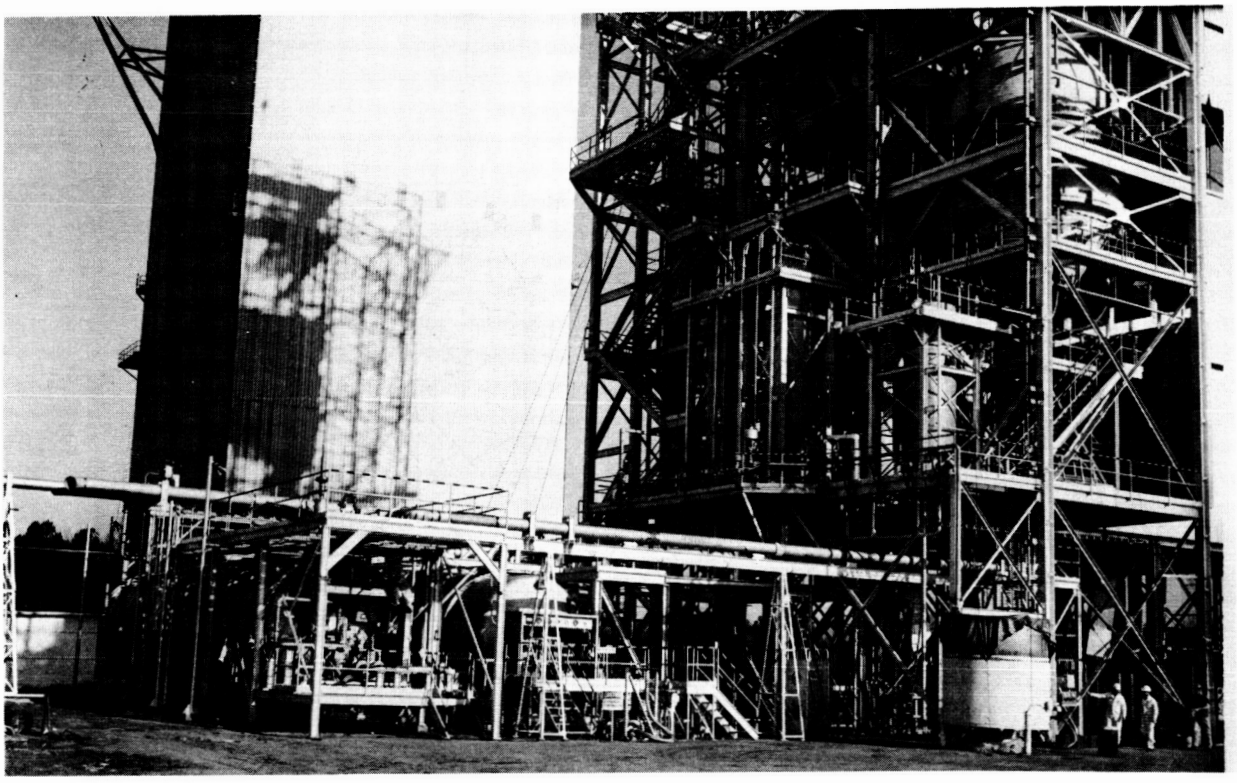

Figure A-1. Cryogenic slosh test facilities.

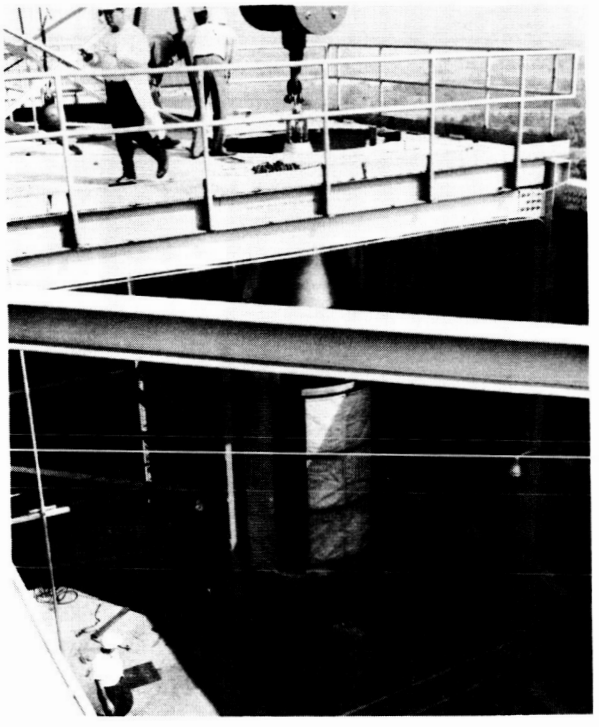

Figure A-2. Low-gravity test facility.

facility will have the capability to calibrate liquid hydrogen flowmeters up to 10.2 cm (4 in.) in size with flow rates of 11.36 m^3/min (3000 gal/min) and will comply with National Bureau of Standards primary standards for flowmeter calibrations. The capability for manufacturing and storing 87.1 m^3 (23 000 gal) of slush hydrogen is planned. The slush manufacturing rate will be approximately 1.89 m^3/hr (500 gal/hr). There are 150 channels of instrumentation available at the facility.

Test Position 302 Vacuum Chamber

This vacuum facility (Fig. A-4) consists of a 6.25 m (20.5 ft) diameter by 10.97 m (36 ft) high 304 stainless steel chamber with associated vacuum pumping equipment, thermal shroud, and liquid hydrogen system. The chamber is dome-loaded with the test item suspended from the dome. A personnel access door is provided on the side of the chamber for final systems checkout prior to chamber evacuation. The interior working area of the chamber is 5.49 m (18 ft) in diameter, and there is 8.08 m (26.5 ft) between upper and lower cold walls.

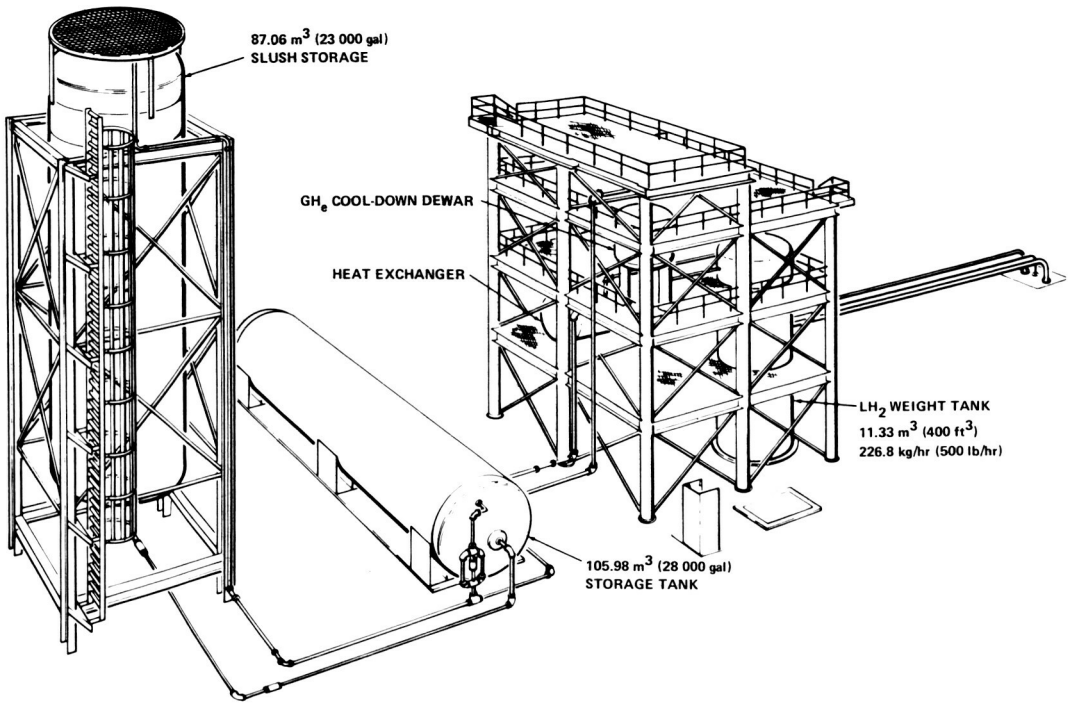

Figure A-3. Hydrogen slush and flowmeter calibration facility

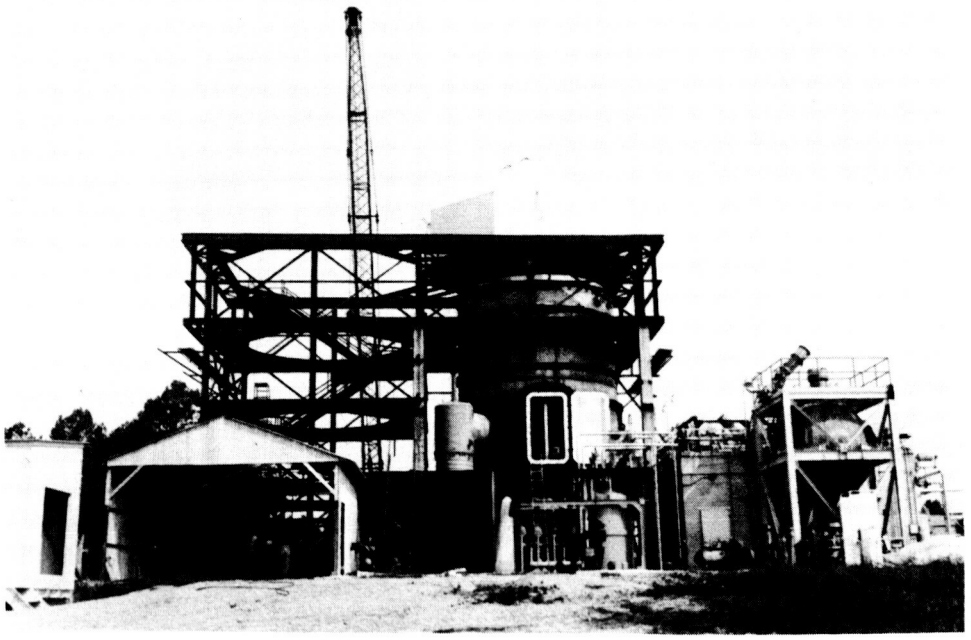

Figure A-4. Test position 302 vacuum chamber.

The vacuum pumping system consists of two 8.50-m^3/min (300-ft^3/min) roughing pumps, two 36.82-m^3/min (1300-ft^3/min) Roots blowers, and two 95-m^3/sec (95 000-liters/sec) oil diffusion pumps. A cold shroud within the chamber provides cryopumping capability and simulates a 77.59° K (-320° F) environment. The cold wall maximum thermal absorption rate is 300 kW.

The chamber is located in a hazardous test area, is designed to perform tests requiring liquid hydrogen, and has a clean, dry, empty ultimate vacuum capability of 133.32×10^{-6} N/m^2 (10^{-6} torr). There are 300 channels of instrumentation available to analyze the test item and support the facility operation.

4.57-m (15-ft) Thermal Vacuum Chamber Facility

The 4.57-m (15-ft) thermal vacuum facility (Fig. A-5) consists of a 4.57 m (15 ft) diameter by 6.10 m (20 ft) high 304 stainless steel chamber with associated vacuum pumping, thermal shroud, quartz lamp array, and liquid hydrogen systems. The chamber is made in two parts, the chamber proper and a flanged dome from which test items are attached.

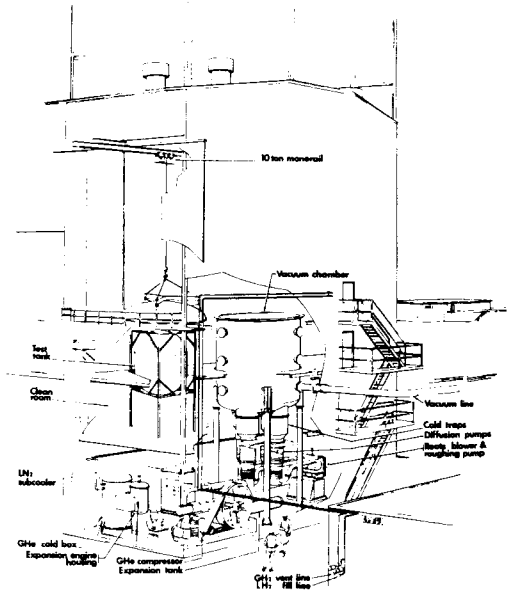

Figure A-5. 4.57-m (15-ft) thermal vacuum chamber facility.

The high vacuum pumping system consists of a 14.16-m^3/min (500-ft^3/min) roughing pump, a 141.60-m^3/min (5000-ft^3/min) roots blower, and four 50-m^3/sec (50 000-liters/sec) oil diffusion pumps.

A cold shroud within the chamber provides cryopumping capability and simulates a 77.59° K (-320° F) environment. The shroud is designed to provide a 20° K cryopumping surface and a 1-kW helium refrigerator system is installed; however, it has not been necessary to operate this system for the hazardous tests conducted to date. The cold wall maximum absorption rate is 30 kW. A normal vacuum chamber pressure of 66.66×10^{-6} N/m^2 (5.0×10^{-7} torr) is achieved with the liquid nitrogen shroud. With the thermal shroud installed inside the vacuum chamber, the interior working area is reduced to 3.66 m (12 ft) in diameter by 4.88 m (16 ft) in height. This facility is also a hazardous one, capable of handling liquid hydrogen and other cryogenic liquids. Approximately 300 channels of instrumentation are available for use with a Beckman 210 data acquisition computer. In addition, a rapid pumpdown system that consists of a two-stage steam ejector can be used to evacuate the chamber to the 1333.2-N/m^2 (10-torr) range to simulate launch vehicle pressure profile ascent rates.

Sunspot I Vacuum Chamber

The facility (Fig. A-6) is a 3.66 m (12 ft) by 5.49 m (18 ft) thermal vacuum chamber for space simulation. The work space inside the cryogenic shroud is 3.20 m (10.5 ft) in diameter by 3.81 m (12.5 ft) high and the ultimate pressure of the facility (clean, dry, and empty) is 9.33×10^{-7} N/m^2 (7×10^{-9} torr). This pressure can be achieved either with the 121.92-cm (48-in.) oil diffusion pump or with the ion/titanium pumping system.

The cryogenic system consists of the liquid nitrogen circulating and control system, the liquid nitrogen shroud, and the purge and warmup system. A 20° K cryopumping array is installed but not operational at this time because of the lack of a 1-kW helium refrigerator. A liquid nitrogen cooled baffle is a part of the diffusion-pumped vacuum system.

The shroud is divided into several control zones, each with an independent throttling control valve to efficiently control distribution of the coolant during periods of uneven distribution of thermal loads.

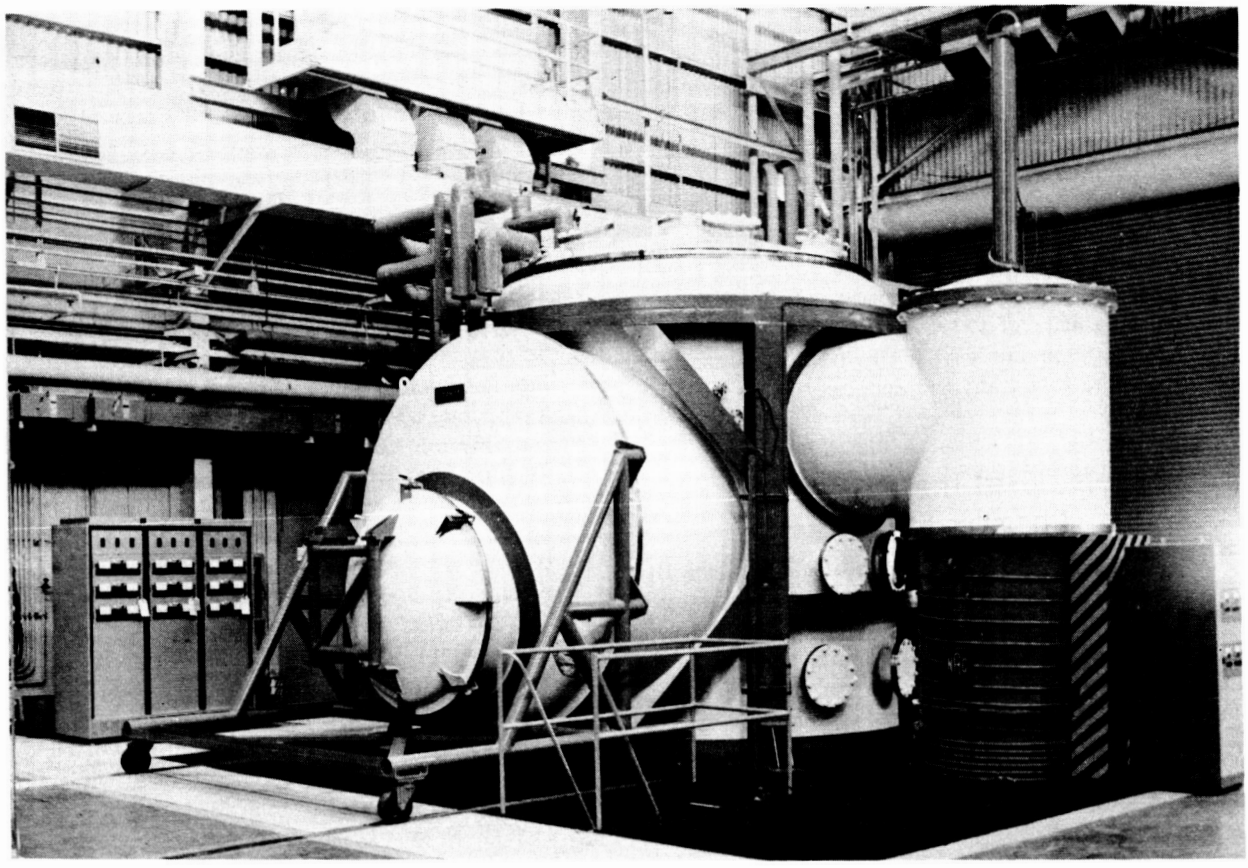

Figure A-6. Sunspot I vacuum chamber.

The shroud is capable of absorbing a load of 189 W/ft^2 on any surface and a total minimum load of 44. 3 kW while maintaining a maximum temperature at any point of 100°K. Additional system features include isolation valves for the cryogenic pump to facilitate pump removal for maintenance or repair. A vent line is provided for use during initial cooldown to prevent unnecessary losses resulting from flowing high temperature gases into the storage dewar.

Additional system features include an isolation valve between the chamber and the oil diffusion pump, viewing ports for either feed-through connections or visual observation of the test article, top or side loading, and a channel instrumentation system for evaluating test article performance.

REFERENCES

1. Gilstad, D. A.; Hyde, E. H.; et al.: Cryogenic Technology Research at MSFC, NASA TM X-53670, Vol. II, Report No. 7, 1967.

2. Subcritical Life Support Cryogen Storage Using High Performance Insulation. LMSC/HREC D 149499, Lockheed Missiles and Space Company, Huntsville, Alabama, February, 1970.

3. Investigations Regarding Development of a High Performance Insulation System. LMSC A994947, Lockheed Missiles and Space Company, Sunnyvale, Calif., Contract No. NAS8-20758, Final Report, December 31. 1969.

REFERENCES (Continued)

4. Frederickson, G. O.; Coes, M. C.; and Nowak, F. A.: Ranking and Selection of Insulation Systems for MNV Application. DAC-63264, McDonnell-Douglas Co., Huntington Beach, Calif., Contract NAS8-21400.

5. Hale, D. V.; and O'Neill, M. J.: Interim Report — Study of Thermal Conductivity Requirements — High Performance Insulation Compressibility Study. TM 54/20-232, LMSC/HREC D149187, Lockheed Missiles and Space Company, Huntsville, Alabama, November, 1969.

6. O'Neill, M. J.; and McDanal, A. J.: Study of Thermal Conductivity Requirements, Multi-Layer Insulation Data Manual. Final Report P225135-II V. 2, Lockheed Missiles and Space Company, Huntsville, Alabama, June, 1971.

7. Arnett, R. W.; et al.: Cryogenic Insulation Standards. MSFC Order No. H-79204A, NBS Project 2750457, Cryogenic Division, Institute for Basic Standards, National Bureau of Standards, Boulder, Colorado, February 15, 1971.

8. Hale, D. V.; and O'Neill, M. J.: Study of Thermal Conductivity Requirements — High Performance Insulation. LMSC/HREC D162128, Lockheed Missiles and Space Company, Huntsville, Alabama, Contract NAS8-21347, Final Report, February, 1970.

9. Hale, D. V.: Interim Report — Study of Thermal Conductivity Requirements, Vol. I, High Performance Insulation Thermal Conductivity Test Program. LMSC/HREC D148611-I, Lockheed Missiles and Space Company, Huntsville, Alabama, January, 1969.

10. Frederickson, G. O.; et al.: Investigation of High Performance Insulation Application Problems. MDC G0275, McDonnell-Douglas Astronautics Company — Western Division, Huntington Beach, California, Contract NAS8-21400, Fourth Quarterly Report, January, 1970.

11. Leonhard, K. E.; Betts, W. S.; Bennett, F. O.; and Tatro, R. E.: Cryogenic Tank Test Program. Convair Report GDC-ERR-1419, General Dynamics/Convair, San Diego, California, December, 1969.

12. Burge, G. W.: System Effects on Propellant Storability and Vehicle Performance. DAC-63061, AFRPL-TR-68-227, McDonnell-Douglas Company, Huntington Beach, California, December, 1968.

13. Guill, J. H.: LH_2 Storability in Space Propulsion Vehicles. Lockheed Demonstration Program LMSC-685104, Lockheed Missiles and Space Company, Sunnyvale, California, February 15, 1968.

14. Sterbentz, W. H.; and Baxter, J. W.: Thermal Protection System for a Cryogenic Spacecraft Propulsion Module. LMSC-A94993, NASA CR-54879, Lockheed Missiles and Space Company, Sunnyvale, California, November, 1966.

15. O'Neill, Mark J.: Study of Thermal Conductivity Requirements, Volume III, Analytical and Experimental Heat Transfer Study of a Venting Cryogen Tank. HREC-6189-3, LMSC/HREC D225135-III, Lockheed Missiles and Space Company, Huntsville, Alabama, Contract NAS8-26189, Final Report, June, 1971.

16. Getty, R. C.: Cryogenic Insulation Development. Convair Aerospace Division of General Dynamics, San Diego, California, Report No. GDC-DDB67-007, Contract NAS8-18021, Final Report (Phase I), January, 1968.

17. Cryogenic Insulation Development. Convair Aerospace Division of General Dynamics, San Diego, California, Report No. GDC-DDB69-002, Contract NAS8-18021, Final Report (Phase II), December, 1969.

REFERENCES (Concluded)

18. Leonhard, K. E.; and Ringwald, R. S.: Development of a Flight-Weight Cryogenic Storage System. Convair Aerospace Division of General Dynamics, San Diego, California, Report No. GDC-ERR-1332, December, 1968.

19. Leonhard, K. E.; et al.: Cryogenic Tank Test Program. Convair Aerospace Division of General Dynamics, San Diego, California, Report No. GDC-ERR-1419, December, 1969.

20. Sterbentz, N. H.; and Baxter, J. W.: Thermal Protection System for a Cryogenic Spacecraft Propulsion Module. Volume 2, NASA CR-54879, LMSC-A794993, Lockheed and Missiles and Space Company, Sunnyvale, California, Contract No. NAS3-4199, November 15, 1966.

21. Leonhard, K. E.; and Ringwald, R. S.: Development of a Flight-Weight Cryogenic Storage System. Eleventh Liquid Propulsion Symposium, Miami Beach, Florida, September, 1969.

22. Brambacher, W. G.; Johnson, D. P.; and Cross, J. L.: Mercury Barameters and Monometers. NBS Manograph 8, National Bureau of Standards, U. S. Government Printing Office, Washington, D. C., May 20, 1960.

23. Hale, D. V.; Sims, W. H.; and Lane, J. H.: A Study of Thermal Conductivity Requirements. Lockheed Missiles and Space Company, Huntsville, Alabama, Contract NAS8-21134, Final Report, October 13, 1967.

BIBLIOGRAPHY

Ficht, L. H.: GAC-4 High Performance Insulation Test. Technical Letter ASD-ASTN-6970, Work Order No. TM-10268-1, Brown Engineering Company, Huntsville, Alabama, June 4, 1970.

Hale, D. V.: Oral Presentation: LMSC/HREC High Performance Insulation Activities, A Study of Thermal Conductivity Requirements. Lockheed Missiles and Space Company, Huntsville, Alabama, Contract NAS 8-21347, June 1, 1969.

Hoover, C. D.: Multiple Docking Adapter Insulation Evacuation Test. Marshall Space Flight Center Memo R-P&VE-PE-67-15, from Robert R. Head to Mr. Wood, Huntsville, Alabama, January 23, 1968.

Lovin, J. K.: Multilayered Insulation Pipe Penetration Study. Technical Proposal, LMSC-D081602, Folder 1, Lockheed Missiles and Space Company, Huntsville, Alabama, February 5, 1971.

McCaleb, H. K.: Mylar and Nylon Net High Performance Insulation Test. Marshall Space Flight Center Memorandum S&E-ASTN-TMM-70-150, Huntsville, Alabama, December 16, 1970.

Multilayer insulation Pipe Penetration Study. Technical Proposal, Lockheed Missiles and Space Company, Huntsville, Alabama, LMSC/HREC D162819, February 5, 1971.

Reynolds, C. L.: Thermal Conductivity of B4A MLI. Technical Letter ASD-ASTN-10,070, Work Order CP-11, from C. L. Reynolds to R. J. Nunnelley, S&E-ASTN-MC, Marshall Space Flight Center, Huntsville, Alabama, December 1, 1970.

DESIGNS FOR ADVANCED INSULATION SYSTEMS

By

J. M. Walters

SUMMARY

This paper describes the design of the principal multilayer insulation (MLI) systems being investigated by Marshall Space Flight Center (MSFC) and its contractors for application to flight-type cryogenic tankage for long-term storage in space vehicles. The MLI systems were designed for application to a 2.67 m (105 in.) diameter cryogenic test tank to simulate full-scale design and installation methods representative of flight-type hardware.

The MLI systems selected for design represent systems suitable for use on space vehicles such as the modular nuclear vehicles that require application of thicknesses up to 15.24 cm (6 in.). The MLI systems are lightweight and structurally efficient.

INTRODUCTION

The design of tankage systems for long-term storage of cryogenic propellants presents the structural design engineer with many delicate but challenging engineering problems. The design of a lightweight insulation system utilizing ultrathin and unique materials is one of these problems. It is recognized that to achieve the utmost in thermal performance, the material, thermal, design, and manufacturing engineering work must be excellent. The research and development programs at MSFC have been directed toward this goal.

Since 1967 three principal types of MLI systems have been investigated:

1. Radiation shields with thin polyurethane spacers.

2. Radiation shields with tufts of dacron needles for spacers, Superfloc.[1]

3. Radiation shields with net spacers.

Each of these systems has been designed for Saturn V flight load environments and for application to the 2.67 m (105 in.) diameter cryogenic test tank shown in Figure 1. The MSFC programs under which these designs were developed are the major topics discussed in this paper.

MULTILAYER INSULATION SYSTEM WITH FOAM SPACERS

MLI systems with foam spacers have been under development by MSFC and Goodyear Aerospace Company (GAC) since 1964. The system was designated as GAC-4 panelized insulation and has the following principal design objectives:

1. The average sidewall equilibrium heat leak for 5.08-cm (2-in.) insulation should not exceed 1704.84 $J/m^2/hr$ (0.15 $Btu/ft^2/hr$).

2. The installed weight of the bumper wall and jacket should not exceed 40.05 kg/m^3 (2.5 lb/ft^3).

3. The system with bumper must prevent a 31.75 mm (0.125 in.) diameter aluminum pellet from penetrating the insulation system to the sidewall of the cryogenic tank at a velocity of 7620 to 9144 m/sec (25 000 to 30 000 ft/sec).

4. The MLI system, assembled in preformed panels, must be capable of being reliably applied to the external surface of large vehicles that are 10.06 m (33 ft) in diameter or larger.

The GAC-4 MLI was designed, fabricated, and installed on the 2.67-m (105-in.) cryogenic tank shown in Figure 1. The system utilized materials and fabrication techniques evolved during the earlier phases of the development program. To test the system, a two-phase program was initiated to demonstrate (1) the single-layer GAC-4 panel arrangement (Fig. 2) in a simulated ascent

1. General Dynamics/Convair trade name.

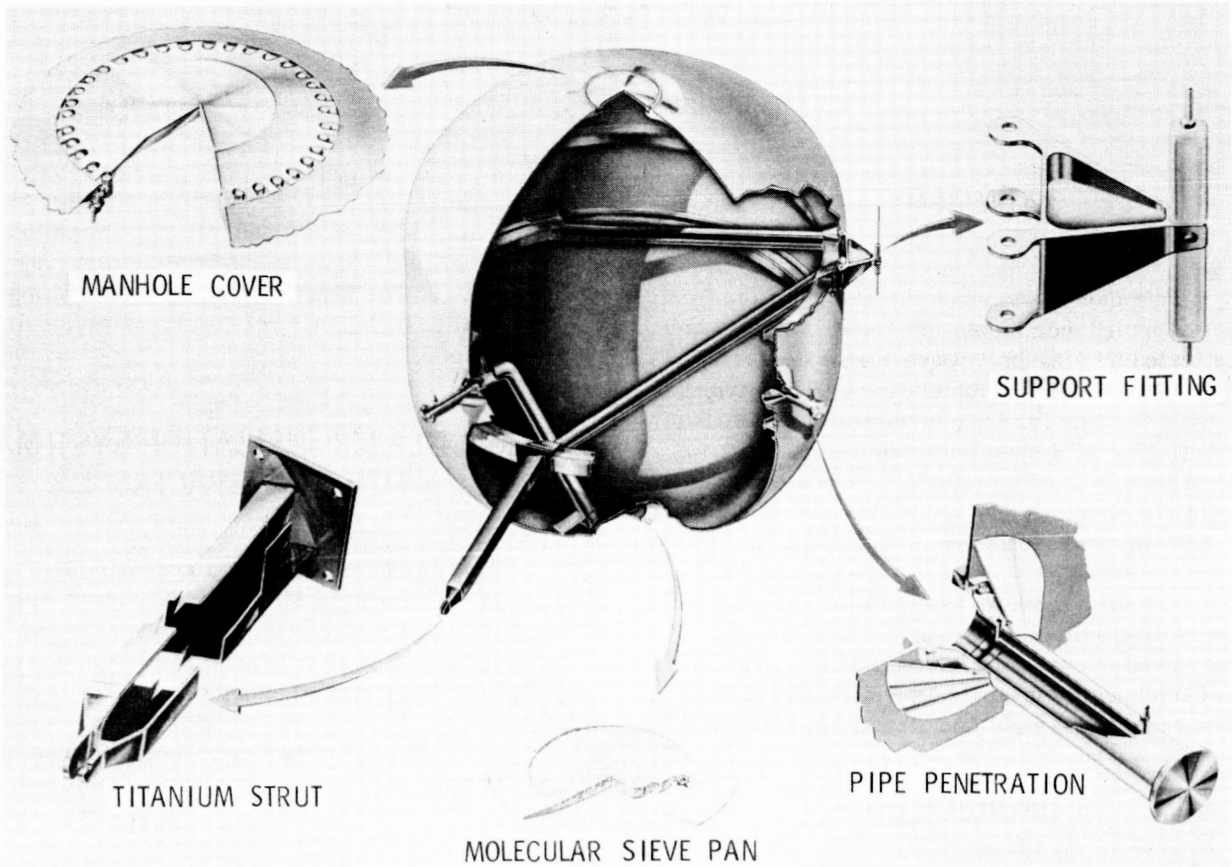

Figure 1. 2.67-m (105-in.) cryogenic test tank.

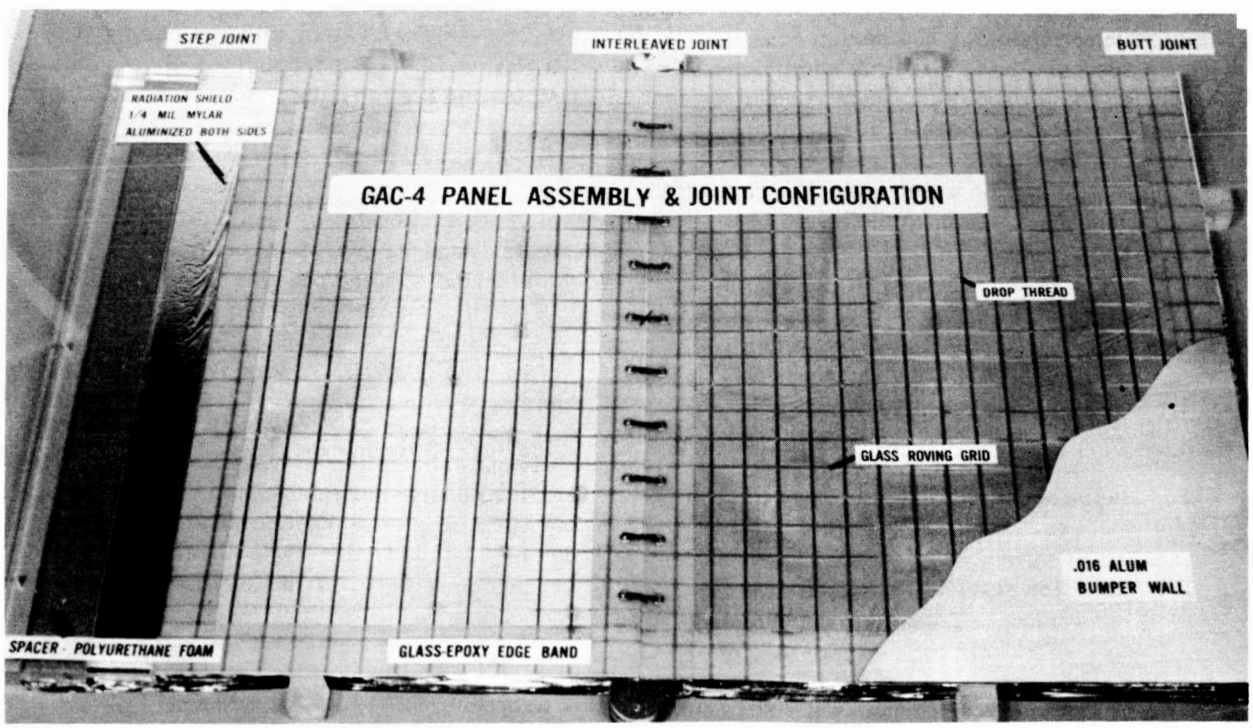

Figure 2. MSFC/GAC cryogenic insulation and micrometeoroid protection system.

acceleration load condition and (2) thermal performance in simulated space.

The GAC-4 MLI system design included two layers of insulation panels that were approximately 2.54 cm (1 in.) thick. Each layer of the MLI system was comprised of eight equal orange-peel-shaped panels with the longitudinal joints of the two layers staggered. The first installed layer is shown in Figure 3. The layer or blanket design includes lightweight fiberglass face sheets to prevent soiling and scratching, fiberglass grid rovings, epoxy-impregnated fiberglass cloth edge-bands, dacron cord lacing, 27 radiation shields, and 26 spacers. A major feature is the nylon zipper fastener that is bonded to the inner fiberglass face sheets; its purpose is to control the gap of the inner surface and to provide continuity in the structural tie. Aluminum eyelets were used in the epoxy edgeband to prevent galvanic corrosion. Results of structural tests of the edge-band design with aluminum eyelets and dacron cord lacing, and nylon zipper joints demonstrated the structural integrity of the main load-carrying elements. The results are shown in Figures 4 and 5.

Acceleration load tests were performed on the inner layer in a simulated ascent load condition. The MLI system was designed to withstand a 6.33-g acceleration load. The acceleration load tests were performed on a rocket sled (Fig. 6) at the Holloman Air Force Base, New Mexico, Air Force Missile Development Center. This test subjected the system to a 5.5-g load with accompanying vibration and acoustic levels and caused no damage to the system.

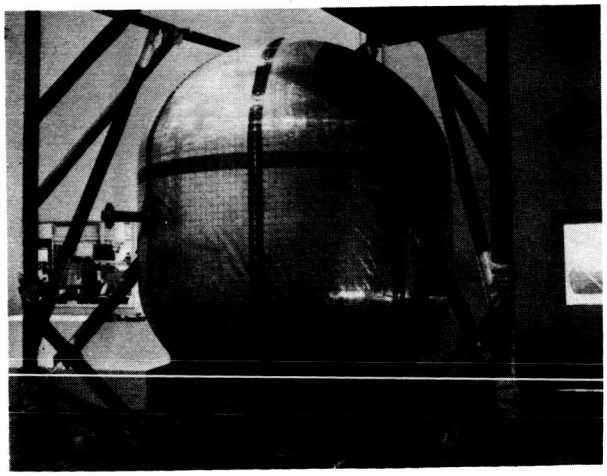

Figure 3. 2.67-m (105-in.) cryogenic test tank GAC-4 MLI system installation.

Frequency, velocity, acceleration, and distance versus time curves from one of the sled test runs are shown in Figures 7 and 8. The MLI system was transported from Akron, Ohio, to Holloman Air Force Base and then to MSFC. It was protected during transit by a purge jacket, as shown in Figure 9, and an outside protective wooden box. While in transit, the protective box suffered damage and the purge

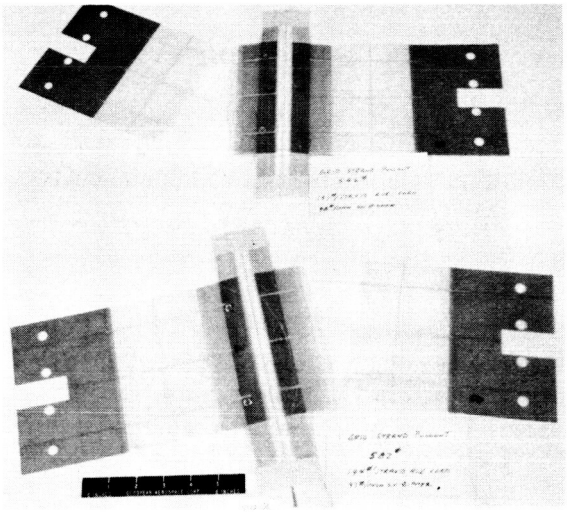

Figure 4. GAC-4 MLI system zipper-fastened grid specimen after tensile test.

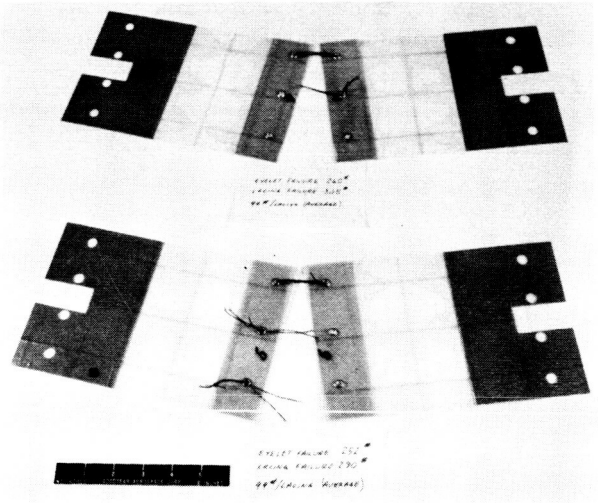

Figure 5. GAC-4 MLI system cord-laced grid specimen after tensile test.

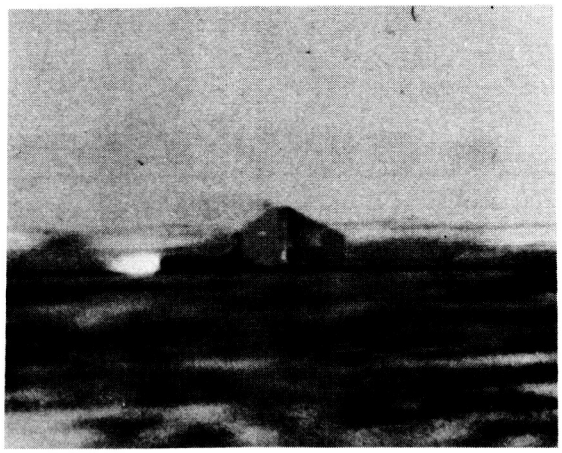

Figure 6. Rocket sled test at Holloman AFB.

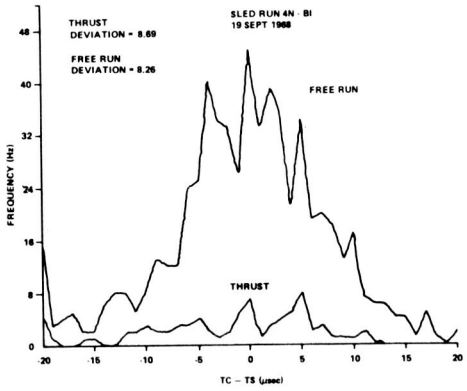

Figure 7. Rocket sled test run velocity and acceleration data.

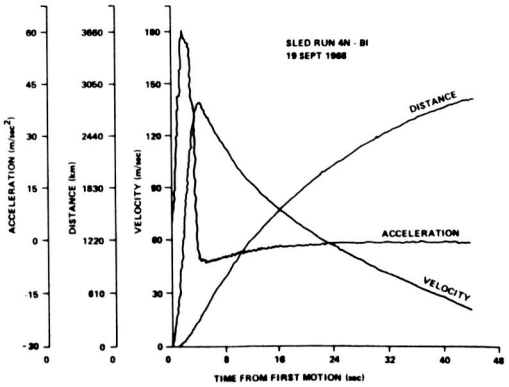

Figure 8. Rocket sled test run vibration and thrust data.

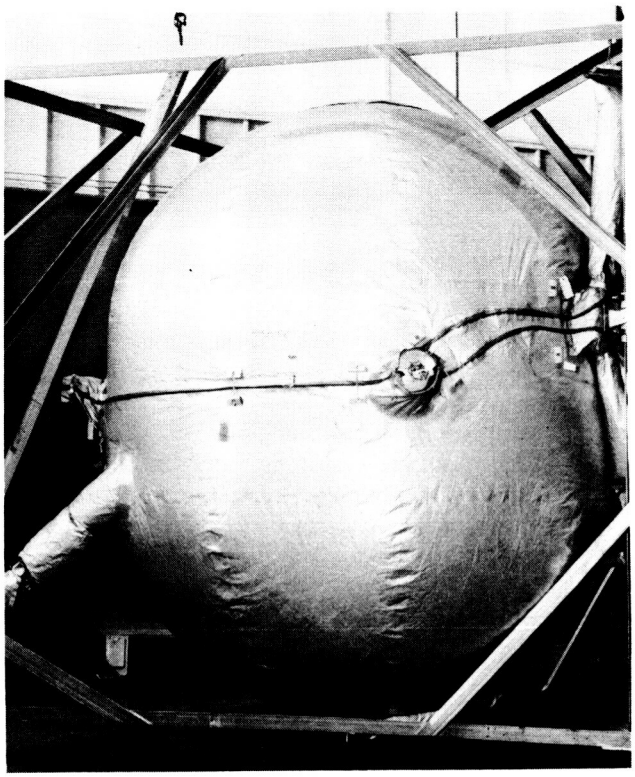

Figure 9. Purge bag for GAC-4 MLI system.

bag and MLI system were damaged by rain water. The only noticeable damage was near a penetration as shown in Figure 10. No attempts were made to replace or repair the system.

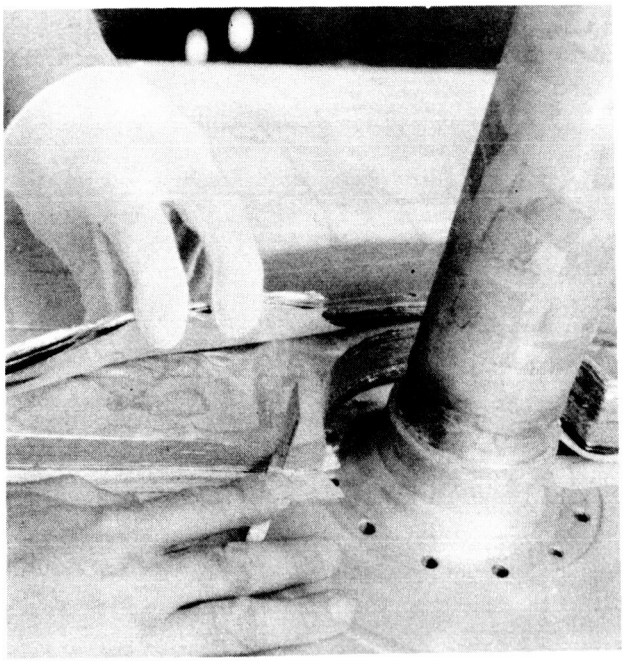

Figure 10. GAC-4 MLI system damage.

The GAC-4 MLI system is shown in Figure 11 with the closeout cover removed after arrival at MSFC from Holloman Air Force Base. No damage to the joints and surface is visible. To inspect the MLI at MSFC, one gore panel was removed, inspected, and reinstalled. The estimated time required for the removal and reinstallation was 15 min. The GAC-4 system proved to be very durable.

Prior to thermal performance testing, a second blanket of MLI was installed at MSFC. The penetrations were removed and a neck tube for fill and drain, vent, etc., was added to the tank. The inner layer was completely removed while the tank was modified. The completed GAC-4 MLI is shown in Figure 12.

The GAC-4 system is an effective micrometeoroid bumper system when used with an appropriate bumper. To qualify the system, hypervelocity impact tests were performed. Representative test damage to the MLI system and aluminum bumper is shown in Figure 13.

MULTILAYER INSULATION SYSTEM WITH SUPERFLOC SPACERS

The MLI insulation system designed by General Dynamics/Convair under MSFC contract

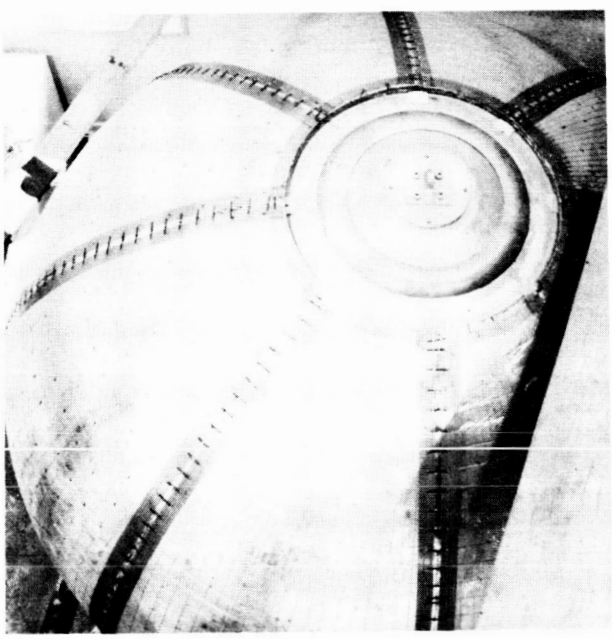

Figure 11. GAC-4 MLI system after rocket sled test.

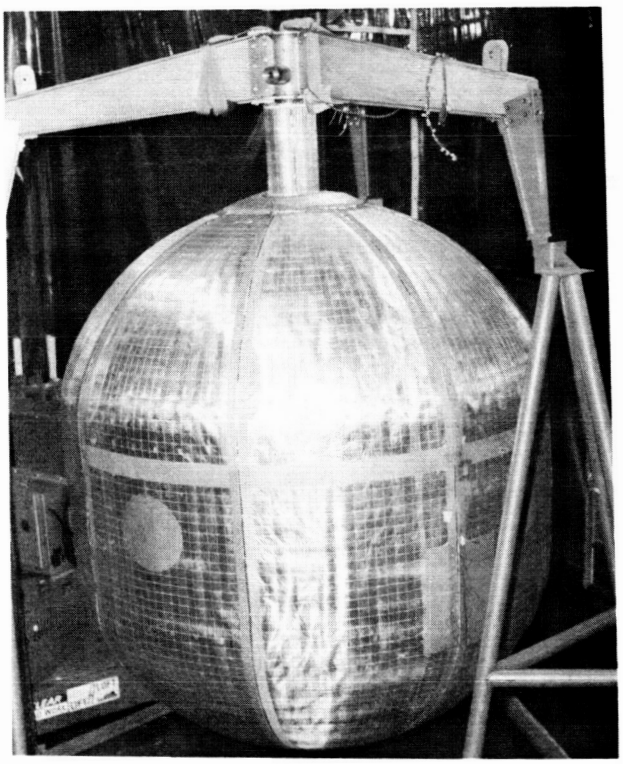

Figure 12. GAC-4 MLI system, two layers, 2.67-m (105-in.) cryogenic test tank.

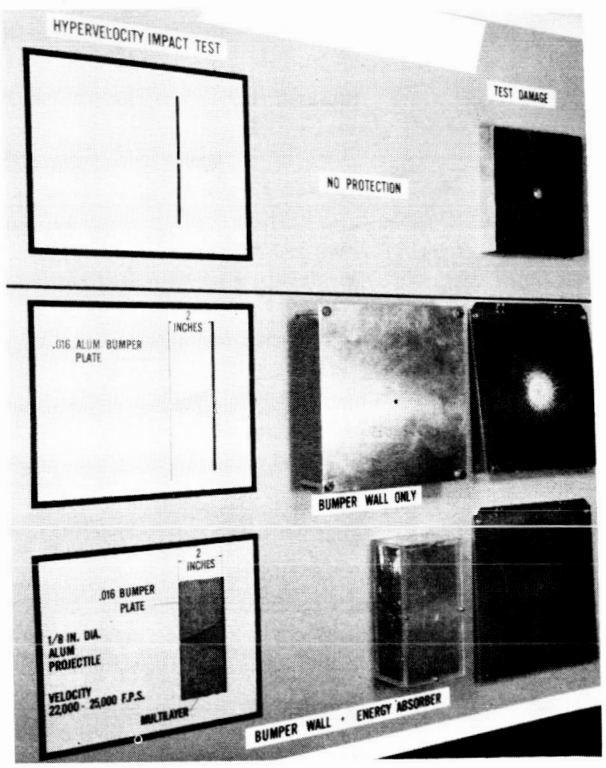

Figure 13. Hypervelocity impact test damage.

NAS8-18021 for the 2.67-m (105-in.) MSFC tank consists of four 2.54-cm (1-in.) Superfloc blanket layers with restraining grommets (Figs. 14 and 15) spaced about the perimeter. The cap blanket is a full 360-deg cone (Fig. 16). The adjacent and remaining blankets are of conical geometry and are segmented. The MLI blankets are interconnected by twin-pin and tri-pin fasteners, and the entire insulation assembly is attached to the tank by unidirectional fiberglass support pins (Fig. 15).

Each blanket segment is offset (Fig. 15) or rotated from the underneath blanket segment so that the seams between the blankets are staggered, thus effecting an overlap of approximately 5.08 cm (2 in.) for each blanket.

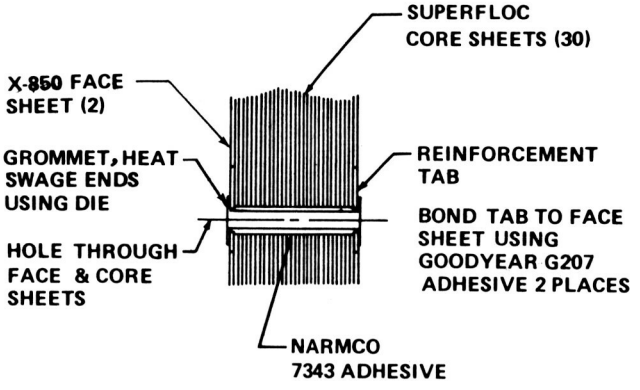

Figure 14. Restraining grommet.

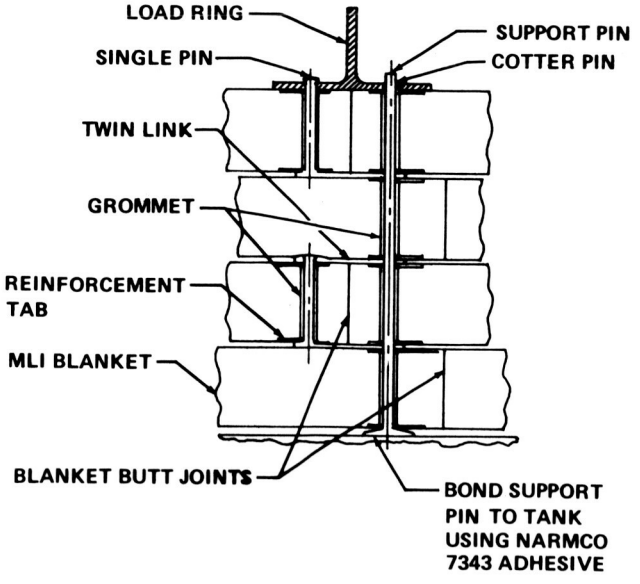

Figure 15. Restraining grommets with support pins installed.

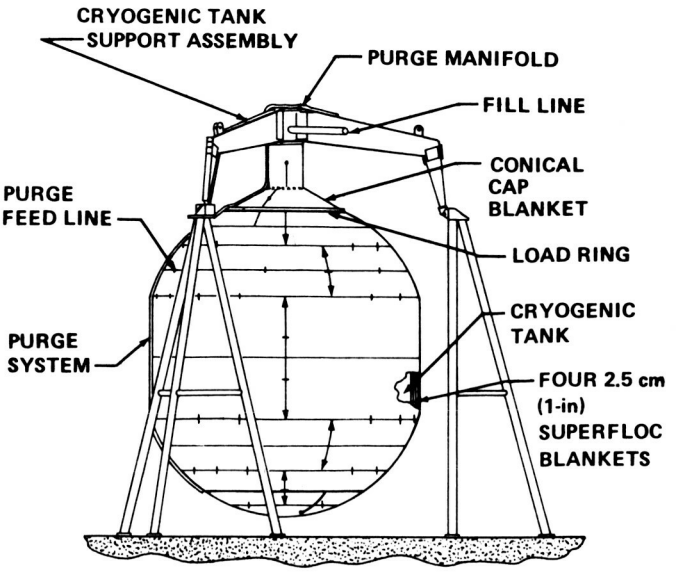

Figure 16. 10.16-cm (4.0-in.) insulation system for 2.67 m (105 in.) diameter tank.

Each blanket consists of 30 radiation shields of Superfloc and 2 face sheets of X-850 with a total thickness of 2.54 cm (1 in.) (Fig. 14). Superfloc is a Convair-developed radiation shield of 0.25-mil Mylar with vacuum deposits of aluminum on both sides. Each radiation shield is separated by dacron fibers that stand out about 10 mm (0.04 in.) above the Mylar base and are arranged in triangular patterns across the sheets. The face sheets are scrim-reinforced Mylar which consists of dacron scrim sandwiched between two layers of aluminized Mylar. Restraining grommets are spaced around the blankets and are bonded to each sheet, as shown in Figure 14. Reinforced polycarbonate resin tabs are located at each grommet location. Each grommet is coated with Narmco no. 7343 adhesive and frozen before installation. The frozen grommet is then inserted into prepared holes in the blanket and allowed to come to room temperature, which causes the adhesive to soften and bond to all sheets. Spacer pins (Fig. 17) are spaced

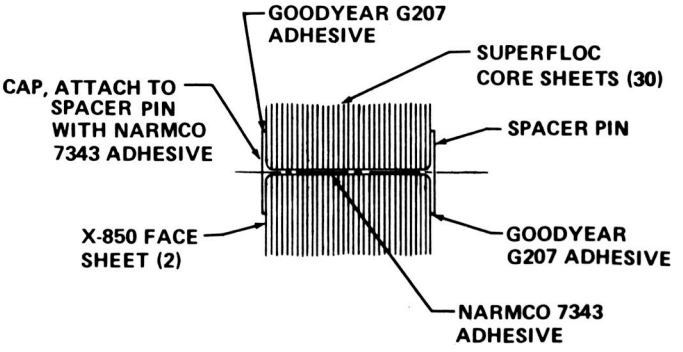

Figure 17. Purge pin installation.

within the center sections of the blankets to control the 2.54-cm (1-in.) density.

The insulation system tank support consists of 18 unidirectional fiberglass pins that have fiberglass bases which are bonded to the tank with the rods extending axially out from the tank (Figs. 15 and 18).

The blanket loads across the seams are carried from blanket to blanket by offset blanket links. Twin-pin fasteners (Fig. 19) are used between blankets at the seams and tri-pin fasteners (Fig. 20) are used where three blankets intersect, as in the case of two corner blankets and another blanket edge. Single- and double-pin fasteners (Fig. 21) are used when two or three blankets are interconnected.

A purge system consisting of a main feeder line extending from top to bottom on the outside of the insulation system and tank is shown in Figure 16. This line feeds manifold lines around the circumference of the tank. The manifold lines connect the purge pins that are located in each blanket section. The purge pins consist of two pieces, a slotted tube and a support flange that is bonded to the outer superinsulation blanket face sheet and accepts the purge manifold fittings (Fig. 22). Low pressure gases feed through the manifolds to the purge pins, penetrate all layers of the insulation in the blankets, and bleed out through the seams, thus purging the whole blanket system.

The 2.67-m (105-in.) tank conical design requires 16 different blanket configurations, whereas a gore design would require only 8 blanket configurations. Thus, a gore design not only reduces manufacturing costs but also has a higher thermal efficiency.

Structural tests conducted during the development of the Superfloc MLI system for the 2.67 m (105 in.) diameter tank consisted of face sheet tearout tests, blanket assembly tests, a blanket vibration test with simulated acceleration load, and Combined Environmental, Vibration, Acceleration, and Thermal (CEVAT) tests.

Face sheet tearout tests were conducted on the reinforced and unreinforced face sheet material, Schjeldahl X-850. Typical test specimen are shown in Figures 23 and 24.

Blanket assembly tests were conducted to evaluate the twin-pin fasteners (Fig. 19) assembled to an insulation blanket.

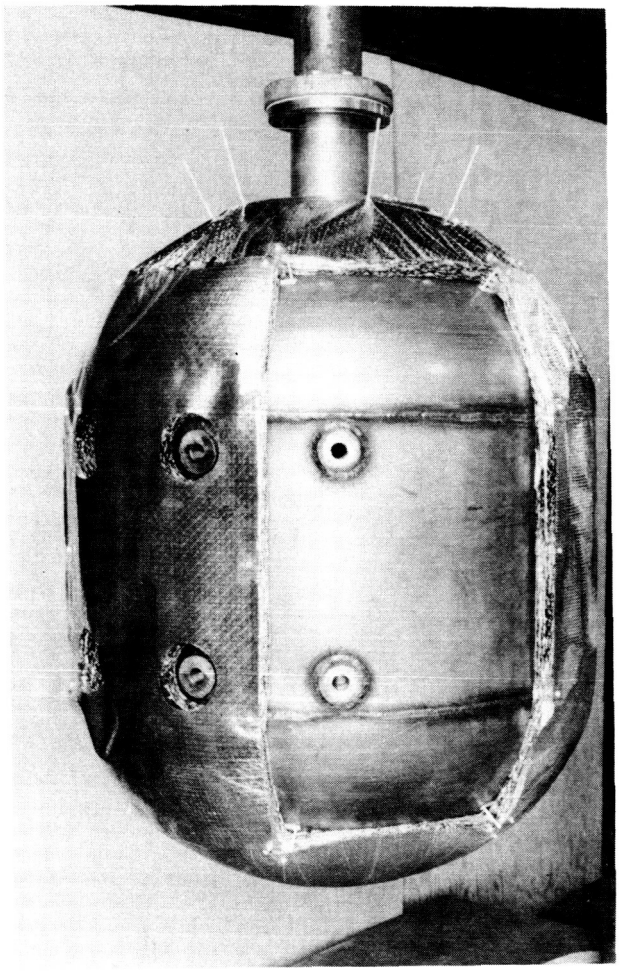

(a)

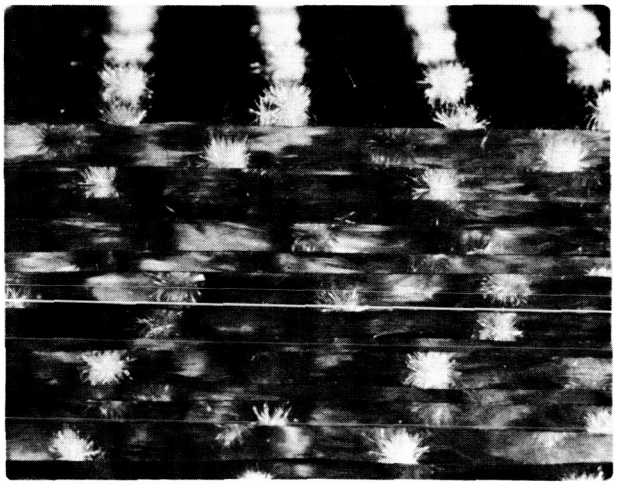

(b)

Figure 18. Superfloc insulation system

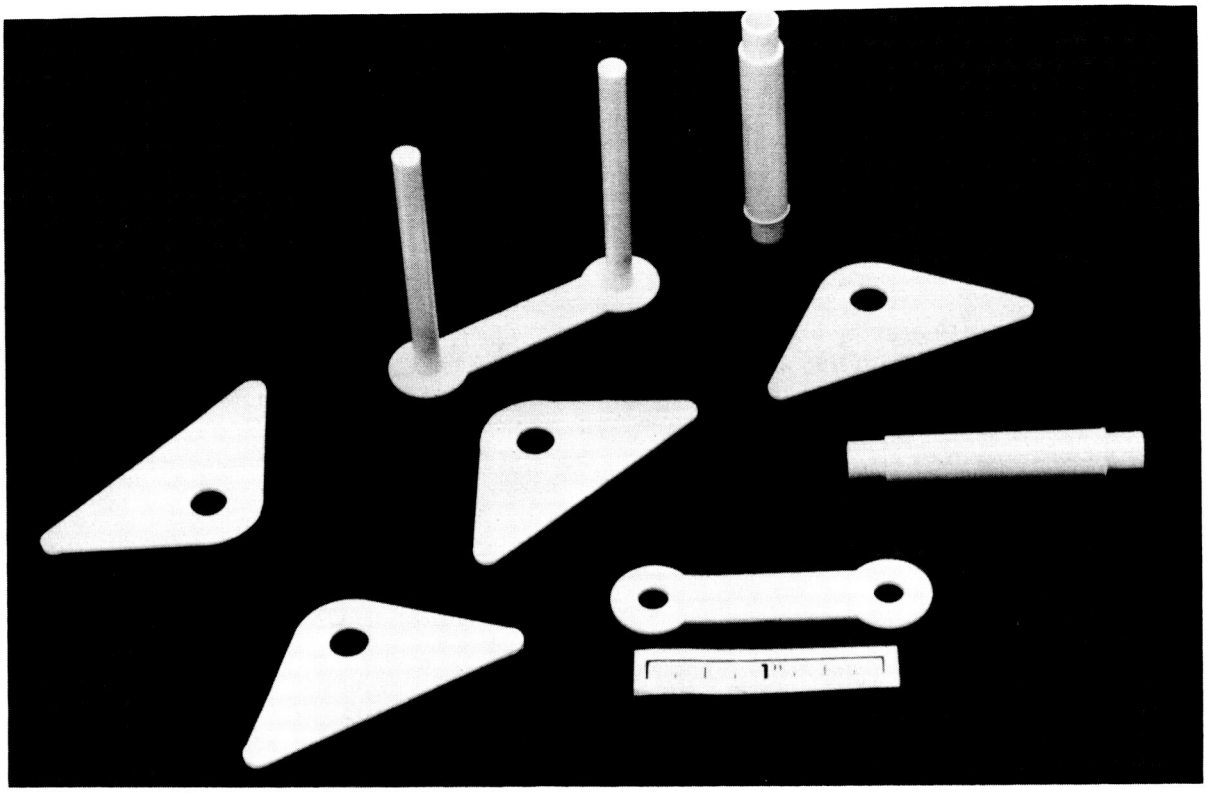

Figure 19. Spacer pin installation.

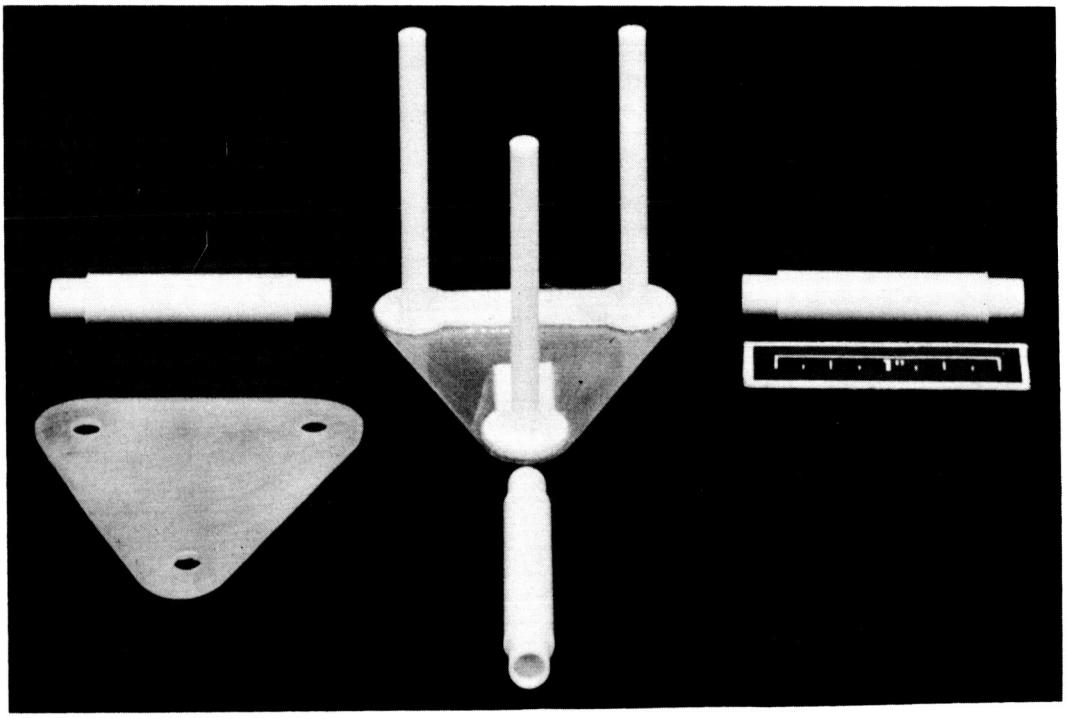

Figure 20. Twin-pin fastener.

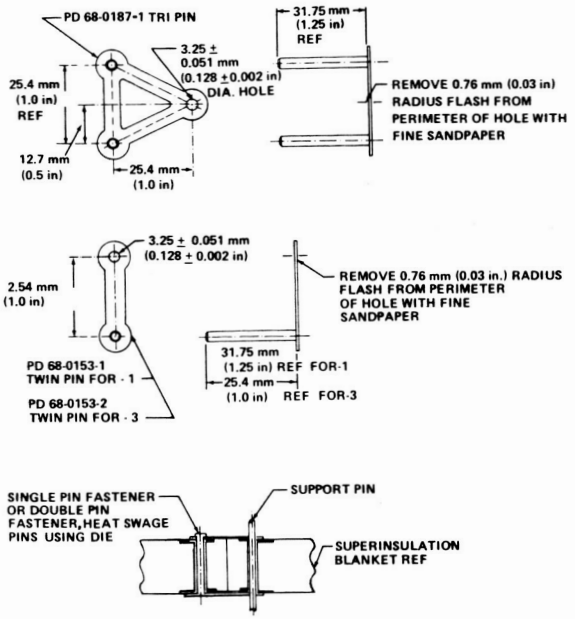

Figure 21. Tri-pin fastener.

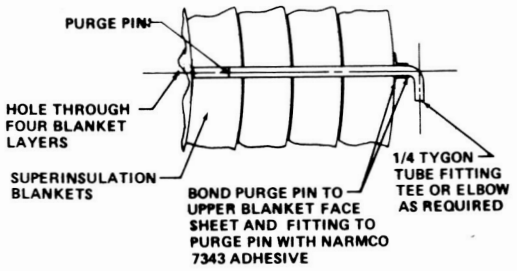

Figure 22. Single-pin and double-pin fastener.

Test specimen are shown in Figures 25 and 26. Insulation blankets, consisting of 30 layers of Superfloc and 2 face sheets of X-850 that contain lexan reinforcements and grommets through the blanket, were assembled and tested in tension as shown in Figures 25, 26, and 27. An ultimate load of 239.9 N (53.9 lbf)/pin at room temperature was reached in the tension test specimen shown in Figures 25 and 26. A tensile test run at liquid nitrogen temperature resulted in a failure at 326.2 N (73.3 lbf)/pin.

A combined vibration and acceleration test was conducted on the 2.54-cm (1-in.) blanket

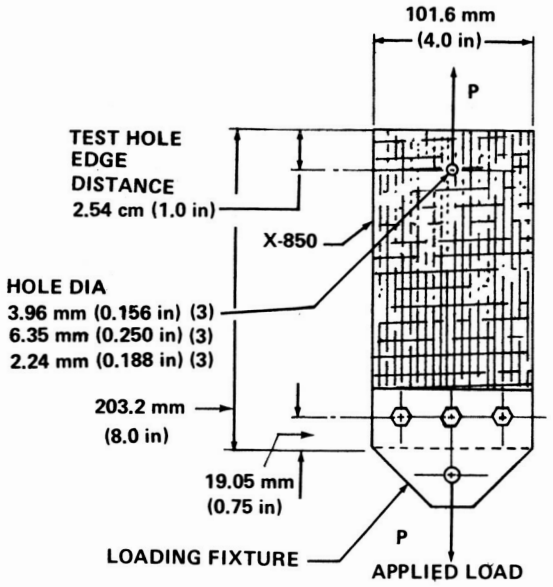

Figure 23. Unreinforced Schjeldahl X-850 test specimen.

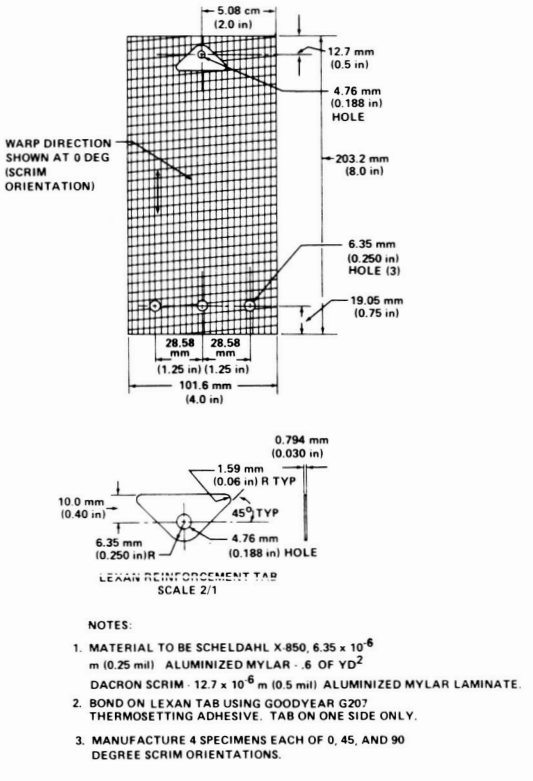

Figure 24. X-850 face sheet test specimen.

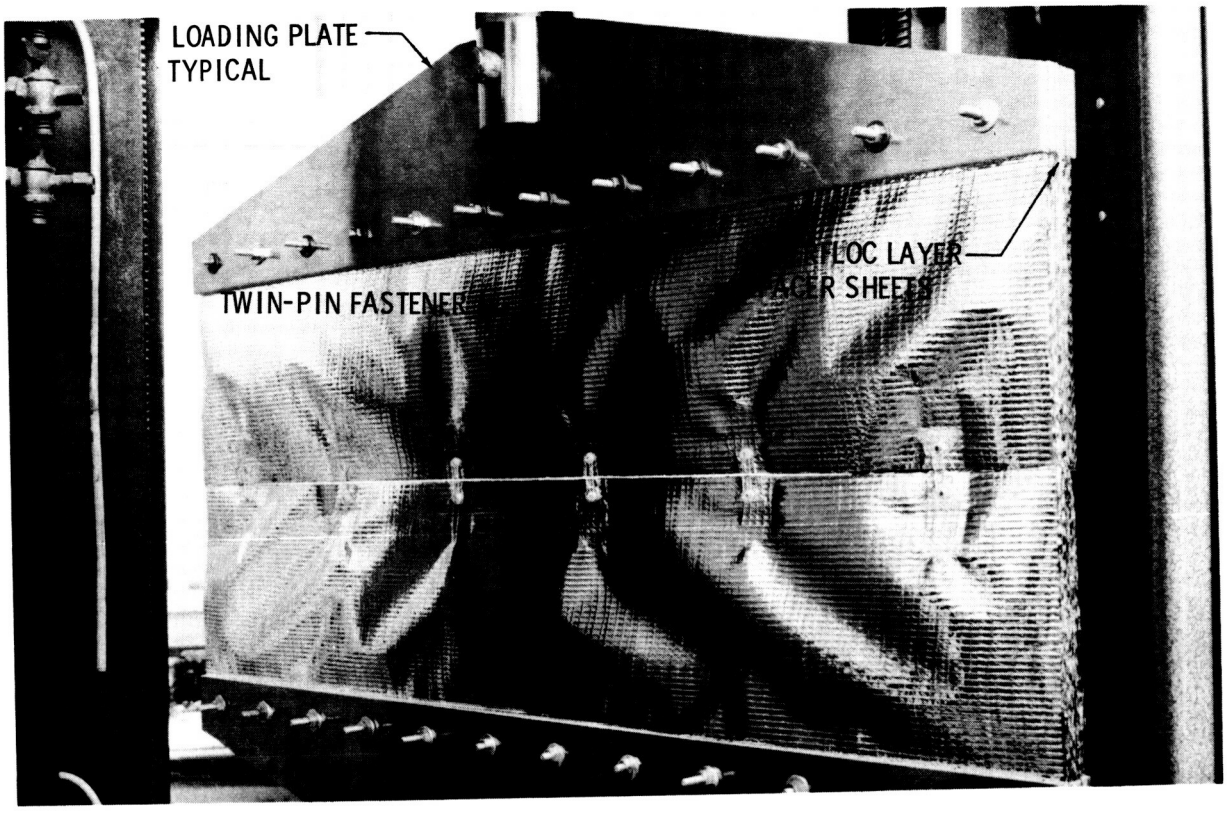

Figure 25. Blanket tension test, unloaded.

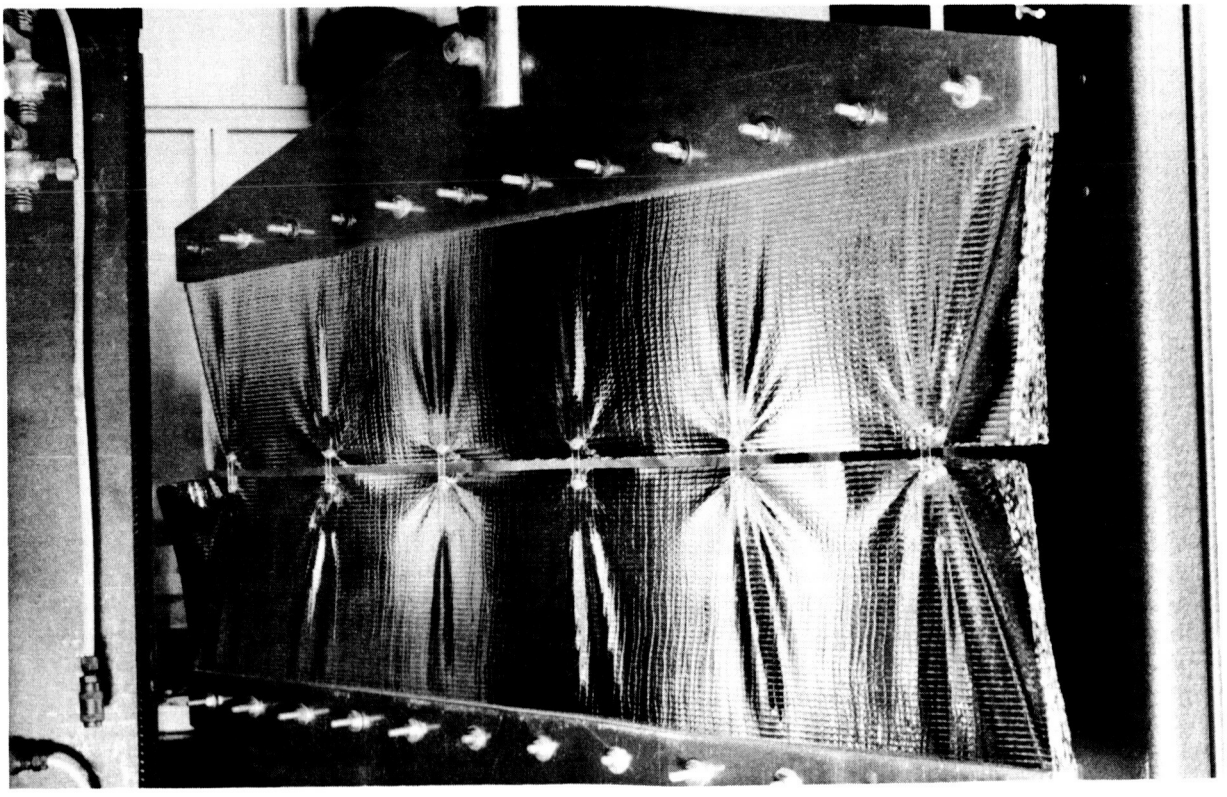

Figure 26. Blanket tension test, loaded.

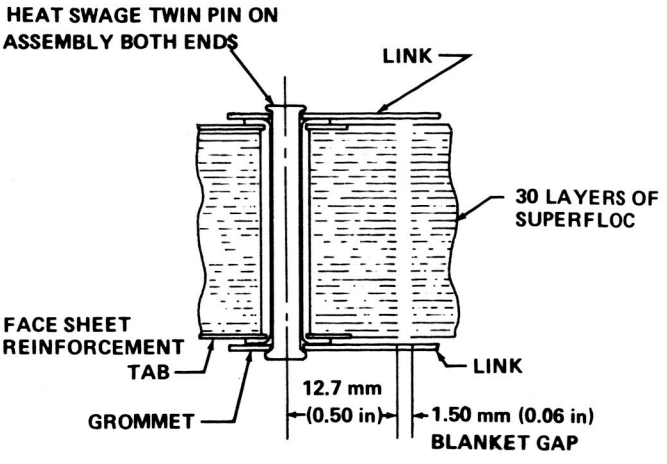

Figure 27. Twin-pin assembly showing heat swage.

assembly shown in Figure 28. Four loads were applied at the design vibration level of 0.3 g^2/Hz at a random frequency of 20 to 150 Hz without any failures. The results of the tension and vibration tests indicated the 2.67-m (105-in.) blanket design was strong enough to withstand a typical Saturn V boost environment (Fig. 29).

To further qualify the insulation system for flight loads, a scale-model system was prepared for CEVAT tests. Four 2.54 cm (1 in.) thick blankets of Superfloc MLI were installed in a 0.635-m (25-in.) tank. The four blankets were then thermally tested, structurally tested in a vacuum chamber, and finally mounted on a centrifuge (Fig. 29) and subjected to the following environments:

1. Linear acceleration up to 20 g maximum.

2. Vibration to 6.3 g at 5 to 300 Hz.

3. Pressure decay rate based on Saturn V trajectory.

4. LH_2 temperature simulator.

The insulated tank was again thermally tested. No thermal degradation or structural damage was observed as a result of the centrifuge tests. The insulation system after the tests is shown in Figure 30. Test acceleration levels are shown in Figure 31.

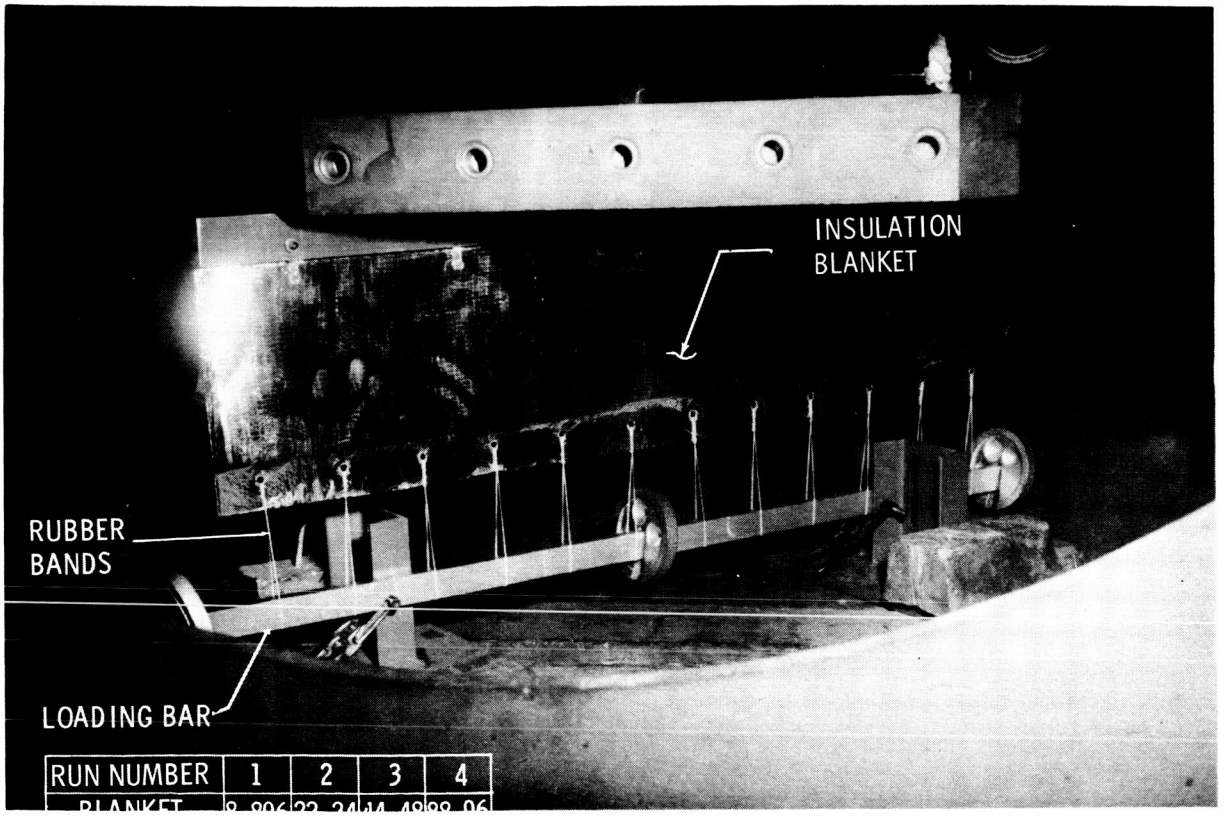

Figure 28. Blanket vibration and acceleration test.

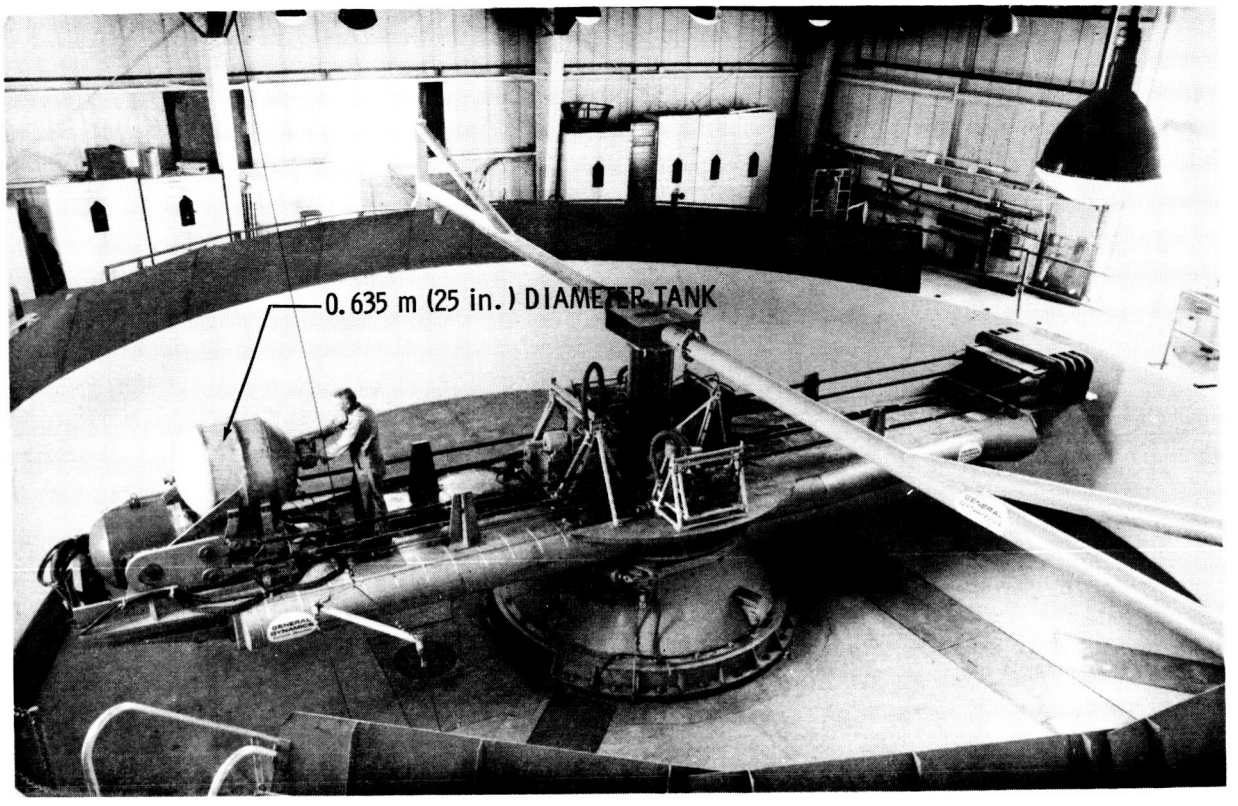

Figure 29. CEVAT centrifuge.

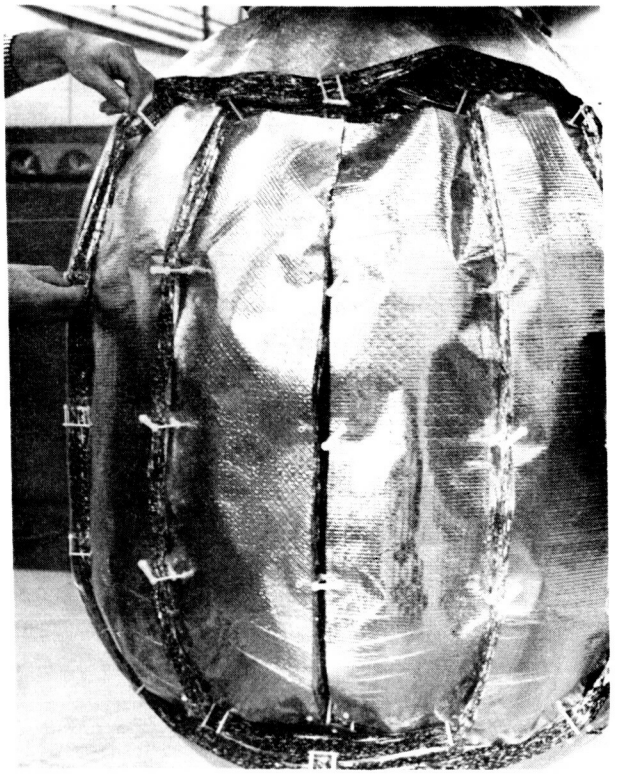

Figure 30. 10.16-cm (4.0-in.) Superfloc insulation system after CEVAT test.

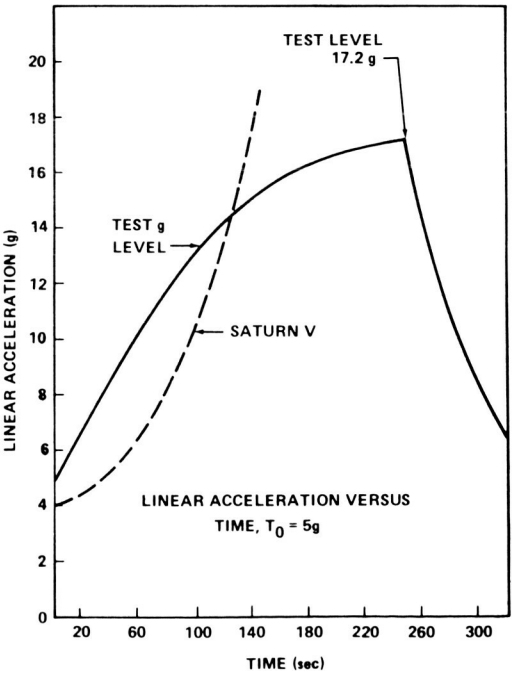

Figure 31. Linear acceleration versus time, CEVAT test.

MULTILAYER INSULATION SYSTEM WITH NET SPACERS

The 2.67 m (105 in.) diameter tank insulation system simulates an MLI system for the Modular Nuclear Vehicle (MNV), shown in Figure 32. This MLI system was designed by the McDonnell-Douglas Astronautics Company, Western Division, under MSFC contract NAS8-21400.

The MLI net spacer system as designed for the 2.67 m (105 in.) diameter tank (Fig. 33) consists of support tube panels, conical panels, main gore panels, patch panels, and manhole cover panels. The panels are to be prefabricated and made from alternating layers of double-aluminized Mylar (DAM) and dacron net spacers between epoxy-impregnated dacron net face sheets. The panels are secured in place by stud button fasteners with heat-sealed caps (Fig. 34).

To carry the structural loads, continuous straps with grommets for attaching were developed and installed on the cold side of each panel and

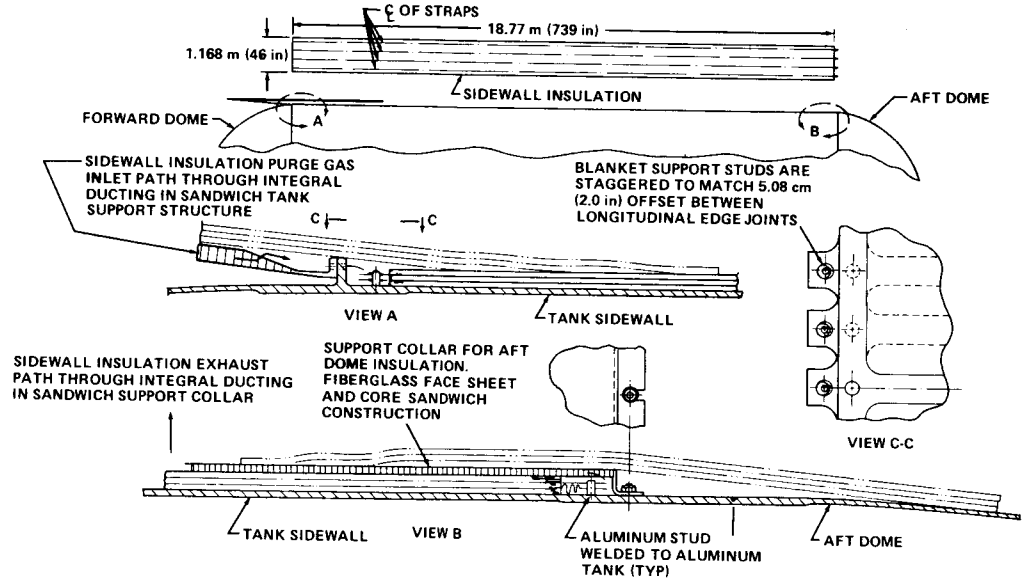

Figure 32. MNV MLI system (net).

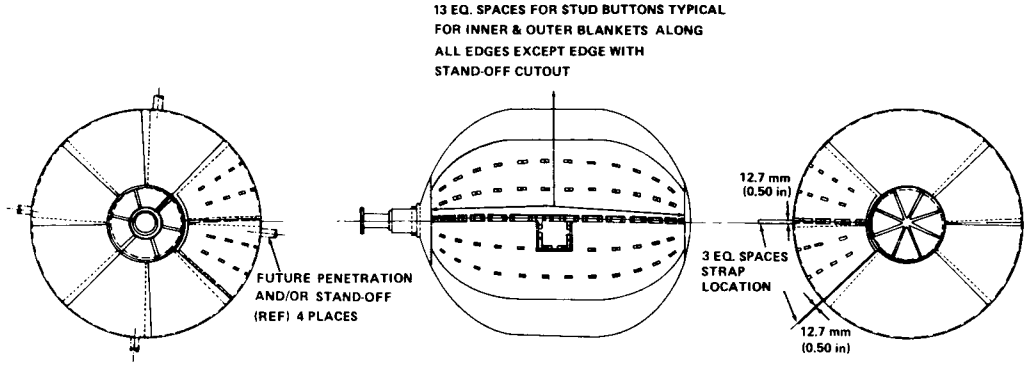

Figure 33. 2.67 m (105 in.) diameter cryogenic test tank.

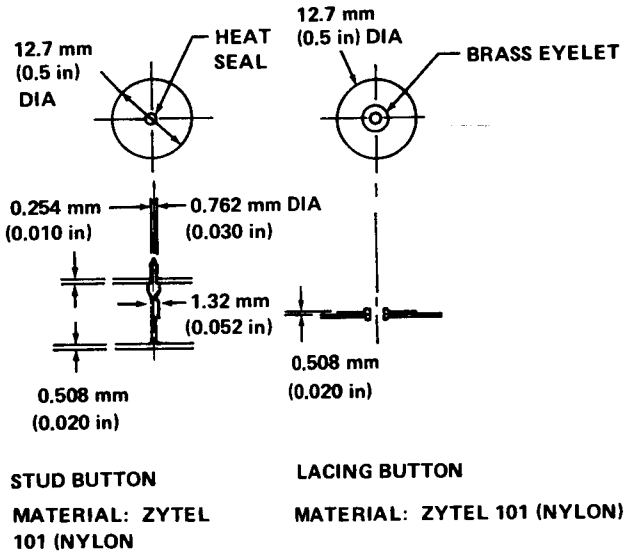

Figure 34. Stud and lacing buttons.

integrated with the face sheets. The load-carrying straps on the warm side of the panels are not continuous, which minimizes shrinkage effects. The continuous load straps (coldest side) provide for differential contraction between the two face sheets of the panel. The thermal contraction comparison of the straps with Mylar is shown in Figure 35.

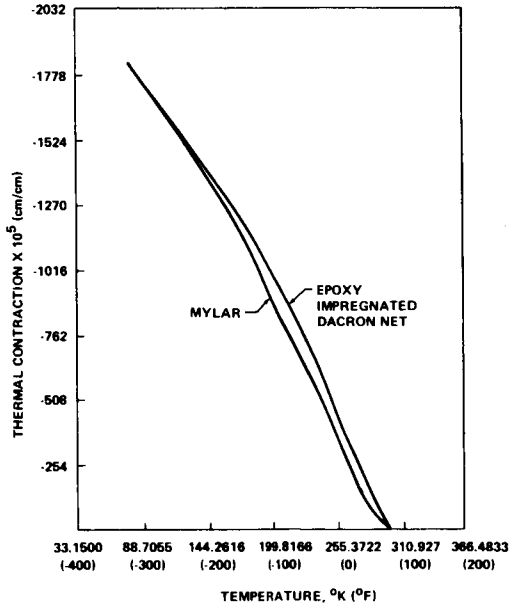

Figure 35. Comparison of thermal contraction.

The panel joints are held together with nomex thread lacing around buttons that are attached with brass eyelets to the epoxy-impregnated edge band of the outer face sheet on each panel. The panels are oversized and are laced tightly to minimize tensile loads that result after filling the tank. The double-lacing method shown in Figure 36 is used.

The MLI system is two panels thick, and the butt joints are offset 5.08 cm (2.0 in.) to prevent a direct heat leak. The tank is covered by 8 inner and 8 outer gore panels attached by the load carrying straps to a support ring which is bonded to the tank head (Fig. 37). The gore panels are secured to a polar cap on the bottom head, shown in Figure 33. Neck tube and conical sections are similar in design to the gore panels. Provisions for attaching tank handling hardware and for installing future penetration designs are shown in Figure 33.

Structural tests were performed on components and the panel configuration. The component tests consisted of static tensile load tests on panel stud-button attachments, a panel face sheet tearout, support straps, an epoxy-impregnated support strap with stud-buttonhole, and a support-strap tab. A typical test setup is shown in Figure 38. To structurally test the basic panel configuration (Figs. 39 and 40), acoustic tests simulating MNV environments (an overall sound pressure level of 158.4) were performed.

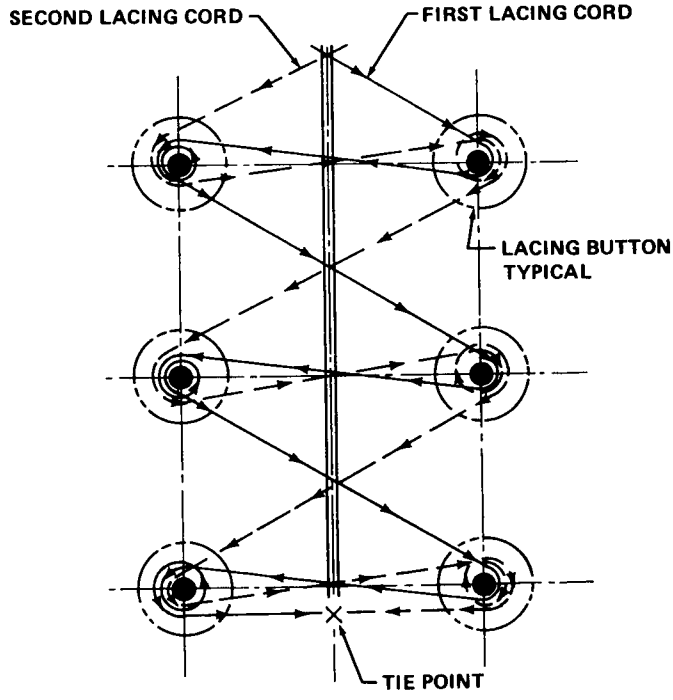

Figure 36. Improved joint lacing pattern.

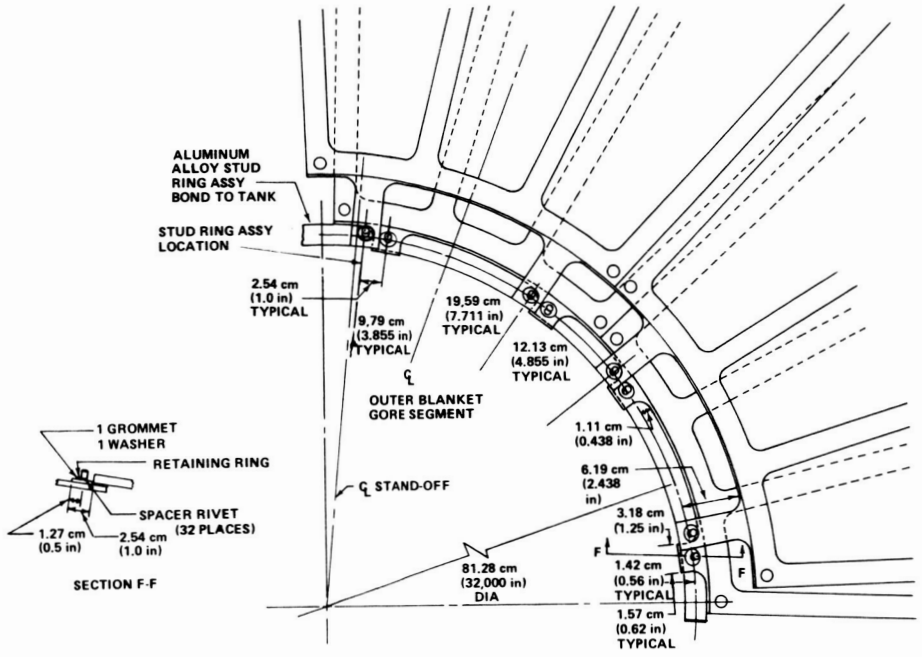

Figure 37. Panel support ring.

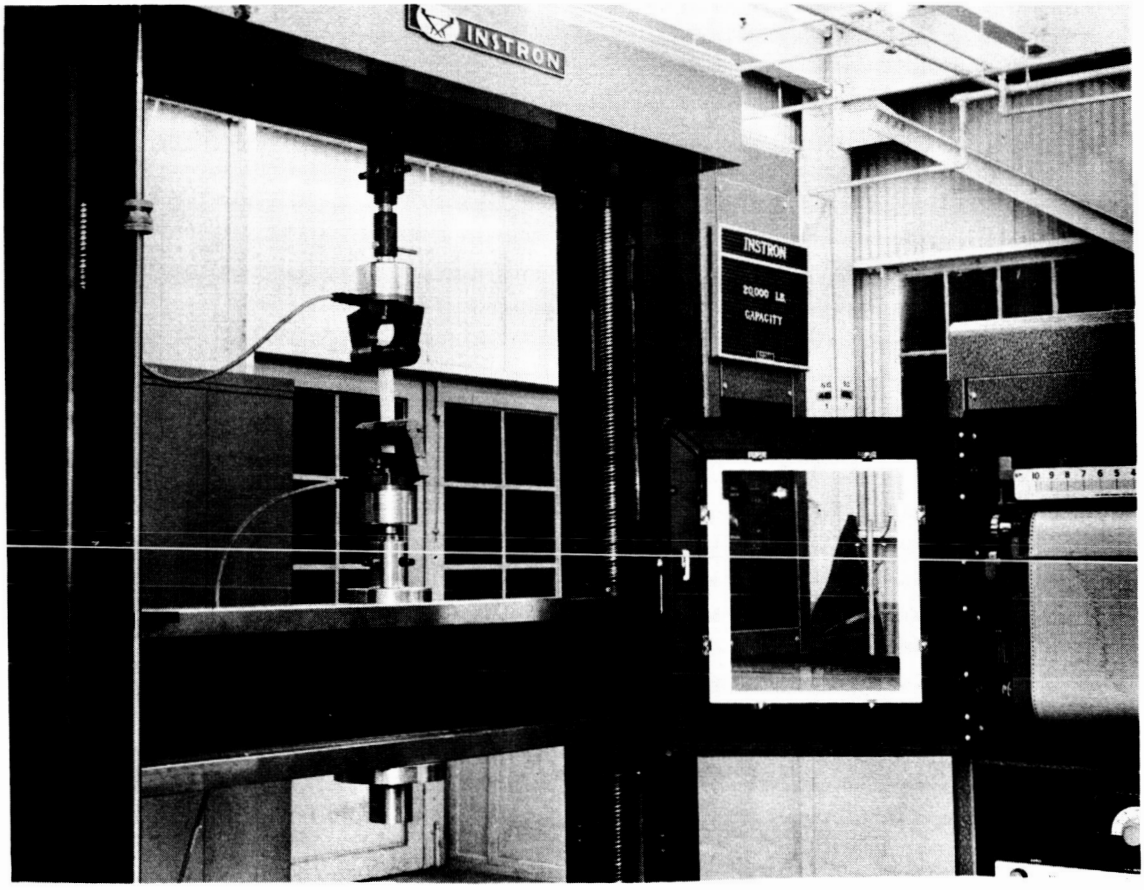

Figure 38. Typical test setup.

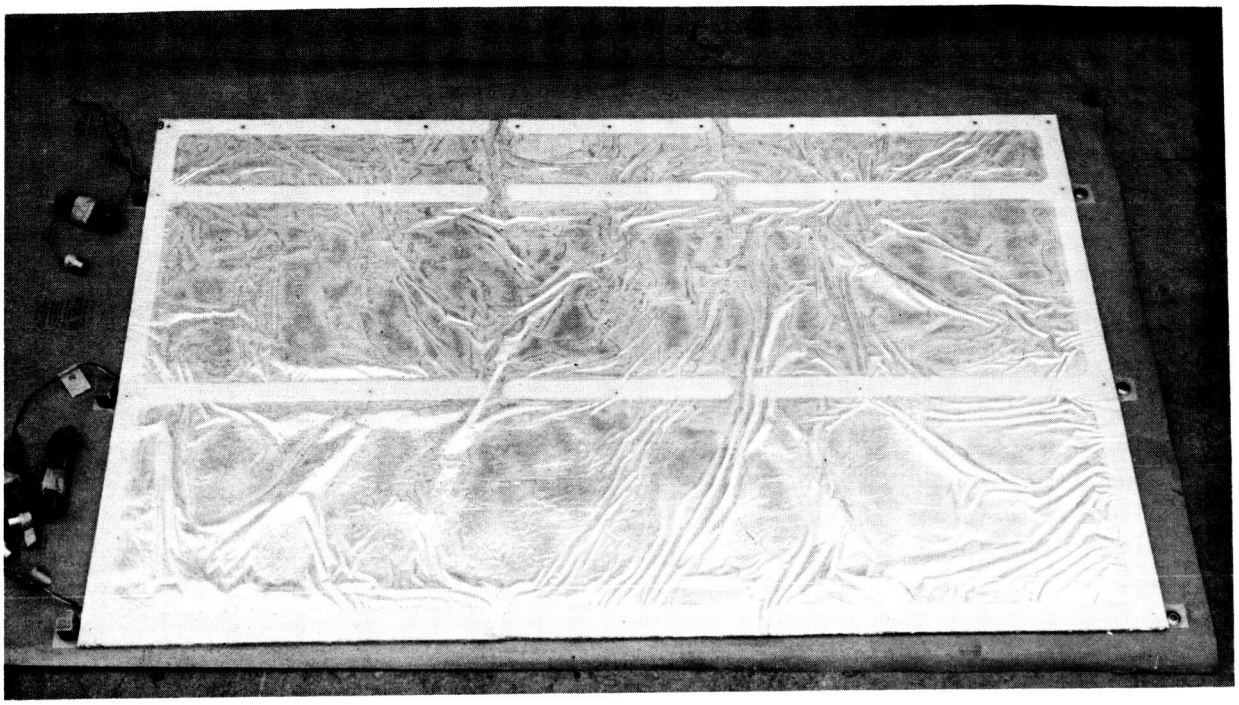

Figure 39. Structural test panel configuration.

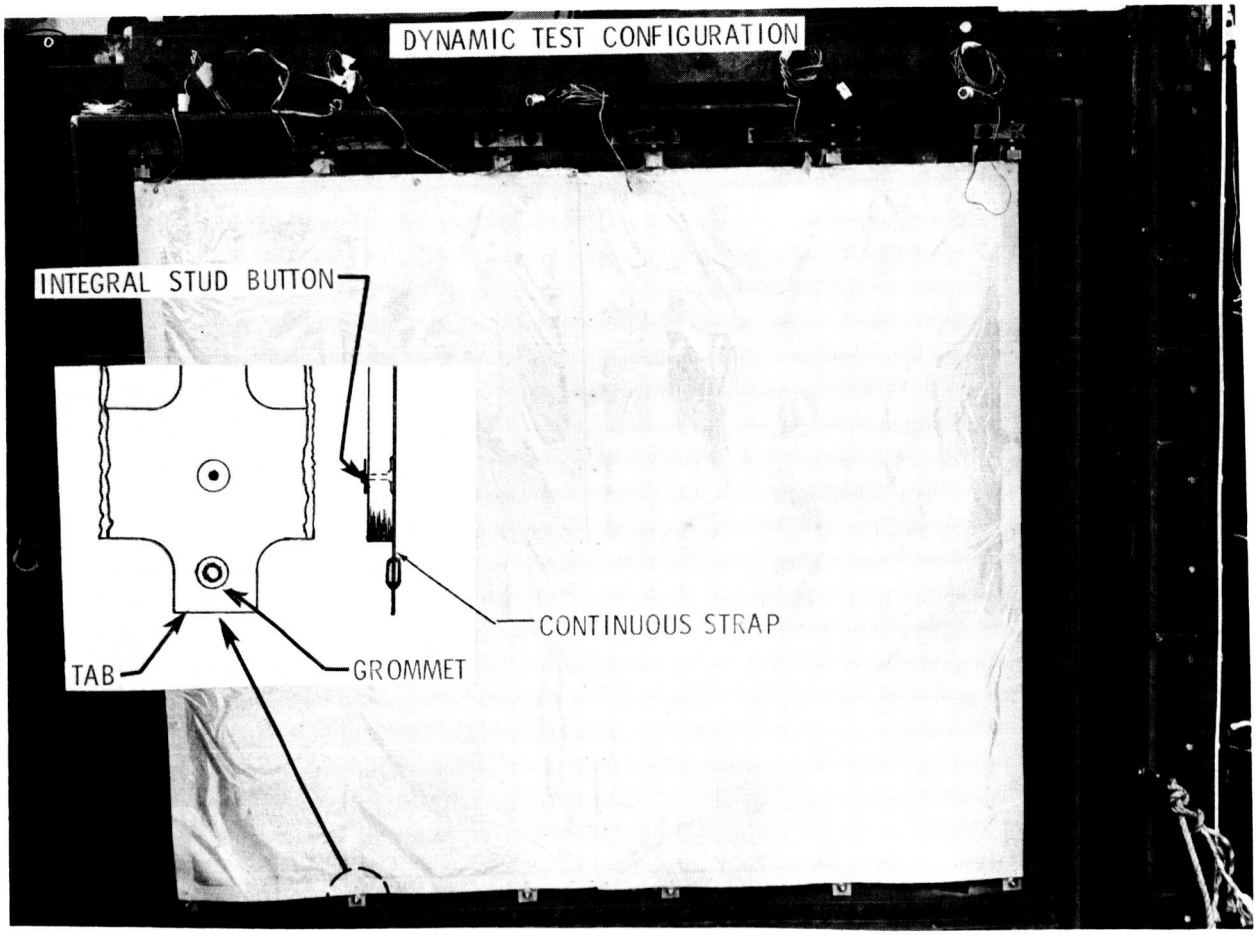

Figure 40. Structural test panel configuration.

The panel configuration was preloaded at the load straps along both sides and subjected to a cryogenic temperature during the test. Figure 40 shows the test specimen installed on the test fixture. Results of this test did not reveal any damage to the face sheets, DAM shields, net spacers, or lacing buttons. The test did reveal an opening in the laced butt joint (Fig. 41). The lacing pattern was modified (Fig. 36) to prevent opening of the joint and to provide a more efficient means of transferring the load.

The end attachments of the load-carrying straps were tested (Fig. 42). A longitudinal acceleration load of 5 g was applied to the straps before and during the panel configuration test. Results of the test indicated no damage around the grommets or to the specimen. Results of the structural tests indicate that the design is structurally adequate for the MNV.

CONCLUSIONS

The structural design of multilayer insulation systems for application to large scale space vehicle cryogenic tankage has been successfully demonstrated for single launch use. The designs studied have been shown to be very lightweight and structurally sound. Structural attachments are still considered to be a source of high weight and heat loss, but these do not necessarily occur simultaneously. Penetrations were considered in the design of all the MLI systems, but further investigations should be made. A summary of various MLI systems' weights is shown in Table 1.

The design of future MLI systems will involve a new and more challenging criterion; that of higher external temperatures combined with the cryogenic, vibration, and acoustic environments to meet space vehicle reusability requirements.

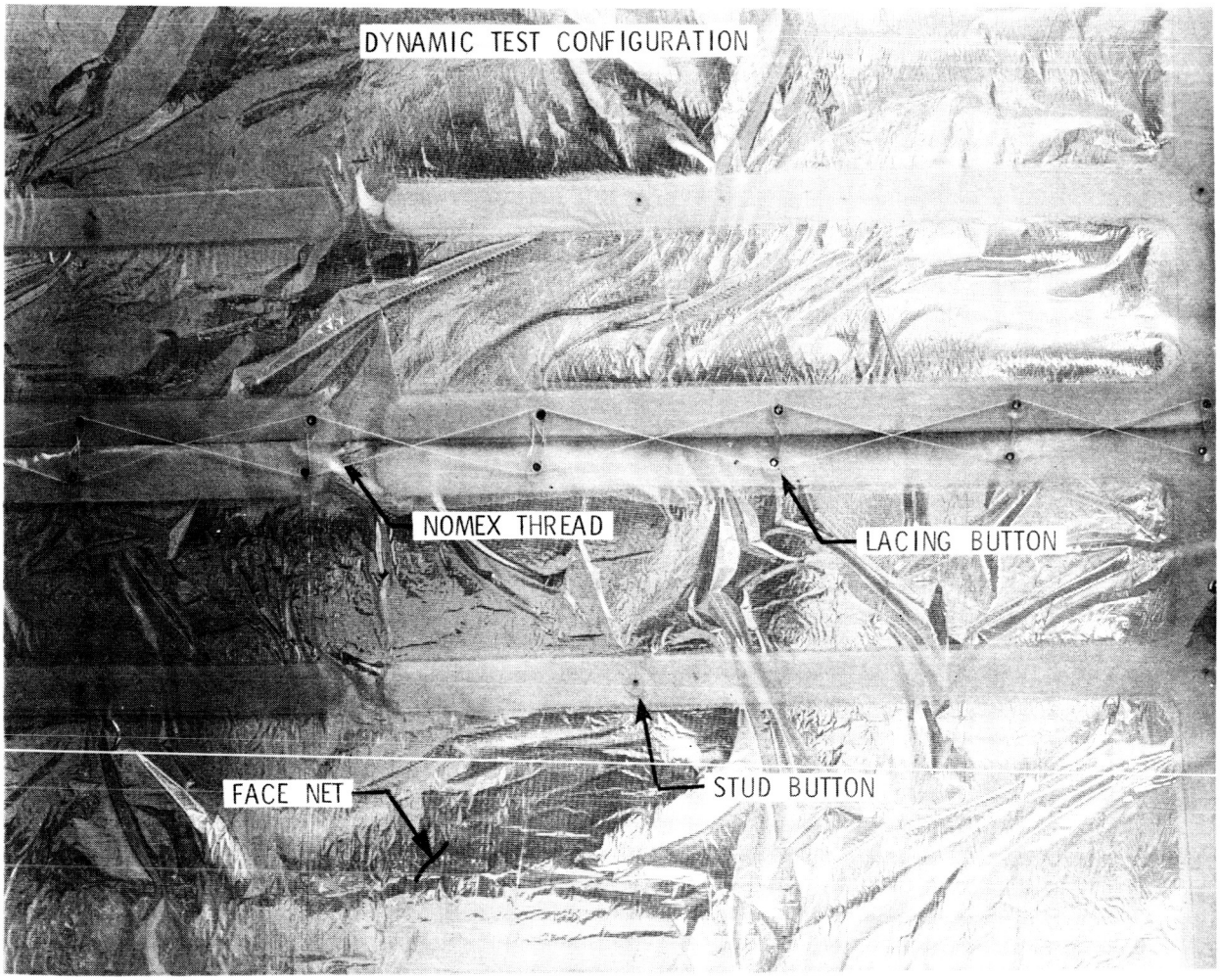

Figure 41. Insulation butt joint after test.

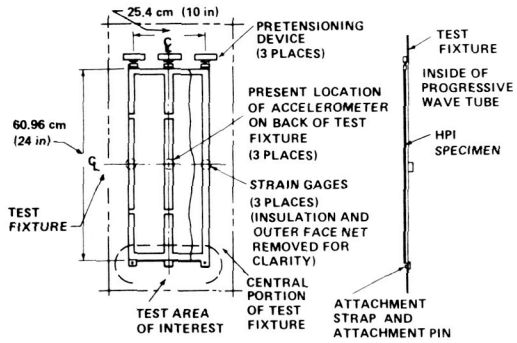

(a)

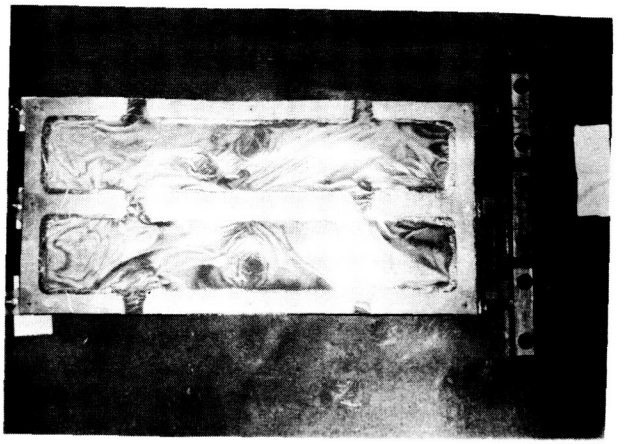

(b)

Figure 42. Attachment strap and load test.

TABLE 1. MLI SYSTEMS WEIGHT SUMMARY, 2.67 m (105 in.) DIAMETER CRYOGENIC TEST TANK

System	System Thickness cm (in.)	Blanket Weight, kg (lb)	Attachments, etc. Weight, kg (lb)	Total Weight Installed, kg (lb)	Total Joint Length, cm (in.)	Total Mean Surface Area, m^2 (ft^2)
GAC-4 NAS8-11747	5.69 (2.24)	57.759 (127.334)	20.593 (45.40)	78.352 (172.734)	7840.98 (3087)	28.908 (311.178)
GAC-9 NAS8-30140	5.08 (2)	48.570 (107.077)	18.144 (40)	66.714 (147.077)	7678.42 (3023)	28.783 (309.830)
GD/C Superfloc NAS8-18021	10.16 (4)	50.368 (111.04)	3.266 (7.20)	53.634 (118.240)	19827.24 (7806)	29.752 (320.253)
MDAC-Net NAS8-21400	1.941 (0.764)	32.749 (72.20)	7.108 (15.67)	39.858 (87.87)	7246.62 (2853)	28.476 (306.525)
GAC-Net NAS8-24884	5.08 (2)	53.854 (118.726)	18.144 (40)	71.998 (158.726)	7678.42 (3023)	28.783 (309.830)

BIBLIOGRAPHY

Nevins, Clyde D.: Designing for Cryogenic Insulation. NASA Technical Memorandum 53670, 1967.

Development of Materials and Materials Application Concepts for Joint Use as Cryogenic Insulation and Micrometeoroid Bumpers. Final Summary Report, Contract NAS8-11747, Goodyear Aerospace Corp. Report No. GER 11676 S/47, June 30, 1968.

Design and Fabrication of the Tooling for Installation of a Composite Insulation System on MSFC 105" Diameter Tank. Final Summary Report, Contract NAS8-24825, Goodyear Aerospace Corp. Report No. GER-14544, September, 1969.

BIBLIOGRAPHY (Concluded)

Development of Materials and Materials Application Concepts for Joint Use as Cryogenic Insulation and Micrometeoroid Bumpers. Final Summary Report, Goodyear Aerospace Corp. Report No. GER 14071 S/11, November 30, 1969.

Application of High Performance Insulation to Large Conical Support Structures. Final Summary Report, Contract NAS8-24884, Goodyear Aerospace Corp. Report No. GER 14518 S/11, October, 1970.

Leonard, K. E.: Cryogenic Insulation Development. Final Report, Contract NAS8-18021, General Dynamics (Convair) Report No. GDC-DDB69-002, December 31, 1969.

Getty, R. C.: Cryogenic Insulation Development. Final Report, Contract NAS8-18021, General Dynamics (Convair) Report No. GDC DDB67-007, January, 1968.

Fredrickson, G. O.: Investigation of High Performance Insulation Application Problems. Quarterly Progress Reports, Contract NAS8-21400, McDonnell-Douglas Astronautics Company, Western Division.

MANUFACTURING DEVELOPMENTS IN INSULATION APPLICATION

By

Iva C. Yates, Jr.

INTRODUCTION

Manufacturing development studies have been conducted at Marshall Space Flight Center (MSFC) and by several contractors to provide information on the fabrication and handling characteristics of a number of candidate multilayer insulation systems. The application of these complex, lightweight insulation systems to large-scale, flight-type cryogenic tankage and other structures has of necessity required the development of new methods, processes, and tooling concepts. The purpose of this paper is to present the results of some of the studies that have contributed to the advancement of cryogenic technology.

The insulation systems that are of primary importance for future application are those using the sliced foam spacers, the net type spacers, the glass fiber paper spacers, and the Superfloc system which consists of tufts of dacron fibers flocked on the surface of the radiation shields. The practical application of these systems to large tankage requires the use of a panel system for ease of fabrication and installation and to provide accessibility to underlying structure and systems. The fabrication of full scale panels and their application to either tanks or mockups provides information on the effects of fasteners, joints, penetrations, and curvature on the applied density of the system. Additionally, these studies provide a basis for ranking systems as to their fabricability, fabrication cost, reproducibility, susceptibility to damage, materials cost, and tooling costs.

FOAM SYSTEMS

One of the first panelized insulation systems developed was the GAC-4 system developed under contract by Goodyear Aerospace Corporation. In this system multiple layers of sliced rigid polyurethane foam and aluminized Mylar are sandwiched between structural glass fiber grids and are stitched with drop threads to form a panel [1].

The development of this system has advanced through materials selection, calorimeter tests, subscale tests, and design phases until finally it has been fabricated and applied to a 2.67-m (105-in.) diameter cryogenic tank. Thermal vacuum tests will be performed at MSFC.

The system designed for the 2.67-m (105-in.) diameter tanks consists of two layers of 2.84 cm (1.12 in.) thick GAC-4 type panels. The thickness is based upon the use of 27 layers of radiation shields and spacers. The radiation shields are 6.35×10^{-4} cm (0.25-mil) Mylar metallized on both sides with aluminum to obtain a room temperature emittance of 0.035 or less. The spacers are rigid polyurethane foam with a nominal density of 28.84 to 30.44 kg/m^3 (1.80 to 1.90 lb/ft^3) and a nominal thickness of 0.069 ±0.008 cm (0.027 ±0.003 in.).

The layer thickness of the panels was based upon the thickness of the single-layer system originally selected for the Multiple Docking Adapter (MDA). The single-layer GAC-4 system was designed, fabricated, and installed on the 2.67-m (105-in.) tank by Goodyear, and a sled test was run at Holloman AFB, New Mexico, to simulate ascent acceleration loads. Subsequently the tank was returned to MSFC where the second layer of insulation was fabricated and installed for a thermal vacuum test to determine the system's effectiveness for thermal protection of liquid hydrogen tanks for space storage of up to 30 days.

For the sled test the tank was configured with a three-point support system. The tank with the single-layer insulation system installed is shown in Figure 1. Subsequently the insulation system was removed, and the tank was modified to provide a single combination structural support and fill and vent line.

The fabrication of GAC-4 type insulation panels is described in detail in Reference 1; however, the key features of the process are discussed in the following paragraphs.

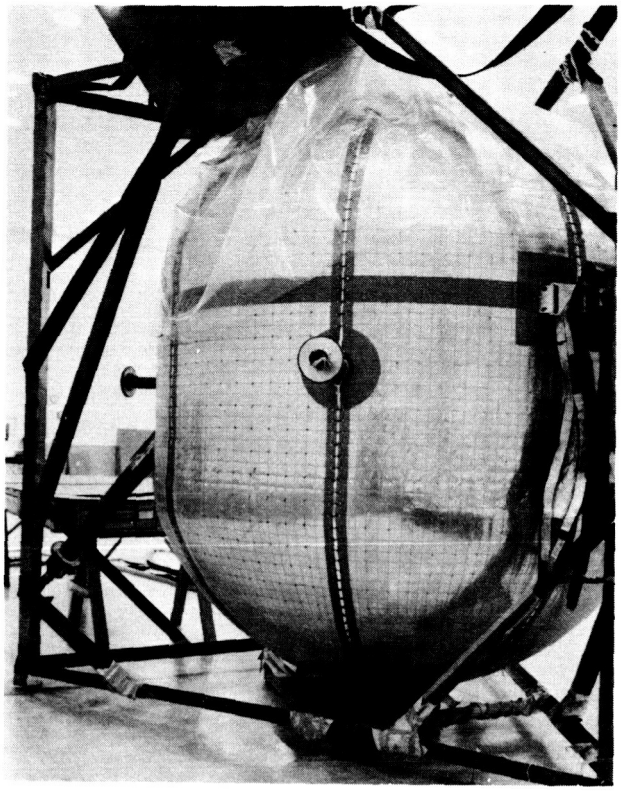

Figure 1. Single-layer GAC-4 insulation on 2. 67-m tank.

Foam Spacer Preparation

Sheets of sliced polyurethane foam are placed on a vacuum screen table and the dust is removed with an ionized air gun (Fig. 2). The sheets are trimmed to a 4. 88-m (16-ft) length with a butt joint between the panels. Annealed, adhesive-coated Mylar strips are then bonded along each long edge and across the butt joint (Fig. 3). The foam sheet is then carefully rolled up in brown paper and placed in temporary storage (Fig. 4).

Radiation Shield Preparation

A roll of 6. 35 $\times$ 10^{-4} cm (0. 25-mil) Mylar, 1. 22 m (48 in.) wide, aluminized on both sides is mounted on the end of a clean flat table. Sheets approximately 4. 88 m (16 ft) in length are rolled out onto the table, taped down, and trimmed. Slits are cut in the Mylar as required to allow it to conform to the compound surfaces (Fig. 5).

Grid and Skin Assembly

The grid skin assemblies are layed up on hard surface forms or molds that are capable of withstanding repeated temperature cycles between 149° C (300° F) and room temperature without deforming or changing the dimensional attributes of the tool. A layup tool fabricated from a high temperature fiberglass laminate as shown in Figure 6 was used. Layup tools representing the inner and outer surfaces of each panel were required. The surfaces of the tools are scribed to locate the edge bands and fiberglass rovings, and they have tooling holes that can be used when the grid is transferred to the panel assembly tool. The tool is prepared, and the type 181 epoxy prepreg stock for the edge bands is layed up on the tool along with additional stock for local reinforcements as required. The urethane-coated fabric used to protect the outer surface of the insulation is applied, and then the "longo" and "circo" 20-end prepreg glass rovings are layed down to form the grid. The rovings are spot-bonded with a small tip heating iron at each intersection and to the edge bands. The layup is then vacuum bagged and placed in an oven for curing. After curing, the assembly is removed from the mold and rough trimmed to within 0. 64 cm (0. 25 in.) of the theoretical trim line. The completed grids are layed out on the tank and marked for bonding of the zippers to the inner grids. The grids with the zippers attached are installed on the tank and checked for fit before panel assembly is begun.

Panel Assembly

An inner fiberglass grid is located on the panel assembly fixture. Strips of 2. 84 cm (1. 12 in.) thick flexible foam spaced approximately 30. 48 cm (12 in.) apart are taped to the grid. The outer grid is then positioned over this and marked for trimming and installation of eyelets. The flexible foam is removed and, beginning with aluminized Mylar, alternate layers of Mylar and foam are layed up. The Mylar layer is taped down as it is installed with the slit ends overlapped and taped to form a smooth layer. The foam is likewise taped down as it is installed; however, the overlap in foam layers is trimmed out to prevent excessive buildup. After the final layer of Mylar is layed up, the outer grid is located and the drop threads are installed on 10. 16 cm (4 in.) centers. The sewing operation is shown in Figure 7.

Panel assembly is completed by trimming the panel using a rotary cutter knife and the trimming

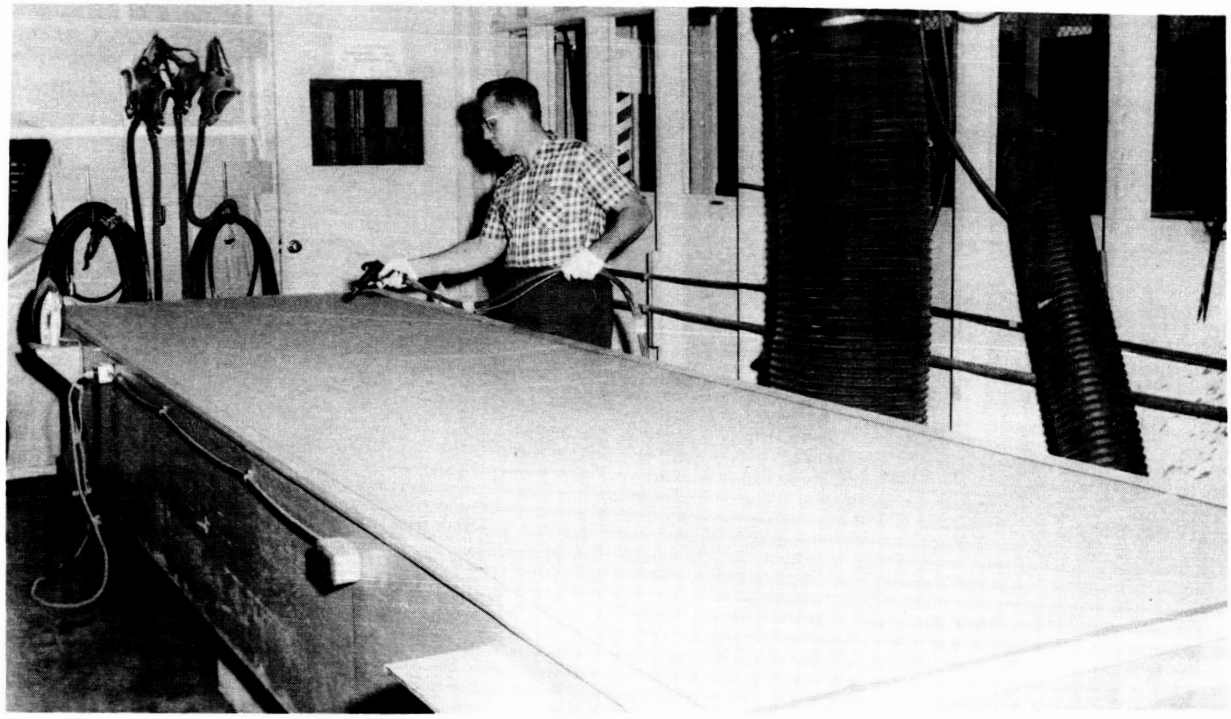

Figure 2. Removing dust from foam spacer.

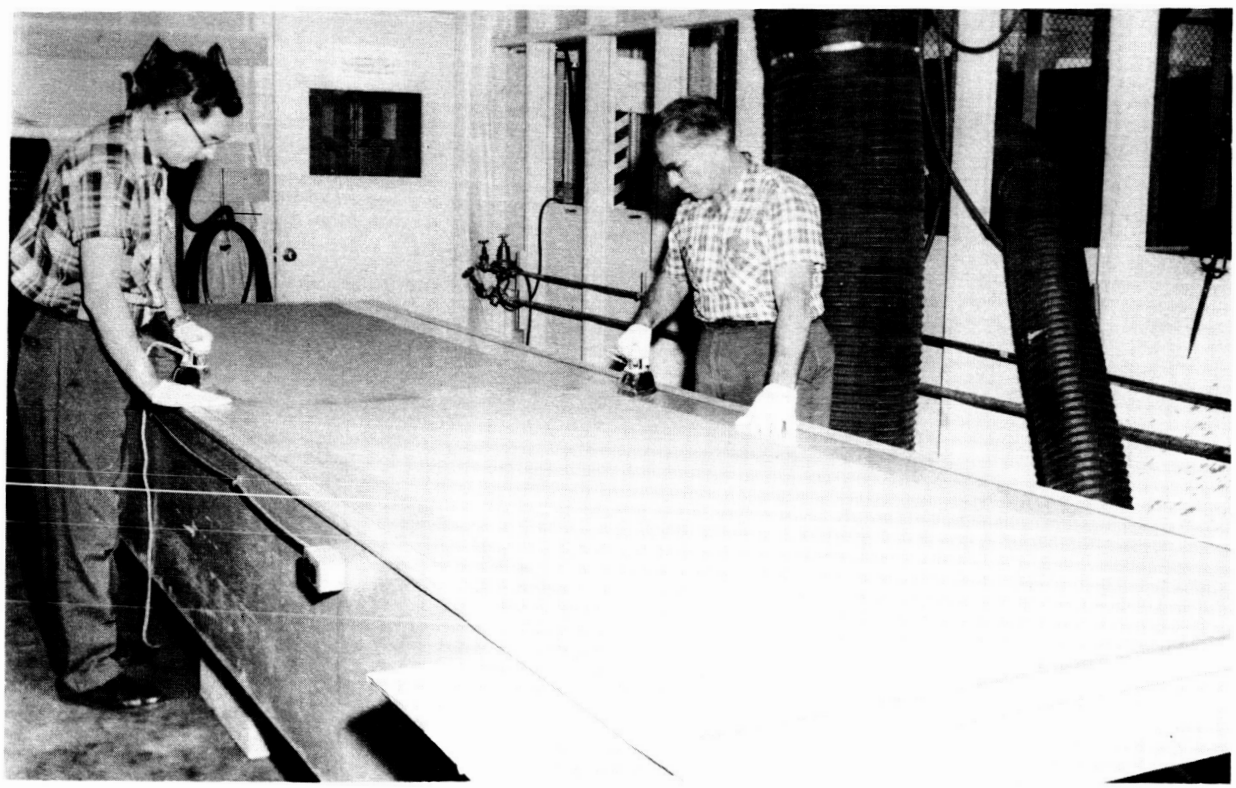

Figure 3. Bonding Mylar strips to foam spacer.

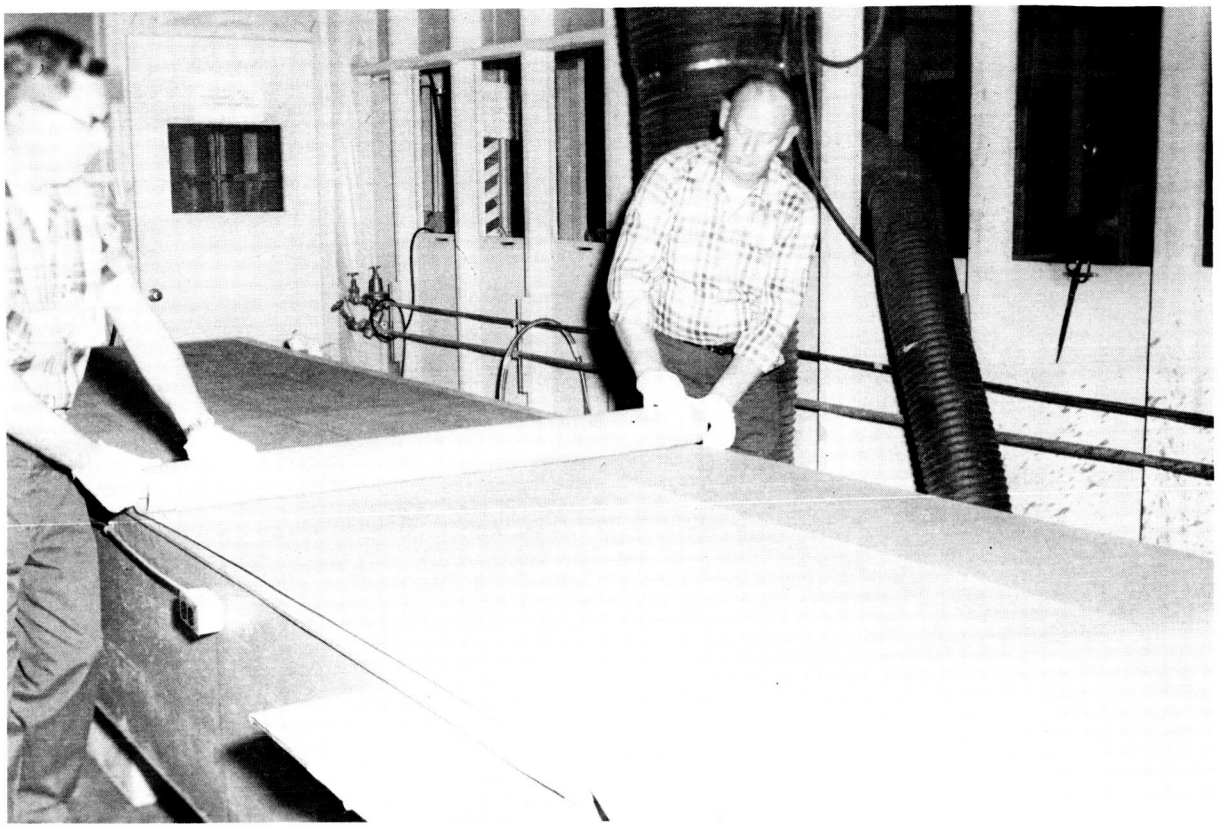

Figure 4. Rolling foam spacer for storage.

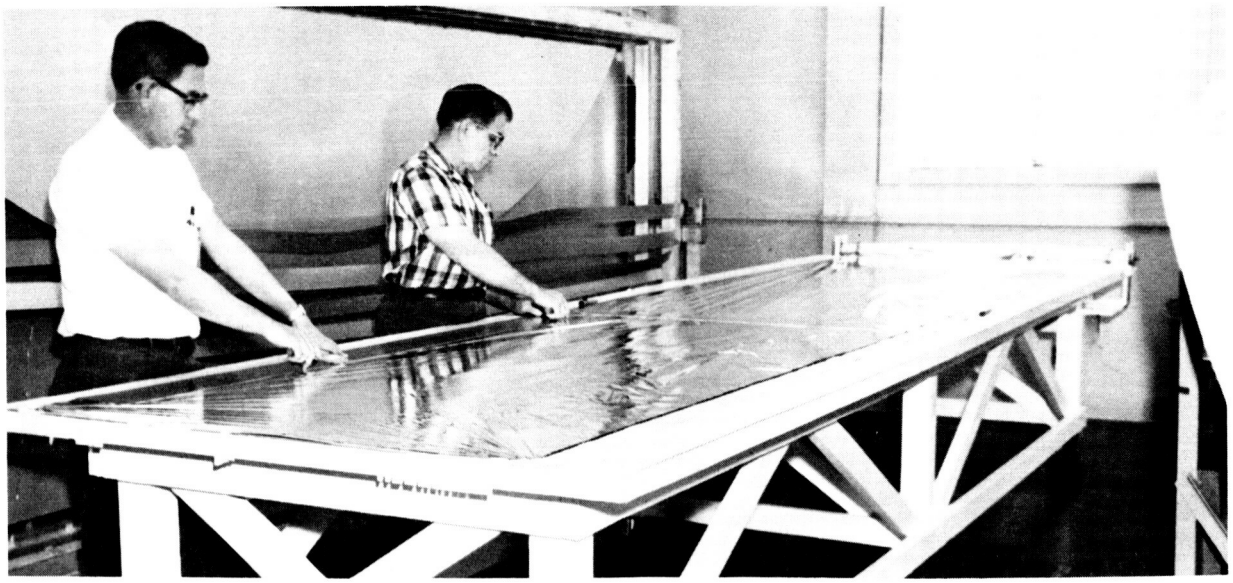

Figure 5. Slitting aluminized Mylar radiation shield.

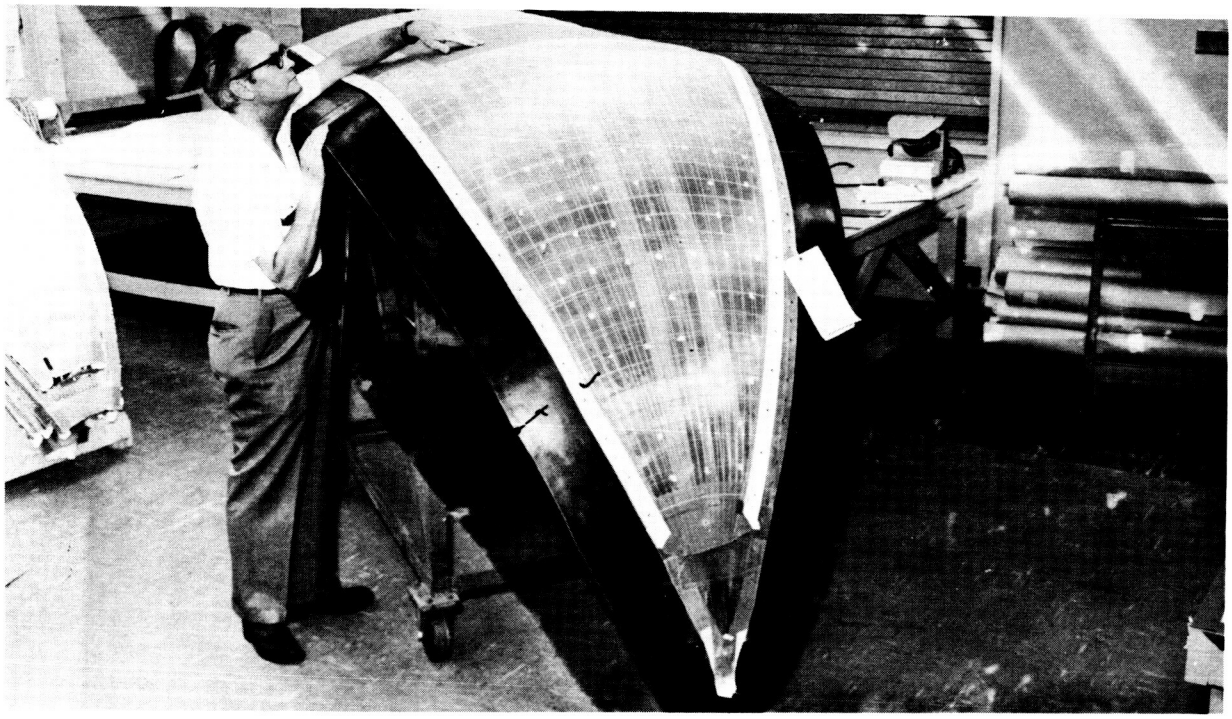

Figure 6. Fiberglass grid.

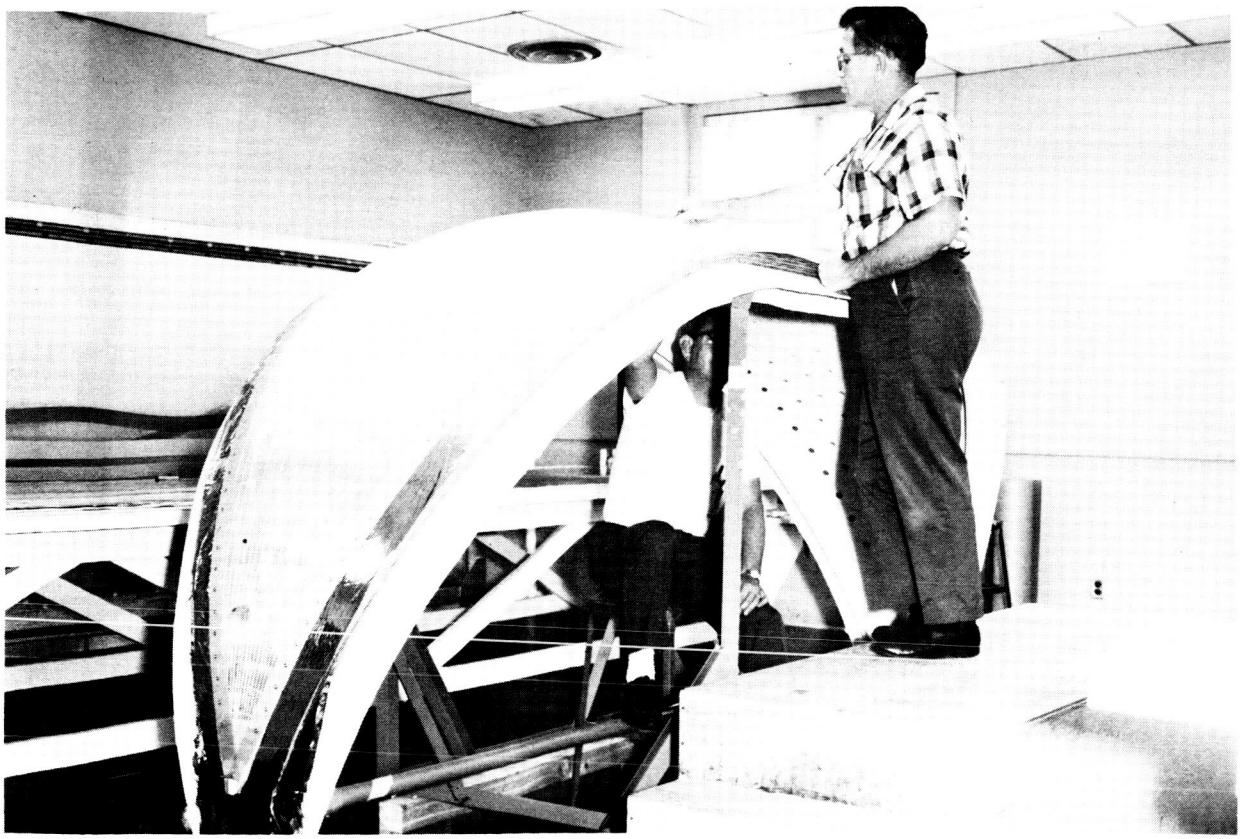

Figure 7. Attaching grids to insulation layup.

fixture. Alternate methods used included a straight edge and a razor knife.

The installation of the panels on the tank is accomplished using the zippers on the inside of each panel and by tying through the eyelets on the outside with a tie cord (Fig. 8).

It was concluded from this study that the design approach was sound and could be applied to tanks of 2.67 m (105 in.) diameter or larger. The grid assemblies impart a degree of rigidity to the panels making them easy to handle and also provide excellent dimensional control of the finished panel. The zippers on the back of the panels are a good solution to the structural problem of connecting the backs of the panels. The lacing of the outer joints provides a means for controlling the gap between panels. The feasibility of using low cost plastic tooling for double curvature panels was demonstrated. The use of knife edge cutting blades in a band saw, or rotary cutter, and hand tools proved to be the most effective cutting methods.

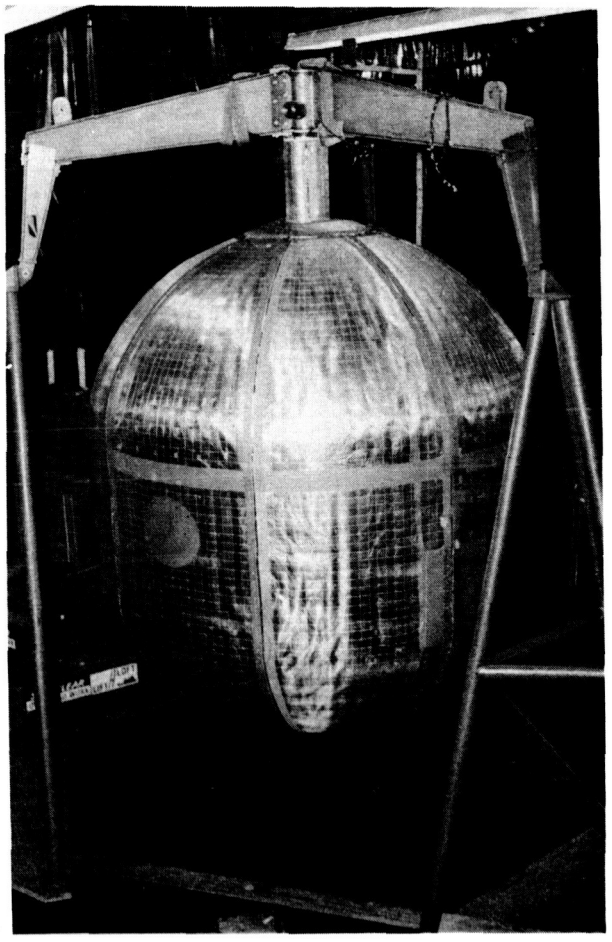

Figure 8. Installation of tie cords.

NET SYSTEMS

Net type materials have been considered by a number of investigators as potentially good spacer material. Nets of a variety of materials have been studied including those made of nylon, silk, dacron, glass, terylene, and polypropylene.

Early investigations were limited to calorimeter and small scale tests. However, in 1967 a study was performed by The Boeing Company to develop manufacturing techniques for application of high performance cryogenic insulation to a 5.08-m (200-in.) torus tank [2]. The multilayer insulation system was required to have a thermal conductivity of 8.67 W/m °K (5×10^{-5} Btu/hr ft °R) or less, a density of 24.3 kg/m^3 (1.5 lb/ft^3), a thickness of 12.70 to 15.24 cm (5 to 6 in.), and good manufacturing producibility and repeatability. The resulting design and detailed manufacturing plan were applicable to insulations using spacers of silk or nylon netting, rigid polyurethane foam, or sliced 1.91-cm (0.75-in.) cell Mylar honeycomb.

In 1968 a follow-on study was performed to demonstrate the manufacturing techniques proposed in the above study [3]. For this study a full scale 45-deg section of the 5.08-m (200-in.) torus tank was fabricated from wood and used to evaluate the application of the insulation system (Fig. 9). The insulation system was composed of five blankets of 2.54 cm (1.0 in.) thick insulation composed of alternate layers of nylon tulle and perforated aluminized Mylar film encapsulated in nylon net. The insulation blankets were attached to the mockup with a combination of plastic studs, nylon threads, and hooks.

Insulation Blanket Fabrication

The insulation blankets were fabricated by laying up the insulation system on a cutting table (Fig. 10) and using flat pattern templates to cut the material to size (Fig. 11). Both ends of the blanket were scarfed by cutting back 1.27 cm (0.5 in.) from the edge of the succeeding cut on every fifth layer in the 55 layer composite to give a smooth taper joint. Nylon tulle, identical to the spacers, was applied to the top and bottom faces and sewn on the edges with

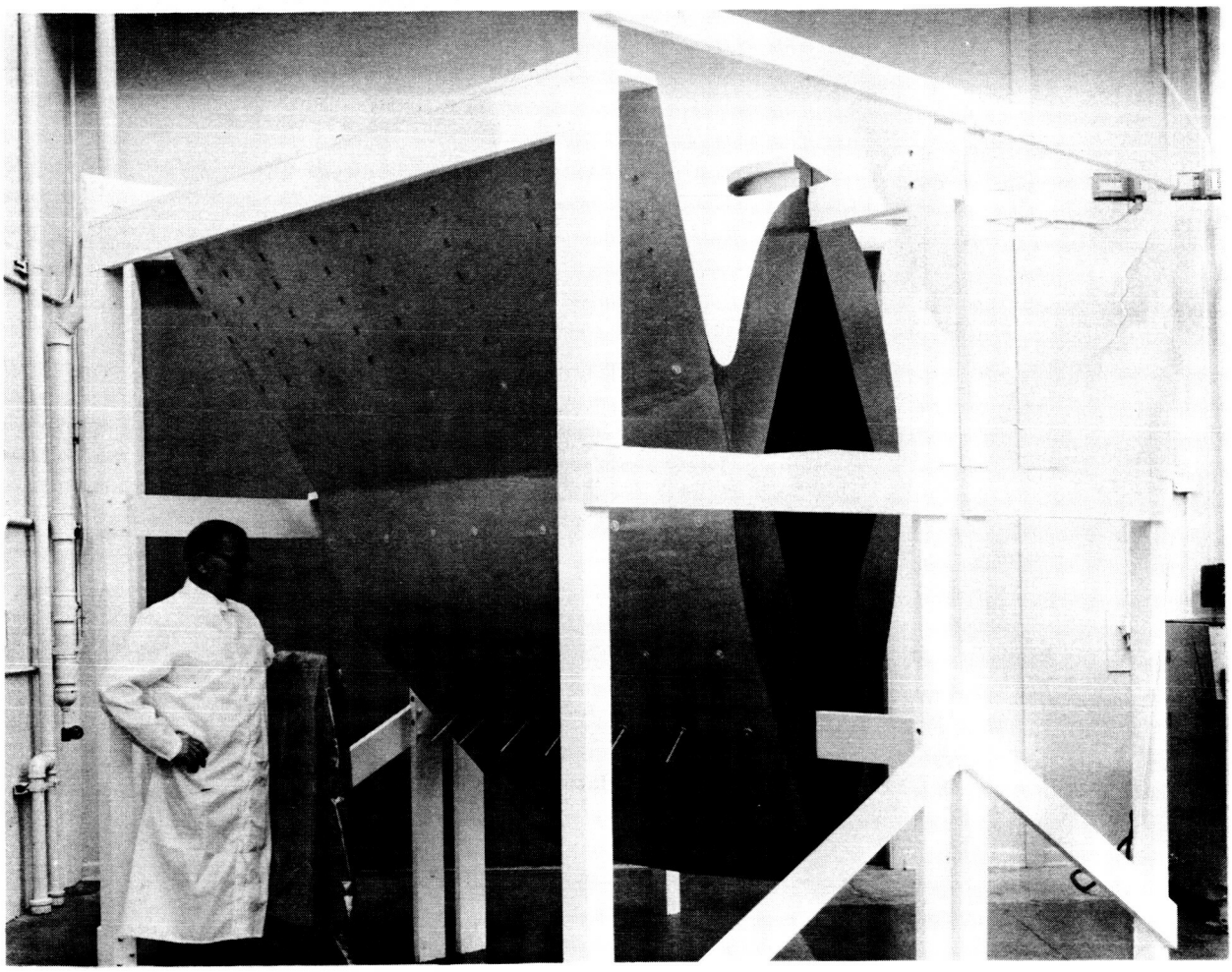

Figure 9. Mockup of torus tank section.

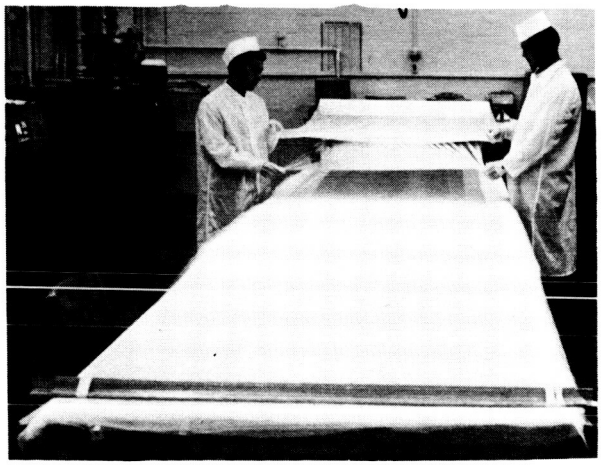

Figure 10. Laying up nylon net/aluminized Mylar insulation.

nylon thread. Buttons and threads were installed on approximately 20. 3-cm (8-in.) centers to prevent lateral shifting of the insulation layers (Fig. 12). A reinforcement tape was sewn to each end of the blankets for attachment to the support.

Fabrication of the insulation blankets in this fashion posed no special problems except that the insulation panel thicknesses were considerably less than anticipated. Earlier thermal conductivity layer density studies had shown that 55 ±5 layers per inch is the optimum density for nylon tulle-aluminized Mylar multilayer insulation. This manufacturing study and subsequent studies have shown that one cannot design to optimum layer density values because it is impossible to obtain them in a real system.

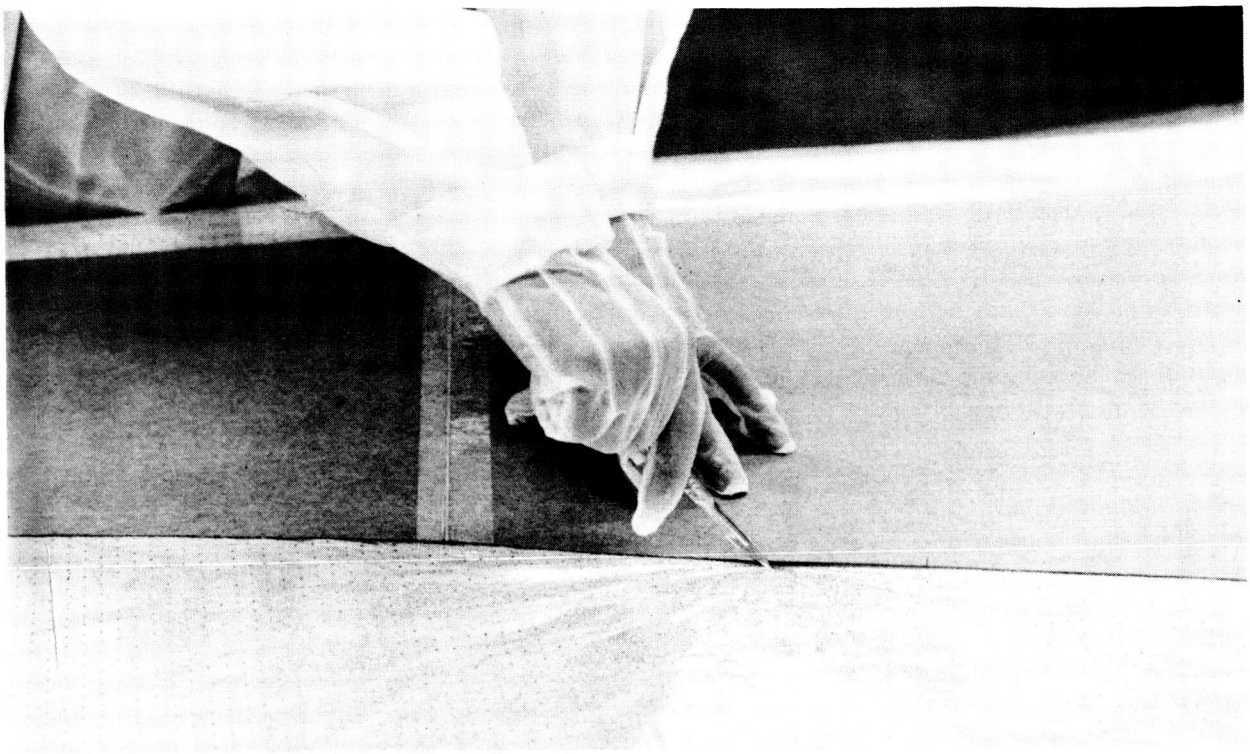

Figure 11. Cutting insulation layup to pattern.

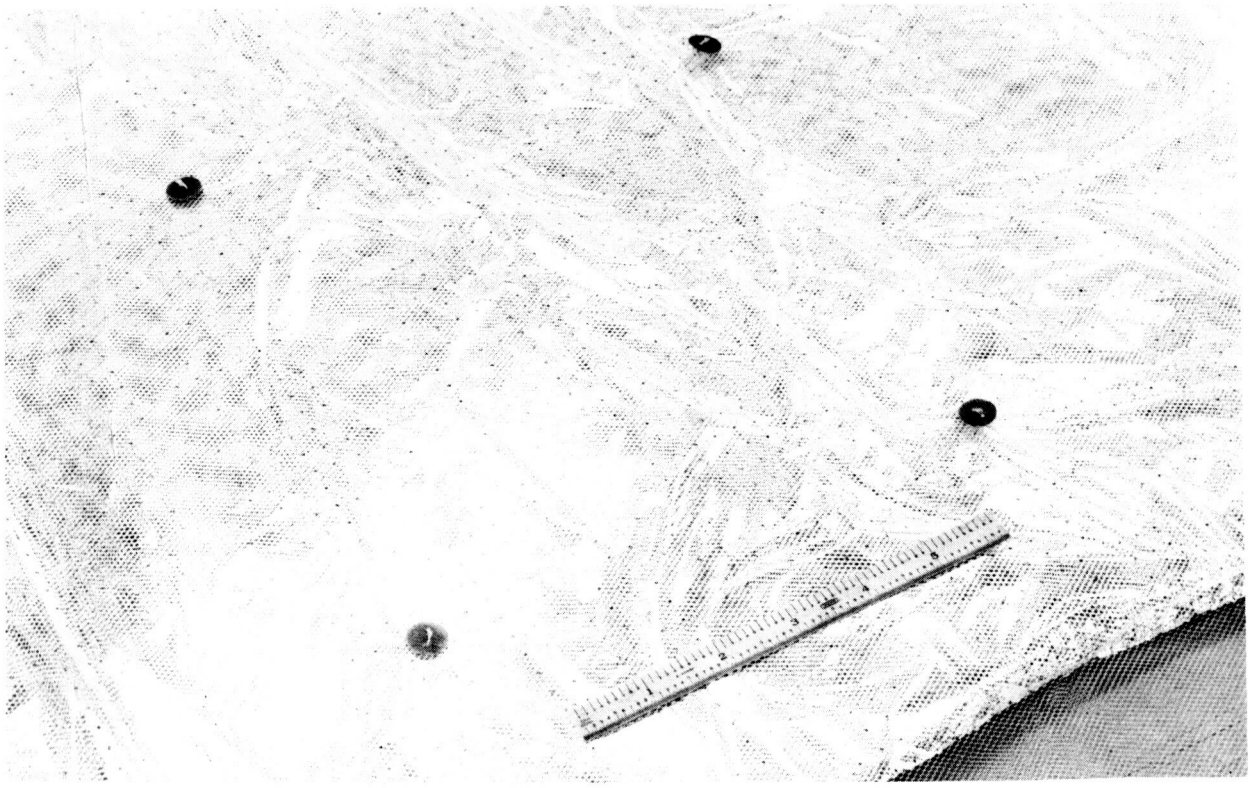

Figure 12. Button and thread installation in insulation blanket.

Installation of Insulation Blankets

The insulation blankets were installed on the tank mockup by marking the position of insulation support studs, followed by marking a hole at each location. The blanket was then installed over the studs, and the retainers were installed and bonded in place. The thread retainers were inserted through the blankets approximately perpendicular to the tank surface. The panels were then attached to the skirt by passing threaded loops over the support clips and tensioning until snug (Fig. 13). The opposite end of the blanket was sewn to the support net assembly using nylon thread (Fig. 14). The blanket butt edges were sewn together with nylon thread to prevent gaps in the insulation blanket.

Installation of the blankets on the mockup presented the problem of compaction of the blankets over areas such as the sump and the upper support studs. This compaction cannot be avoided with this type of insulation at this thickness; however, some improvement can be made by more careful location of holes for the stud support. The thread retainers proved to be totally unsatisfactory because of the difficulty in penetrating the blankets with the thread perpendicular to the tank and in line with the attach buttons bonded to the tank. This caused improper tensioning of each layer. The use of segmented stud supports would alleviate the problem with a slight penalty to the total insulation heat flow.

More extensive studies were performed by McDonnell Douglas Astronautics Company — Western Division on 12 different multilayer insulation systems to rank them on a fabricability basis. Systems using nylon net and dacron net were ranked first and second. This ranking considered fabrication cost, predictability, susceptibility to damage, and material cost [4].

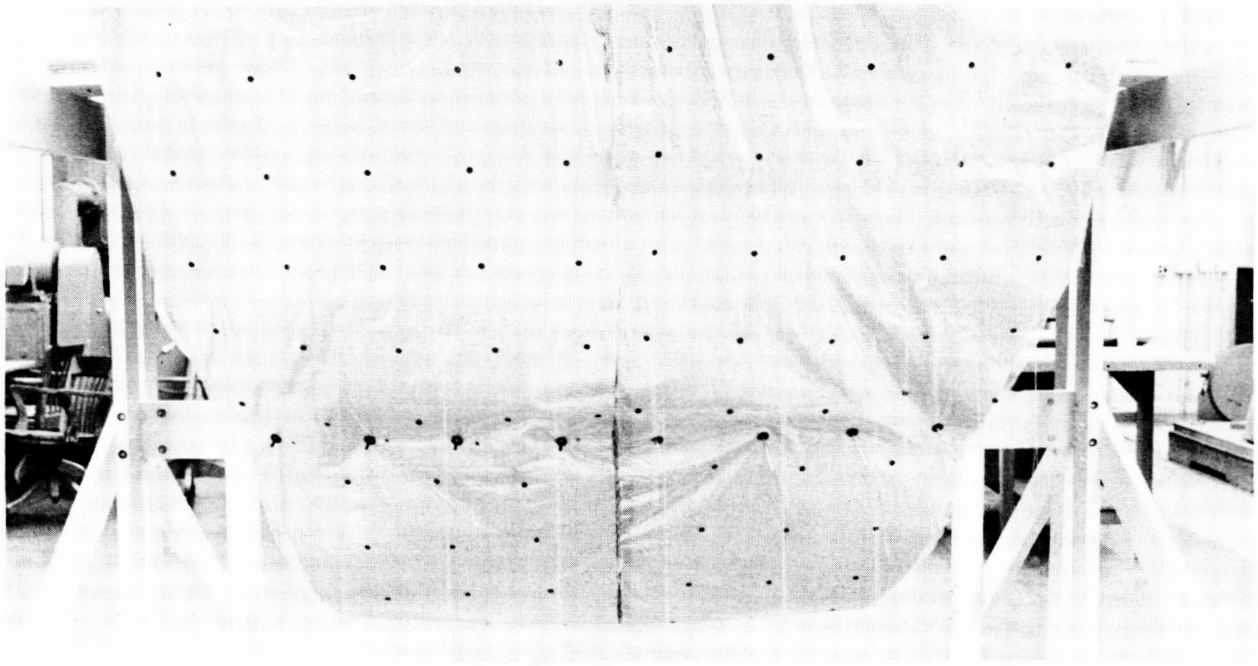

Figure 13. Installation of insulation blankets.

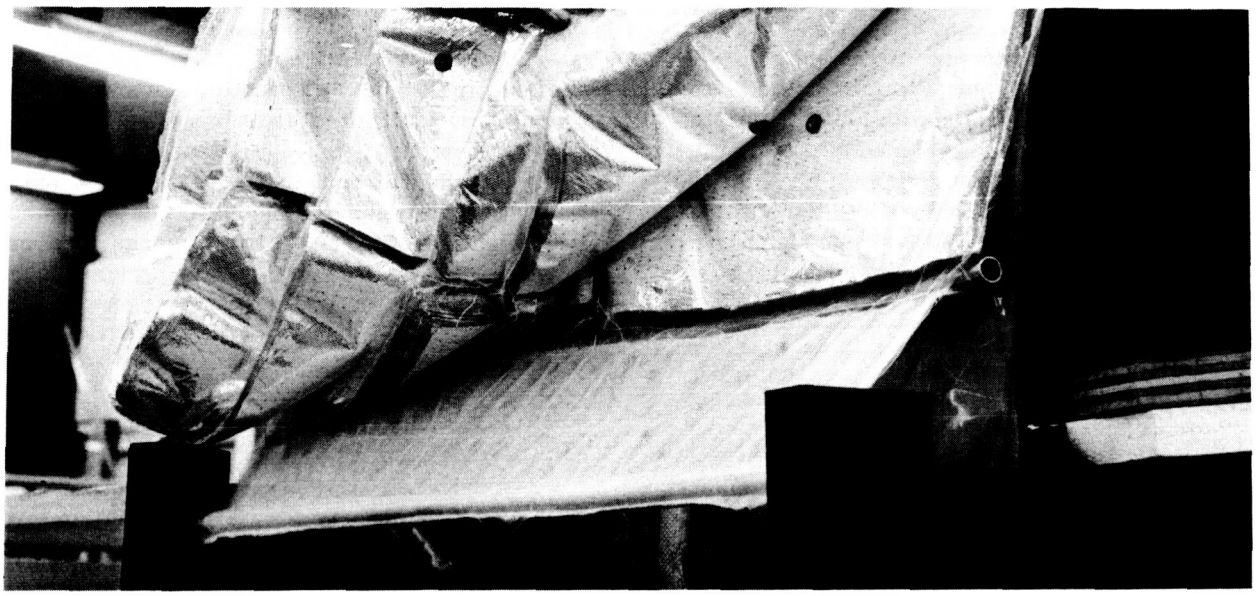

Figure 14. Attachment of blankets to support net.

Application of a Net System

A study was undertaken by Goodyear Aerospace Corporation to perform design studies and materials and manufacturing process investigations, and to provide engineering documentation and manufacturing plans for a purged multilayer high performance insulation system for a 2.67 m (105 in.) diameter tank [5]. A requirement of the study was that the multilayer system should consist of alternate layers of aluminized Mylar reflective shields and net spacers in panels or blankets. The thermal performance objective was a thermal conductivity of less than 1.43 W/m °K (1.4×10^{-5} Btu/hr ft °F) between 540° R and 40° R with a natural density of 36.9 kg/m^3 (2.3 lb/ft^3) or less.

The study built on previous attempts to design and fabricate a multilayer insulation using net spacers. Fiberglass grids similar to those used with the GAC-4 foam type system were selected for this application. Over 100 commercially available net spacer materials were reviewed in an effort to find a suitable off-the-shelf material. However, none of these met the insulation density objectives, and a custom woven dacron net, style B/4B, was selected for thermal evaluation and verification of the design on a mockup of the 2.67-m (105-in.) tank. The mockup represents the critical section of the tank, the intersection of the upper bulkhead and the conical support. A view of the mockup with the demonstration panels installed is shown in Figure 15.

Insulation Panel Fabrication

One blanket was fabricated for the upper bulkhead and one for the conical support to verify the design. The grids for the conical support were fabricated on a flat plate using techniques similar to those developed for the GAC-4 system. The grids for the bulkhead panel were fabricated on the mockup itself. An assembly fixture was made for the conical panel. A section of the mockup was drilled and used

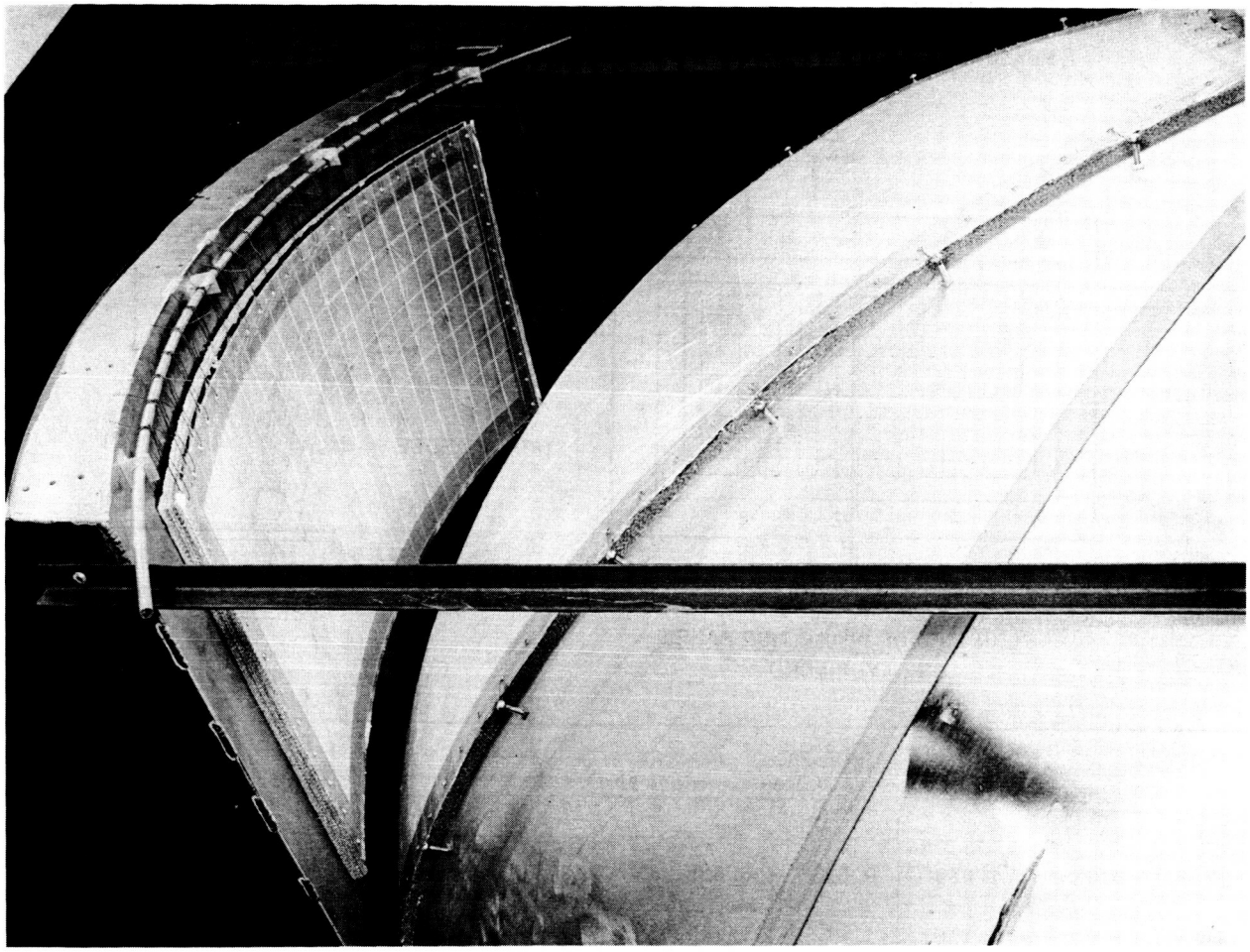

Figure 15. Insulation panels on mockup of cone-supported, 2. 67-m tank.

for assembling the bulkhead panels. Fabrication of the panels was straightforward using techniques previously described. The discrepancy between the predicted 88 layers per inch and the actual thickness achieved on the layup mold may be seen in Table 1. The number of layers was increased to 110 in an effort to attain the desired 2. 54 cm (1 in.) thickness. However, the center area remained 3 to 12 percent low. The average panel thickness was 2. 21 cm (0. 87 in.). The layup of the bulkhead panel also required more layers of insulation than the predicted 88 layers per inch (Table 2). For this panel, an additional 11 layers were added in an attempt to reach the desired 2. 54 cm (1 in.) thickness. With the addition of the 11 layers a dimensional check showed an average thickness of 2. 54 cm (1 in.) in all areas except the knuckle radius area. This area was close to the trim line, and the thickness deficiency was attributed to the combined effects of a small radius of contour and the localized tension and compression resulting from taping the insulation layers during the layup process. It should be noted in the table that there was considerable recovery of thickness in the knuckle area after trimming.

The basic fabrication techniques developed on earlier programs adapted well to the dacron net panels. Cutting a composite of net spacers and aluminized Mylar required compression of the insulation in the area to be trimmed to prevent movement of the spacers and tearing of the shields (Fig. 16). Knife-edged tools must be kept sharp to avoid snagging the nets. Multilayers with net spacers are very soft and yield under light loads. The tying of drop threads required extra care to avoid compression of the insulation. Panels with net spacers distort easily; therefore, they should be handled on contour forms that will retain the fabricated shape.

TABLE 1. CONICAL INSULATION PANEL THICKNESS CHECK DURING PANEL FABRICATION

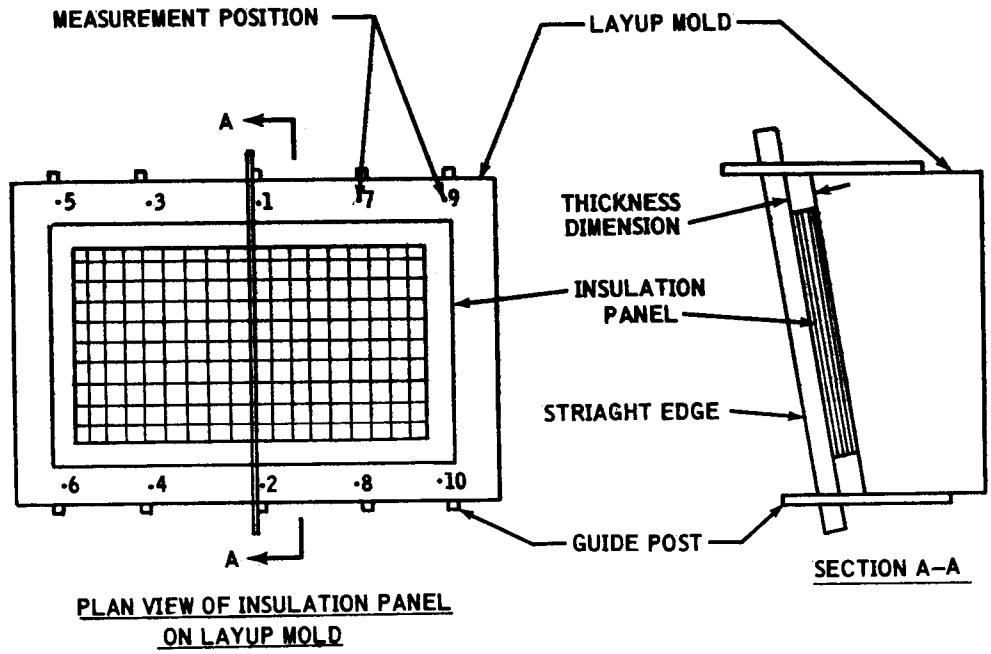

Number of Shields	Measurement at Positions Shown Above (cm)									
	1	2	3	4	5	6	7	8	9	10
22	0.635	1.635	0.635	0.635	0.762	0.635				
44	1.031	1.110	1.110	1.110	1.27	1.189				
66	1.422	1.549	1.524	1.506	1.753	1.524				
88	1.727	1.854	1.803	1.930	2.286	2.057				
110	2.223	2.459	2.301	2.380	2.54	2.54	2.464	2.301	2.54	2.54
After Top Grid[a]	2.058	2.058	2.109	2.134	2.159	2.134	2.134	2.210	2.286	2.286
After Top Grid[b]	2.032	1.981	1.956	1.956	2.032	1.981	2.007	2.032	2.058	2.134

a. After sewing of drop threads and 3 days settling.
b. After 4 weeks settling.

TABLE 2. THICKNESS MEASUREMENTS RECORDED DURING FABRICATION OF DOME INSULATION PANEL

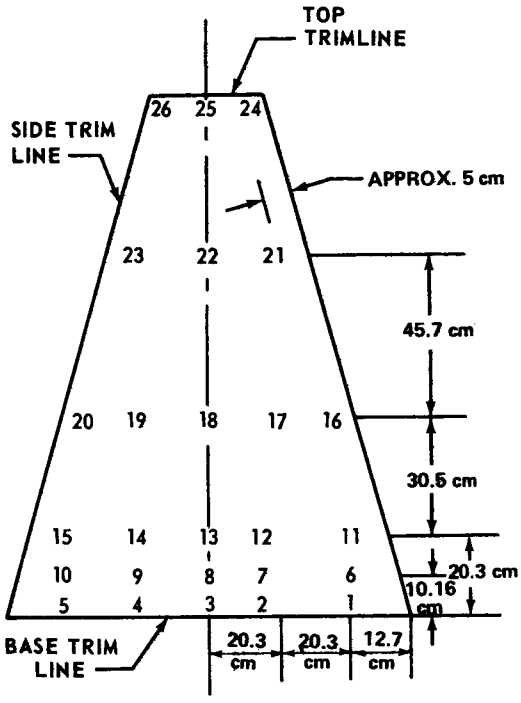

THICKNESS MEASUREMENT LOCATIONS – 69QS1786 PANEL

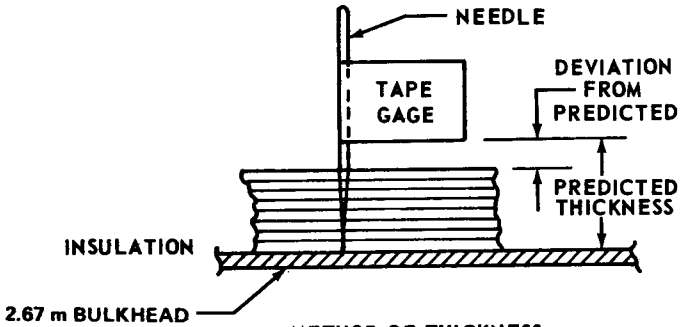

METHOD OF THICKNESS MEASUREMENT

	Panel Thickness (cm)								Panel Thickness (cm)						
	Layer 22	Layer 44	Layer 50	Layer 66	Layer 88	Layer 99	Layer 99[a]		Layer 22	Layer 44	Layer 50	Layer 66	Layer 88	Layer 99	Layer 99[a]
1	0.30 Ave.	0.97 Ave.	0.792	1.270	1.588	1.745	2.380	15					2.380	2.380	2.380
2			0.953	1.427	1.745	1.745	2.141	16	0.30 Ave.	0.97 Ave.	1.031	1.666	1.984	2.301	1.905
3			0.792	1.270	1.745	1.905	2.223	17			1.270	1.824	2.54	2.616	2.54
4			0.953	1.427	1.588	1.666	2.141	18			1.349	1.745	2.54	2.616	2.54
5			0.953	1.270	1.824	1.905	2.380	19			1.189	1.745	2.380	2.54	2.54
6				1.524	1.905	1.905	2.103	20			1.109	1.745	2.380	2.54	2.380
7				1.587	1.984	2.223	2.54	21	0.46 Ave.	1.09 Ave.	1.031	1.524	2.380	2.223	2.301
8				1.587	1.984	2.223	2.54	22			1.270	1.824	2.459	2.692	2.459
9				1.587	1.905	2.223	2.54	23			1.109	1.824	2.54	2.616	2.616
10					2.223	2.223	2.380	24			1.109	1.745	1.984	2.380	2.380
11				1.587	2.062	2.062	2.223	25	0.30 Ave.		1.109	1.905	2.54	2.692	2.54
12				1.745	2.223	2.380	2.54	26			1.109	1.905	2.38	2.616	2.54
13				1.666	2.223	2.380	2.616	b	0.64	1.270	1.43	1.91	2.54	2.69	2.69
14				1.824	2.223	2.380	2.616								

a. After trim plus 4 days.
b. Predicted thickness based on 88 layers/inch.

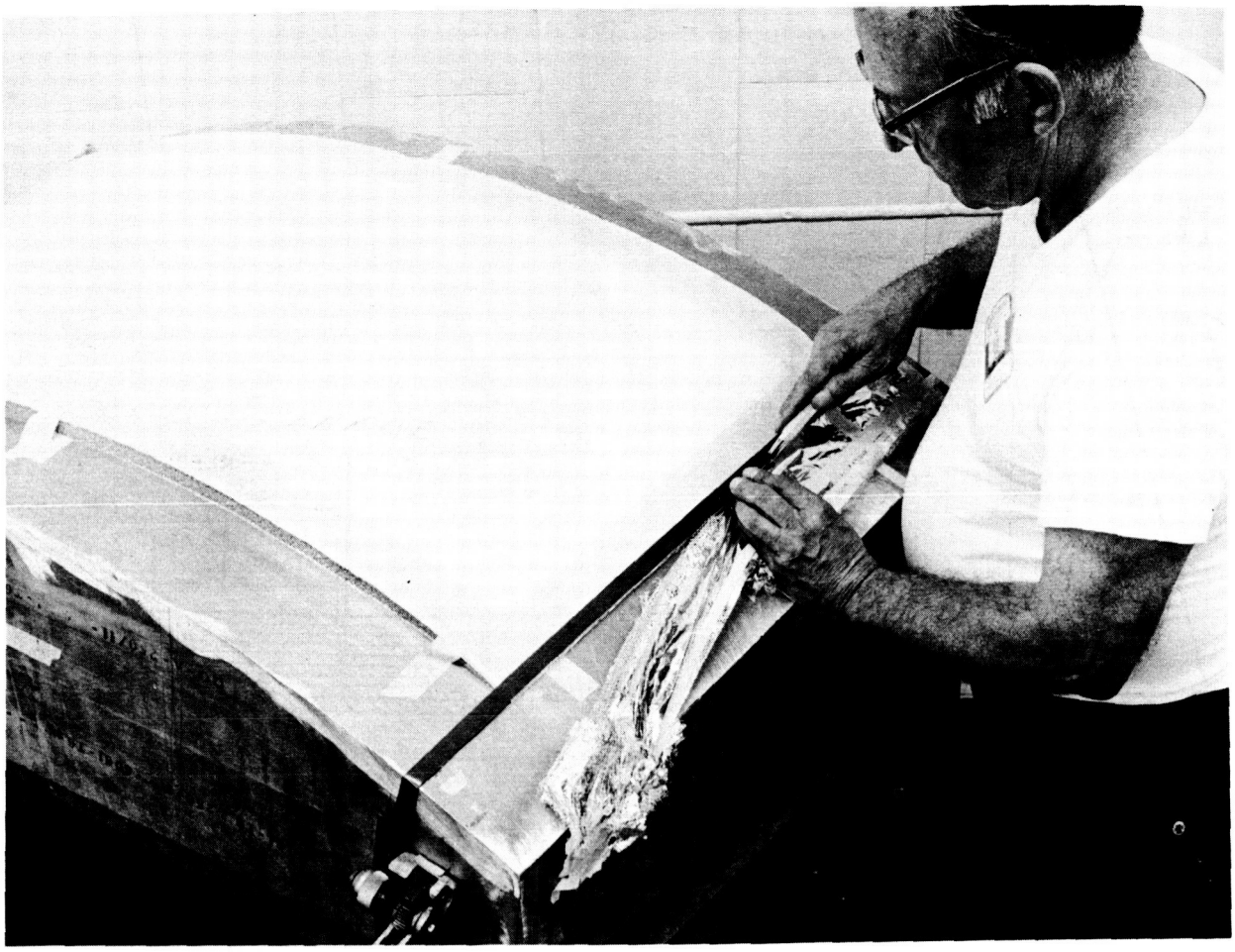

Figure 16. Trimming insulation panel.

GLASS FIBER PAPER SYSTEMS

The two glass fiber paper systems that have been studied extensively are:

1. Tissuglass — A borosilicate glass fiber paper manufactured by Palflex, Inc. with a nominal thickness of 1.52×10^{-5} m (0.6 mil) and a nominal density of 224.28 kg/m^3 (14 lb/ft^3).

2. Dexiglass — A borosilicate glass fiber paper manufactured by C. H. Dexter and Sons with a nominal thickness of 7.11×10^{-5} m (2.8 mil) and a nominal density of 200.25 kg/m^3 (12.5 lb/ft^3).

Of the two, the tissuglass spacer is preferred on the basis of fabricability studies as well as the lower thermal conductivity and density of the composite insulation. Studies of this system have been performed by Lockheed Missiles and Space Company (LMSC) and McDonnell Douglas Astronautics Company — Western Division (MDAC-W). As a result of in-house studies at LMSC and studies performed by LMSC under contract NAS8-20758 [6], a design was evolved that improved the fabricability of the fragile paper systems. The insulation materials were encapsulated in dacron net with reinforced dacron webbing (Fig. 17). The insulation materials were prevented from shifting by using a heat-sealed nylon stud and button concept (Fig. 18). In these studies panels were layed up flat and then draped around the contoured tank. Inconsistencies in layer density caused by wrinkling of the insulation are unacceptable because of the resulting uncertainties in thermal performance.

A subsequent study performed by MDAC-W has shown the improvements that can be made in layer density control by fabricating the blankets on a contour tool. In this study of high performance insulation

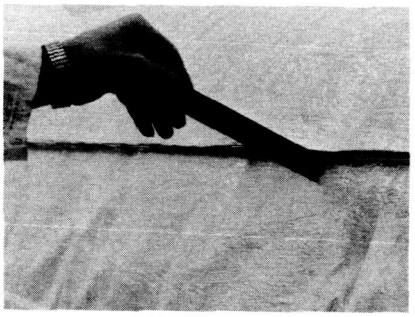

Figure 17. Tissuglass/aluminized Mylar insulation blankets.

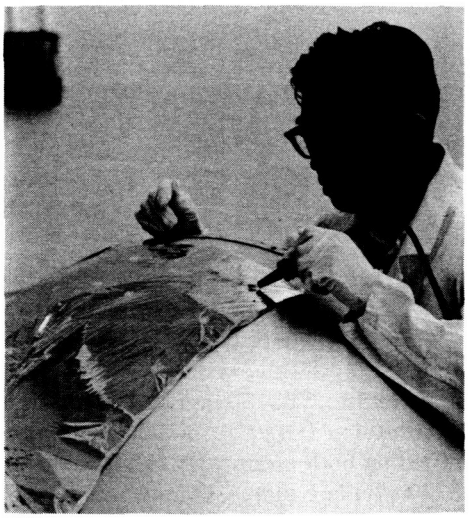

Figure 18. Heat sealing nylon button and stud.

application problems, contract NAS8-21400, full scale mockup sections of the modular nuclear vehicle (MNV) forward dome and sidewall were fabricated and used to demonstrate the fabricability and design feasibility of insulation blankets for this application.

Shown in Figure 19 is the mockup of a section of the MNV forward dome. The surface represents the contour of the 10.06 m (33 ft) diameter $\sqrt{2}$ ellipsoidal dome. The mockup is approximately 1.83 m (6 ft) wide at the base where the dome joins the

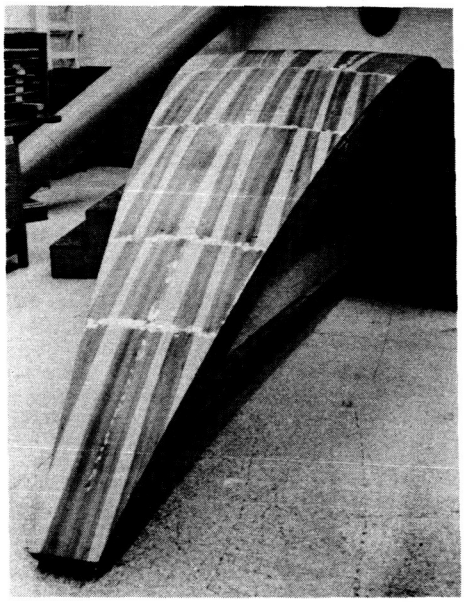

Figure 19. Mockup of 10.06-m ellipsoidal dome.

cylinder. The mockup served two purposes: (1) it provided a cutting and layup surface for blanket fabrication, and (2) it served as a mockup for demonstrating insulation production methods. A mockup of similar construction was used for the sidewall of the cylinder. It was 1.22 m (4 ft) wide by 4.88 m (16 ft) long and was curved to simulate the 10.06 m (33 ft) diameter of the tank.

The need for contouring the insulation during fabrication is shown in Figure 20 where a single layer of 15 gauge Mylar is layed up on the dome mockup. Note the wrinkled areas even on this large contour. In the fabrication of blankets it was necessary to make contour cuts, overlap, and tape each radiation shield to obtain reasonably good layer density control (Fig. 21).

A fiberglass top plate tool (Fig. 22) was used to control blanket thickness (density). The tool is positioned above the layup surface and is applied after the blanket components have been stacked. The tool is supported at the edges by machined spacers to control panel thickness. The tool has holes that match those in the mockup for insertion of the

Figure 20. Layup of radiation shield on dome mockup.

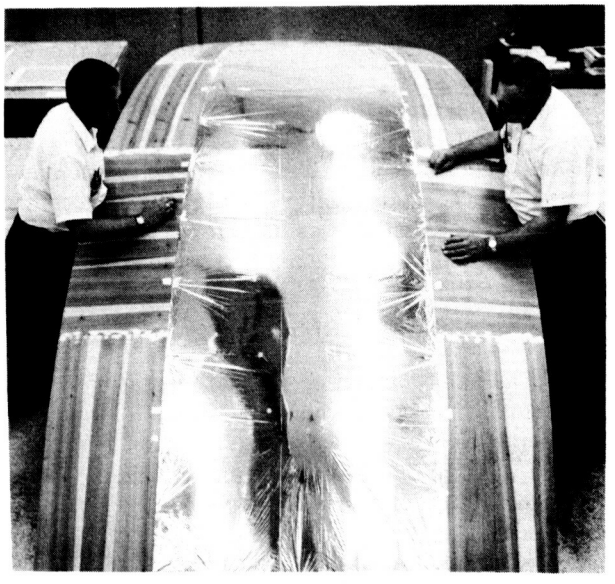

Figure 21. Radiation shield after contour cuts and taping.

fasteners. A completed dome section insulation panel is shown on the dome mockup in Figure 23.

1. General Dynamics/Convair Division trade name.

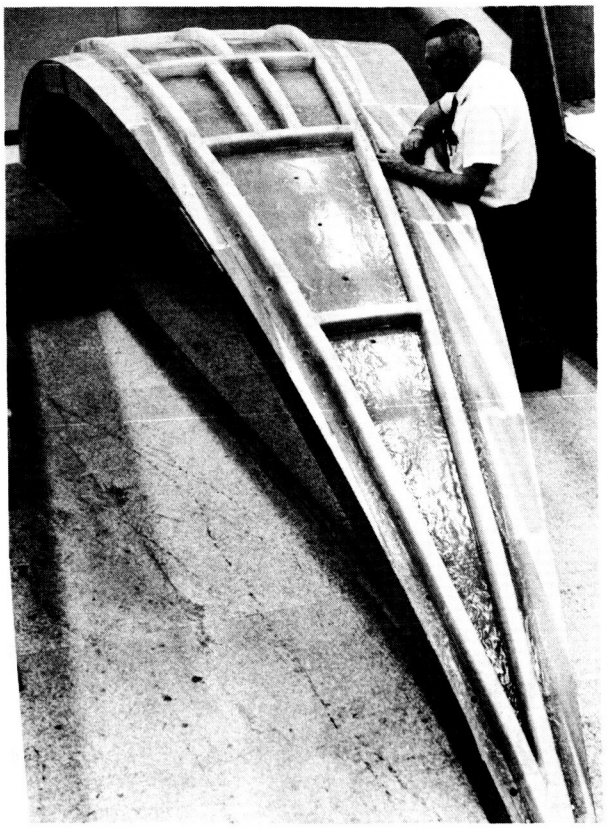

Figure 22. Fiberglass top plate tool.

SUPERFLOC SYSTEMS

Superfloc,[1] developed by General Dynamics/ Convair Division (GD/C), is a thin Mylar film aluminized on both sides with tufts of dacron fibers bonded to it on one side. Film thicknesses of 25 gauge (0.00025 in.) and 15 gauge (0.00015 in.) have been used (Fig. 24). Spacing of the tufts of dacron can be varied according to the application.

This system has a very good thermal performance although it is very sensitive to design treatment and manufacturing techniques. GD/C has demonstrated in IRAD studies and NASA-sponsored studies that manufacturing techniques have been developed and can be applied to make this system workable.

Superfloc systems have been designed and applied to a 63.5-cm (25-in.) tank (Fig. 25) that

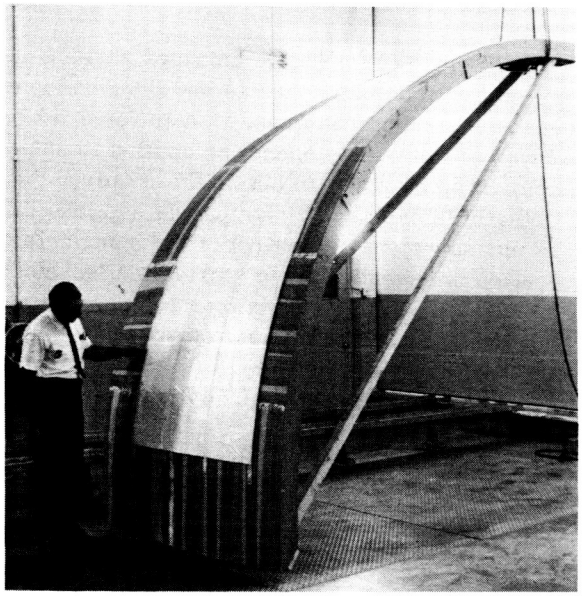

Figure 23. Completed dome insulation blanket on mockup.

was a scale model of the MSFC 2.67-m (105-in.) tank [7] and to a 2.21-m [87-in.] ellipsoidal tank.

Manufacturing techniques used in blanket fabrication are similar in many respects to those used for other systems. Contour tools are used to tailor the individual layers of Superfloc. These are then layed up on a tool and trimmed to size (Fig. 26). Note that strips of polyurethane foam are inserted along the edges of the layup to support the Superfloc during trimming.

CONCLUSIONS

It is concluded that manufacturing technology is available for the application of any of the aforementioned systems to a vehicle. However, it has been shown that good tooling is required to meet the design tolerances that are required for repeatable thermal performance. The use of inexpensive fiberglass or wood tools has been successful in the studies

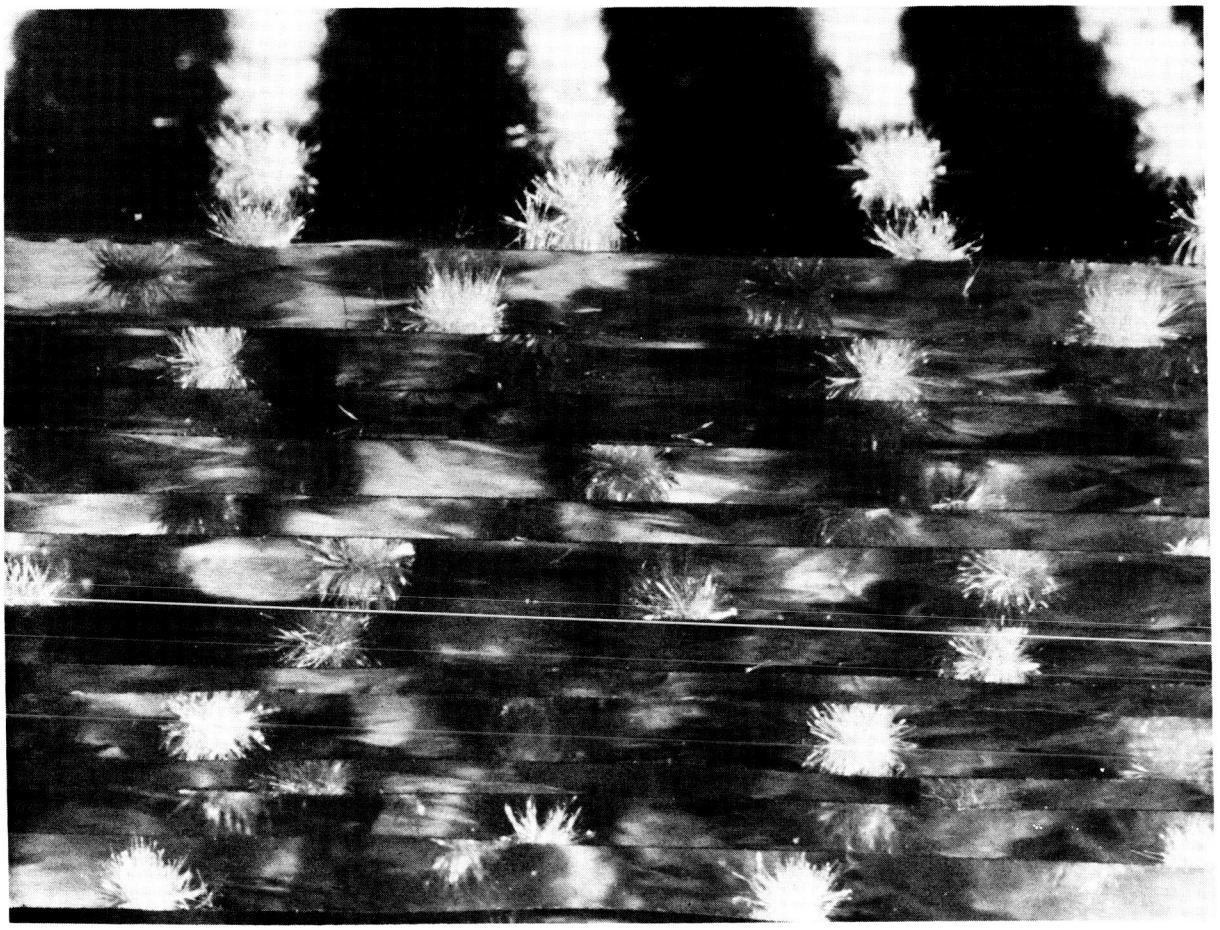

Figure 24. Layers of Superfloc insulation.

referenced in this report, and similar tooling could be used for production.

The use of full scale mockups pays off in the verification of design concepts and the development of manufacturing techniques. Layer densities based on layup of flat panels cannot be applied to contour panels. The only way to obtain the required data is to actually fabricate full size panels and take thickness measurements. Control of the manufacturing operation is essential since fabrication techniques are critical and minor variations can cause major discrepancies in the thickness of insulation panels. Once they are fabricated, care must be exercised in storing and handling the insulation panels.

Future applications of multilayer insulations, particularly those involving high temperature materials, will require additional studies to enable familiarity with process characteristics.

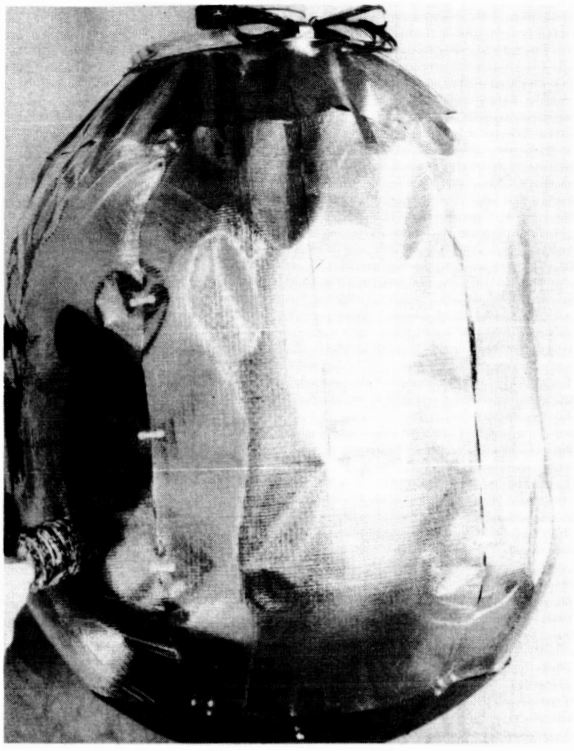

Figure 25. Superfloc on scale model tank.

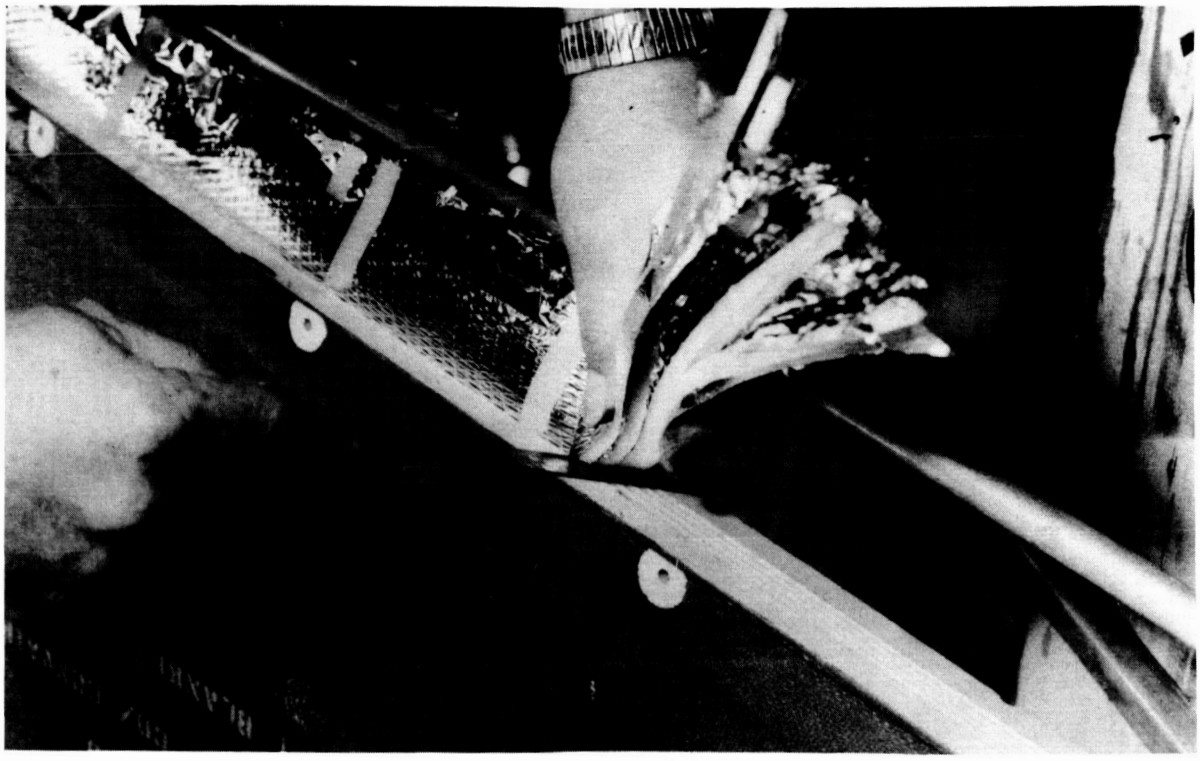

Figure 26. Trimming Superfloc insulation blanket.

REFERENCES

1. Development of Materials and Materials Application Concepts for Joint Use as Cryogenic Insulation and Micro-Meteoroid Bumpers. Annual Summary Report, Contract NAS8-11747, Goodyear Aerospace Corporation, Report No. GER 11676 S/47, June 30, 1968.

2. Development of Manufacturing Techniques for Application of High Performance Cryogenic Insulation. Final Report, Contract NAS8-21172, The Boeing Company, Report No. D2-109005-1, October 1967.

3. Demonstration of Manufacturing Techniques for Application of High Performance Cryogenic Insulation. Final Report, Contract NAS8-21341, The Boeing Company, Report No. D-139267-1, September 1968.

4. Investigation of High-Performance Insulation Application Problems. Fourth Quarterly Report, McDonnell Douglas Astronautics Company – Western Division, Report No. MDC G 0275.

5. Application of High Performance Insulation to Large Conical Support Structures. Final Report, Contract NAS8-24884, Goodyear Aerospace Corporation, Report No. GER-14518 S/11, October 1970.

6. High Performance Thermal Protection Systems. Final Report, Contract NAS8-20758, Lockheed Missiles and Space Company, Report No. LMSC-A964947, December 31, 1969.

7. Cryogenic Insulation Development. Final Report, Contract NAS8-18021, General Dynamics Convair Division, Report No. GDC - DDB69-002, December 31, 1969.

MULTILAYER HIGH PERFORMANCE INSULATION MATERIALS

By

J. M. Stuckey

SUMMARY

A number of tests are required to evaluate both multilayer high performance insulation samples and the materials that comprise them. Some of the techniques and tests being employed for these evaluations and some of the results obtained from thermal conductivity tests, outgassing studies, effect of pressure on layer density tests, hypervelocity impact tests, and a multilayer high performance insulation ambient storage program at the Kennedy Space Center are presented in this paper.

INTRODUCTION

Experience to date indicates that no one multilayer high performance insulation system will meet all the requirements for the various space missions. Requirements other than thermal conductivity-density products will undoubtedly affect the selection of some of the multilayer insulation (MLI) to be employed and, accordingly, the materials involved. In selecting materials for MLI systems, consideration must be given to such properties as weight, thermal conductivity, optical properties, thermal expansion (contraction), strength, temperature limitation, outgassing, reliability, reusability, etc. In addition, materials are required for fabricating and attaching the systems to the structure. This discussion will not attempt to cover all phases of material testing, but will be limited to some of the tests and programs now being used to evaluate materials and MLI samples at the Marshall Space Flight Center (MSFC).

DISCUSSION

Thermal Conductivity

Thermal conductivity tests are performed using an ADL Model 12 calorimeter. Figure 1 is a schematic of the calorimeter. To determine the minimum thermal conductivity, several tests are required that entail determining equilibrium boiloff data at various separations between the hot and cold plates. The inital tests are performed at separations between the plates that are somewhat greater than the free stacked height of the insulation samples; subsequent tests are carried out at decreasing separations between the hot and cold plates. The separation distance between the hot and cold plates is used to calculate a theoretical layer density in number of reflective shields per centimeter and/or inch of thickness. Tests are run using either LN_2 or LH_2, as deemed desirable, for the cold face temperature. The thermal conductivity curves determined for two MLI samples composed of alternate layers of double-aluminized Mylar reflective shields with dacron net spacers in one case and nylon net in the other are presented in Figure 2. The data show that the thermal conductivity for both systems at first decreases and then increases as the separation between the plates of the calorimeter becomes smaller. The data also show that for the nylon net system, increasing the layer density from 10 to 26 shields per centimeter of thickness causes very little change

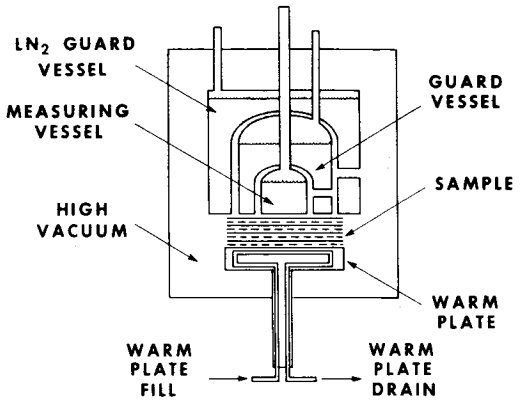

Figure 1. Schematic of thermal conductivity apparatus.

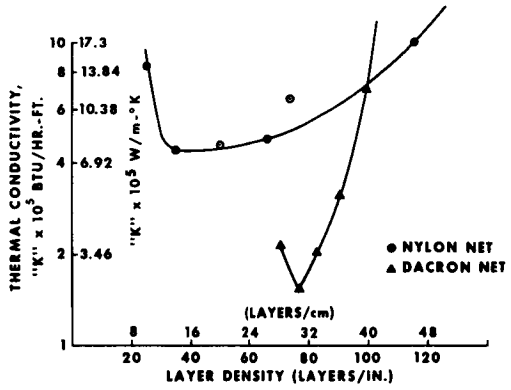

Figure 2. Thermal conductivity as a function of layer density.

in thermal conductivity. At the same layer density, the thermal conductivity of the dacron net sample is approximately one-third that of the nylon net sample. The thermal conductivity K determined for the dacron net sample was 2.68×10^{-5} W/m °K (1.55×10^{-5} Btu/hr ft °R) and for the nylon net sample was 8.3×10^{-5} W/m °K (4.8×10^{-5} Btu/hr ft °R).

Outgassing

The difference in thermal conductivity between the two MLI samples using net spacers appears to be partially a result of sizing, finish, or a lubricant on the nylon net. In the Skylab I program, the allowable outgassing for materials with respect to the Apollo Telescope Mount (ATM) is controlled by MSFC document 50M02442, "ATM Material Control for Contamination Due to Outgassing." Briefly stated, the outgassing requirements are as follows:

1. The rate of weight loss of the material during temperature cycling from 25° C to 100° C shall not exceed 0.2 percent/cm^2/hr when heated at a rate of 2° C/min.

2. Steady-state rate of weight loss at 100° C shall not exceed 0.04 percent/cm^2/hr.

The outgassing characteristics of several samples of nylon net were evaluated for potential use in MLI systems; some of the samples failed to meet the outgassing requirements. A sample of nylon net considered for application on the Skylab was heated in an evacuated chamber for 72 hr at 93° C. Offgases from the sample were analyzed by chromatographic and infrared techniques and showed the presence of hydrocarbon materials. Slow outgassing of the finish on the nylon net may effectively raise the pressure in the sample being tested above that in the chamber. Increased pressure in the sample would result in a higher thermal conductivity and would increase the boiloff. The dacron net sample is heat-set and contains no finish. This material has been qualified to meet the requirements of document 50M02442 for use on the Skylab. Since the netting materials are not designed for aerospace applications, it is not unusual that outgassing and other difficulties are sometimes encountered with various samples.

Effect of Pressure on Layer Density

As shown previously in the thermal conductivity testing, pressure compresses multilayer insulation samples. Compression of the MLI blanket will adversely affect the thermal protection both by decreasing the thickness and by tending to increase the thermal conductivity of the thinner blanket. The instron unit has been used to evaluate the relative compressibility of MLI samples. The effect of pressure on the thickness of a dacron net/double-aluminized Mylar sample is shown in Figure 3. Here it is seen that 0.454-kg pressure on a 30.5 cm diameter specimen decreases the thickness approximately 17 percent, and 4.54-kg pressure decreases the thickness nearly 32 percent. A weight of 0.454 kg is equivalent to 60.9 N/m^2 (8.84×10^{-3} psi) At a pressure of 6.89 N/m^2 (1×10^{-3} psi), the thickness is decreased approximately 9 percent. Although these tests show the weight sensitivity of the dacron netting/double-aluminized Mylar, some other systems such as crinkled single-aluminized Mylar (NRC-2), which depends on layer density control from the crinkled condition of the reflective shield, are affected to a much greater extent. These data show the importance of controlling layer density during blanket fabrication and installation to obtain an installation with a predictable thermal performance.

Variation in Thermal Conductivity Determinations

To further complicate the evaluation and selection of high performance MLI systems, wide

variations in test results on thermal performance for the same insulation samples are reported by various contractors and government agencies. The thermal conductivities of three MLI samples as determined at three different laboratories are shown in Table 1. For the double-aluminized Mylar/tissuglass system, there is nearly a 600-percent variation in thermal conductivities as determined by MSFC, McDonnell-Douglas Astronautics Co., and Lockheed Missiles and Space Co. For the system using nylon net, the variation is nearly 200 percent. The variation for Superfloc is 340 percent. The number in parenthesis in Table 1 shows the calculated layer density; again, there are wide variations. These results emphasize the need for establishing a standard procedure for determining thermal conductivity values. A funded program is planned to resolve this problem.

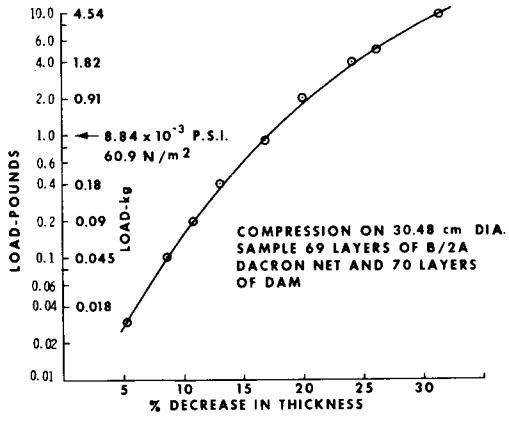

Figure 3. Effect of pressure on MLI sample thickness.

Hypervelocity Impact Tests

Another factor being considered is the protection required to prevent micrometeoroid penetrations as man's stay in outer space is increased. For long term missions and in some cases even for relatively short term missions, MLI systems are required both for environmental control and for cryogenic storage. To evaluate the protection afforded by MLI systems for preventing micrometeroid penetration, hypervelocity impact tests are conducted using a light gas gun. The light gas gun of the Materials Division of Astronautics Laboratory is shown in Figure 4. The target is located at the far end. The capabilities of the light gas gun are briefly summarized as follows:

1. Projectile velocity capabilities are over 7.6 km/sec.

2. Projectile mass can easily be controlled from 10 to 600 mg.

3. Complete instrumentation for determining projectile velocity and integrity is included.

4. Gun variables are instrumented to maximize projectile velocity predictability.

TABLE 1. THERMAL CONDUCTIVITY

MLI System	Marshall Space Flight Center		McDonnell-Douglas Astronautics Co.		Lockheed Missiles & Space Co.	
	Thermal Conductivity, K, $\times 10^5$ W/m °K ($\times 10^5$ Btu/hr ft °R)	Layer/cm	Thermal Conductivity, K, $\times 10^5$ W/m °K ($\times 10^5$ Btu/hr ft °R)	Layer/cm	Thermal Conductivity, K, $\times 10^5$ W/m °K ($\times 10^5$ Btu/hr ft °R)	Layer/cm
DAM[a]/Tissuglass	4.5 (2.6)	74[b] (188)	0.77 (0.44)	32[b] (82)	4.0 (2.3)	39[b] (100)
DAM[a]/Nylon Net	8.3 (4.8)	26[b] (67)	7.7 (4.4)	36[b] (91)	4.5 (2.6)	31[b] (80)
Superfloc	3.8 (2.2)	17[b] (42)	1.5 (0.86)	11[b] (29)	1.1 (0.65)	12[b] (30)

a. Double-aluminized Mylar.

b. Number of layers per inch of thickness.

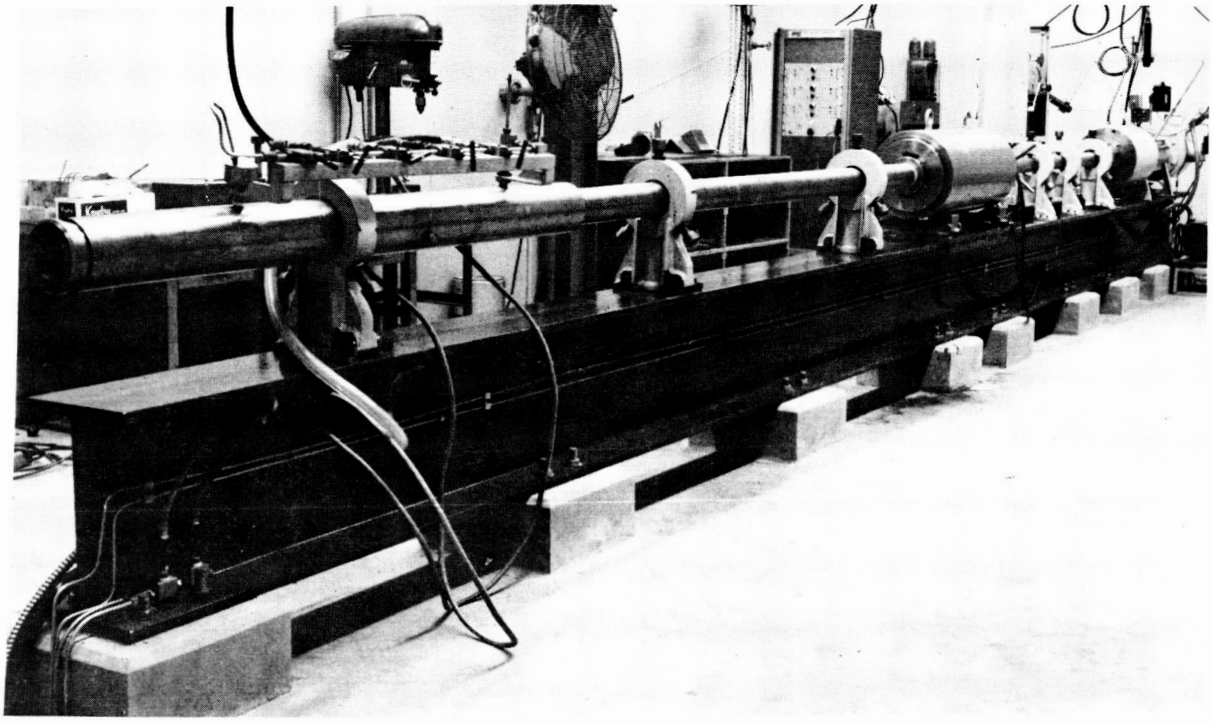

Figure 4. Light gas gun.

5. Sequential photographs are taken of the projectile during impact.

6. Two shots per day are possible.

Figure 5 shows the results of a projectile passing through an MLI sample consisting of double-aluminized Mylar/red foam. The sample was located immediately behind a bumper. Continued dispersion of the projectile is shown by the increase in size of the damaged area as the projectile passed through the insulation.

MLI Ambient Aging Program

In another program a test is underway to evaluate the possibilities of damage to MLI systems in uncontrolled storage, particularly at Kennedy Space Center (KSC). At MSFC and at other locations, damage to the aluminized surfaces of reflective shields has been encountered when moisture accumulated within MLI blankets or specimens. In most cases the moisture accumulation was a result of the freezing-out of moisture in the air onto cold surfaces after tests using cryogens were conducted. To evaluate the potential moisture accumulation within insulation blankets during uncontrolled storage at KSC, an MLI ambient storage program was initiated there during January, 1968. The MLI samples in the program, after a few additions, essentially include all the systems of interest. Most of the specimens are 60.96 by 60.96 cm (24 by 24 in.) and have from 30 to 120 radiation shields. The samples are protected from direct wind, rain, and sunlight by storage in a well ventilated, unheated building. Periodic inspections of the samples were made during the first year, and every 3 months thereafter. One radiation shield from each concept was removed from the inner section of the samples during each inspection and returned to MSFC for emissivity and absorptivity measurements. Minor damage has been encountered in all samples with tissuglass spacers and with crinkled single-aluminized Mylar reflective shields (NRC-2). The NRC-2 samples developed very small bare spots, mostly in the wrinkled or creased area. All samples with tissuglass spacers developed small white dots on the reflective shields (probably corrosion). These dots were detected during the 12-month inspection, and the dots appear to be

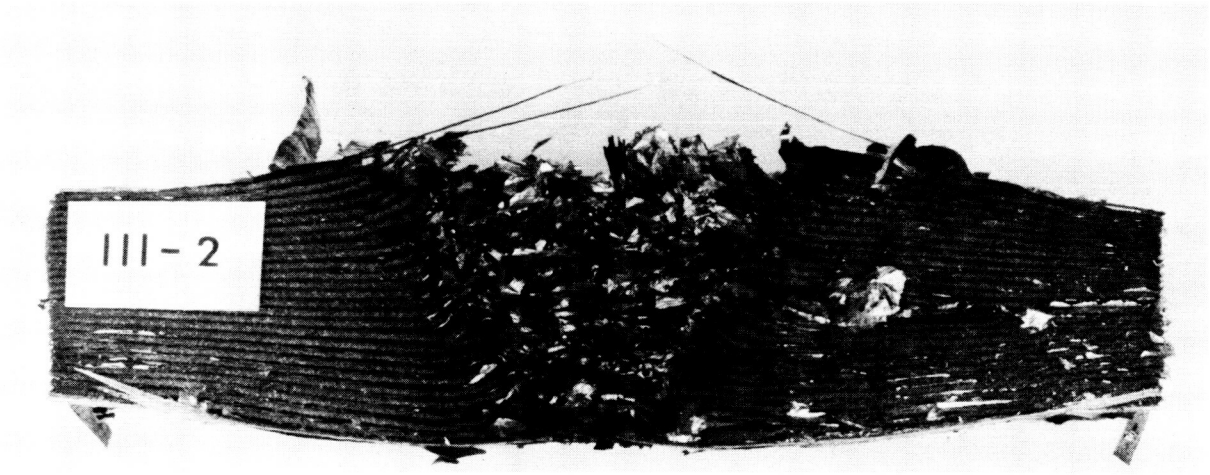

Figure 5. Hypervelocity impact test on an MLI sample — double-aluminized Mylar/red foam.

slowly increasing in size and number. Emissivity and absorption measurements on reflective shields do not show any significant change, however. The only concept that failed completely consisted of perforated double-aluminized Mylar with no spacer. One of the damaged radiation shields from a failed sample is presented in Figure 6. About half of the shields in each sample were affected. The size of the affected area decreases as the distance from the center increases. The outer approximately 25 percent of the shield showed no appreciable corrosion. This same type of failure occurred in all samples of a duplicate set exposed at a different time.

Tentative conclusions from the high performance insulation ambient storage program at this time are as follows:

1. Short term interruptions of dry gas purge should not be detrimental to flight MLI systems while stored at KSC.

2. Ambient conditions can result in moisture accumulation within MLI blankets leading to corrosion or reaction of the aluminum on the reflective shields.

3. Perforation of the reflective shields increases the chance of moisture accumulation within MLI blankets.

4. Spacers between the reflective shields decrease the chance of moisture accumulation within the MLI samples.

CONCLUSIONS

1. Numerous tests are required for evaluation of both MLI samples and the materials that comprise them for qualification for flight usage.

2. There is a need for establishing a standard procedure for determining thermal conductivity.

3. Test results indicate that outgassing of materials may be a factor affecting the thermal performance of MLI systems.

4. Some MLI systems are quite sensitive to pressure, and slight pressure results in a drastic increase in layer density.

5. Hypervelocity impact tests show the potential of MLI for affording protection against micrometeoroid penetration.

6. The MLI ambient aging program at KSC has shown that short term interruption of the required dry gas purge should not be detrimental, but under certain conditions, moisture can accumulate within MLI blankets resulting in deterioration of the aluminized surfaces.

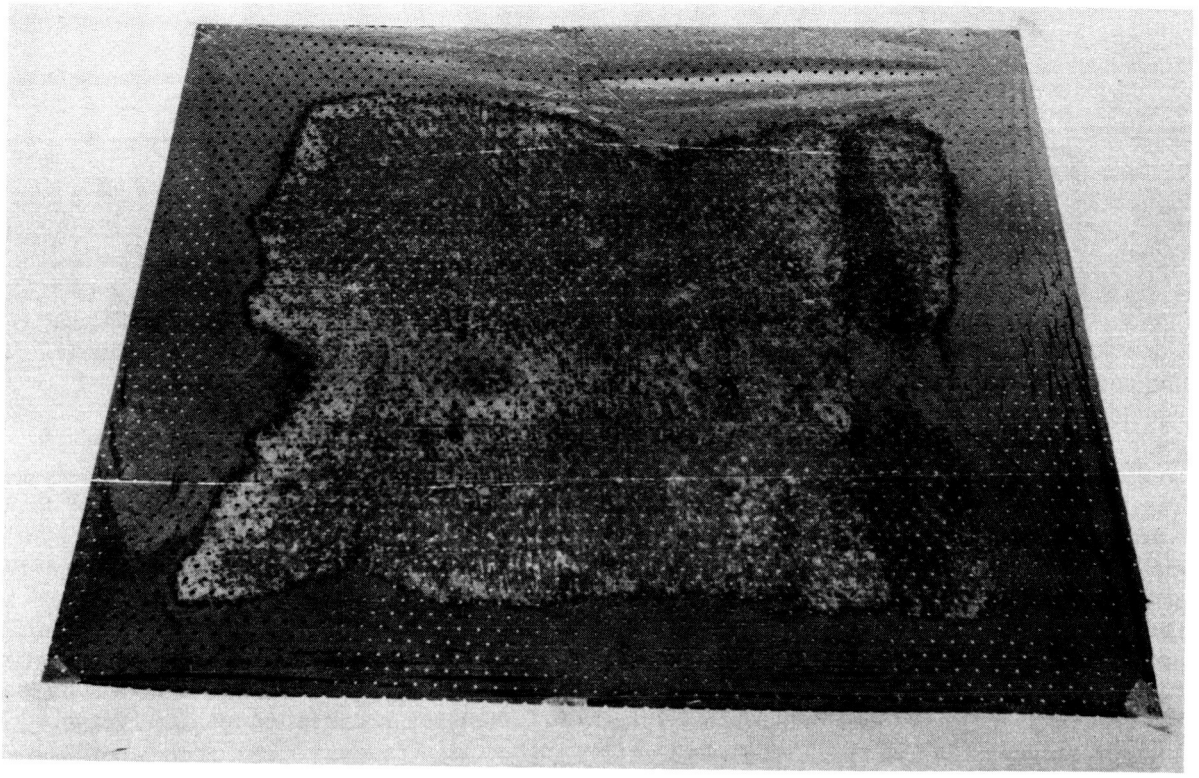

Figure 6. Damaged radiation shield.

SUPERCONDUCTING MAGNETS AND DEVICES FOR SPACE VEHICLES AND EXPERIMENTS

By

Eugene W. Urban

INTRODUCTION

During the past several years many new devices employing one or more of the fascinating properties of superconductors have been proposed. Some of these have passed through the conceptual stage and have become, or are now being developed into, practical instruments whose capabilities greatly exceed those of their conventional counterparts. In the following, the capabilities of some of the more promising of these devices that have potential applications to the space program will be considered, and research in the Space Sciences Laboratory of Marshall Space Flight Center related to such applications will be discussed.

Superconductors are materials that lose all electrical resistance when cooled to a sufficiently low temperature. Most superconductors are metals in elemental, alloy, or compound form; but certain metal nitrides and carbides are superconductors, and considerable work has been done in recent years to determine whether organic superconductors can be formed. Two general classes of superconductors exist; the characteristic properties of these classes and the devices into which they can be incorporated show a relatively sharp division.

TYPE I MATERIALS AND DEVICES

Most of the elemental superconductors such as tin, lead, and several others are in the class called Type I. Their transition temperatures or Onnes temperatures, T_c, above which they are not superconducting, are low; i.e., from a maximum of 9.2° K down to milli-degree Kelvin. They have immeasurably small resistivities and exhibit the Meissner effect, in which magnetic flux is totally excluded from a specimen when it is superconducting. Their critical magnetic fields, H_c, above which they lose their superconductivity, are also low; i.e., corresponding to inductions on the order of a few tenths to a few thousandths of a tesla. These considerations indicate that devices using Type I materials are inherently restricted to low magnetic field, low temperature applications. However, within these restrictions, many different instruments have been proposed and many of those are actively being developed or have been developed.

Table 1 lists several types of detectors that have been studied recently, together with an indication of typical sensitivities. Some of these instruments are based on one of the two Josephson effects, which are characterized by the flow of either direct or extremely high frequency alternating current at a thin insulator gap between two superconductors. In a typical geometry, such a junction is used to count the individual quanta of magnetic flux that are present because of an ambient field which is to be measured, for example, or that result from the flow of a very small current whose magnitude is to be determined. Fully developed laboratory instruments employing this concept are available commercially and have been employed in such applications as femtovoltmeters and to make magnetocardiograms for comparison with standard electrocardiograms. A number of promising radio-frequency (RF) and microwave devices are shown in Table 2. Of particular interest for space instrumentation are high Q structures. High Q structures are fabricated as thin film microstrips and could be incorporated into such apparatus as channelizing filters for surveillance receivers; complex or multiple microwave, infrared, and processing circuitry for array radars; extremely narrow band or steep skirt-rejection filters; recirculating memories; and delay circuitry. In addition, work has been performed on a sensitive material properties analyzer in which a wide variety of samples can be inserted without contacts into a tuned, high Q cavity. From simple nondestructive measurements of frequency and Q changes and absorbed power, remote determination can be made of such parameters as

dielectric constant, loss tangent, mobilities, relaxation times, carrier densities, etc.

TABLE 1. LIST OF SUPERCONDUCTING DETECTORS

Infrared
Bolometer
Josephson Junction: 10^{-14} W, wavelength range 0.1 mm to 1.0 mm
Magnetic Field (10^{-23} W noise power)
Magnetometer: 10^{-12} T change in 10^{-5} T field
Voltmeter: 10^{-15} V
Ammeter: 10^{-12} A at virtually zero input impedance
Temperature
Josephson Junction Noise Thermometer
Nuclear Radiation
Total Dose Monitor

TABLE 2. LIST OF SUPERCONDUCTING RF AND MICROWAVE DEVICES

Transmission Lines: 100 MHz to 12 GHz; 170 psec response to step
Mixers: 10 to 13 GHz; 10^{-18} W/Hz
RF Amplifiers
Signal Sources
Computer Memory Elements
Resonators:
Helical: $Q > 10^7$ at 100 MHz
Strip or Ring: $Q > 5 \times 10^5$ at 14 GHz
Cavity (Charged Particle Accelerators): $Q > 10^9$ at 1.3 GHz
Materials Properties Analyzer
Measure Frequency Change, Q, Absorbed Power
Determine Dielectric Constant, Loss Tangent, Properties of Relaxation Processes and Carrier Traps, Mobility, etc.

TYPE II MATERIALS AND DEVICES

The Type II superconductors are generally alloys, such as Ti-Nb, and compounds, such as Nb_3Sn; niobium and sometimes vanadium are also considered to be Type II. Those materials of greatest technological interest have relatively high values of T_c (10° K to 20° K), high critical magnetic fields, H_{c2} (greater than 5 T), and can carry very large current densities (greater than 10^4 A/cm^2) in the presence of high fields. For example, a commercial Ti-Nb alloy conductor may carry 13 000 A/cm^2 at 8 T. The great advantage of these materials is that when they are operating in a dc mode, they dissipate no power and, therefore, generate no heat. Thus, not only can superconducting solenoids develop much higher continuous fields than can conventional magnets, but they can do so without the enormous electric power input and cooling fluid requirements of the conventional devices.

Research and general-purpose superconducting magnets using simple winding configurations are commonly employed. In addition, more complicated winding geometries have been employed in a number of special-purpose magnets. Table 3 lists several types of magnets in each category and gives details of the largest existing magnets in two applications. In Table 3, "standard" refers to relatively straightforward cylindrical solenoid configurations, while "special" includes all nonsolenoid or combination systems. For example, an energy storage magnet with an optimized energy density might be built with a multilayer, variable-pitch winding in a toroidal shape.

A major cosmic ray experiment proposed for the second mission of the High Energy Astronomical Observatory (HEAO) satellite will employ a pair of identical superconducting magnets in a cryogenic system designed to operate for 1 year. Each 0.75 m diameter magnet will develop a maximum field of approximately 2.5 T and will store an energy of 1 MJ. They will be wound as standard solenoids. One coil will serve as a cosmic ray deflector for particle momentum analysis; the second coil is included to counterbalance the very large torque that would act on the spacecraft, if a single magnet interacted with the earth's weak magnetic field.

TABLE 3. TYPICAL SUPERCONDUCTING MAGNET APPLICATIONS

Standard Coil Configurations
Laboratory Magnets: 14 T central field, 15 cm bore diameter, 35 cm length, 2 MJ stored energy
Particle Accelerators
Magnet Levitation (Thermonuclear)
Wind Tunnel Model Levitation
Bubble Chamber Magnets: 2 T central field, 5 m bore diameter, 3 m length, 45 Mg conductor mass, 80 MJ stored energy
Special Coil Configurations
Thermonuclear Containment
Active Space Radiation Shielding
Rotating Machinery
Energy Storage
Gyroscope Rotor Suspension
Vechicle Levitation
Track Guided Free Flight, Takeoff and Landing

Levitation is a fascinating application of the large fields that can be realized with superconducting magnets. Suspension of one magnet without physical contact in a vacuum chamber above another outside the chamber has been demonstrated in at least two laboratories that use the systems in thermonuclear research. A wind tunnel model suspension and maneuvering system was built and demonstrated at the University of Virginia, and the National Magnet Laboratory has studied a magnetic technique for externally maneuvering a medical diagnostic probe or catheter tip via the arterial system into otherwise inaccessible regions of the body.

Of direct interest to aerospace is a concept of high speed vehicle levitation in which the eddy currents generated in a nonsuperconducting metal sheet by a superconducting magnet moving relative to it would provide strong repulsive fields. The Department of Transportation is funding two feasibility studies of a high speed passenger train system in which magnets would be carried on the train and eddy currents in a shaped aluminum track would provide lifting and centering forces. The same concept could be applied to a space shuttle or aircraft landing system, either emergency or routine, in which magnets would be located in a landing strip and the eddy current sheet would form the lower skin of the vehicle.

Rotating electrical machines offer promising uses of superconducting coils. The British have operated a large homopolar power station motor with a stationary superconducting field winding. Groups in the U. S. have studied motors and generators with both stationary and rotating superconducting field windings. Thus far, it has not been possible to construct superconducting armatures, since moving flux in the presence of currents in a superconductor leads to heating and unacceptable refrigeration loads.

Two notable problems exist in the field of high field superconductivity, especially in relation to space applications. These are (1) the low operating temperatures that must be maintained continuously during operation and (2) the fact that high field superconductors are inherently unstable from a thermal-magnetic standpoint and must be stabilized in a manner that increases the mass and complexity of the conductors. Stable conductors are currently fabricated with many fine strands of superconductor twisted in a tight helix in a high purity copper matrix of 0. 07 cm to 0. 25 cm diameter. Such conductors minimize or eliminate the chance of an accidental magnetic disturbance that could generate sufficient heat to cause a rapid propagating magnet shutdown. Nevertheless, the mechanisms for the initiation of magnetic disturbances are still not well understood and research is still required on this problem. Through better knowledge in this area, it may be possible to reduce further the amount of nonsuperconducting material in a magnet.

The temperature restriction means that a liquid helium coolant source, either closed cycle with a local refrigerator or open cycle with large helium storage volume or periodic resupply, must be provided along with a carefully designed and constructed cryostat to contain the device. For a ground-based system these large masses and volumes are primarily an inconvenience, although increased costs enter into the conductor manufacture and refrigeration supply. However, for a space system, the penalties for nonoptimum design are very large, if not prohibitive. First, a potentially unnecessary stabilizer mass and the added magnet-dewar structure resulting from the larger coil volume must be launched. Secondly, liquid helium refrigeration resupply in an open cycle means greatly increased total launch weights and the presence of experiment-conducting helium gas in the vicinity of the spacecraft. Alternatively, closed-cycle cooling would

require a refrigerator, a large generator (cyrogenic refrigerator power requirements increase rapidly as the superconducting device operating temperature decreases), and radiators for the refrigerator and the generator. Similar, though scaled down, refrigeration problems would be encountered for spaceborne low field superconducting instrumentation systems such as magnetometers or signal detectors.

It is apparent that significant reductions in the mass of the cryogenic system of a superconducting device could be made with even modest increases in the temperature at which the device must be operated. This in turn indicates the importance of finding superconductors with higher Onnes temperatures.

RESEARCH PROGRAM

The Space Sciences Laboratory superconductivity research program has had the following general goals: (1) to solve the system mass and power problem through better understanding of magnetic instabilities and transition temperature behavior of superconductors, and (2) to study device concepts for flight instruments and experiments. Specific tasks currently in progress are described below.

Magnetic Properties

Measurements are being made of the magnetic and thermal response of Type II superconductors to changing magnetic fields and these data are being compared to the behavior calculated from theoretical models. In a typical measurement, a hollow cylindrical sample of superconductor is suspended in the bore of a large superconducting magnet, as shown in Figure 1. As the magnetic field is changed smoothly, magnetic flux penetrates the superconductor; flux motion is detected by pickup coils. The slow penetration of flux in a process called flux flow leads to steep spatial gradients in the magnetic field within the specimen and, therefore, generates diamagnetic currents in it. These circulating currents depend on the strength of the local magnetic field in much the same way as do the conduction currents in a superconducting wire in a magnet. By making flux-flow measurements, it is possible to infer how the currents and fields are distributed within the sample. It is also possible to observe the onset of so-called limited instabilities, which are precursors to large, rapid field collapses in the superconductor and are known as flux jumps. Flux jumps are the chief cause

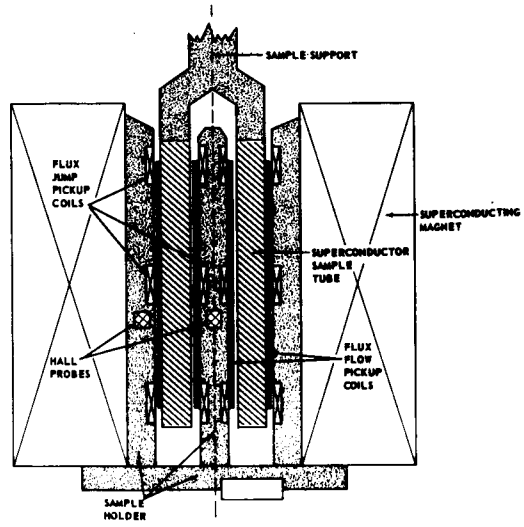

Figure 1. Schematic of flux jump-flux flow experiment sample holder.

of power losses in, and even complete shutdown of, inadequately stabilized magnets. An understanding of the conditions under which they initiate and their mode of propagation is essential to our attempts to specify the characteristics of inherently stable materials. Figure 2 shows a portion of a typical flux-flow measurement. Here the voltage on a pickup coil outside the cylindrical sample is plotted versus the applied magnetic field as the field is increased at a constant rate. Flux jumps, which appear as very short pulses on this time scale, occur in a fairly regular manner and greatly alter the internal field and the subsequent flux flow. Analysis of the linear regions of curves such as that shown in Figure 2 led recently to the proposal of a new empirical formula for the dependence of the superconducting current on the magnetic field in a specimen and other parameters. A portion of a flux-flow voltage record in which a regular oscillatory instability builds up to the flux-jump breakdown is shown in Figure 3. The new supercurrent formula is being used to determine theoretically how such oscillations and flux jumps are generated.

New Superconducting Materials

Three techniques are being employed to produce promising new superconducting materials that may have higher Onnes temperatures and critical

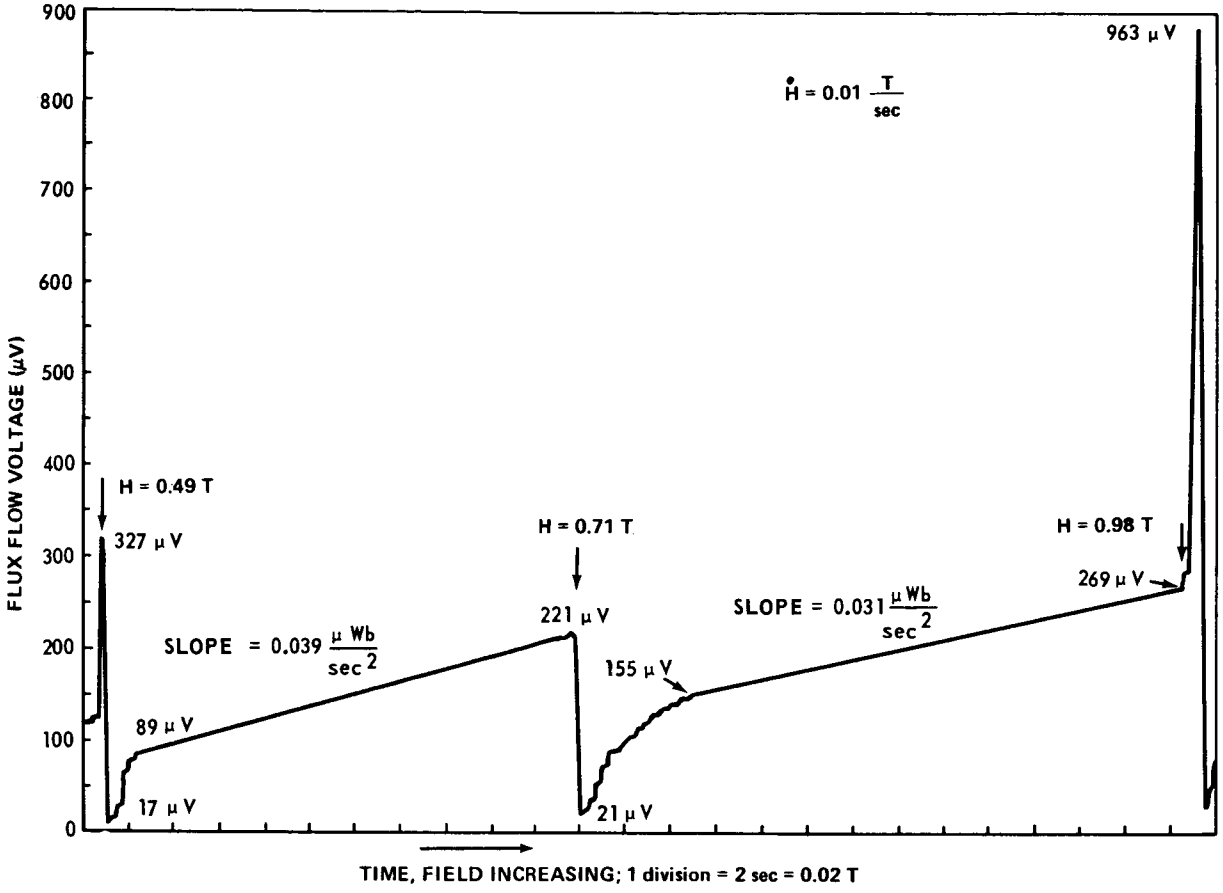

Figure 2. Typical flux-flow voltage data.

fields. These materials are the A-15 or beta-tungsten structure compounds of which Nb_3Sn is the best known and is the only one commerically available in conductor form. Others being studied include Ta_3Sn, Nb_3Al, Nb_3Ga, Nb_3Si, V_3Sn, V_3Gs, V_3Al, and several three-component A-15 systems. Two of the preparation techniques, arc melting and vapor diffusion, have been known for some time but have not been applied to some of the materials covered here. The third technique, in which the reactant powders are heated and compacted by the shock wave from a high explosive detonation, is new and unique. It offers the possibility of producing very promising compounds that have not been formed by the more standard methods, notably Nb_3Si and V_3Al. After formation, the materials are analyzed through measurement of their Onnes temperature behavior and their critical magnetic fields by X-ray diffraction studies and, in the case of the large explosion samples, by Picklesimer, photomicrograph, and electron microprobe analysis. The photomicrograph in Figure 4 shows a circular cross section region of Nb_3Sn along the axis of a compacted cylinder. In Figure 5 vapor diffusion samples prior to and after reaction and two explosively formed specimens are shown.

Transition Temperature Studies

Although most superconducting properties are very well understood theoretically, it has not been possible to explain precisely how the Onnes temperature of a particular material will depend on its electronic and structural properties. This phase of our research seeks to establish the relationship between Onnes temperature and the microscopic properties of a number of superconducting alloy systems, notably the Nb-Mo system. High frequency sound waves are an effective probe of the electronic structure of a substance. Sharp pulses of acoustic energy in the frequency range from 10 MHz to 100 MHz are generated by a quartz transducer along specific crystallographic axes of a single crystal of

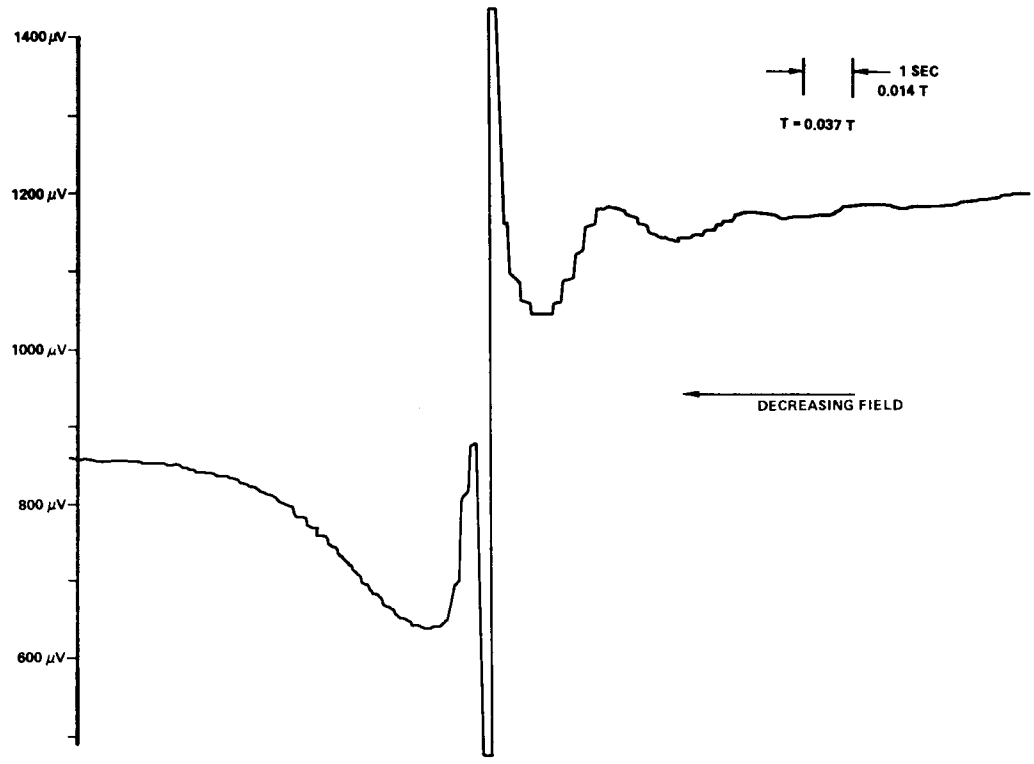

Figure 3. Oscillatory flux-flow voltage data.

superconductor. By measuring the travel time and amplitude change of the pulse echos, ultrasonic velocity and attenuation can be determined with a sensitivity of one part in 10^6 as a function of crystallographic direction and alloy composition. Conclusions can then be drawn concerning the detailed superconducting properties of the alloy. This research thus reveals additional significant information on the problem of specifying the parameters of superconductors that would have higher Onnes temperatures.

Superconducting Devices

An experimental program is currently being initiated to study the application of sensitive superconducting devices to flight experiments and to support the development of apparatus for a satellite test of general relativity. Of particular interest are Josephson effect instruments, including magnetometers for voltage, current and field measurements, and high sensitivity infrared detectors. At present, material properties are being measured by means of a magnetic-flux-conserving superconducting loop susceptibility bridge whose readout is made by a commercial Josephson junction instrument, known as a symmetric superconducting quantum interference device (SQUID). Experience with this apparatus will permit more rapid development of potential flight devices.

The relativity experiment referred to is being developed by Stanford University for the Space Sciences Laboratory. Relativistic precession of a rapidly spinning superconducting gyroscope ball will be read out by means of a closed superconducting loop that will detect extremely small angular changes

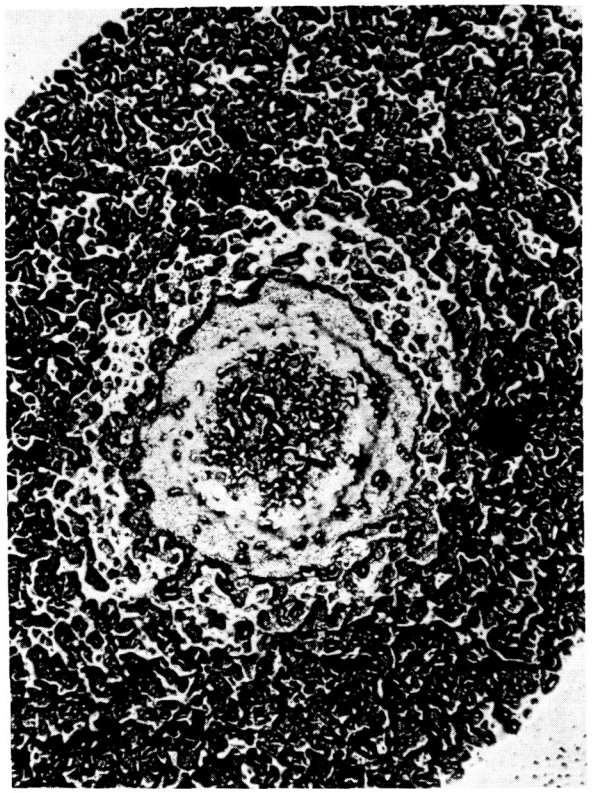

Figure 4. Photomicrograph of cross section of explosively compacted Nb_3Sn.

in the very weak spontaneous magnetic moment of the spinning ball. The high degree of perfection of the gyro ball and its electrostatic suspension system leads to an almost impossible spin-up problem. Theoretical and experimental research will be conducted to determine whether the gyro could be spun up while in the normal state (heated to a few degrees above the Onnes temperature) and then cooled to superconductivity in a controlled manner so that absolutely no external magnetic flux would be trapped in the ball and thus disrupt the readout system.

CONCLUSION

Superconductivity research in the Space Sciences Laboratory of MSFC is oriented toward those problems that tend to restrict the greater application of superconducting devices in space research and technology. These include magnetic problems of high field magnets, increasing operating temperatures, and development of useful competitive superconducting instruments.

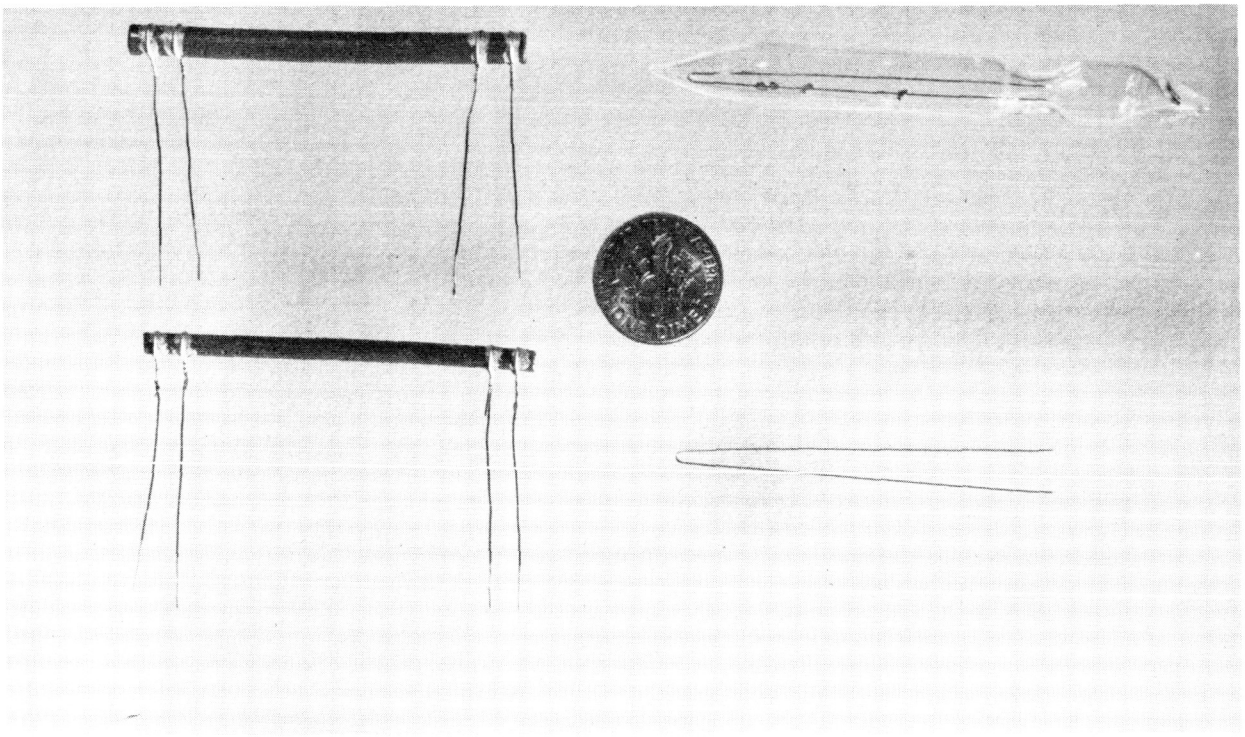

Figure 5. Explosively compacted and vapor diffusion reaction samples.

CRYOGEN ACQUISITION IN ORBIT

By

L. J. Hastings

SUMMARY

During the past 3 years, in-house and contracted cryogen acquisition research at Marshall Space Flight Center (MSFC) has concentrated on two acquisition methods, acquisition by acceleration and acquisition by passive capillary systems. Acquisition by continuous acceleration is considered the state-of-the-art method; however, this method is not attractive for future applications from weight and mission compatibility standpoints. Other methods such as intermittent acceleration, positive expulsion, dielectrophoresis, and capillary systems are untried on cryogen vehicles. The most promising of these are intermittent acceleration, capillary systems, and a combination of the two.

Liquid control by acceleration, either continuous or intermittent, requires proper precautions against the tendency for slosh amplification upon a sudden acceleration decrease. MSFC drop tower tests have shown that excessive slosh amplification will occur when slosh baffles are not used. However, a ring baffle located at the liquid surface will effectively reduce the amplification to acceptable levels.

The best technique for analytically simulating the complex liquid motions resulting from intermittent propellant settling is the Marker and Cell (MAC) computer technique. This approach provides both pictorial and tabulated data output describing fluid configurations, pressure contours, and velocity vectors. Characteristics of many low-gravity fluid mechanics problems in addition to the resettling problem can be similarly analyzed. An MAC program has been adapted to the MSFC 1108 computer system.

A theoretical method for determining equilibrium interface configurations in axisymmetric containers of arbitrary shape has been investigated. A single differential equation was derived from the principle of minimum surface and potential energy using the calculus of variations. This equation, in conjunction with boundary conditions, container shape, and contact angle, can be numerically solved for the desired surface profile using the Runge-Kutta iteration technique. The method imposes no significant limitations on contact angle or Bond number and is easily programmed for computer solutions. Representative theoretical results concerning the influences of contact angle, Bond number, and container fill level on surface shapes were determined. The theoretical results obtained agreed with experimental data.

Often, drop tower evaluations of fluid dynamics have resulted in the superimposition of equilibrium surface formation transients upon the phenomena of primary interest. Therefore, the behavior of a zero contact angle liquid-vapor interface after a sudden reduction in acceleration was experimentally investigated. The interface profiles and certain oscillation amplitudes were measured as a function of time and acceleration level using cylindrical and spherical containers. Based on the measured surface profiles, estimates were made of the time required for a surface to attain quasi-equilibrium.

A systems design study has been performed to determine the feasibility of using capillary devices for low-gravity propellant control in large scale cryogenic vehicles. Initially, the thermodynamic and heat transfer problems were defined and methods were derived for their solution. Some of the problems considered were vapor formation within a surface-tension expulsion device, interface control during venting and pressurization, propellant settling, residual propellant prediction, and bubble motion under the influence of thermophoretic and buoyancy forces. Based upon information derived from the solution of these problems, capillary control concepts were developed for two representative missions; an S-IVC restart mission and a lox tanker propellant transfer mission. These designs were then compared to dielectrophoretic, settling, and bladder transfer systems on the basis of weight penalty, cost, reliability, and safety. Both mission studies concluded that surface tension systems offer sufficient promise to warrant additional study. The most promising capillary concepts were developed through a preliminary design phase.

The fluid mechanic problems associated with surface tension retention and control have been investigated experimentally in a 2. 1-sec drop tower. Disturbing accelerations were applied normal and parallel to flat perforated plate barriers and screen barriers to evaluate interface stability and damping ability. The critical Bond numbers for square- weave screen and perforated plates were 0.45 and 0.84 respectively with accelerations normal to the surfaces. Critical Bond numbers ranging from 0. 85 to 2. 5 resulted with lateral accelerations applied to a wide range of barrier configurations. Settling dynamics were best damped with two parallel perforated plates and dutch-twill weave screen.

The effects of surface orientation and reduced gravity on Freon 113 nucleate boiling have been investigated using a 4-sec drop tower. Results of this study demonstrate that the pool boiling curve is a function of both acceleration level and surface orientation. Also, downward shifts of the boiling curve in zero gravity were indicated, and significant vapor accumulations were noted on the vertical heated surfaces. Further tests in a 1. 34-sec drop tower with LN_2 and LH_2 generally confirmed the preceding findings. Additionally, it was established that the superheat required to initiate boiling was independent of body forces; however, the incipient heat flux will shift downward with decreasing gravity.

LIST OF SYMBOLS

Symbol	Meaning
a	local acceleration, m/sec^2
B_N	Bond number based on radius
D	container diameter, m
FR	Froude number
g	standard acceleration of gravity, m/sec^2
R	container radius, m
R_0	characteristic container dimension, m
t_p	interface oscillation period, sec
$\bar{t}_p$	nondimensionalized oscillation period
t_t	total interface damping time, sec
$\bar{t}_t$	nondimensionalized damping time
Z	vertical dimension, m
β	kinematic surface tension, m^3/sec^2
ρ	liquid density, kg/m^3
σ	liquid surface tension, N/m
$\Delta \zeta_\ell$	maximum low gravity slosh amplitude, m

INTRODUCTION

Orbital cryogen acquisition is the process of acquiring a cryogen in a low- or zero-gravity environment. Upon consideration of future space missions (Table 1), it becomes apparent that all the major missions require cryogen acquisition for engine restart and/or propellant transfer.

TABLE 1. MISSIONS REQUIRING ORBITAL CRYOGEN ACQUISITION

Mission	Transfer	Engine Restart
Space Shuttle		X
Space Shuttle Payload	X	
Space Tug	X	X
Nuclear Shuttle	X	X
Propellant Depot	X	
Space Station	X	

Table 2 summarizes the various acquisition concepts usually considered and the basic advantages and disadvantages of each. One basic approach is control of the bulk liquid by settling acceleration, either continuous or intermittent. Another approach is represented by passive acquisition in which the bulk propellant is allowed to migrate randomly within the tank and the passive system provides liquid access regardless of the liquid location. An approach usually considered for enabling engine restart is that of partial volume control. In this approach, a small portion of propellant is continuously controlled and the control volume is sized such that the engine can restart and thrust for a period corresponding to the propellant resettling time.

TABLE 2. ACQUISITION TECHNIQUES

	TECHNIQUE	FEATURES
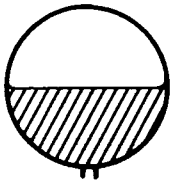 ACCELERATION	● CONTINUOUS ACCELERATION	PROVEN; WEIGHTY
	● INTERMITTENT ACCELERATION	PREDICTABLE; WEIGHTY; MISSION COMPATIBILITY?
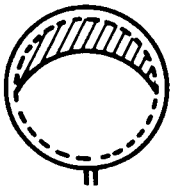 PASSIVE	● CAPILLARY SYSTEMS	PASSIVE; LIGHT; REUSABLE; IMMATURE; COMPLEX FOR LARGE TANKS
	● DIELECTROPHORESIS	PREDICTABLE; REUSABLE; COMPLEX; SAFETY/LOX?
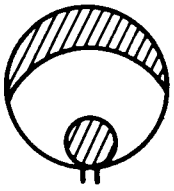 PARTIAL VOLUME CONTROL	● BLADDERS/BELLOWS	POSITIVE EXPULSION; CYCLE LIFE? UNDEVELOPED FOR LARGE TANKS

Thus far, engine restart has dictated the propellant acquisition requirements. The S-IVB/Saturn V and Centaur have used what is now considered the current state-of-the-art method; that is, a continuous settling thrust or linear acceleration. This technique is reliable and predictable, but for missions on the order of days rather than hours, it becomes unacceptable from a weight standpoint. Intermittent propellant resettling is predictable with some technology extension, although it has not been attempted on large scale or cryogenic vehicles. However, it too has a weight disadvantage and can cause undesirable mission constraints.

Other more advanced methods of cryogen acquisition are capillary, dielectrophoretic, and positive expulsion systems. However, neither of these systems has been used in a cryogen flight application.

Capillary systems are passive, lightweight, and reusable. Thus, the method is promising but presently is immature from a technology standpoint and is complex for large tank systems, especially when thermal conditioning is considered.

Dielectrophoretic systems operate by inducing polarization forces in a fluid through an applied electric field. Since no moving parts are involved, the system can be considered essentially passive. The method provides reasonably predictable effects and can be arranged so that it requires no thermal conditioning system since it actively repels vapor. Its disadvantages are weight, complexity, and safety, especially when used in lox.

Bladders, bellows, etc., are often used in small tank systems for storable propellants. Considerable efforts have been expended in recent years on extending such methods to cryogen systems since the expulsion process is positive. However, the cycle life is questionable and technology for large tank systems is undeveloped. Metallic diaphragms are presently the most promising technique of this class.

A REVIEW OF MSFC RESEARCH

Much of the MSFC research conducted in recent years concerning low-gravity fluid mechanics and heat transfer has been an outgrowth of the vigorous research program in support of the S-IVB/Saturn V orbital engine restart mission. Although the S-IVB-203 orbital experiment and the first S-IVB engine restart occurred almost 5 years ago, the data resulting from these programs have provided a strong foundation for present research.

Recent MSFC achievements in the area of propellant acquisition can be generally divided into two categories, acquisition by acceleration and acquisition by passive capillary systems. In-house and contracted programs completed during the last 3 years are listed and briefly described in the following paragraphs.

In-House Research

Projects completed during 1968 and 1969 concentrated on propellant control by continuous acceleration. Low-gravity equilibrium liquid-vapor interface shapes were investigated analytically; the results are described in Reference 1. Low-gravity interfaces were also experimentally evaluated using the MSFC drop tower[1]; these experimental data are presented in Reference 2. Low-gravity sloshing was a primary concern. The control of slosh amplification resulting from a sudden acceleration decrease was evaluated analytically and by drop tower experimentation. The slosh amplification, oscillation periods, damping, etc., are documented in Reference 3.

Instrumentation suitable for determining propellant location and quantity in a low-gravity environment has also been a problem related to cryogen acquisition. Thus, the performance characteristics of various liquid-vapor sensors were established using the drop tower; these are documented in Reference 4.

In the area of heat transfer, the influence of low-gravity environments on boiling heat transfer phenomena in Freon 113 was experimentally assessed and is reported in Reference 5.

During the past year, in-house projects have been directed more specifically toward design support of the space shuttle and space station missions. Thus, the projects have not existed long enough to have been completed and documented. One such project is an orbital liquid transfer experiment designed to investigate the hydrodynamic problems involved in a zero-gravity capillary system for acquisition and transfer. An experimental prototype has been assembled, and initial tests in the KC-135 aircraft were conducted in March, 1971. The experiment orbital carrier is "to be determined", but the experiment is suitable for a Skylab I type environment with minimum interface requirements.

Contracted Research

Studies contracted for or completed during the 1967 through 1970 time period have emphasized the utilization of capillary acquisition systems, although much of the resulting technology is applicable to other acquisition concepts. The first study contracted in the subject time period was an evaluation by General Dynamics of the S-IVB-203 orbital experiment fluid mechanics and heat transfer data. The experiment was used as a basis to update existing analytical models and to create new models. Repressurization, closed tank pressure rise, flash boiling/depressurization, and propellant sloshing/settling were the general topics studied [6]. As a result of an extension to this contract [7], a Marker and Cell (MAC) computer code for analyzing complicated propellant dynamic and heat transfer phenomena was developed.

The capabilities of various capillary devices to retain liquid against acceleration disturbances and to dampen liquid dynamics were investigated by Martin-Marietta Corporation. The results of this study are primarily experimental drop tower data [8]. No heat transfer or thermodynamic problems were examined under this contract.

The most comprehensive study of capillary systems involved their application to cryogen vehicles. This study was performed by General Dynamics and resulted in example capillary acquisition system designs for propellant transfer and engine restart missions. The design approaches and designs are

1. The MSFC drop tower design and operational procedures/capabilities are described in "Low Gravity Fluid Mechanics and Thermodynamics Experiments in a Drop Tower Facility," by W. B. McAnelly and W. J. Covington, NASA TM X-53765, February 1969.

are presented in References 9 and 10. Additionally, parametric data and design principles for general application have been documented in Reference 11. This particular study represents the first comprehensive study of capillary cryogen acquisition systems and should be of significant value to the present shuttle and station programs.

A study performed by the University of Michigan has complemented the MSFC boiling heat transfer studies by testing with cryogens (LN_2 and LH_2) as opposed to a storable test liquid. Interim results are presented in Reference 12.

Because of the broad spectrum of subjects researched and reported in the preceding references, only selected details and results are presented in subsequent sections of this paper. Material is presented from References 1, 2, 3, 5, 7, 8, 9, 10, and 12.

SLOSH AMPLIFICATION

In the case of propellant positioning by continuous low acceleration (on the order of 10^{-4} to 10^{-5} g), slosh amplification problems can occur if proper precautions are not taken. Liquid sloshing amplitudes that are relatively small during a high thrust period can attain very high amplitudes when the liquid kinetic energy is suddenly converted to potential energy in a low-gravity field. This problem was experimentally investigated at MSFC and results were obtained concerning maximum slosh amplitudes, with and without baffles, slosh period, center of gravity shift, slosh damping, and liquid-vapor configurations. Data on the subjects of slosh amplitude and period of oscillation are summarized in the following.

Slosh Amplitudes

The behavior of a liquid column oscillating in the fundamental antisymmetric mode and subjected to a sudden reduction in axial acceleration was investigated using the MSFC drop tower facility to obtain a controlled low-gravity environment for durations of up to 4.3 sec. Tests were conducted in 15.2 cm diameter cylinders using petroleum ether, a zero contact angle liquid, as the test fluid. The test conditions provided Bond numbers ranging from 12 to 100 and Froude numbers ranging from 0.03 to 22 based on tank radius (R). Engineering results that have general application in the design of propellant control systems were obtained. In addition, the liquid behavior for the specific S-IVB/Saturn V geometric configuration and energy conditions at orbital insertion, both with and without the baffle and deflector installed, was evaluated.

The pictorial qualitative data obtained are presented in Figure 1, where slosh amplification with and without slosh baffles is shown. As demonstrated in the case without baffles, the amplification was sufficient for the liquid to move up to and cross the upper dome. With the addition of a 1.8-cm ring baffle at the liquid level, however, the amplification was limited to only a few liquid globules.

From a quantitative standpoint, the maximum liquid amplitude in the low-gravity environment was evaluated in the form of the measured amplitude as a function of the instantaneous energy conditions at drop. The maximum low-gravity amplitude ($\Delta\zeta_\ell$) was defined as the difference between the measured maximum amplitude and the instantaneous amplitude at the instant of drop. Figure 2 shows the measured maximum liquid amplitudes, nondimensionalized by tank radius (R), as a function of the square root of the Froude number. Results are shown for tests both with and without the baffle and deflector.

In the tests without the baffle and deflector, there was some data scatter and a single curve representative of all the data could not be defined. However, the maximum amplitude along the upper boundary of the data region varied from $\Delta\zeta_\ell/R = 0.63$ to $\Delta\zeta_\ell/R = 1.8$ over a Froude number (FR) range of 0.028 to 14.6 and is defined by the empirical relation,

$$\Delta\zeta_\ell/R = 0.99\,(FR)^{[0.018\,\ell n\,(FR) + 0.177]}$$

The numerical data with the baffle in the tank were obtained from tests in which the nominal liquid level was below the baffle position. Figure 2 shows that at any given Froude number, the slosh baffle significantly reduced the maximum liquid amplitude compared to the unbaffled amplitude. These results do not fully emphasize the effectiveness of the baffle as a propellant control device. The primary value of the baffle is in reducing the liquid kinetic energy (hence Froude number) during the high-gravity condition, in comparison to the energy that would exist if the baffle were not in the tank.

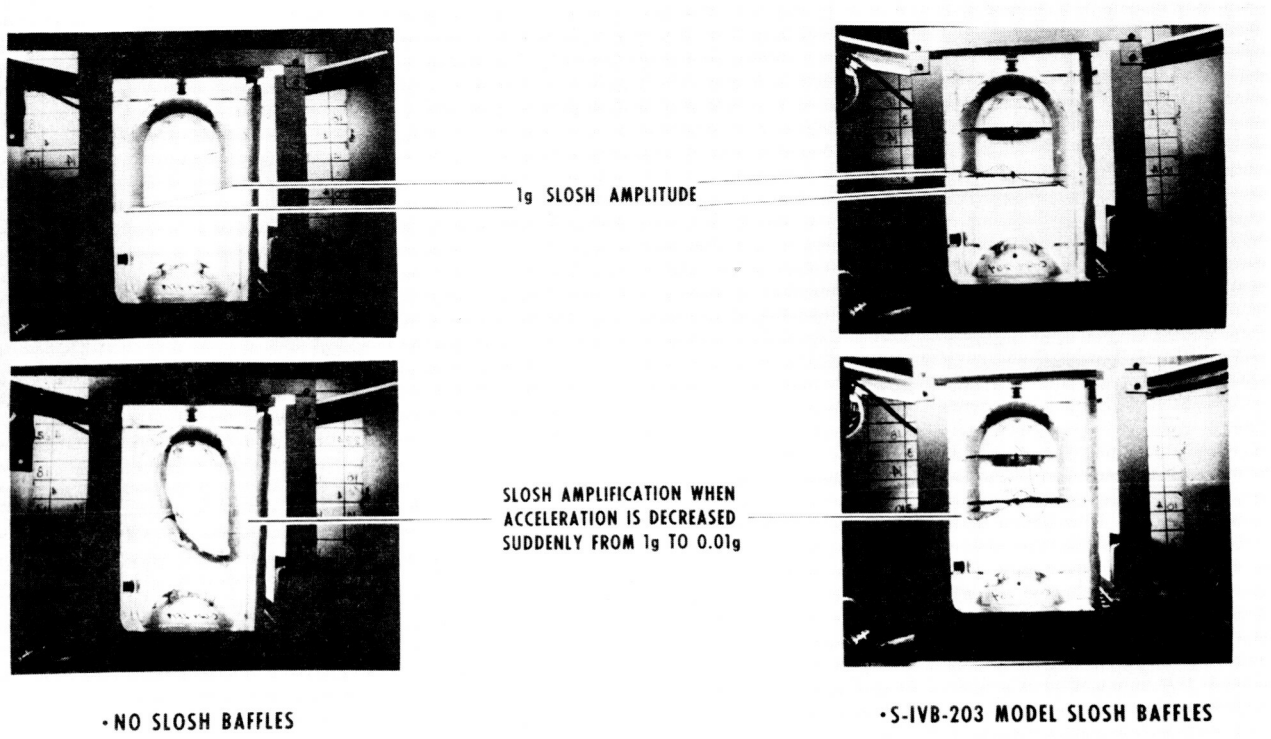

Figure 1. Slosh amplication, MSFC drop tower.

Period of Oscillation

The measured wave periods as a function of Bond number are shown in Figure 3. Also shown is the theoretical wave period as determined from the Satterlee-Reynolds equation [13]. There is no obvious tendency for the measured wave period to deviate significantly from the Satterlee-Reynolds equation at either low or high Bond numbers. Since the experimental wave periods were measured from the first complete cycle of motion under the reduced-gravity environment and these measured data agree so closely with the theoretical period, it is concluded that, for all practical purposes, the liquid column shifts frequency instantaneously with changes in apparent gravitational field.

PROPELLANT RESETTLING – MAC METHOD

The prediction of complex fluid motions is becoming practical with the development of more efficient computing methods and faster, larger computers. The Marker and Cell method, developed at Los Alamos Scientific Laboratory for incompressible fluids with a free surface, is suitable for evaluating many low-gravity and zero-gravity fluid and heat transfer problems. The method is a finite-difference technique for integrating the equations for nonsteady viscous fluid flow. The computational procedures enable a pictorial and numerical output of computed results. The computational region consists of a mesh of rectangular cells and a set of marker particles that define the fluid configuration. Marker particles are specified on the grid network at the beginning of a problem to denote the fluid position. With each time step, new velocities are calculated and the marker particles are moved with the local velocity.

One problem that the MAC program has been used to assess is that of propellant resettling. Example pictorial data resulting from a propellant settling analysis are shown in Figure 4. The LH_2 in a 6.1 m diameter tank with two ring baffles was resettled at 0.337 g. The computed fluid motions, velocity vectors, and pressure isobars were output both pictorially and in tabulated data form. The small details of the liquid motion cannot be resolved; however, the dominant features can be clearly resolved. The initial perturbations existing in the

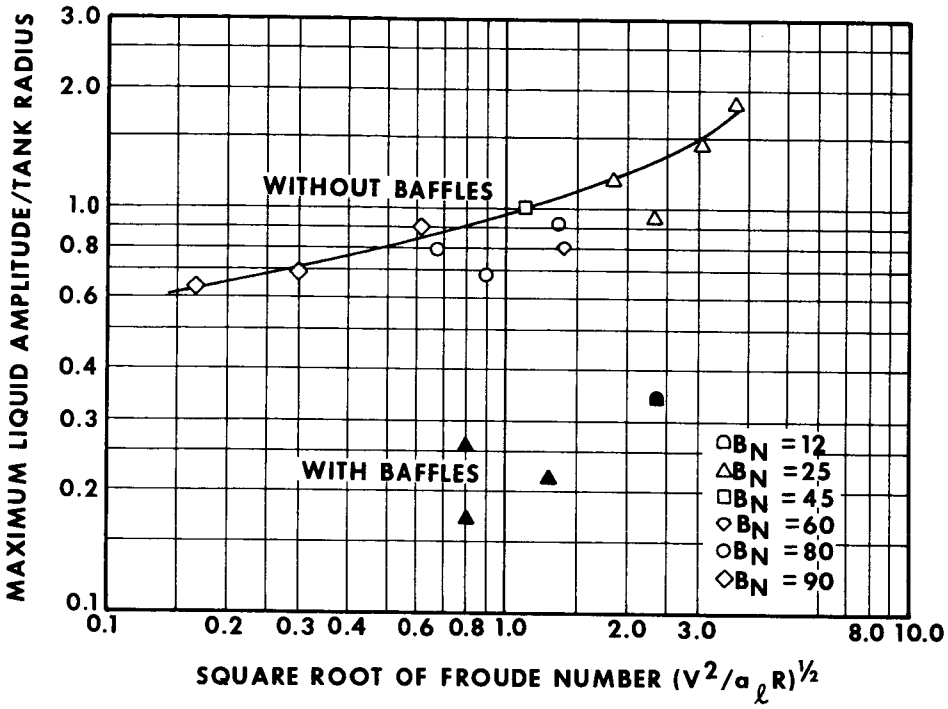

Figure 2. Maximum liquid amplitude following a sudden reduction in acceleration.

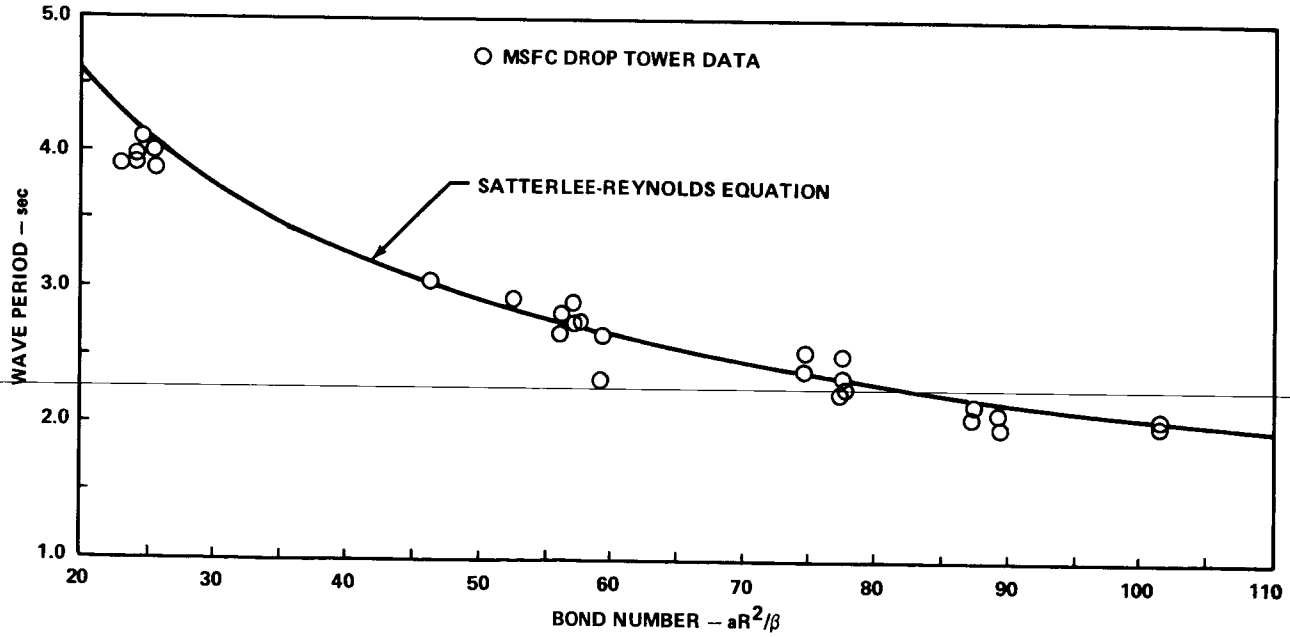

Figure 3. Experimental/theoretical slosh wave period versus Bond number.

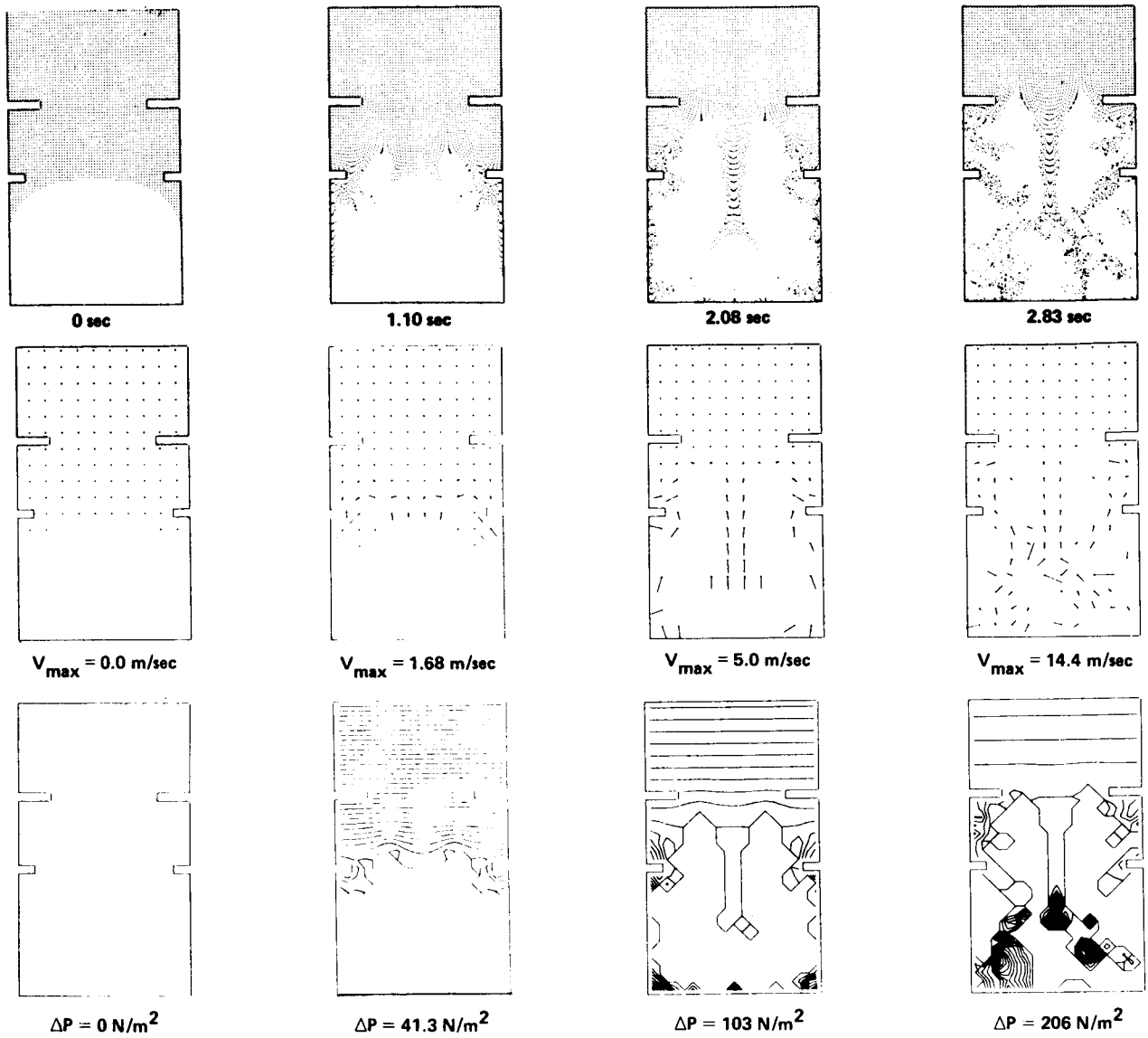

Figure 4. Propellant settling — Marker and Cell computer output.

liquid-vapor interface are important to the resulting settling motions. The curved surface in this case enhanced liquid flow down the walls. Otherwise the center jet of liquid would have been even more dominant. The interference of the baffles is also evidenced both in the fluid motion and the pressure contour plots. After 2.5 sec the settling motions become quite chaotic and the run could not be continued without using excessive computer time. Further developments with the MAC technique under a present contract with Lockheed Missiles and Space Company will alleviate the problem with the addition of curved boundaries and surface tension.

In addition to the subject computer analysis of liquid resettling, an extensive drop tower investigation was sponsored, and the results are described in Reference 14. These experimental results compare almost perfectly with the MAC simulations in the few cases compared thus far.

It should be noted that the MAC technique can also be used to assess temperature stratification/destratification, liquid outflow/inflow, mixing by diffusion and circulation, and surface tension retention capabilities.

THEORETICAL EQUILIBRIUM SURFACE SHAPES

In environments devoid of any disturbances except that of low acceleration or gravity, surface tension forces become comparable to those of gravity, and equilibrium liquid-vapor interface shapes may radically depart from the near flatness observed in normal gravity. This is especially true of the many liquids that exhibit wall contact angles at or near 0 deg.

A convenient form of the basic interface differential equation was derived from the familiar principle of minimum surface and potential energy using the calculus of variations. The use of a polar coordinate system eliminated the convergence difficulties encountered in the previous solutions. Also, the derivation enabled the incorporation of a Bond number based on a characteristic container dimension into the basic differential equation, as opposed to a Bond number based on interface radius of curvature.

The basic differential equation and boundary conditions dependent on container shape were programmed for a GE-235 computer so that surface shapes for any particular combination of Bond number, vapor volume, and contact angle can be determined. The computer solution utilizes the Runge-Kutta numerical technique and imposes no significant limitations on contact angle or Bond number.

Representative surface shapes were computed to determine the influence of contact angle, Bond number, and container fill level for three container shapes; cylindrical, spherical, and spheroidal. It was determined that, in a cylinder, the influence of Bond number on interface deformation is maximum between Bond numbers of 2 and 20 and becomes negligible for Bond numbers greater than approximately 200. In spherical or spheroidal containers, the empty fraction has a significant effect on the interface profile. Also, unlike the cylinder, a contact angle of 90 deg does not assure negligible interface distortion in spherical or spheroidal containers. The limiting contact angle is that angle measured in the liquid between a horizontal plane corresponding to the infinite Bond number liquid level and the tangent to the container boundary.

Example computed interface shapes for a prolate spheroid for four different fill levels and Bond numbers of 5, 20, 50, and 100 are presented in Figure 5.

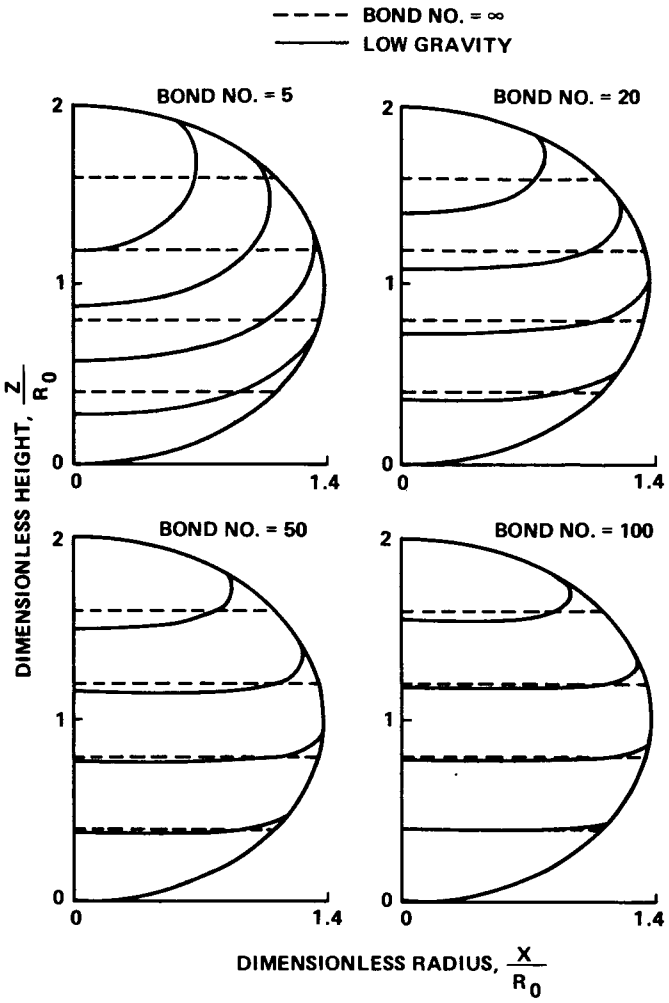

Figure 5. Zero-degree contact angle interface shapes in an oblate spheroid.

The plotted data have been nondimensionalized by one-half the vertical height of the spheroid, R_0. Also, R_0 is the characteristic length dimension used in the Bond number.

The theoretical profiles were compared with experimental data from Reference 15 and exceptional agreement was obtained (Fig. 6). In fact, if the actual contact angle is known, it is believed that the static equilibrium interface profiles can be computed with greater accuracy than they can be measured because of the distortion and reflection problems inherent in such experimental measurements. Typical correlations for surface shapes in a cylinder are shown in Figure 6.

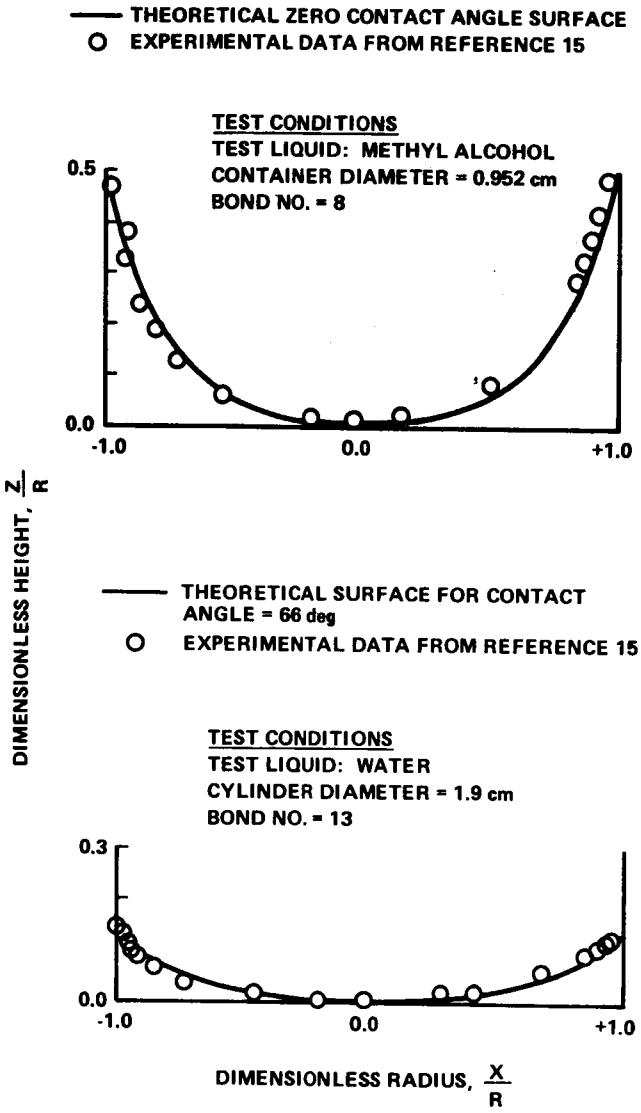

Figure 6. Experimental and theoretical interface shapes in a cylinder.

EQUILIBRIUM INTERFACE FORMATION TRANSIENTS

During the investigation of certain fluid behavior phenomena in the MSFC drop tower, difficulties sometimes were encountered in analyzing the data because the dynamics of equilibrium liquid-vapor interface formation were superimposed on the dynamics of primary interest. Therefore, to assess the influence of these interface formation dynamics on other fluid behavior phenomena, an experimental study of interface formation transients was made. Drop tower tests were conducted using petroleum ether as the test liquid and with a 15. 2 cm diameter cylinder and spherical segment. Representative data from the tests with the cylinder are presented in the following paragraphs.

Significant oscillations of the interface were observed in all tests, and although the interface oscillation magnitudes and frequency were a function of Bond number, the same general behavioral pattern appeared in all of the tests performed. Some of the shapes assumed by the interface are shown in Figure 7. The photographs shown are from a typical test at a Bond number of 48.

The test data indicated that, except for very high Bond numbers (on the order of 400 or greater), the time for a surface to attain complete equilibrium in containers about 15. 2 cm or greater in diameter cannot be measured using drop tower testing. Secondary oscillation modes will persist throughout the test period and will exhibit negligible damping. However, results were obtained that enabled estimates to be made of the time required for a surface to attain a state of quasi-equilibrium. It was assumed that the primary vibrational mode of the surface formation transients is represented by the interface centerpoint oscillations; then, the frequency and magnitude of the "overshoot" were used to estimate the primary period of oscillation and the damping decrement, respectively, where overshoot depth was measured from the normal gravity liquid level. These measured amplitudes and oscillation periods were then used to estimate the period of time required for the surface to attain quasi-equilibrium.

However, the MSFC data could not be applied directly to other container diameters and fluids. Other investigators [16, 17] have shown that interface oscillations are related to fluid properties and container diameter (D) by the following relation:

$$\text{Oscillation Period} \approx \left(\frac{\rho}{\sigma}\right)^{1/2} (D)^{3/2}$$

This relation does not consider viscous effects; however, the influence of viscosity is generally accepted as being negligible in comparison with surface tension for containers of practical size.

If the preceeding equation is used to nondimensionalize the measured surface response times, the MSFC experimental data can be scaled to various 0-deg contact angle fluids and cylindrical containers. The nondimensionalized versions of the oscillation period, $\bar{t}_p$, and damping time, $\bar{t}_t$, are presented respectively in Figures 8 and 9 as a

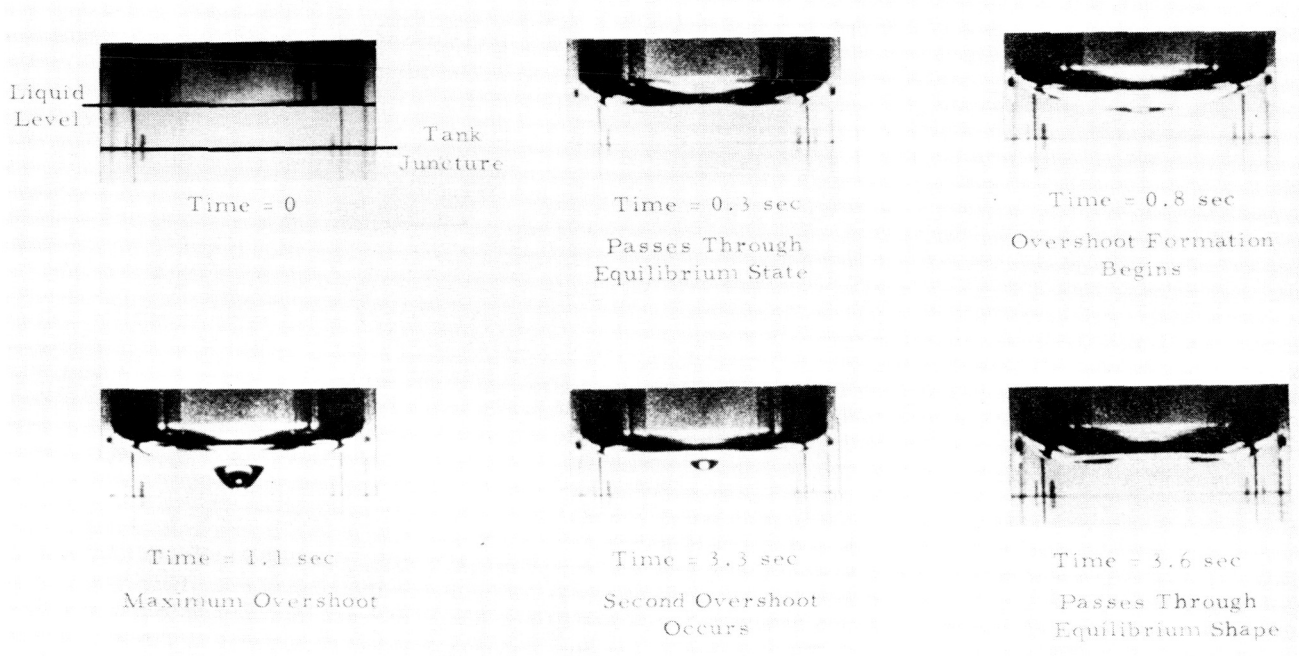

Figure 7. Experimental interface shapes in a cylinder at a Bond number of 48.

function of Bond number and are defined by the following empirical relations:

$$\bar{t}_p = \frac{t_p}{(\rho/\sigma)^{1/2} (D)^{3/2}} = \frac{0.847}{(B_N)^{0.39}}$$

and

$$\bar{t}_t = \frac{t_t}{(\rho/\sigma)^{1/2} (D)^{3/2}} = \frac{6.12}{0.0345\ B_N}$$

The usefulness of Figures 8 and 9 (i.e., the usefulness of the relations for $\bar{t}_p$ and $\bar{t}_t$) is illustrated in the following examples:

1. If a drop tower test objective requires that a petroleum ether surface attain quasi-equilibrium within 2 sec after test initiation at a Bond number of 80, then a container diameter of about 8.6 cm would be necessary. An oscillation period of 0.8 sec would occur in the test.

2. In a full-scale vehicle, an oscillation period of 445 sec would exist in a 6.6 m diameter container of liquid hydrogen at a Bond number of 80, and approximately 1130 sec would be required for the interface to attain quasi-equilibrium after injection into the low gravity environment.

Although a major portion of an experimental interface usually oscillated throughout a test, the interface curvature near the container walls appeared to agree rather well with the theoretical equilibrium shape in that same region during a significant portion of each test period. At times the entire interface matched the theoretical configuration reasonably well. Deviations of the measured interfaces from the theoretical interfaces were attributed to the experimental surface oscillations and optical distortion.

CAPILLARY DEVICES IN CRYOGENS

Prior to 1968, consideration of capillary devices in propellant management problems was restricted to storable propellants in cryogen systems. In 1968 a study was initiated that emphasized the heat transfer and thermodynamic problems involved in the use of capillary devices in large scale cryogenic vehicles. The study objectives were (1) to generate data of a general and parametric nature that would enable application to a wide range of missions and (2) to design example systems for orbital engine restart and propellant transfer. The S-IVC and S-IIB manned Mars flyby missions were used as design drivers for the restart and transfer problems, respectively.

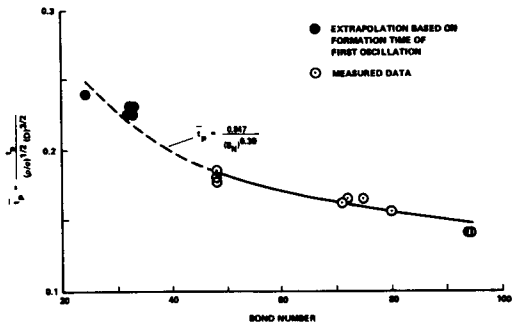

Figure 8. Nondimensionalized interface oscillation period in a cylinder versus Bond number.

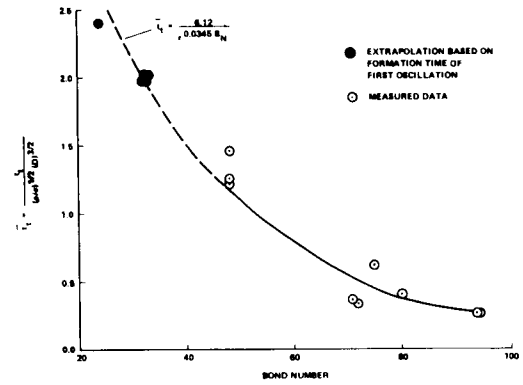

Figure 9. Nondimensionalized time required for interface to attain quasi-equilibrium in a cylinder versus Bond number.

S-IVC Orbital Restart

The S-IVC mission consists of three S-IVC vehicles (modified S-IVB vehicles) assembled in orbit. The second S-IVC is required to restart in orbit after 30 days and was the basic problem of interest in this study. The mission ground rules are shown in Table 3. The restart system employed a thermodynamic vent system for main tank pressure control and a capillary device (restart basket) for propellant control (Fig. 10). The general philosophy was to maintain control of and properly condition sufficient liquid propellants for idle mode engine restart and resettling of bulk propellants.

Two problem areas required consideration, fluid mechanics and thermodynamics. Fluid analyses involved assessment of low-gravity fluid behavior phenomena such as propellant resettling time, start basket spillage, vapor ingestion because of settling dynamics, basket refill, and suction dip. The time required to resettle the propellants determines start basket size in the case of a single engine restart[2]. Surface tension retention at 10^{-4} g to 10^{-6} g can be accomplished with relatively coarse screens or perforated plates. However, the restart thrust (0.337 g) dictates that a fine mesh screen be used to prevent spillage from the basket. During the reorientation sequence, extreme turbulence can be encountered which can cause vapor to be entrained in the liquid flowing into the basket. Also, after propellant resettling, the propellant flow rate into the basket must exceed the feedline flow rate or the liquid cannot displace the vapor from within the basket that was formed before the bulk liquids settled at the basket. Finally, sufficient start basket volume margin must be allowed to prevent vapor ingestion because of suction dip near the end of the reorientation process.

Thermodynamic requirements are, basically, that vapor formation within the liquid reservoir resulting from boiling and evaporation be precluded. Since it is generally believed that zero gravity will lower the heat flux required for incipient boiling, great care must be taken to minimize heat leaks through structural attachment points. In addition to localized surface boiling, bulk boiling (or flash boiling) can occur if the main tank pressure should drop below the saturation pressure of the restart liquid. Uncertainties involved in predicting zero-gravity heat transfer phenomena have resulted in general acceptance of the requirement for an active cooling system to maintain the reservoir liquids in a subcooled state.

FLUID SYSTEM

The resultant LH_2 start basket configuration is illustrated in Figure 11. The reservoir volume is based on a propellant settling time of 10 sec, which

2. In multiple orbital restart missions, the particular mission profile can significantly influence restart volume requirements if some of the engine burn periods are insufficient for propellant resettling and start volume replenishment.

TABLE 3. S-IVC MISSION GROUND RULES

Configuration:	S-IVB LH_2 Tank J2S Engines No Recirculation System S-IVB Pressurization System
Orbital Environment:	490-km Circular Orbit 10^{-6} g Drag Acceleration Total Orbital Heating = 626 W Forward Dome and Joint Area = 58.6 W Cylinder Wall = 50 W Aft Dome and Joint Area = 138 W Common Bulkhead = 380 W
Vehicle Conditions:	60 Percent Liquid Hydrogen Level Thermodynamic Vent Separator $(6.9 - 13.8) \times 10^4$ N/m^2 Band 30-day Mission Duration 17.2×10^4 N/m^2 Tank Pressure
Orbital Restart:	Idle Mode Operation LH_2 Flow Rate = 1.3 kg/sec Vehicle Acceleration = 8.23×10^{-3} g Main Engine Operation LH_2 Flow Rate = 33.7 kg/sec Vehicle Acceleration = 0.337 g

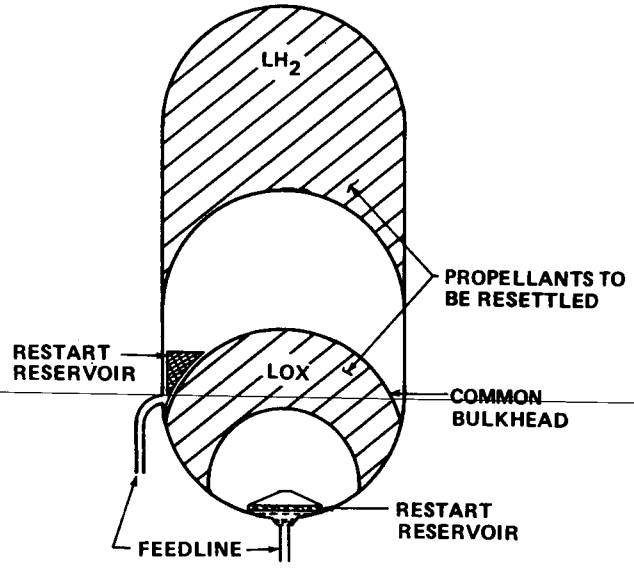

Figure 10. S-IVC acquisition concept for engine restart.

was estimated using the MAC computer program previously described. The settling time dictated a basket volume of 5.6 m^3, and the shape minimized the surface area (25.6 m^2) that, in turn, minimized thermodynamic cooling requirements. The basket is constructed predominantly of solid material with 1.90 m^2 of 200 by 1400 mesh screen (dutch-twill weave) on the front and sides. The top of the basket has an opening of 0.065 m^2 with a 200 by 600 mesh screen. The screen area at the top is such that the pressure loss because of vapor flow across the screen exceeds the liquid pressure head and thereby inhibits liquid spillage. A pull-through suppression screen was placed at the top of the outlet and, based on subscale S-IVC outflow test correlations, should limit residuals to 1.12 m^3. The 200 by 1400 mesh deflector screen was added to resist the passage of vapor forced into the basket as a result of vapor impingement during resettling. It was estimated that velocities must exceed 6 m/sec for vapor to break through the outside basket screen surfaces. MAC computer analyses indicated maximum velocities of 16.5 m/sec.

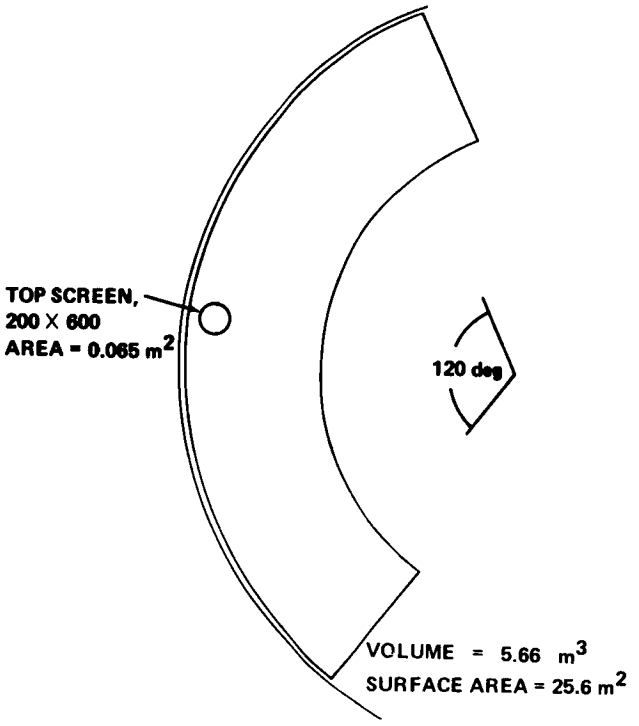

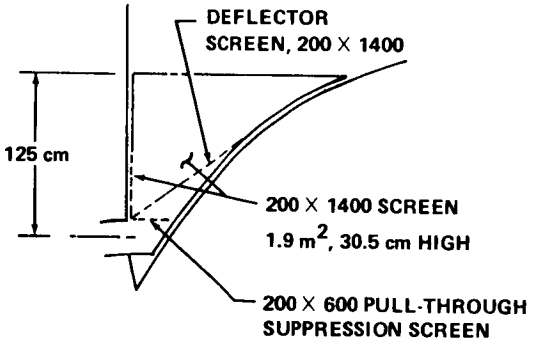

Figure 11. S-IVC LH_2 capillary restart basket.

The lox restart reservoir design is based on considerations similar to those in the LH_2 case. The resulting design is shown in Figure 12. The reservoir volume is 1.12 m^3 and the reservoir has a screen flow area of 0.88 m^2 with a 200 by 600 mesh screen.

The heat exchanger vent system described later requires a continuous supply of liquid hydrogen. Screen capillary collectors are employed to assure the liquid supply. The 5 cm diameter tubes constructed of 200 by 600 dutch-twill screen mesh

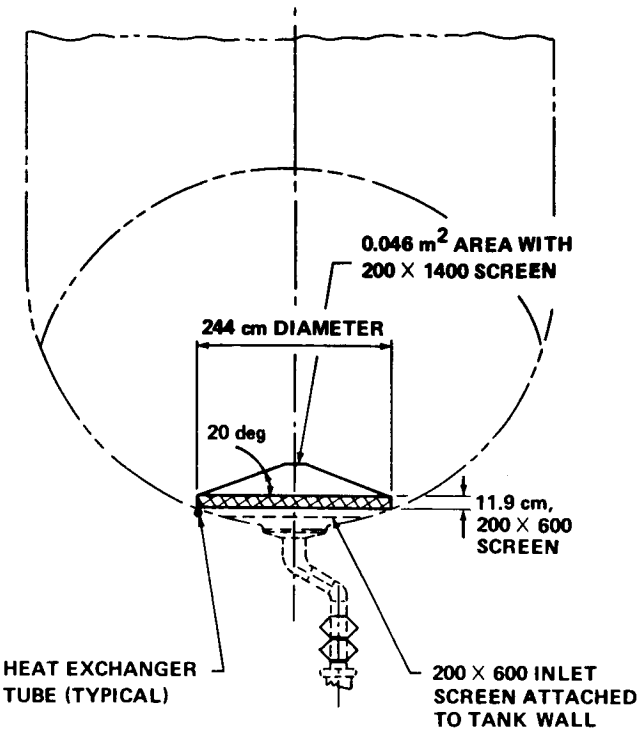

Figure 12. Oxidizer tank reservoir arrangement.

guarantee liquid containment against orbital drag and attitude control maneuvers. The selected configuration of three tubes, 120 deg apart, should assure sufficient liquid contact since the LH_2 tank is 60 percent full. The flow pressure drop would be on the order of 4.78 N/m^2 and this is well within the 334 N/m^2 surface tension retention capability of the screen.

The total hardware weights for the LH_2 and lox systems are 179 kg and 67 kg, respectively, including thermal conditioning hardware.

THERMODYNAMIC SYSTEM

The overall thermal control system selected for the S-IVC restart scheme is illustrated in Figure 13. The basic proposed system uses heat exchangers to cool the start baskets and to maintain constant pressure in the LH_2 and lox tanks. It should be noted that the system operates independently of the main tank pressure vent control system. This allows the restart system cooling flow to be fixed.

The start basket cooling system inlet liquid is expanded to about 68 940 N/m^2 and is then passed

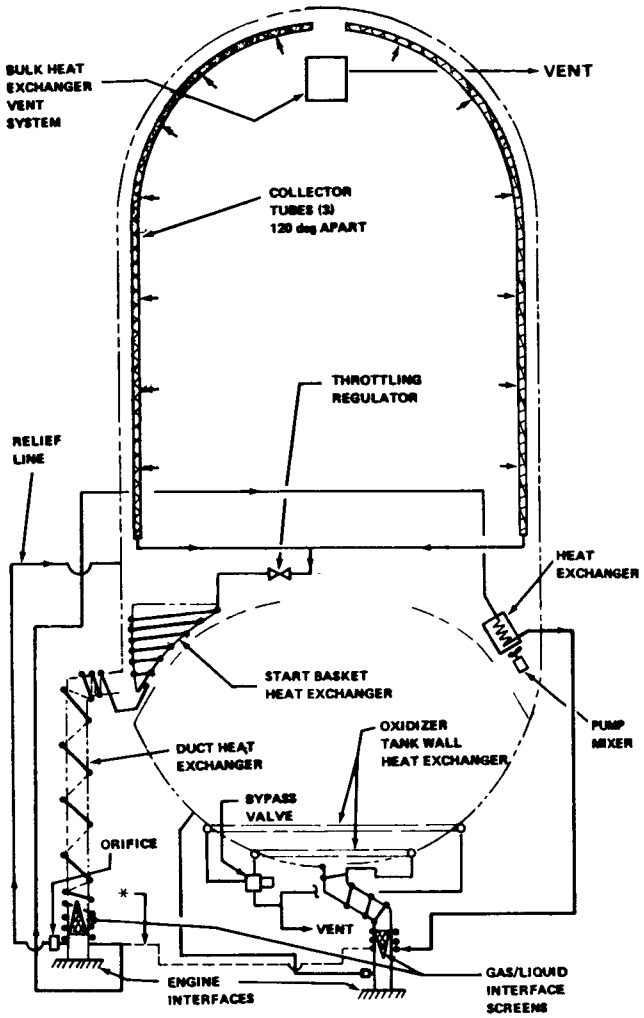

Figure 13. S-IVC heat exchanger system schematic.

around the LH_2 start basket and feedline to maintain subcooled conditions, thereby preventing vapor formation. The cooling coils are routed from the feedline either to an LH_2 bulk heat exchanger integrated directly with a mixer, or directly to the lox tank. The routing depends on whether or not sufficient cooling capacity remains in the vented fluid after passing over the feedline to effectively assist in cooling the LH_2 propellants. Thermal conditioning of the lox restart basket is accomplished by cooling the outside of the lox tank in the vicinity of the basket. The coils are finally passed over the lox feedline and vented to space. A total vent flow rate of 4 kg/hr proved sufficient to provide all the necessary cooling.

Examination of the overall heating data and the LH_2 basket location (Fig. 13) illustrates that the basket area near the common bulkhead is the most critical area to be cooled. Stagnant superheated gas can be formed in the region between the basket and bulkhead if sufficient cooling is not provided. It was estimated that the total maximum heat to be absorbed up to the basket outlet is about 293 W.

A maximum ullage pressure drop below saturation of 960 N/m^2 was estimated. Resulting bulk boiling would not create sufficient vapor within the basket (about 2 percent) to cause problems.

The LH_2 feedline is connected to a heat source from which it cannot be effectively insulated. Initially, the feedline will be wet, and if the contained liquid is allowed to evaporate, substantial vapor would be forced into the basket. Thus, removal of the 29.3 W generated by the feedline must be intercepted by the vent cooling system. A conical screen was placed in the line near the engine interface to prevent vapor migration up the line and to optically suppress incident radiation from downstream heat sources.

The lox tank external wall surface near the start basket was wrapped with cooling coils sufficient to remove a minimum of 280 W and thereby prevent vapor formation within the basket. One coil was attached above the start basket to provide additional tank cooling as required. The fluid circulation through the additional loop is controlled by a switch that senses oxygen tank pressure. A continuous flow passes through the start basket and feedline cooling coils.

A further concern was the possibility of lox freezing. The system was sized such that a minimum temperature of 67.3°K would occur, thereby assuring temperatures above the freezing point of 55.6°K. Additionally, mixing within the tank minimizes the possibility of localized overcooling.

A minimum feedline cooling capability of about 20 W was provided with the remaining cooling capacity. A tube length of 10 m was required. Total tube lengths (1.27 cm inside diameter) of 114.3 and 30.5 m resulted for the LH_2 and lox systems respectively. The flow pressure drops were 6.2×10^3 and 11.7×10^3 N/m^2 for the LH_2 and lox portions respectively.

S-IIB/Lox Tanker

In the S-IIB mission, a lox tanker is required to remain in orbit with a full tank for 163 days prior

to the transfer of lox to the S-IIB. This study resulted in the design of a capillary acquisition system for the lox tanker. Table 4 summarizes the lox tanker ground rules.

The basic objective of the study was to provide a continuous flow of vapor-free liquid out of the tanker under essentially zero-gravity conditions with intermittent 10^{-3} g disturbances. The concept proposed is shown in Figure 14. The liquid is acquired by eight screen channels which provide a continuous flow of liquid provided certain conditions are satisfied. It is essential that the channels have a high surface area for maintaining continuous contact with the liquid, especially near the end of the transfer when the propellant level is low and residual minimization is of concern. The outflow pressure drops cannot exceed the screen surface tension retention capabilities. The channels are required to retain liquid against momentary disturbances, and the channels must be thermodynamically conditioned to prevent vapor formation resulting from boiling, either because of heat leaks or tank pressure drops. The fluid and thermodynamic system results are described in subsequent paragraphs.

FLUID SYSTEM

As mentioned previously, the channel system should maintain constant contact with the bulk liquids insofar as possible. The continuous low-gravity level of 10^{-6} g resulting from drag creates a Bond number of approximately 6. Therefore, the ullage bubble will be essentially spherical and the walls will be continuously wetted. The proposed channel system takes advantage of the wetted wall condition; thus, channel uncovering should not occur until near the end of the transfer period. A cylindrical screen shell is used as a liquid reservoir to provide uninterrupted flow should the channels be momentarily uncovered.

Propellant transfer rate strongly influences transfer efficiency. The flow rate and area, which is a function of liquid contact, must be such that the pressure drop does not exceed the screen retention capacity. An assessment of minimum flow area conditions near the end of the transfer prompted the addition of a channel about the tank equator, thereby increasing the flow area and reducing frictional flow losses.

The sensitivity of tank residuals to channel geometry is illustrated by the following example results. Minimization of channel size reduces the unusable liquid trapped within the channels but increases pool residuals within the tank for a given flow rate. For instance, a 23-μm screen channel size of 3.82 by 35.6 cm resulted in a minimum total residual of 1230 kg at a flow of 24 kg/sec. Substituting a channel height of 3.56 cm increased the minimum residuals to 1540 kg[3].

The 200 by 600 mesh screen mesh channels (3.82 by 35.6 cm) provide a total surface area of 66.5 m^2. The reservoir is 1.22 m in diameter by

TABLE 4. LOX TANKER GROUND RULES

Configuration:	LMSC Tanker for S-IIB Receiver (5.537 m Diameter Sphere)
Orbital Environment:	185 × 490 km Transfer Orbit 10^{-6} g Drag Acceleration 10^{-3} g Disturbances Possible Total Orbital Heating is Equivalent to 3640 kg Boiloff in 163 days
Vehicle Conditions:	163-day Mission Duration 10×10^4 N/m^2 Tank Pressure Thermodynamic Vent Separator 95 percent Initial Liquid Oxygen Level
Orbital Propellant Transfer:	Transfer Flow Rate = $\frac{90\ 000\ \text{kg}}{90\ \text{min}}$

3. The residuals could be virtually eliminated if a low settling acceleration of approximately 6.5×10^{-4} g was used during the last 200 sec of the transfer period.

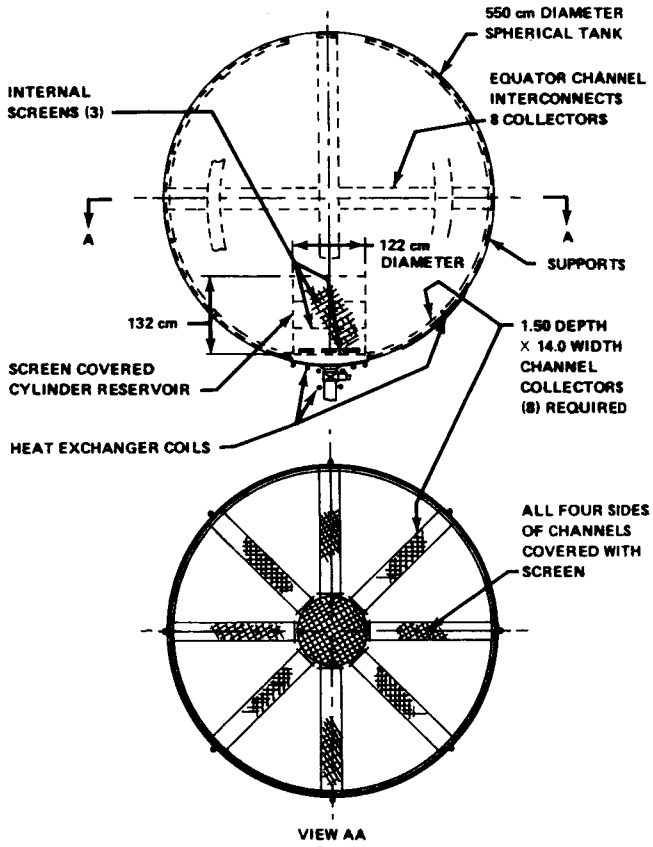

Figure 14. Oxidizer tanker capillary acquisition arrangement.

1. 32 m high (7. 15 m^2), consists basically of a perforated structural shell, and is covered with 200 by 600 mesh screen, except for the top. The top has a 165 by 800 mesh screen so that the initial vapor ingestion occurs at the top rather than at the sides. The three internal horizontal screens are also 165 by 800. The total acquisition system weight (including the thermal system) was 194 kg. All screens, the channel, and the reservoir were made of aluminum.

THERMODYNAMIC SYSTEM

The thermal considerations for the S-IIB/lox tanker system are similar in many respects to those described for the S-IVC restart system. Prevention of vapor formation within the channels required assessment of the following:

1. Heat leak by conduction through structural supports.

2. Heat transfer to superheated gas in contact with a channel. This problem is not as serious as in the S-IVC case since liquid should be in continuous contact with the channels and thereby keep the screens wetted. Evaporated liquid should be replaced by wicking.

3. As in the S-IVC case, bulk boiling resulting from a tank pressure drop should not be a problem since pressure decreases were predicted to be small (963 N/m^2).

Thus, channel and reservoir structural heat leak is the most critical problem, especially since the relatively low lox cooling capacity must be distributed as uniformly as possible over a large surface area and to many potential "hot spots."

The basic system proposed utilizes a thermodynamic vent system with liquid at the heat exchanger inlet. The collector channels are tapped to provide this liquid. After cooling critical areas, the vented fluid is routed to a bulk heat exchanger/mixer system within the tank pressure control[4]. The total vent flow rate available was determined by requiring that tank pressure be maintained constant. The flow distribution problem was minimized by assuming that each cooling circuit had a throttling device and that liquid is taken from each channel or reservoir to be cooled.

Several basic internal channel cooling methods such as that represented by Figure 15 were examined. However, in each case the total coolant tube heating was too high. It was ultimately determined that the cooling tubes had to be located external to the tank walls with direct attachment only at critical areas. Such an arrangement is shown in Figure 16. Destratification by mixing is especially important in this concept since the channels are not directly cooled. Screened areas were assumed wetted constantly because of wicking.

The coolant flow loops are illustrated in Figure 17. A total of 80 attachments with a cooling requirement of 26 W was estimated. About 29 W was allotted to cool other areas. A flow rate of 9. 8 kg/hr was split into 10 equal flow passages (9 channels and a reservoir/pump area) with a flow length per passage of 9 m. A total pressure drop of 550 N/m^2 was calculated using 0. 32 cm tubing.

4. A separate bulk heat exchanger system could have been used for tank pressure control with separate on-off flow requirements.

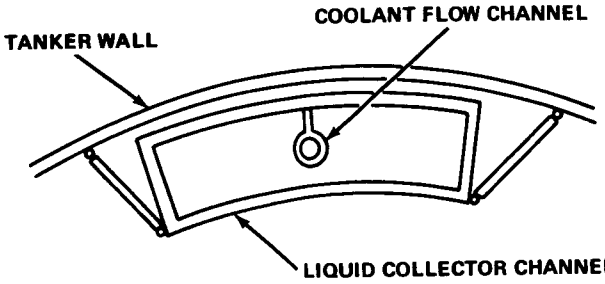

Figure 15. Lox tanker cooling with cooling channels inside the collector channels.

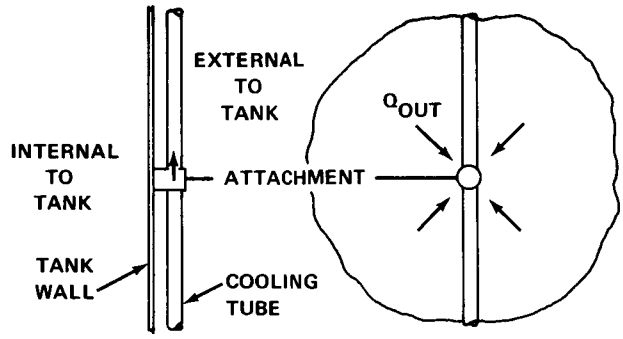

Figure 16. Lox tanker external cooling tube attachment.

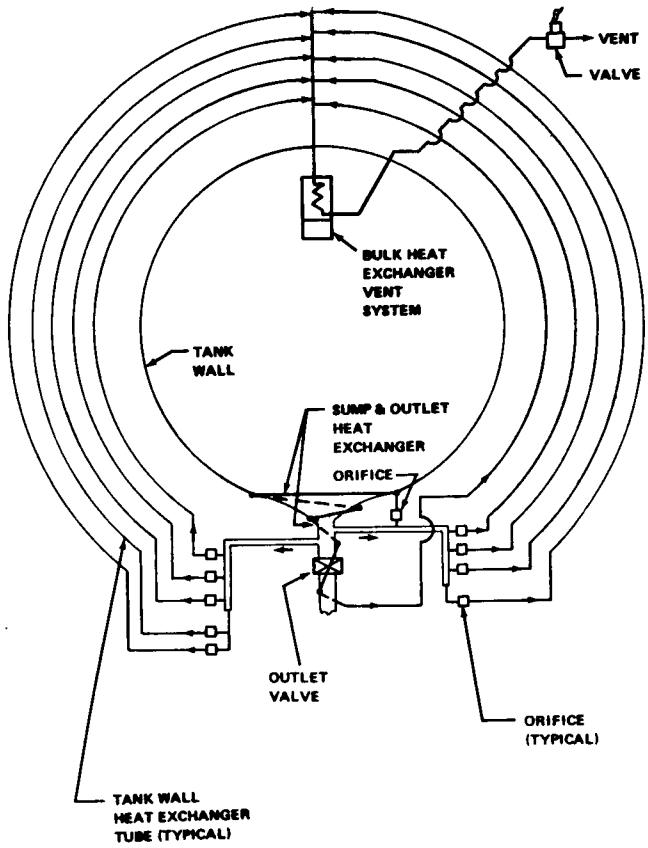

Figure 17. Lox tanker heat exchanger schematic.

Systems Comparison

Capillary systems were compared with dielectrophoretic, bladder, and settling systems for both the S-IVC and lox tanker missions. Comparisons were made on the basis of system weight, reliability, cost, and safety. The weights were based on preliminary analyses.

S-IVC system weight comparisons are best illustrated by considering Figure 18, which presents system weights for the candidate concepts versus propellant settling time. Obviously, all system weights increase with increasing propellant settling time except the bladder system. The settling method weights were estimated assuming that all vapor flowed to the main engine operating in the idle mode and that the thrust did not provide useful propulsion since the actual thrust with random liquid-vapor mixtures would be unpredictable. Idle mode settling requires a minimum of 25 sec and a weight penalty of 270 kg.

Surface tension and dielectrophoretic systems require approximately 10 sec settling time since liquid flow to the engine is assured. Capillary system weights for systems of all stainless steel, stainless with aluminum supports, and all aluminun are presented. The all aluminum system weight of 192 kg represents the minimum weight system. An all aluminum dielectrophoretic system weighs approximately 406 kg. The estimated polymetric bladder system weight is 514 kg based on a bladder placed along the longitudinal tank axis that expandec against the bulk liquid.

From a reliability and cost standpoint, linear acceleration was rated best. However, it is significant that if more than one restart is required, the fixed weight penalty of the surface tension system enhances its standing relative to linear acceleration Safety in lox is questionable with the dielectrophoretic system. The bladder reliability for such a large container is questionable.

Weight comparisons made for the lox transfer mission are summarized in Table 5. Two settling systems were considered, one using a continuous

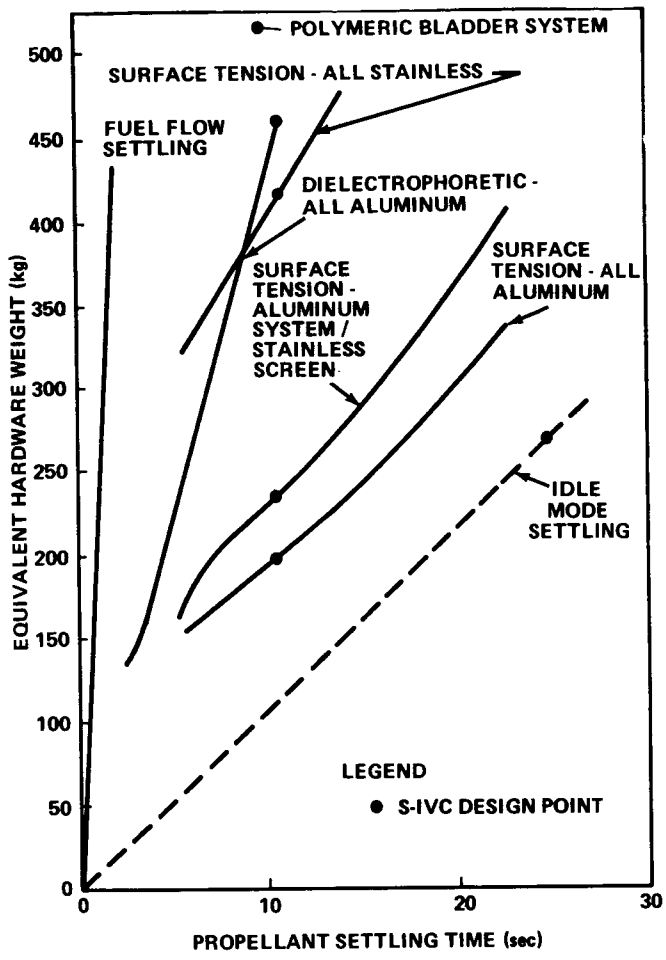

Figure 18. Hardware weight comparison for S-IVC restart system.

acceleration of 3×10^{-5} g and the other using an increased scavenging acceleration of 6.5×10^{-4} g near the end of the transfer to reduce residuals. The scavenging acceleration was assumed also in the residual estimates for the other systems.

The weights, with scavenging, range from 730 kg for linear acceleration to 466 kg for the bladder system. From a total viewpoint, the linear acceleration is most reliable and therefore will probably be used whenever the mission capabilities are not greatly compromised. The surface tension system is competitive, however. Its basic weakness results from the lack of technology and it is, therefore, somewhat less reliable. The bladder and dielectrophoretic systems have the same reliability problems that were mentioned for the S-IVC case.

LIQUID CONTROL WITH CAPILLARY DEVICES

The basic objective of this program was to experimentally investigate, using drop tower testing, the ability of screen barriers and perforated plate barriers to position and control fluids against low-acceleration environments. The program was divided into four problem categories:

1. Liquid-vapor interface hydrostatic stability provided by perforated plates and square-weave screens when subjected to accelerations normal to the capillary barrier.

2. Schemes for preventing passage of settled liquids through capillary barriers.

3. Liquid-vapor interface stability provided by capillary barriers against accelerations parallel to the barrier surface.

4. Liquid refill of capillary annuli and vapor entrapment.

Test Procedure

Approximately 300 drop tests were conducted in a 2.1 sec drop tower using various axial and lateral accelerations, container sizes, and test liquids. Methanol, carbon tetrachloride, Freon-TF, and chloroform were selected as test liquids to simulate the surface tension and wetting properties of a wide range of space propellants. The fluid behavior data were provided by 16 mm movies of liquid motions in transparent cylinders.

Experiment Results

HYDROSTATIC STABILITY

A total of 77 drop tests was conducted to determine the hydrostatic stability of perforated plates and square-weave screens against axial accelerations normal to the barriers. Accelerations were constant and ranged from 0.0013 to 0.055 g. In all cases, the initial liquid surface was slightly above the barrier surface. Cylinders that were 25 cm high and 12.7 cm in diameter were used with the barrier placed 10 to 15 cm above the bottom.

TABLE 5. LOX TANKER WEIGHT COMPARISONS

Transfer Method / Type of Penalty	Settling (kg)	Settling with Scavenging (kg)	Aluminum Surface Tension, Channels (kg)	Aluminum Surface Tension Channels, Stainless Screens (kg)	Stainless Surface Tension, Full Liner (kg)	Dielectro-phoresis (kg)	Bladder (kg)	All Stainless, Surface Tension Channels (kg)
Vent System	4.5	4.5	12	12	23	4.5	4.5	0.90
Transfer System	45.5	45.5	189	236	310	222	74.0	376
Residuals	855	15	15	15	15	15	420	15
Secondary Propulsion	318	665	352	352	352	352	-	352
Added Pressurant	-	-	-	-	-	-	13.5	-
	1223	730	568	615	700	593	512	744

The results for perforated plates are presented in Figure 19, which is a plot of pore radii versus the ratio of kinematic surface tension (β) to acceleration. The straight line corresponding to a Bond number of 0.84 (based on pore radius) is generally the dividing line between stable and unstable regions. Thus, the critical Bond number criteria previously determined by other investigators [18] with glass tubes was verified.

The data for square-weave screens are presented in Figure 20. Unlike the plates, however, the critical Bond number for pore stability is 0.45 (based on one-half the weave opening). This lower Bond number is attributed to three-dimensional effects of the screen weave on the interface shape; i.e., the interface at each pore is not necessarily perpendicular to the acceleration vector as in the perforated plate case.

LIQUID SETTLING/DAMPING

The objective of the liquid settling/damping tests was to determine the capability of various barriers to dissipate settling liquid forces and retain the liquid. The tests were similar to those described previously except that the initial liquid level was below the barriers[5]. The liquid level ranged from 5 to 8 cm below the barrier. Settling accelerations from 0.022 to 0.04 g resulted in Bond numbers from 30 to 135. The barrier performance was categorized into the seven damping regimes shown in Figure 21. Categories A through D allowed liquid passage ranging from none to very little. The remaining categories, E through G, allowed liquid passage ranging from moderate to substantial. It should be noted that there is no definite line of demarcation from one category to the next.

During the testing, it was ascertained that liquid flow along the walls always contacted the barrier first and tended to "wet" the surface before the central column of liquid impinged. This wetting action significantly enhanced barrier performance, and, therefore, some tests were conducted with a ring deflector to prevent the wall flow effects.

5. In the previous hydrostatic stability tests, it was noted that if the initial liquid level was very slightly below the barrier, then the stability was significantly affected.

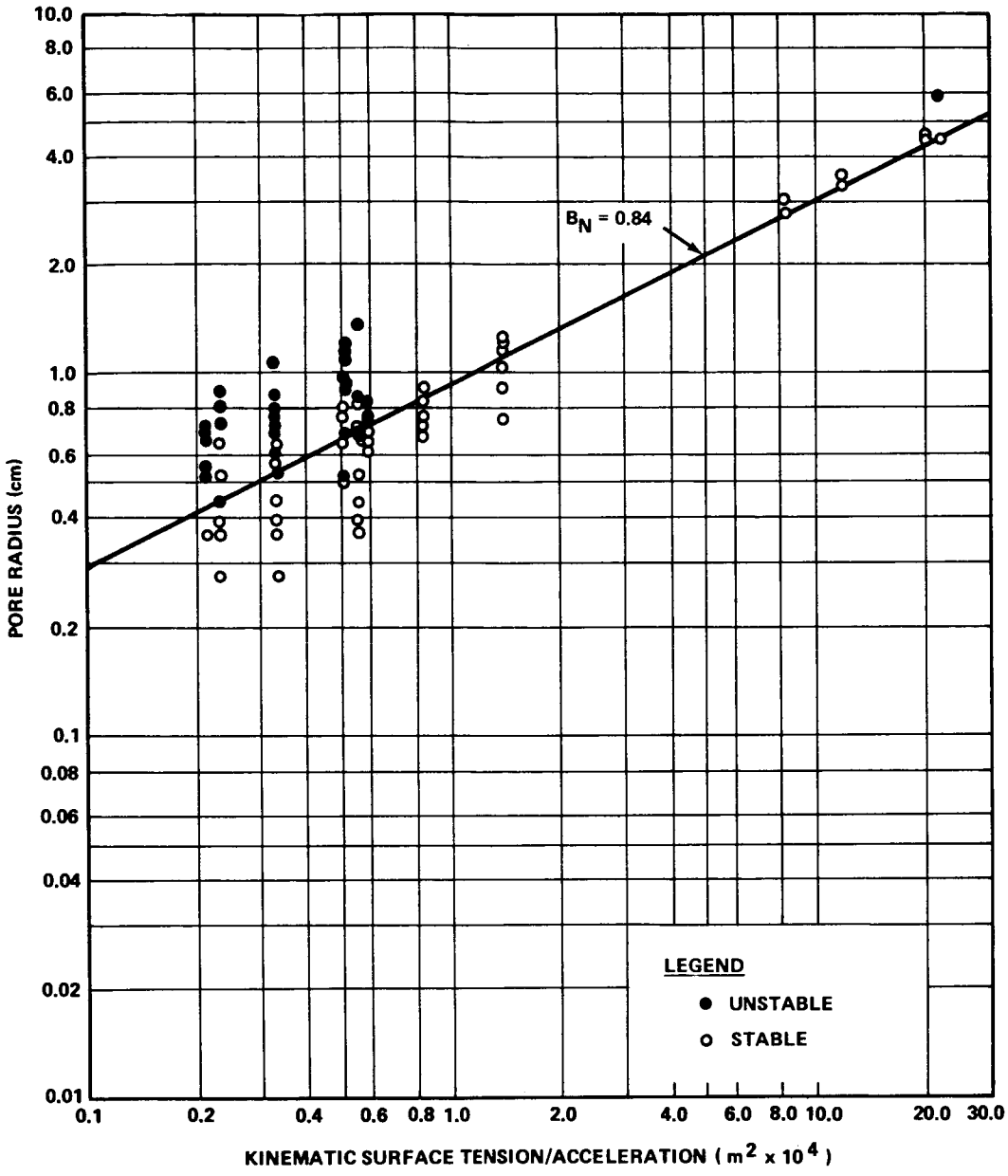

Figure 19. Perforated plate stability characteristics.

Barriers evaluated included single- and double-perforated plates, multi and single tubes, single- and double-layer square-weave screen, and single-layer dutch-twill screen. The open-to-closed area ratio ranged from 0 to 0.575. The dutch-twill intricate weave has no open area normal to the acceleration. The double plates were arranged so that the hole openings were staggered.

The damping performance for selected barriers (single square-weave and dutch-twill screens, and single and double perforated plates) versus Weber number[6] is presented in Figure 22. The single-plate and square-weave screen results are for tests without a wall flow deflector. The dutch-twill and double-plate results are for tests with and without the deflector. As opposed to tests without barriers,

6. Weber number is based on liquid approach velocity and pore radius.

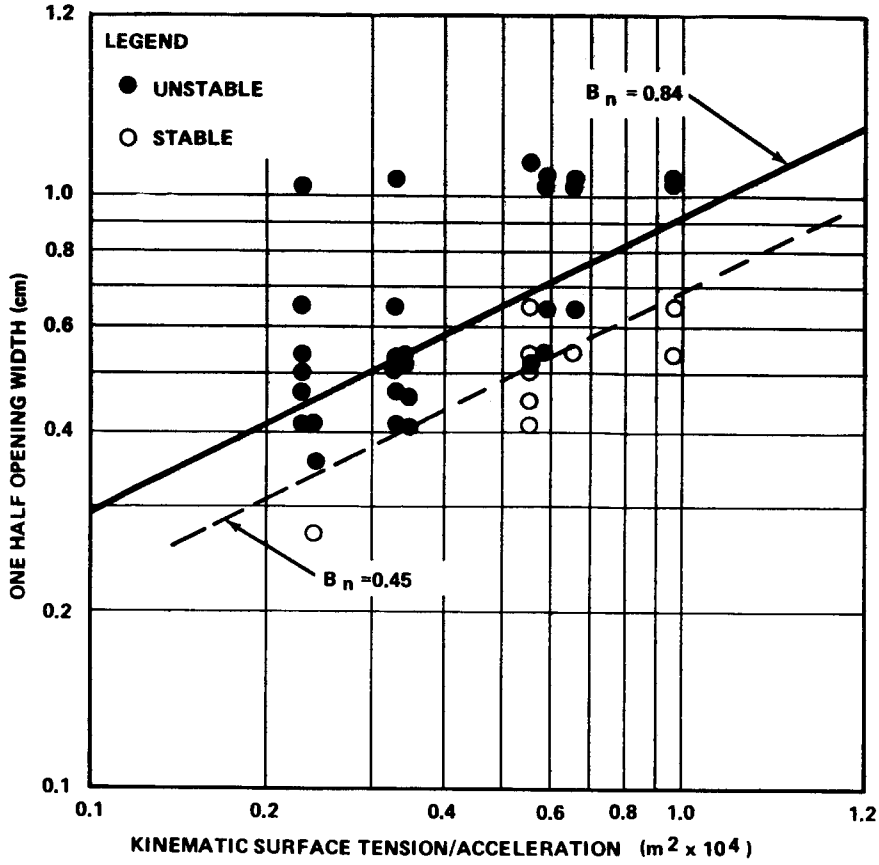

Figure 20. Square-weave screen stability characteristics.

only the dutch-twill and double-plate tests demonstrated no noticeable deflector influence and provided good damping for all tests.

Single-plate results indicated poor damping for open-to-closed area ratios greater than 0. 43 (ratios between 0. 176 and 0. 43 were not tested). A significant deflector influence was noted. For example, category B damping at a Weber number of 0.626 occurred without the deflector on the same plate, and category E damping at a Weber number of 0.463 occurred with the deflector on the same plate.

Apparently the torturous liquid passage paths provided by the dutch-twill and double-plate barriers enhanced the energy dissipation and capillary wetting action, which, in turn, provided good barrier performance.

HYDROSTATIC STABILITY/HORIZONTAL ACCELERATIONS

Perforated plates and screens were subjected to a range of accelerations parallel to the barrier surface and with the liquid surface at or above the barrier surface. The data were evaluated using a modified Bond number based on pore radius times maximum distance between any two pores and lateral acceleration. The critical Bond number ranged from 0. 85 to 2. 5. The open-to-closed-area ratio had a marked effect on stability; i. e. , stability decreased with increasing area ratio. Area ratios from 0 (dutch twill) to 0. 36 were tested.

CAPILLARY ANNULI REFILL

If the external surface of a capillary annulus is wetted before the annulus itself is liquid filled,

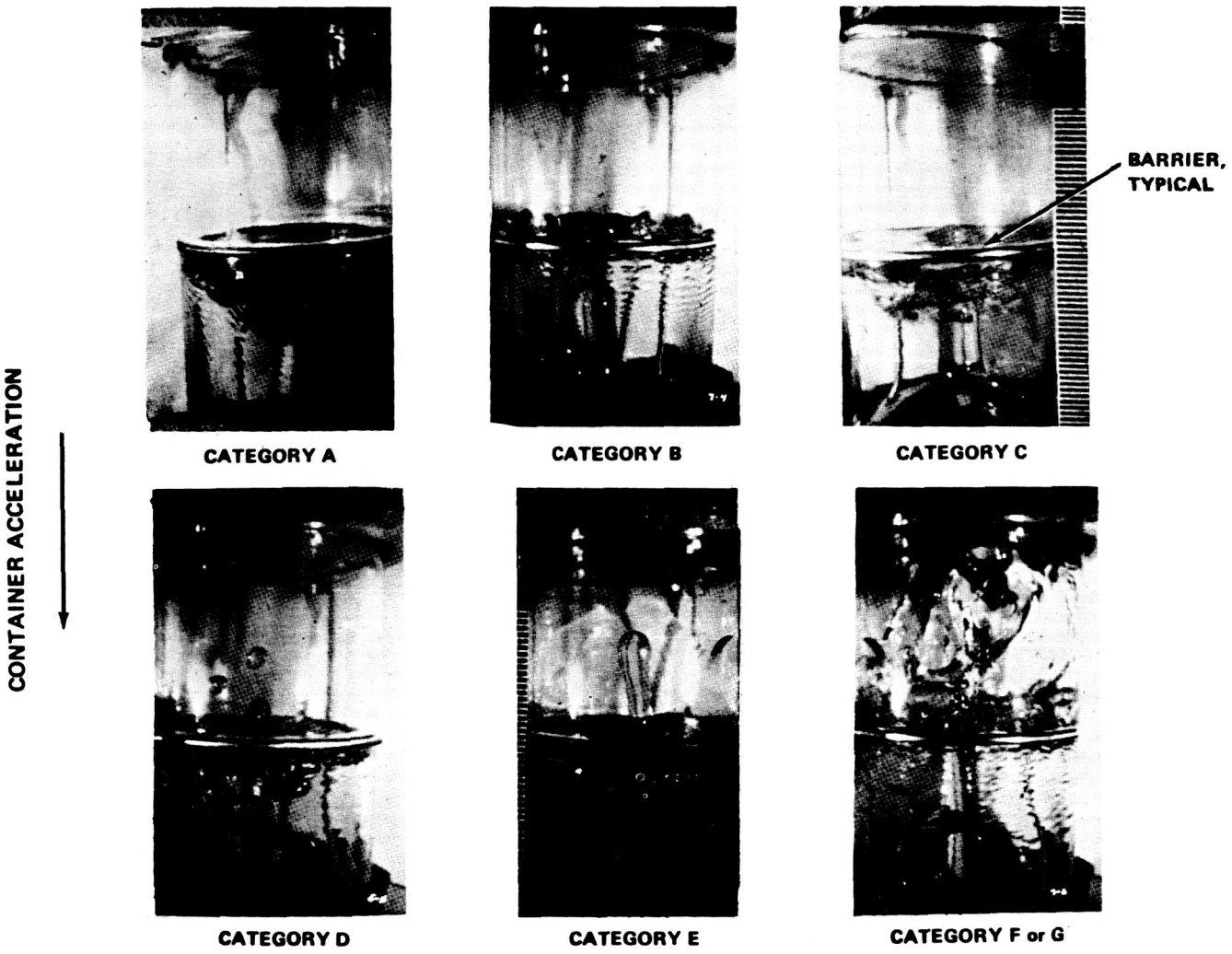

Figure 21. Typical barrier damping categorization.

then vapor entrapment occurs. This problem was analytically and experimentally assessed. The basic conclusion was that a barrier such as dutch twill enhances the surface wetting action; therefore, vapor entrapment is likely, especially in zero gravity. The problem can be minimized somewhat by using square-weave screens.

BOILING HEAT TRANSFER

As mentioned previously, the effects of boiling heat transfer and vapor formation must be considered in the design of capillary acquisition systems. The specific phenomena of boiling heat transfer as affected by reduced gravity have been experimentally investigated at MSFC and at the University of Michigan. Example MSFC data and a few brief comments on the University of Michigan work are presented in the following.

MSFC Boiling Data

Prior to the MSFC studies, it had been generally concluded that the boiling process was not significantly affected by reduced gravity, at least during the brief test periods available with drop towers and KC-135 aircraft. Most of this prior experimentation involved the use of small heat transfer surfaces or configurations that eliminated the effects of orientation. The MSFC experimentation employed heater surfaces that were large compared with the induced-gravity bubble size, and various orientations were evaluated.

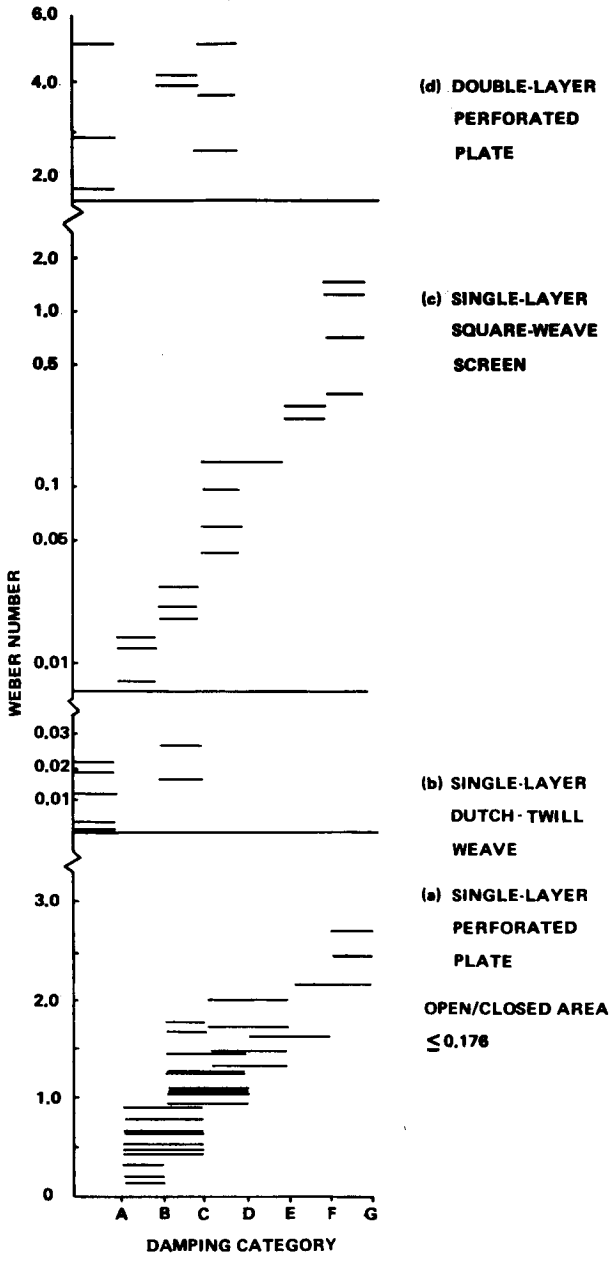

Figure 22. Damping performance of selected barriers.

The tests were conducted in the MSFC drop tower, which provides a free-fall time of about 4.1 sec. Two test surfaces, 5 by 10 cm and 5 by 5 cm, made of 0.16 cm copper were used. Most of the tests were conducted with the 5 by 10 cm surface however. Saturated Freon 113 was the test liquid used. Surface temperatures were provided by four copper-constantan thermocouples and the boiling phenomena were photographed with two 16-mm cameras at 400 frames/sec.

The general test procedure was to heat the surface to steady-state conditions and then lower the surface into the Freon. The heater power was turned off upon the initiation of low gravity and the resulting temperature-time decay was measured. Prior to each drop test, a normal gravity test was conducted to provide a direct comparison with the reduced-gravity results. Three surface orientations were assessed; vertical, horizontal facing upward, and horizontal facing downward.

Example photographic data describing vapor formation conditions on a vertical surface at normal and reduced gravity (0.01 g) are presented in Figure 23. The reference wire, 0.10 cm in diameter, can be used to estimate bubble departure size. As expected, the normal gravity bubbles were quite small and departed almost as rapidly as they were formed; however, in reduced gravity the departure diameters were about 5 to 10 times larger. Also, the slow moving bubbles departing from the lower portion of the surface tended to coalesce and accumulate with those above such that a vapor boundary layer began to form. Such vapor accumulation tendencies, especially during long orbital periods, can certainly affect heat transfer mechanisms and create significant vapor quantities in undesirable locations.

The type of thermal data obtained is illustrated in Figure 24. The measured temperature decays for two horizontal surfaces, one facing upward and one downward, are presented for normal and reduced gravity (0.01 g). With the heated face upward, the reduced gravity heat transfer exceeds that of normal gravity. However, with the surface facing downward, normal gravity heat transfer significantly exceeds that of reduced gravity. With a vertical surface, the normal gravity boiling heat transfer is slightly higher than in the low-gravity case.

Thus, it is concluded that both gravity level and surface orientation affect boiling heat transfer phenomena. The decrease in the boiling heat transfer coefficient for the vertical and horizontal surface facing downward indicates that a reduction in acceleration level to zero might cause a downward shift in the boiling curve for all orientations.

University of Michigan Data

Recently the University of Michigan has concentrated on incipient and steady boiling of cryogens subjected to reduced-gravity conditions. The parameters varied included: test fluid (LN_2 and

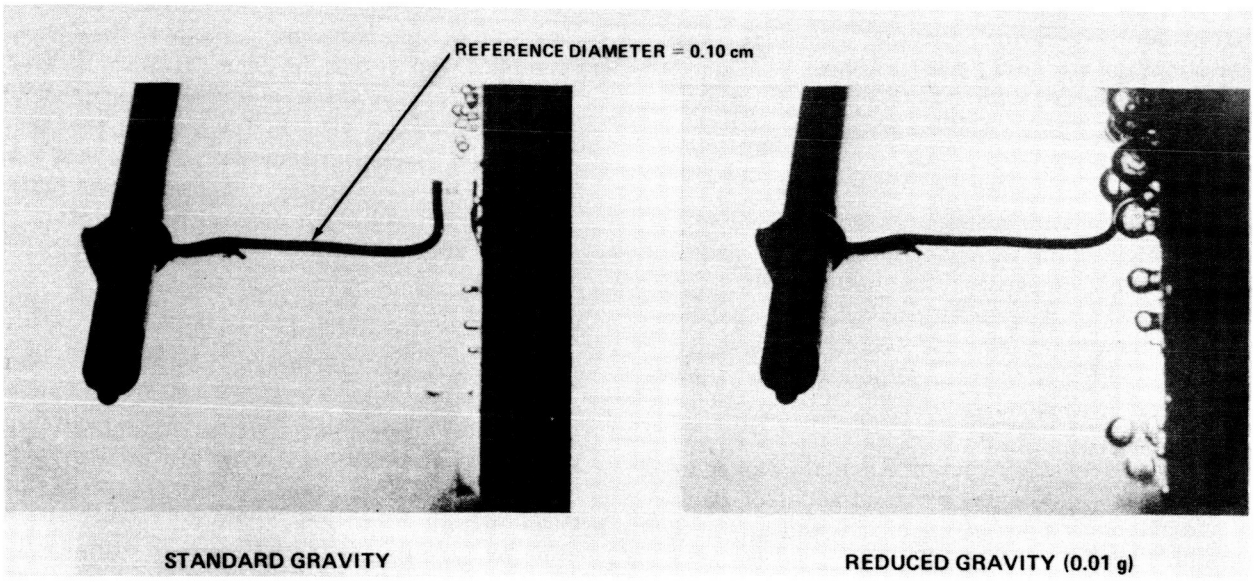

Figure 23. Boiling on a heated vertical surface.

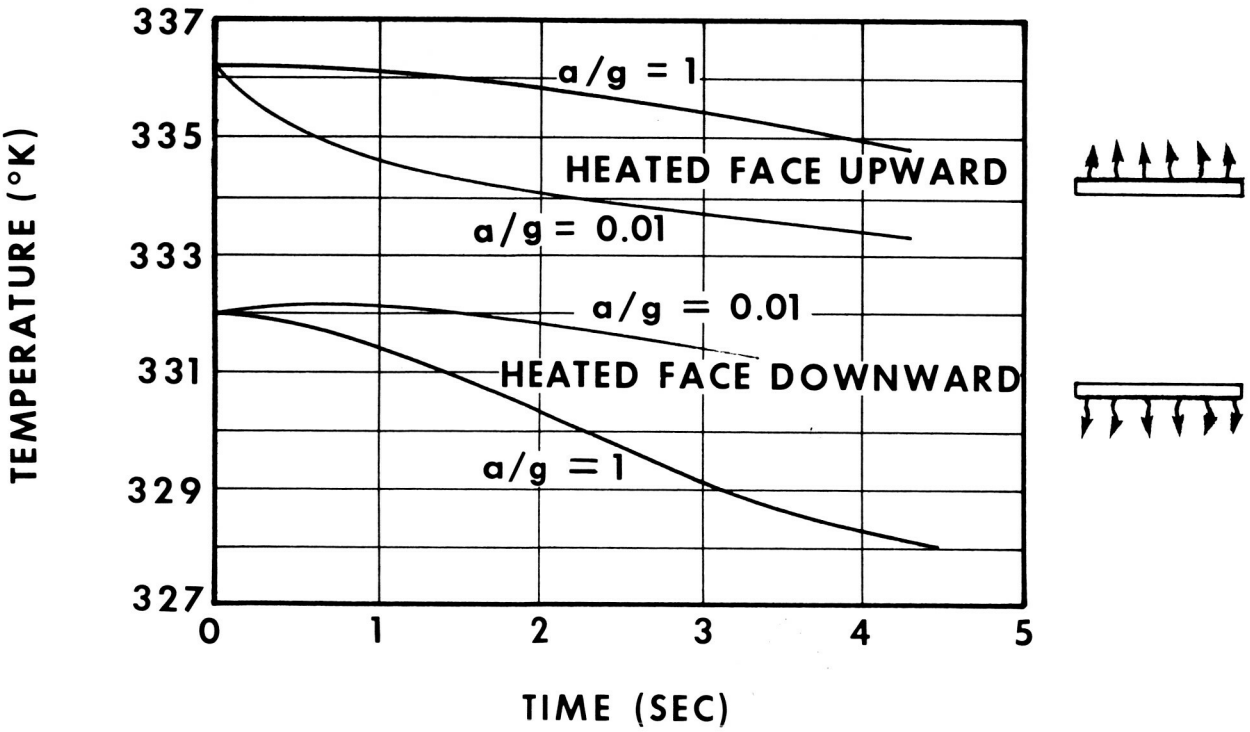

Figure 24. Comparison of standard-gravity and reduced-gravity heat transfer from a horizontal surface.

LH_2); heater surface temperature, geometry, and orientation; gravity level; and pressure. Reduced gravity was obtained with a 1.34 sec drop tower. As in the MSFC study, the transient calorimeter technique was used.

The LH_2 nucleate boiling curve was generated using a 2.5 cm diameter sphere at reduced[7] and normal gravity. In general, the boiling curve shifted downward at reduced gravity. For example, the peak nucleate heat flux for saturated liquid at 15.8×10^4 N/m^2 shifted from 63 000 W/m^2 at 1 g to 25 200 W/m^2 at reduced gravity.

The transient calorimeter technique was adapted to flat surfaces to determine the influence of geometry and orientation on boiling of LN_2 and LH_2 at normal and reduced gravities. A vertical cylinder was used to simulate a vertical flat plate at 1 g. A 7.6 cm diameter disc, in which the center 2.54-cm-square section constituted the measuring section, was used to determine the influence of orientation in LN_2 at 1 g and at reduced gravity. It was observed that for a given saturation temperature, the low-gravity heat flux is greater than that for 1 g in the horizontal down orientation, less for the horizontal up orientation, and less with the vertical orientation (heat flux in between the two horizontal positions). In reduced gravity, the geometry becomes influential in the way in which the liquid momentum is retained during the short test time. This indicated the importance of long-duration, reduced-gravity tests in determining the true nature of "near zero" gravity boiling heat transfer. Tests with the disc in liquid hydrogen were conducted only at 1 g, and the results were qualitatively similar to those with LN_2.

Measurements of incipient boiling at 1 g and at low gravity were made using a transient technique with a platinum wire in both LN_2 and LH_2. A step increase in power was applied, and from the transient wire temperature measurements, it was possible to observe when nucleate boiling began. It was observed in both LN_2 and LH_2 that the maximum heater superheat at nucleation was independent of the body forces present. Thus, it appears that in zero gravity, heat is removed primarily by conduction within the liquid. Whether or not boiling occurs is dependent upon heat leak rate, liquid conduction, and heat leak/zero gravity duration.

CONCLUSIONS

Orbital cryogen acquisition is a definite requirement for engine restart and/or propellant transfer on all major future missions. At present the most promising methods, especially for large scale vehicles, are acquisition by linear acceleration and acquisition by capillary systems. These two general approaches have been emphasized by MSFC in recent years. Many of the technology "tools" for acquisition by acceleration have been or are being developed. Continuous acceleration has been proven reliable through flight experience but is costly from a weight standpoint. Intermittent acceleration and propellant settling requires some state-of-the-art extension since it has not been attempted on a large scale cryogen vehicle. The method though is not always compatible with mission flexibility or profile. For multiple duty cycles, the weight costs can be significant also.

Capillary acquisition systems offer the advantages of reusability, passiveness, low weight, and mission flexibility. The major disadvantage is that of an undeveloped technology. The method does not lend itself to verification through ground testing. Hence, the lack of orbital experimentation with capillary systems has allowed the development of a significant technology gap. It is recommended that the experimental aspects of the method be vigorously pursued to enable its timely application to upcoming missions.

7. Reduced gravity or zero gravity denotes a maximum of 0.008 g which occurred because of drag forces during the free-fall drop tests at the University of Michigan.

REFERENCES

1. Hastings, L; and Rutherford, R.: Low Gravity Liquid-Vapor Interface Shapes in Axisymmetric Containers and a Computer Solution. NASA TM X-53790, October 1968.

2. Hastings, L. J.: Experimental Study of the Response of a Static Liquid-Vapor Interface After a Sudden Reduction in Acceleration. NASA TM X-53841, June 1969.

3. Toole, L. E.; and Hastings, L. J.: An Experimental Study of the Behavior of a Sloshing Liquid Subjected to a Sudden Reduction in Acceleration. NASA TM X-53755, August 1968.

4. Adams, R. G.; Bynum, B.; James, A. L.; and Hastings, L. J.: Performance Characteristics of Liquid-Vapor Sensors Operating in a Reduced Gravity Environment. NASA TM X-53840, May 1969.

5. Littles, J. W.: Nucleate Pool Boiling of Saturated Freon 113 in a Reduced Gravity Environment. NASA TM X-53942, August 1969.

6. Bradshaw, R. D.: Evaluation and Application of Data from Low-Gravity Orbital Experiment. Report No. GDC-DDB-70-003, General Dynamics Convair Division, April 1970.

7. Burton, K. R.; and Anderson, B. J.: Evaluation and Application of Data from Low Gravity Orbital Experiment, Phase II, Marker and Cell Method for Solution of Fluid Dynamics Problems. Report No. GDC-DDB70-004, General Dynamics Convair Division, July 1970.

8. Alexander, E. A.; et al.: Experiment Investigation of Capillary Propellant Control Devices for Low Gravity Environments. Report No. MCR-69-585, Martin Marietta Corp., June 1970.

9. Blatt, M. H.; et al.: Low Gravity Propellant Control Using Capillary Devices in Large Scale Gryogenic Vehicles. Report No. GDC-DDB70-007, General Dynamics Convair Division, August 1970.

10. Blatt, M. H.; et al.: Low Gravity Propellant Control Using Capillary Devices in Large Scale Cryogenic Vehicles. Report No. GDC-DDB70-008, General Dynamics Convair Division, August 1970.

11. Blatt, M. H.; et al.: Low Gravity Propellant Control Using Capillary Devices in Large Scale Cryogenic Vehicles. Report No. GDC-DDB70-006, General Dynamics Convair Division, August 1970.

12. Merte, H.: Incipient and Steady Boiling of Liquid Nitrogen and Liquid Hydrogen Under Reduced Gravity. Technical Report No. 7, University of Michigan, November 1970.

13. Satterlee, H. M.; and Reynolds, W. C.: The Dynamics of the Free Liquid Surface in Cylindrical Containers Under Strong Capillary and Weak Gravity Conditions. Technical Report LG-2, Stanford University, May 1964.

14. Bowman, S. E.: Cryogenic Liquid Experiments in Orbit, Volume I: Liquid Settling and Interface Dynamics. NASA CR-651, December 1966.

15. Chin, J. H.; et al.: Analytical and Experimental Study of Liquid Orientation and Stratification in Standard and Reduced Gravity Fields. Report No. 2-05-64-1, Lockheed Missiles and Space Company, July 1964.

16. Siegret, C. E.; Petrash, D. A.; and Otto, E. W.: Time Response of Liquid-Vapor Interface After Entering Weightlessness. NASA TN D-2458, 1964.

REFERENCES (Concluded)

17. Benedikt, E. T.: Scale of Separation Phenomena in Liquids Under Conditions of Nearly Free Fall. ARS Journal, vol. 29, no. 2, February 1959, pp. 150-151.

18. Masica, W. J.; et al.: Hydrostatic Stability of the Liquid-Vapor Interface in a Gravitational Field. NASA TN D-2267, May 1964.

LONG TERM CRYOGENIC STORAGE SYSTEM INTEGRATION

By

R. E. Stonemetz, J. H. Pratt, and T. W. Winstead

SUMMARY

The post-Apollo space effort will consist of short-to-intermediate duration, near-earth missions and long duration planetary missions utilizing high energy cryogens for rendezvous propulsion and transportation. Efficient propellant management of cryogen storage containers is required to preclude high launch rates and thus meet mission demands.

The possibility of achieving efficient propellant management is enhanced significantly by recent developments in thermal management subsystems, including zero-gravity vapor venting, destratification mixing, hydrogen reliquefaction, and solar shields. These disciplines are pertinent to long term cryogen storage and are capable of effecting significant improvements in current storage systems.

This paper will survey Marshall Space Flight Center's research achievements in the thermal management areas of liquid hydrogen storage systems in deep space and low orbit environments. These concepts are also applicable to lox storage systems.

LIST OF SYMBOLS

Symbol	Meaning
m_{VT}	total mass vented from tank, kg
$\dot{m}_V$	tank venting rate, kg/hr
P_P	mixer input power, W
h_V	specific enthalpy of vented vapor, J/kg
h_L	specific enthalpy of liquid, J/kg
$\dot{Q}_E$	tank heat flux, J/hr
λ	heat of vaporization, J/kg
e	vapor density to liquid density in the tank
θ	total mission time, hr
TF	time fraction, percent
D_0	mixer jet diameter, m
P_0	mixer fluid power, W

INTRODUCTION

Efficient thermal management of cryogen propellant storage systems requires minimizing the environmental heat flux, controlling the effects of in-tank heat distribution on tank pressure rise rate, and providing efficient energy release to preclude overpressurization of the storage tank. The environmental heat flux to the cryogen tank can be minimized with high performance insulation (HPI) and may be further reduced with a solar shield. Typical high performance insulation results in a liquid hydrogen tank heat flux of 0.158 W/m^2 in deep space and 0.79 W/m^2 in low earth orbit. These values were used in this investigation and no further discussion of HPI will be made. Subscale solar shield testing reveals tank heat flux reductions of 60 percent in deep space and 15 percent in low orbit.

Energy must be released from a cryogen storage tank to prevent overpressurization. A vent system designed for a zero-gravity environment that releases energy by venting superheated vapor will optimize cryogen losses. Typical losses are 10 percent of initial mass for deep space missions employing 10 m diameter cryogen tanks and 20 percent for 30 day

system was located 0.6 m from the tank bottom with the capability to orient the mixer outlet flow axially down the tank, radially, or axially up (arrow) as shown in Figure 3.

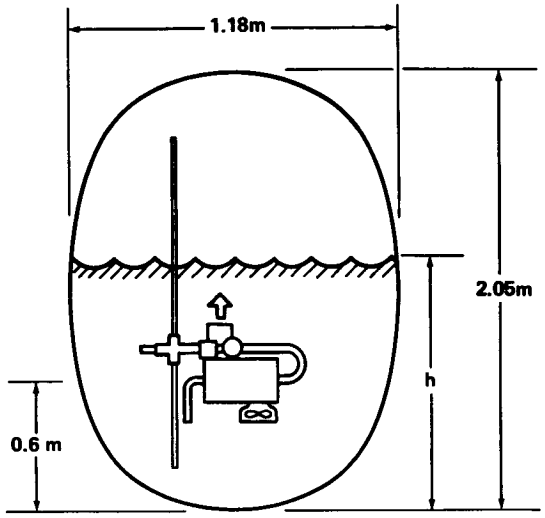

Figure 3. Test tank system installation.

Mixer orientation for the first test series was radial resulting in a slow ullage pressure response when actuated with liquid at the inlet. Figure 4 shows a very shallow pressure decay following actuation. This is attributed to a lag in mixing the fluid to obtain energy transfer between the ullage and the liquid.

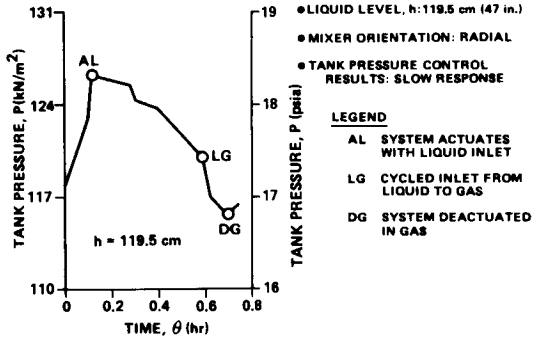

Figure 4. Tank pressure history, first test series.

The second test series was conducted with the mixer oriented to discharge axially up the tank (Fig. 3). Ullage pressure response was very good in all cases as shown in Figure 5. The increased time required for energy transfer between the ullage and the liquid for smaller ullage fractions is evident when Figures 4 and 5(b) are compared.

The mixer was oriented in a downward direction for the third test series (Fig. 6). Figure 6(b) shows results at a liquid level of 1.2 m. The tank pressure decay with liquid at the vent inlet was very slow because there was very little ullage-to-liquid energy exchange. Tank pressure decay was nonexistent with a liquid vent inlet and a 1.8-m liquid level as depicted in Figure 6(c). In this case, the energy transfer from the ullage to the vented fluid was less than the energy input to the ullage from the wall and penetrations. This was attributed to the poor fluid mixing characteristics when the mixer outlet flow was directed downward.

Liquid was not detected in the vented fluid during transient startups or steady-state operation during any test. These tests also demonstrated that tank fluid mixing and liquid-to-ullage coupling are significant for efficient pressure control and that the heat exchanger being located at the tank end with mixer discharge toward the opposite end promotes maximum liquid-to-ullage coupling, which results in efficient pressure control.

Flight System Design Considerations

The primary considerations for a flight system design are flow rate and duty cycle. An optimum duty cycle considers hardware lifetime, reliability, and system effective weight. The tradeoff parameters that affect duty cycle are mixer work, which puts energy into the system, Joule-Thompson subcooling, which removes energy from the system, and mission duration and tank size, which determine tank heating rate (energy input). The weight of vented propellant is determined by

$$m_{VT} = \theta \left[\frac{\dot{Q}_E}{\dot{m}_V \left(\frac{e\lambda}{1-e} + h_V - h_L \right) - P_P} \right]$$

and the vent flow rate as a function of the fraction of total mission time that the system operates can be determined by

$$\dot{m}_V = \frac{\dot{Q}_E / TF + P_P}{\frac{e\lambda}{1-e} + h_V - h_L}$$

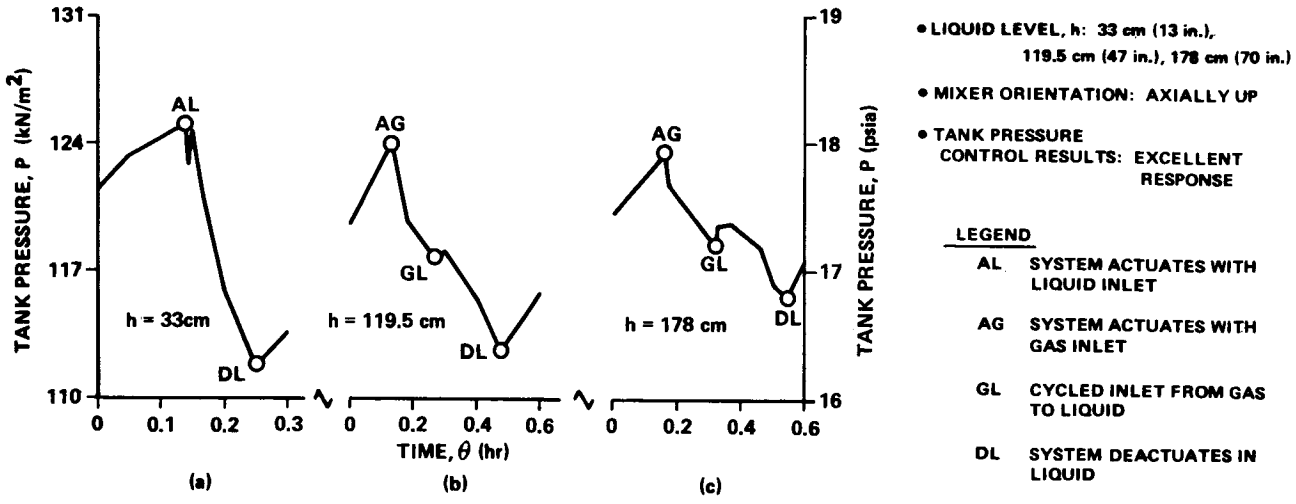

Figure 5. Tank pressure histories, second test series.

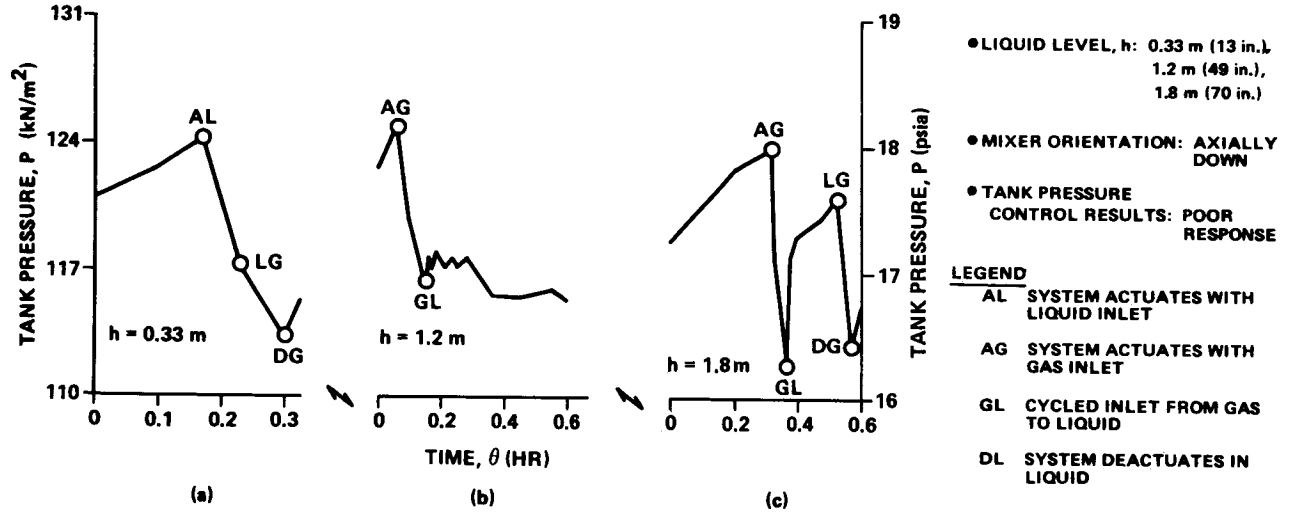

Figure 6. Tank pressure histories, third test series.

The vent rate plotted as a function of system operating time (duty cycle) for two flight-size tanks is presented in Figure 7. The effect of operating time on system effective weight is illustrated in Figure 8 as a vent penalty and compared to the hypothetical case of saturated vapor venting, $\dot{m}_V = \dot{Q}_E/(h_V - h_L)$. The thermodynamic vent system incurs a greater boiloff penalty when operated more than 25 percent of the mission time; this is primarily a result of the energy input from the pump mixer having a greater influence on tank thermodynamics than J-T subcooling. However, the opposite is true for a system operating less than 25 percent of the mission time, and optimum system weight results when the vent system is operated approximately 10 percent of the mission time.

LOW-GRAVITY TANK THERMODYNAMICS

Several analytical models have been developed to predict tank pressure buildup rates and in-tank temperature distributions during long term storage of cryopropellants in the low-gravity environment. These models consider vapor heating, local boiling, and conduction and convection heat transfer processes between tank walls and the propellant. Currently, there are no general discriminators to indicate which of these heat transfer modes is dominant. However, each analysis indicates that significant temperature stratification is probable, and each indicates the need for active propellant destratification mixer systems.

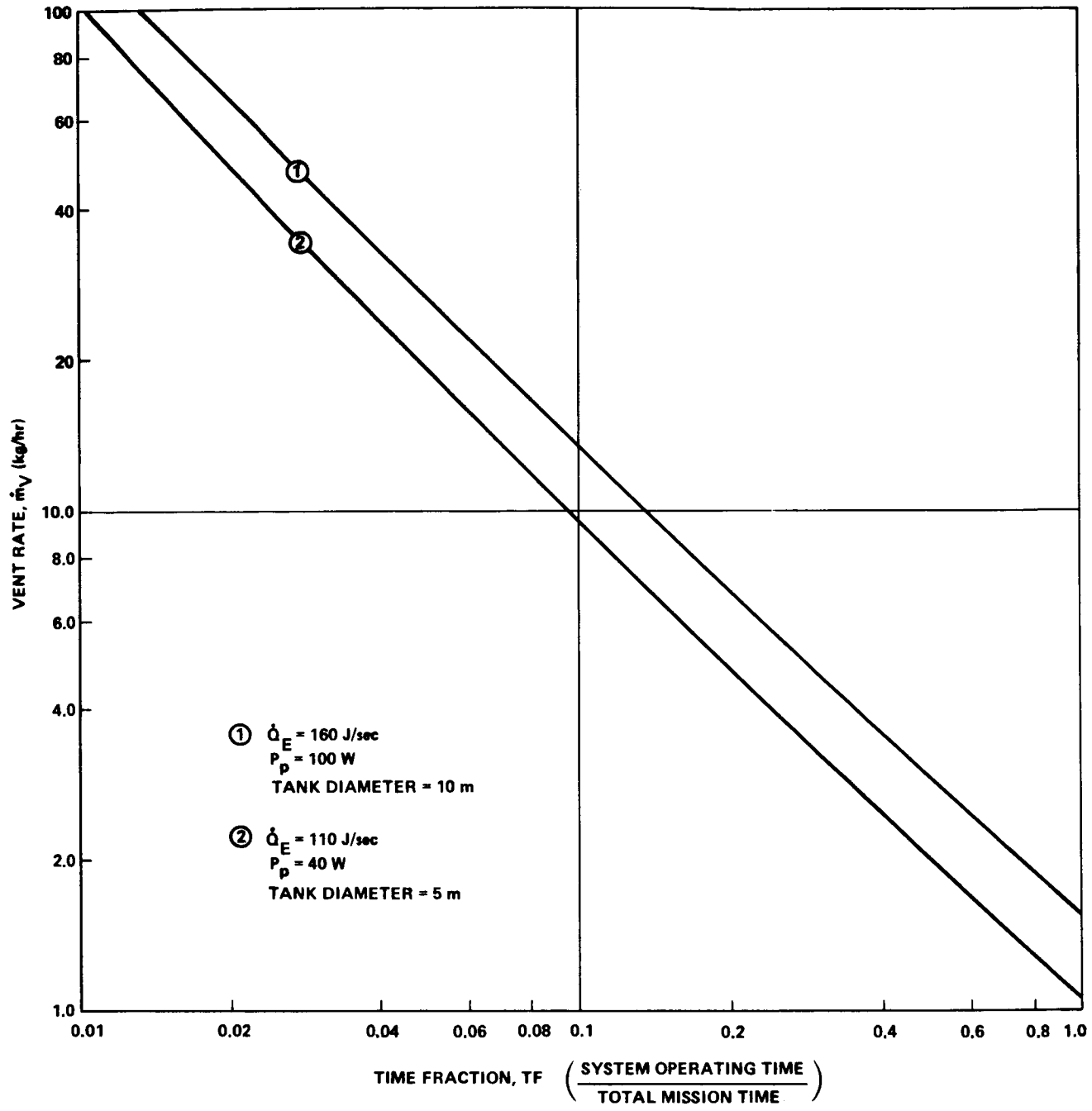

Figure 7. Vent rate as a function of system operating time.

Various concepts have been evaluated for destratification mixer systems with two fundamental premises: (1) the mixer system could be utilized to maintain tank pressure in applications where the heat absorption capability of slushed, gelled, or subcooled propellants is employed; and (2) the mixer system may be integrated with or redundant to the mixer required for a thermodynamic vent system.

Considerations for various mixer concepts are summarized in Table 2, which shows that axial jet mixers are concluded to be superior. Salient considerations for this conclusion are discussed for each of the concepts in the following paragraphs.

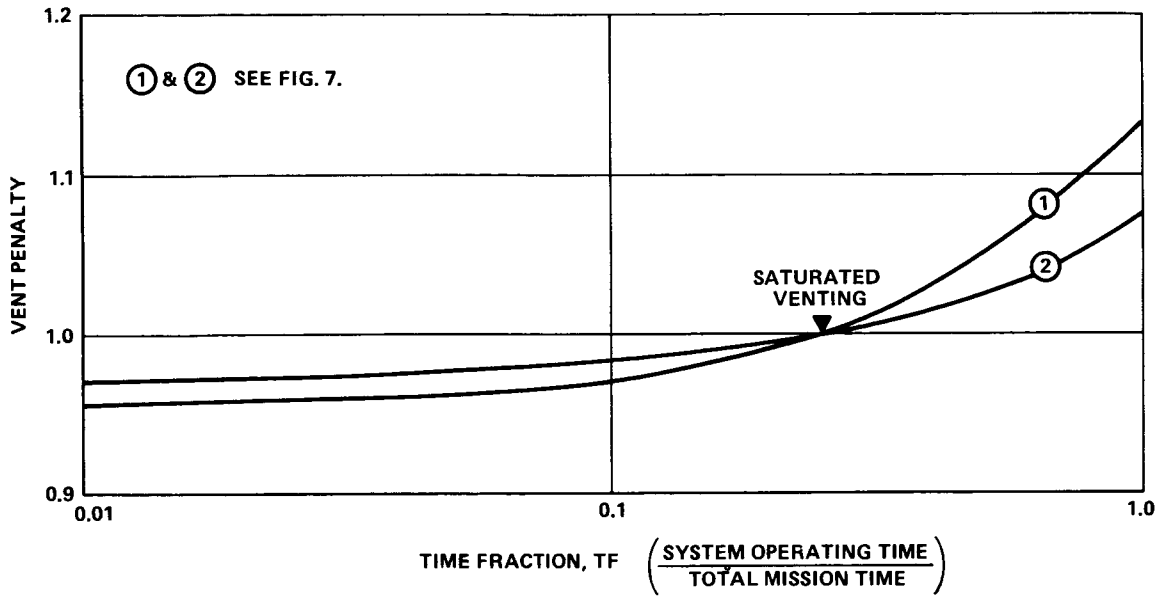

Figure 8. Duty cycle influences on propellant management.

TABLE 2. COMPARISON OF DESTRATIFICATION MIXER SYSTEM CONCEPTS

		CONSIDERATIONS				REMARKS
		PERFORMANCE	WEIGHT	SIMPLICITY	FLEXIBILITY	
PADDLE WHEEL		SUPERIOR WITH LARGE LIQUID FRACTION			INADEQUATE WITH LOW LIQUID FRACTION	N/A
DUCTED FLOW					INADEQUATE	N/A
ULLAGE MOTION	APS THRUST		EXCESSIVE			N/A
WALL HEX			EXCESSIVE			N/A
RADIAL JET		ACCEPTABLE	ACCEPTABLE	LOW-COST REDUNDANCY	ACCEPTABLE	ACCEPTABLE
AXIAL JET		SUPERIOR	SUPERIOR	LOW-COST REDUNDANCY	ACCEPTABLE	PREFERRED

Paddle Wheels

Using paddle wheels to stir bulk liquids is the most efficient method of achieving mixing. This concept is limited, practically, to use with high liquid volume fractions, since paddle wheels are not efficient when surrounded by vapor. Also, the bulk liquid would be rotated within the tank, which would create undesirable vehicle attitude control requirements in some storage applications.

Ducted Flow

The concept of pumping fluids from one point to another point in the tank through ducts is an acceptable mixing method for large liquid-to-tank-volume fractions, but effective mixing is degenerated as the liquid fraction is decreased. Under optimum considerations, this concept is less efficient than jet pumps.

Auxiliary Propulsion System Thrust

Using alternately opposing vehicle thrusting to mix propellants does not appear feasible for most applications because of excessive auxiliary propulsion system propellant weights. However, it is likely that thrusting to maintain vehicle attitude control will partially destratify storage tanks.

Wall Heat Exchanger

The weight of wall heat exchangers and the complexity of attaching heat exchangers for simple maintenance and acceptable tank wall-heat exchanger thermal contact are both severe disadvantages to this concept. Intercepting heat by the wall heat exchanger such that zero-gravity propellant acquisition devices will not be exposed to boiling heat transfer has some merit for localized applications and may be optimum for small tanks considering total system integration.

Jets

Mixing of the bulk fluid by jet action appears optimum. Radial-flow jets have been evaluated and are not efficient because of dissipation of energy at the tank wall. Axial-flow jets afford greater mixing efficiency and are recommended as the prime candidate for destratification mixers.

An intensive study on design and performance parameters has been completed for axial jet mixers [2]. Model tests were conducted to verify mixer performance predictions using water in 0.3 m and 3.0 m diameter tanks [2,3]. These studies indicate that small (1 to 5 cm) axial jet mixers operating at low fluid output power (1 to 10 W) are adequate to destratify a 10 m diameter tank. Typical mixing times for a 10 m tank are on the order of 1 hour, and the mixer power impact is not unreasonably limited by the immaturity of the stratification prediction methods.

Figure 9 shows the recommended limiting design criteria for an axial jet pump. The criteria are based on the conditions that the mixer will be surrounded by the tank ullage vapor, that the ullage "bubble" must be dissipated, and that liquid subsequently will be drawn into the mixer to destratify the tank. The criteria make allowance for an ullage bubble diameter equal to tank diameter and consider that redundant mixers would be at several locations within the tank such that one or more mixers would be surrounded by vapor at any given time.

The effects of system input power and mixer diameter on system weight and size are illustrated

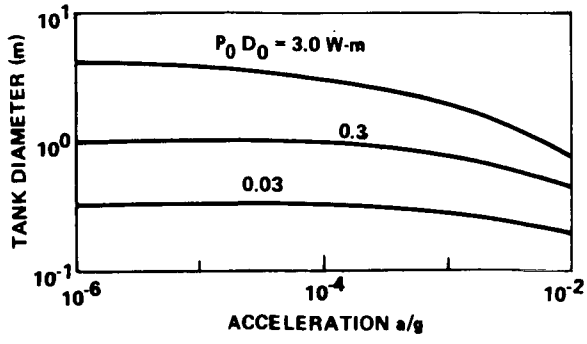

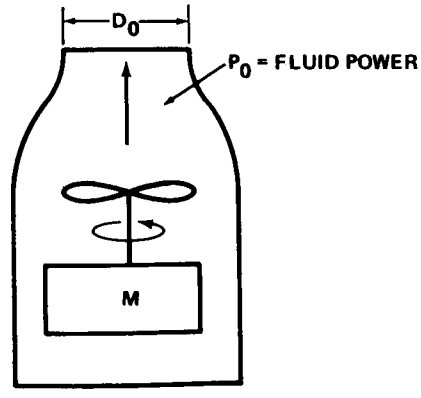

Figure 9. Bubble breakup criteria.

in Figure 10. Hardware and power system weights are shown separately to indicate the drivers in selecting optimum system weight. A majority of the power system weight is delta-boiloff resulting from low mixer efficiency. The impact on system weight is dependent on the number of duty cycles required and the duration of the mixer operation.

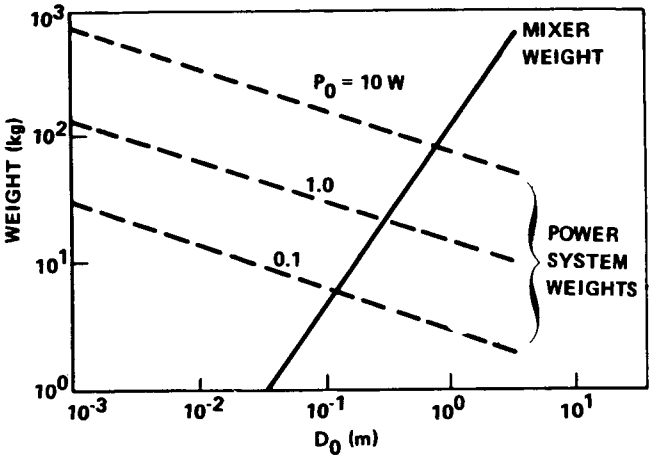

Figure 10. Axial jet mixer system weights.

Figure 11 presents results of mixing analysis for a 10 m diameter tank considering a range of stratification buildup times and illustrates the effect of fluid power on system weight.

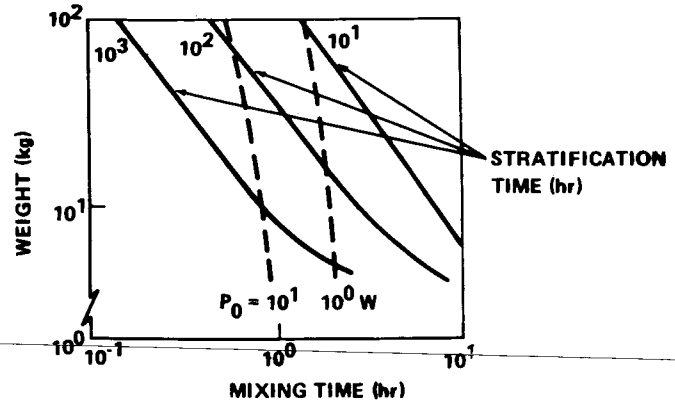

Figure 11. Effects of sequence and power.

Practical considerations indicate that optimum vehicle costs will result when 1 to 5 cm diameter axial jet destratification mixers powered by 1- to 10-W synchronous electrical motors are used. These considerations include using state-of-the-art components for up to 500 hours of duty life. While the studies indicate that mixer system weights could be reduced by developing smaller components, this does not appear to be justified at this time, since the potential weight reductions are modest and efficiencies are likely to suffer with component miniaturization.

HYDROGEN RELIQUEFACTION SYSTEM

Hydrogen reliquefiers have been investigated [4] as a means of reducing the net boiloff loss during long term storage. The considerations for using a reliquefier are component weights, reliquefaction fraction, power requirements, and mission parameters such as storage duration, tank size, and boiloff rate. The concepts that were considered are (1) self-powered, (2) total refrigeration, and (3) power-assisted systems. The self-powered partial reliquefier uses energy from a portion of the hydrogen vapor to compress the remaining vapor that is to be reliquefied. Low reliquefaction fraction and high hardware weights degrade the desirability of a self-powered hydrogen reliquefier. A closed-loop total reliquefier has obvious advantages for extremely long missions, but has high power requirements and is weighty because of the required space radiators, etc. These factors, along with development risk considerations, have eliminated the closed-loop concept as a candidate at this time. The most promising concept is a power-assisted partial reliquefier (PAPR) that utilizes a portion of the boiloff flow as a heat sink and energy source to help drive the compressor. A prototype PAPR is currently being developed and will be considered in this paper.

Parametric studies indicate that a PAPR design should consider only vapor supply conditions; integration with the thermodynamic vent system (discussed previously) is indicated.

Approximately 50 percent of the hydrogen vent vapor is compressed, then cooled, and expanded as a liquid back into the tank. The remaining 50 percent of the hydrogen vapor is heated by the high pressure stream in a counter-flow heat exchanger, expanded to a low pressure that produces work to help drive the compressor, and is then heated to a higher temperature and converted to paraortho equilibrium before it is vented overboard.

A schematic of the thermodynamic cycle is shown in Figure 12 and will be discussed by corresponding numbered locations on the schematic and T-S diagram.

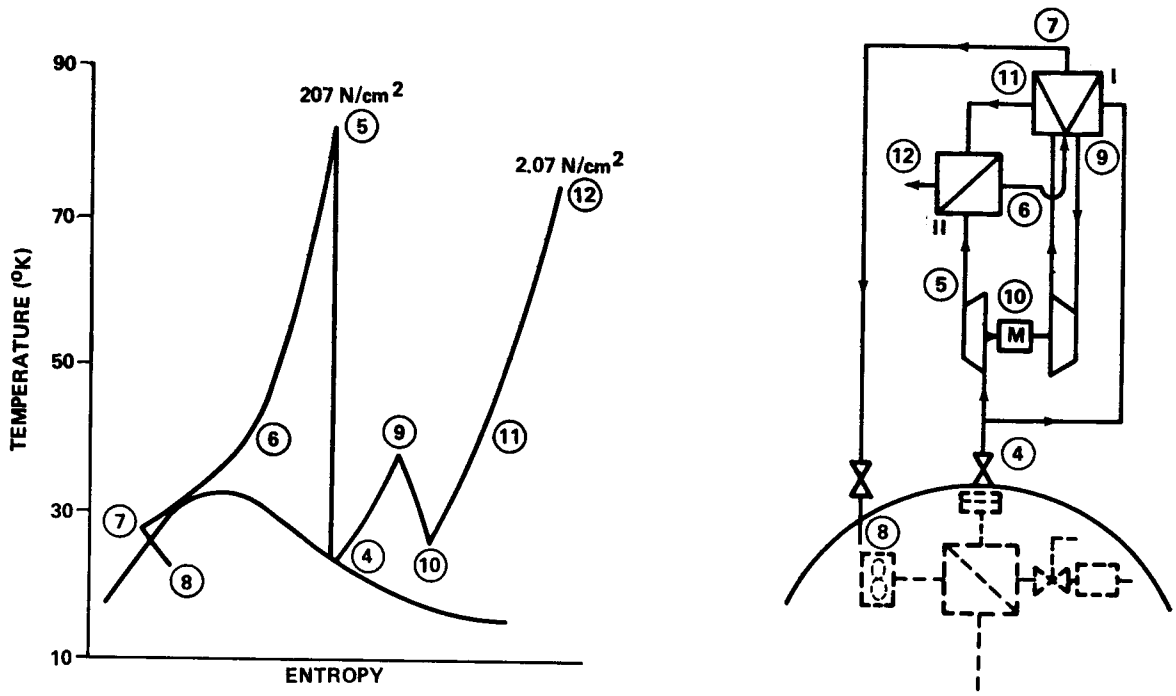

Figure 12. Thermodynamic cycle for the power-assisted partial reliquefier.

As shown in Figure 12 superheated vapor enters the reliquefier from the vent system at (4) and is divided into two approximately equal streams. First, consider the portion of hydrogen vapor that is to be reliquefied. It is compressed from (4) to (5), cooled in heat exchanger II from (5) to (6), further cooled in heat exchanger I to (7), and expanded through a Joule-Thompson valve into the tank as a liquid at (8). The portion of hydrogen vapor that is to be used as a heat sink and vented overboard is ducted through the dual-pass heat exchanger I from (4) to (9) and expanded through a positive displacement expander to extract work and reduce temperature to (10). The vapor is then re-routed through heat exchanger I to (11) and through heat exchanger II to (12) where it is vented overboard. A catalyst in the vented gas flow stream of heat exchanger II accelerates the parahydrogen conversion to paraortho equilibrium hydrogen. The paraortho equilibrium hydrogen has approximately 50 percent greater heat capacity than the parahydrogen vapor, as shown in Figure 13. This increased heat capacity results in a greater heat sink per pound of vented vapor and thus increases the fraction of vapor that can be reliquefied.

A prototype partial hydrogen reliquefier was developed to verify the design concept and demonstrate system operation. The prototype unit is a miniature, coupled, reciprocating, compressor-expander engine with an electric drive motor and two wound-finned tube heat exchangers incorporating a paraortho conversion catalyst. The thermodynamic cycle design point is based on a supply of saturated parahydrogen vapor at a pressure of 20.7 N/cm^2 and a temperature of 23°K. The reciprocating machinery, shown in Figure 14, has the following specifications:

- 41.3 percent reliquefaction at 1.8 kg/hr with paraortho hydrogen conversion.
- Size — 0.61 m diameter by 1.22 m high.
- Weight — 91 kg.
- Power — 300 W.
- Speed — 6.66 rps.

All hardware was fabricated, and preliminary checkout for system cryogenic testing identified a compressor seal problem. The compressor is a two-stage, piston-cylinder, positive-displacement system that uses piston rings for seals to the cylinder (Fig. 15). Inadequate sealing of the compressor seals was discovered, and four different ring configurations were installed and tested in the compressor with limited success. The seal problem is aggravated by the low operating speed (6.66 rps), the short

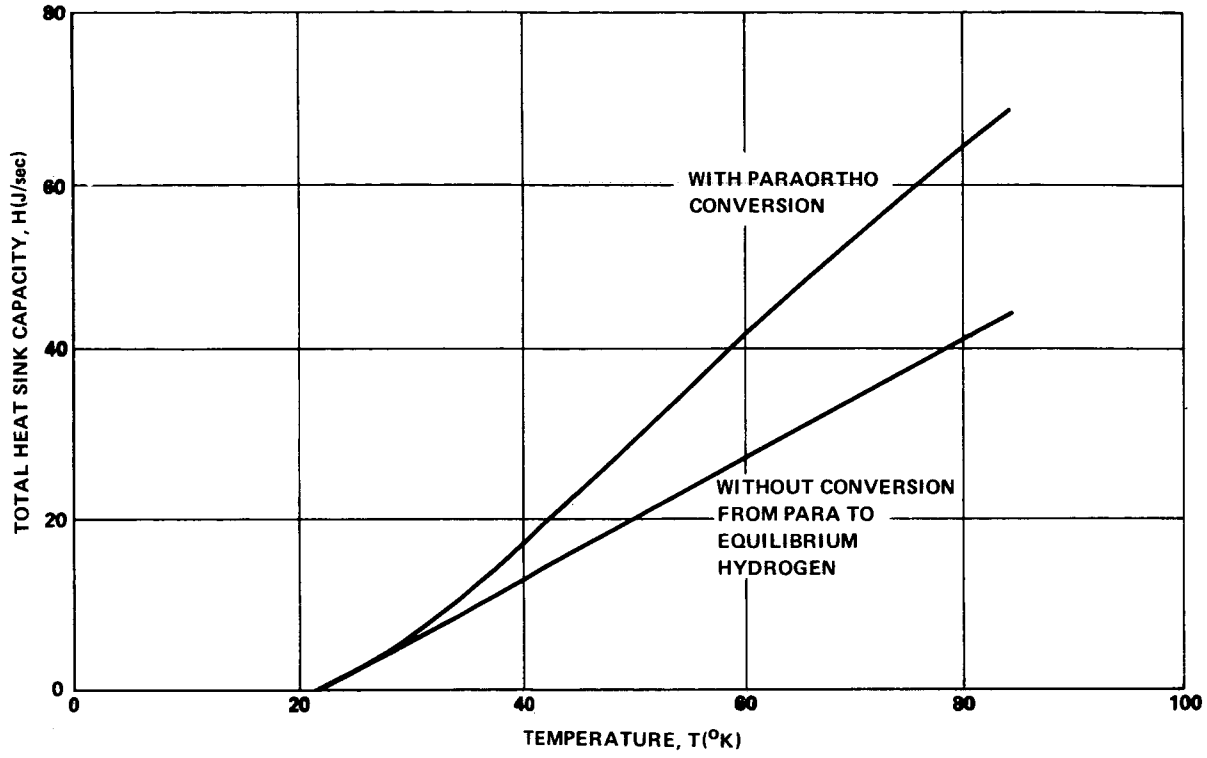

Figure 13. Heat sink capacity of hydrogen.

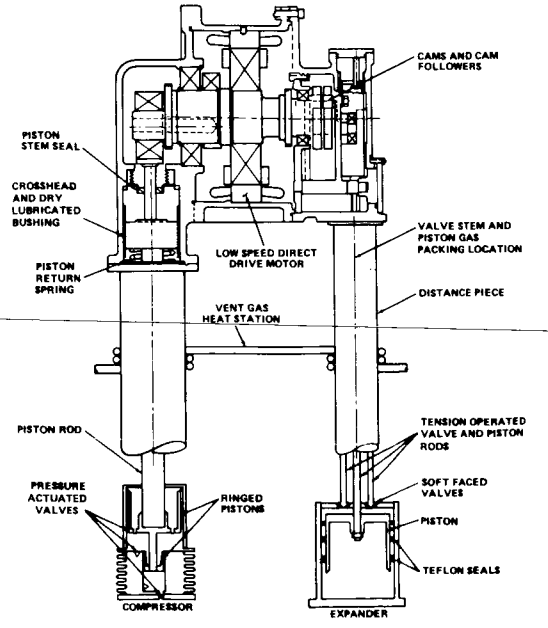

Figure 14. Prototype reciprocating machinery.

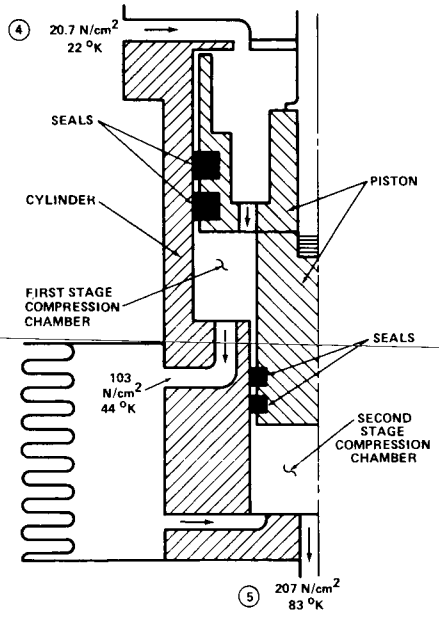

Figure 15. Compressor, piston seal arrangement.

piston stroke (≈ 2.5 cm), and the reversing pressure across the seals. Improved seal configurations are currently being designed and tested to resolve the problem.

A cryogenic test facility, consisting of a cryostat and cryogard tank, has been assembled to provide realistic operating conditions for verification of the prototype reliquefier performance. The optimum reliquefaction fraction and lifetime characteristics of the reciprocating machinery will be determined during cryogenic testing.

SOLAR SHIELD

Solar shields have been evaluated for additional thermal protection of cryogen space storage systems. The primary objective of a solar shield is to minimize the solar heating incident upon the cryogenic tanks by intercepting, reflecting, and reradiating thermal energy from the vehicle. Studies indicate that the heat transfer rate to cryogenic tankage can be reduced by 10 to 15 percent in low orbit and by 50 to 60 percent for deep space missions [5]. An analytical and experimental development program [6] has been conducted to select appropriate materials and verify operational techniques with subscale tests. The sizes and weights of typical solar shield applications are shown in Figure 16.

An inflatable solar shield has been developed that is folded and stowed in a small, dense configuration during launch, thus making it compatible with the high-gravity loadings during boost flight. During long term cryogen storage periods, the solar shield is deployed, inflated, and rigidized so that it will be structurally sound after the inflation gas is vented. The solar shield is jettisoned after use.

The inflatable solar shield design objectives are to accommodate the environment during boost and to provide maximum surface area with minimum weight during space operations. Although the expected shield loadings in the operational environment are extremely low, the structure must be able to withstand vehicle attitude maneuvering loads and meteoroid impacts.

The inflatable shield concept has been successfully demonstrated by the Echo II satellite program, in which an aluminum-Mylar-aluminum tri-laminate was boosted into orbit, deployed, and inflated to form a sphere. However, the Echo program did not employ the rigidization scheme. The Echo II program did provide a shell material (designated GT-15 by the G. T. Schjeldahl Company); however, an additional materials development program was conducted for each component of the inflatable solar shield. The GT-15 skin material is a three-ply laminate consisting of 0.00089 cm thick mylar with 0.00046 cm thick aluminum foil bonded to each side. This material has sufficient strength and flexibility for use as an expandable structure, but a reinforcement system is required for adequate load carrying capacity of the shield, particularly near the vehicle attach area. Studies show that the deployed solar shield must be able to survive attitude loadings of 0.001 to 0.01 g during orbital operations. The method developed to reinforce the GT-15 sphere consists of bonding a thin layer of flexible, open-cell polyurethane foam to the sphere and impregnating the foam with a monomeric material that can be rigidized upon command.

The scheme selected for rigidizing the polyurethane foam is a self-rigidizing vinyl monomer, tetraethylene glycol dimethacrylate, mixed with a benzoyl peroxide initiator, methyl ethyl ketone diluent, and a Cab-O-Sil thixotropic agent to produce

a chemically active solution. The foam is impregnated with this solution to form a flexible material that may be stored under controlled temperature (< 410°K) and/or oxygen environment. Polyester adhesive (Schjeldahl A-55) was selected as the adhesive to bond foam to the GT-15 skin because of its compatibility with the monomer, acceptable bond strength, and adaptability to machine lamination techniques.

Since the solar shield is a likely thermal control subsystem for a nuclear powered vehicle, the effects of a 4×10^6 ergs/gram-carbon nuclear radiation (gamma) environment on the rigidization material were investigated and found to be negligible.

Rigidization of the foam occurs when the monomer is polymerized by an exothermic reaction, resulting in a clear, rigid, cross-linked polymer. The rigidization process is initiated by a polymerization accelerator, N-diethylanaline (DEA), which flows past the monomer impregnated foam after the solar shield is inflated. Convective cooling by the helium inflation gas necessitated that the foam be bonded to the outside of the GT-15 skin and shrouded with two aluminized mylar sheets for thermal radiation shielding. A sketch of a solar shield is shown in Figure 17.

A subscale test program was conducted to investigate the thermal and structural performance of the solar shield. A small scale thermal test program was conducted in a simulated space environment using an LN_2 cold wall vacuum chamber and carbon arc lamps to simulate the solar radiation. The effects of thermal control coatings, internal reflective membranes, and solar vector/vehicle axis misalignment were assessed. A high emittance band of carbon-doped polyester over one-half the backside (shaded) area of the shield was found to be effective in reducing the vehicle-side shield temperatures by about 20 percent. The internal reflective membrane, also made of GT-15, is effective in reducing shield temperatures on the shaded (vehicle) side. An alodine thermal control coating was selected because of its durable optical properties for use on the outside hemispherical surface facing the sun. The effects of several combinations of thermal control coatings and membranes are shown in Figure 18. These data indicate that solar misalignment of the shield and vehicle axis will not have an adverse effect on the net radiation to the vehicle as long as direct solar energy is not incident upon the vehicle.

Structural tests were conducted to evaluate the load-carrying capability of thin-shell spherical models. The small-sphere structural tests were conducted in a centrifuge at 170°K. The 0.8 m diameter models with a 0.32-cm rigidized foam reinforcing cap covering one-fourth of the surface area failed at 7 g and the 0.39 m diameter models failed at 30 g. The 0.39 m diameter models with 0.64 cm thick foam did not fail at the centrifuge maximum of 30 g. Three larger scale 4.6 m diameter solar shield models were structurally tested in simulated space conditions. A mechanical fixture failure on two tests and a foam impregnation problem on one test prevented complete structural evaluation of the large scale spheres. The spheres supported themselves under a 1-g loading, which correlates to an approximately 0.01 g loading on a 18.4 m diameter sphere in an operational environment. These tests verified that a large, rigidizable structure can be fabricated, folded, packaged, transported, deployed, and rigidized under space conditions.

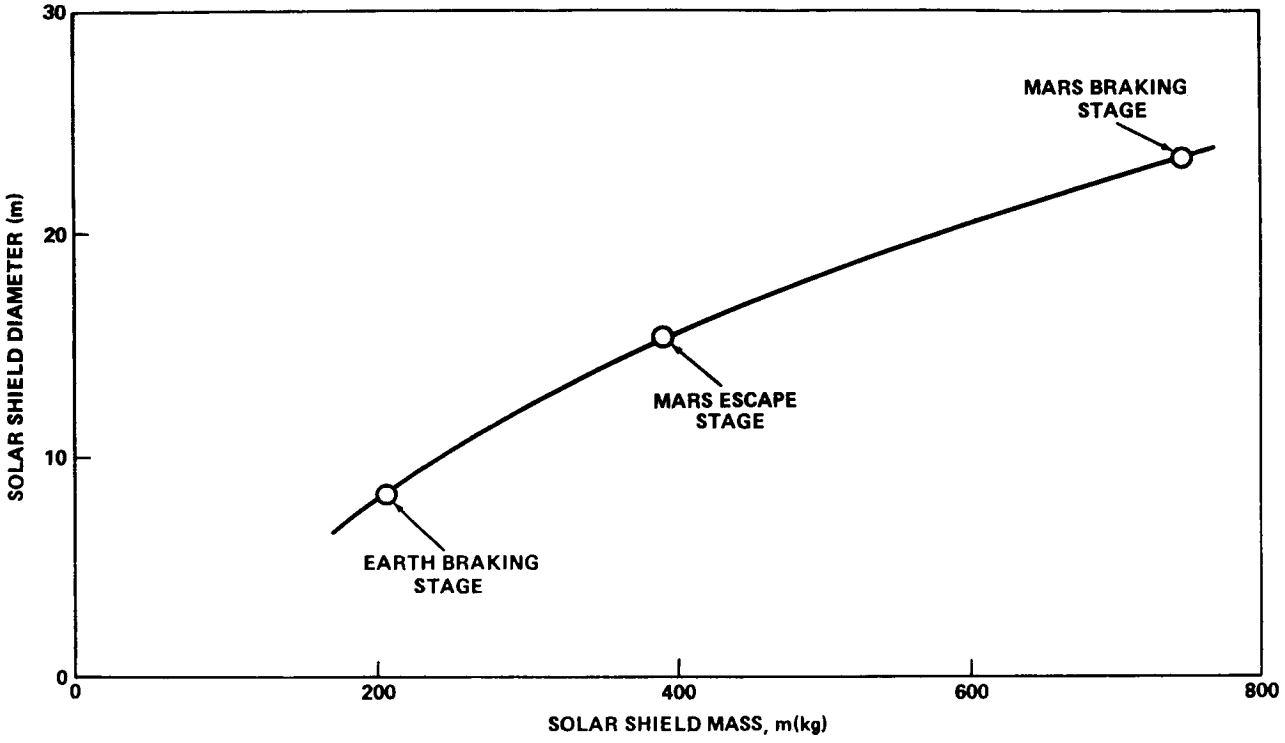

Figure 16. Typical inflatable solar shield sizes.

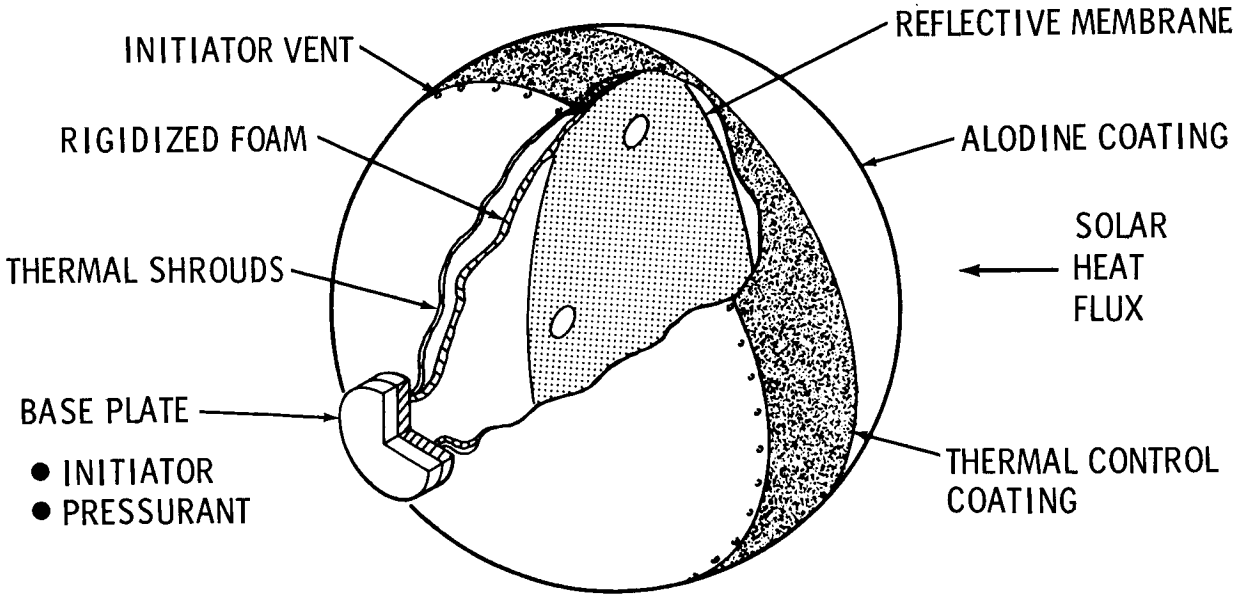

Figure 17. Inflatable solar shield configuration.

LONG TERM CRYOGEN STORAGE SUBSYSTEMS INTEGRATION

The current status of the four liquid hydrogen storage subsystems is summarized in Table 3. The characteristics of these disciplines are such that they complement and/or supplement each other to effect greater flexibility in mission design. Integration of these disciplines into a total storage system concept has been performed based on actual or expected prototype characteristics and HPI performance. There are numerous concepts for control systems to effect proper

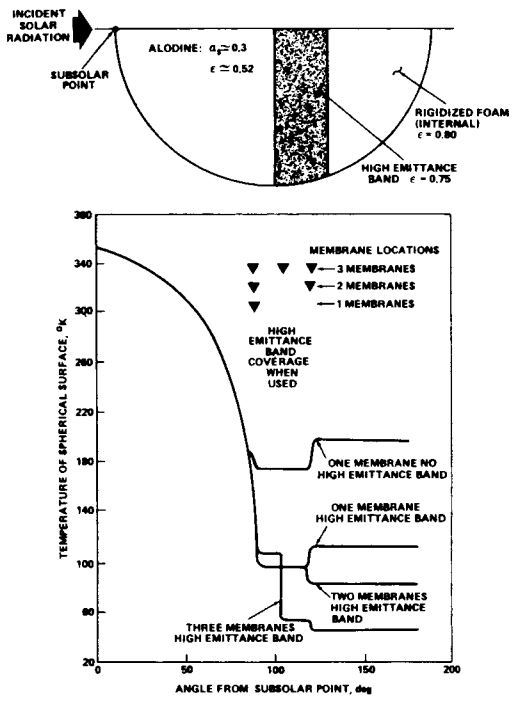

Figure 18. Predicted solar shield temperature distributions.

sequencing of the subsystems, but they will not be addressed in this discussion.

Long Term Missions

Total system performance in a deep space environment is presented in Figure 19. The performance of the integrated systems is referenced to the hypothetical boiloff loss resulting from venting saturated vapor. However, since liquid/vapor locations are random, the thermodynamic vent system (TVS) is considered to be a baseline configuration. Propellant savings of up to 30 percent are available with the addition of a solar shield (SS), 45 percent with a reliquefier (PAPR), and up to 60 percent by using both the reliquefier and solar shield. The reliquefier not only enhances the performance of the vapor venting system but also optimizes the vent system duty cycle from 10 to approximately 40 percent of the total mission time. This increases the vent frequency while decreasing the vent system flow rate (Fig. 7) and reliquefier weight.

TABLE 3. TECHNOLOGY DISCIPLINE SUMMARY

Disipline	Status
Zero-Gravity Vapor Vent	Prototype H_2 thermodynamic vent system developed
Distratification Mixer	Prototype axial jet mixer developed; 1-g, H_2O correlations adequate
Reliquefaction	Open-loop concept feasible; prototype performance verification planned
Solar Shield	Subscale prototype developed; structural scaling inadequate

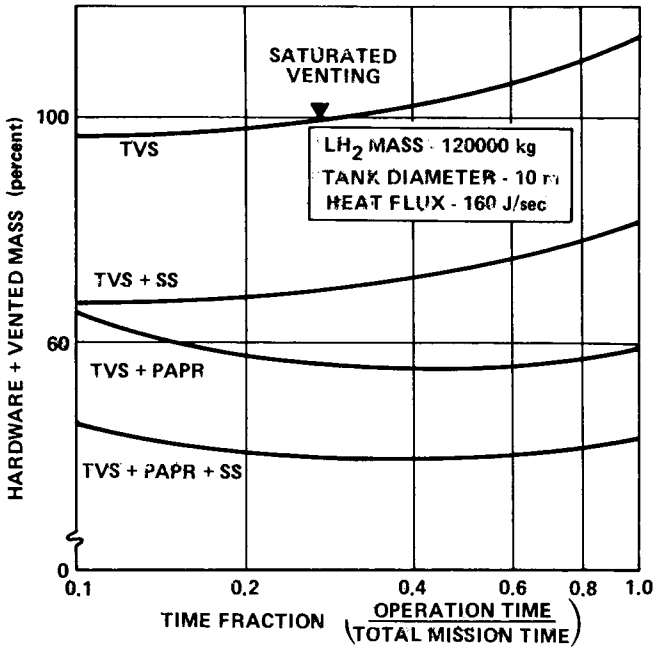

Figure 19. Subsystems integration performance for long term deep space missions.

Intermediate Term Missions

Figure 20 presents system performance as a function of mission duration in low orbit. The TVS is considered a baseline configuration weighing approximately 10 kg. Any system other then the

TVS will result in a small reduction in vehicle payload for mission durations of less than 7 days. Thereafter, the reliquefier enhances the storage system performance since it reduces the net boiloff by about 40 percent for a 30-day mission. The poor performance of a spherical solar shield in low orbit eliminates it as a potential subsystem candidate because of degradation by the albedo and planetary radiation.

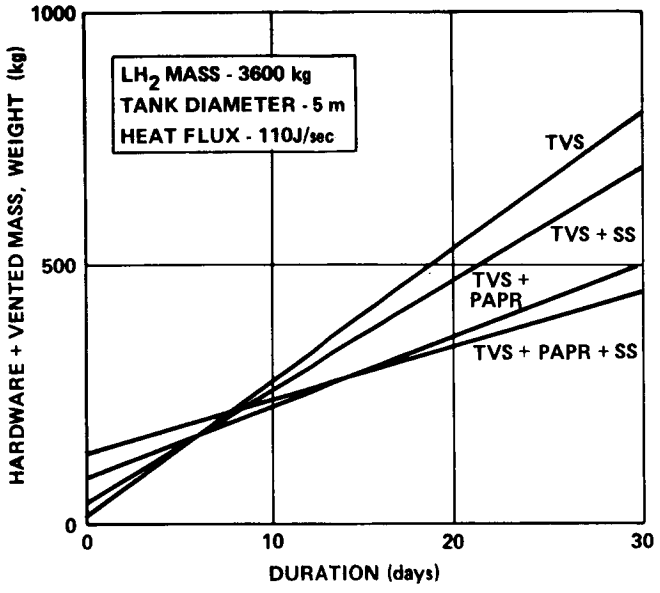

Figure 20. Subsystems integration for low orbit missions.

CONCLUSIONS

Efficient propellant thermal management of a cryogen storage system requires subsystems that are capable of minimizing the effects of tank heat flux, in-tank heat distribution, and energy release from the tank. Minimization of the environmental heat flux can be accomplished with high performance insulation, and it can be further reduced with a solar shield. The effects of in-tank heat distribution on ullage pressure can be minimized by using a destratification mixer subsystem. Energy must be released from the tank to preclude overpressurization; this requires a vent system capable of venting vapor only in a zero-gravity environment. The performance of a zero-gravity vapor vent system can be enhanced by coupling to a reliquefaction system.

A detailed cryogen storage system analysis is required to determine the applicable subsystems necessary to achieve optimum performance for any given mission. A trade and optimization study is necessary to determine a control system commensurate with the objectives of the destratification mixer and zero-gravity vapor vent subsystems.

This investigation has revealed significant increases in performance when a reliquefier and solar shield in conjunction with a zero-gravity vapor vent system are utilized. Application of a reliquefier and solar shield in long term deep space missions may effect a 60-percent reduction in propellant loss, compared to that associated with the vapor vent system only.

Significant improvements in storage system performance are possible for low earth orbit applications; for the typical system that was evaluated, system performance gains were realized for mission durations exceeding 7 days. Spherical solar shields are generally not competitive for low earth orbit applications.

REFERENCES

1. Stark, J. A.; and Blatt, M. H.: Cryogenic Zero-Gravity Prototype Vent System. General Dynamics Convair Division, Contract No. NAS8-20146, October 1967.

2. Poth, L. J., et al.: A Study of Cryogenic Propellant Mixing Techniques. Report No. FZA-439-1, General Dynamics Fort Worth Division, Contract No. NAS8-20330, November 1, 1968.

3. Van Hook, J. R.; and Poth, L. J.: Study of Cryogenic Fluid Mixing Techniques. Report No. FZA-450-1, General Dynamics Fort Worth Division, Contract No. NAS8-24882, September 15, 1970.

4. Gibson, L. A.; and Wilkinson, W. K.: Extraterrestrial Reliquefaction of Cryogenic Propellants. Final Report, General Dynamics Fort Worth Division, Contract No. NAS8-5298, December 11, 1965.

5. Jones, L. R.; and Barry, D. G.: A Study of Lightweight Inflatable Shadow Shields for Cryogenic Space Vehicles. Report No. FZA-395, General Dynamics Forth Worth Division, Contract No. NAS8-11317, January 31, 1965.

6. Doughty, R. O.: An Analytical and Experimental Development Program for Inflatable Solar Shields. General Dynamics Fort Worth Division, Contract No. NAS8-21132, May 22, 1969.

BIBLIOGRAPHY

Kunkle, Elden: Hydrogen Reliquefier. Air Products and Chemicals, Inc., Allentown, Pennsylvania, Contract No. NAS8-21203, (Study in Progress).

ADVANTAGEOUS USE OF SLUSH AND GELLED SLUSH IN SPACE VEHICLES

By

J. Z. Adamson*

SUMMARY

During the past decade, three primary advantages of using a mixture of solid and liquid hydrogen (slush) in rocket propellants have been recognized: (1) the increased loading resulting from increased density, (2) the increased mission duration resulting from the increased heat capacity, and (3) increased mission flexibility. Additional potential advantages of using gel mixtures are the achievement of positional stability in a zero-gravity environment, reduced sloshing, and reduced vaporization. Recently, the advantages of combining both slush and gel have been recognized. These advantages are: (1) a reduction in the gelling agent necessary, (2) the achievement of active positioning, and (3) a potential increase in impulse density (Table 1).

This paper attempts to establish the need for and direction of future testing in this area based upon MSFC and MSFC contractor-supported research in the field within the past 3 years. The need for extended mission capability as indicated by present mission planning is outlined and the expected schedules are presented. A condensed version of analytical and testing conclusions as related to storage systems and slush is given. The significant results of slush flow testing and its possible influence on vehicle propulsion systems are presented, and the characterization and preparation of gels are discussed in relation to future applications, advantages, and disadvantages.

TABLE 1. ADVANTAGES OF SLUSH, GELS, AND SLUSH-GEL MIXTURES

Slush
● Increased Payload Capabilities
● Increased Storage Duration
● Mission Flexibility
Gels
● Positional Stability
● Reduced Sloshing
● Reduced Vaporization
Slush-Gel Mixtures
● Reduced Gelling Agent
● Active Positioning
● Increased Impulse Density

INTRODUCTION

Slush, a mixture of frozen particles and triple-point liquid, has a heat capacity and density greater than that of a normal boiling liquid. The heat absorbing capacity of 60-percent slush hydrogen is 8.60×10^{4} J/kg (37 Btu/lb) greater than the saturated liquid at 1 atm (a 57-percent increase). The density is increased by 16.5 percent.

Long duration space missions require propellants that can be efficiently stored and that have a high specific impulse. Slush and subcooled cryogens fulfill both requirements. Engine performance is improved by reducing pumping volume, a shift of maximum specific impulse occurs at the reduced oxygen-fuel ratio, and the capability to absorb heat input increases storage duration while reducing insulation, venting, and tank size.

Mission planning indicates that slush/gel technology, which will be useful in the space shuttle and nuclear shuttle programs, will be needed between

* The author gratefully acknowledges the assistance of Mr. Eric H. Hyde and Mr. Armis L. Worlund of MSFC and Mr. Jesse Hord, Mr. C. F. Sindt, and others of the National Bureau of Standards in collecting information for this paper. The contractors who have contributed to this program are Teledyne-Brown Engineering Co., Lockheed Missiles and Space Co., and Aerojet General Corp.

1972 and 1988. Figure 1 indicates missions that could benefit from application of slush or gel technology. During the past 3 years MSFC has sponsored a number of studies both in-house and with contractors [1-4] relative to manufacturing, handling, and instrumenting slush systems. For a number of years MSFC has planned a manufacturing and testing facility to familiarize Marshall personnel with slush and its unique technology, and to develop the needed instrumentation for space vehicle operation. To achieve optimum vehicle performance, a working knowledge of pressure drop and heat transfer as a function of velocity and pipe diameter is necessary. The intent of the first phase of facility operation is to verify the scale-up of the freeze-thaw process developed by the National Bureau of Standards (NBS), to extend the aging period of slush to more than 4 days, and to study fluid flow problems such as mixing methods and power, slosh, vortexing, and bridging. An additional need is to stay abreast of the state-of-the-art in production techniques, gels, and ground handling. The most important by-product of this effort is the development of a trained engineering group, in-house, that will be familiar with and available for problem solving in the proper time frame (1975 to 1978).

ANALYSIS

The feasibility of subcooling liquid hydrogen was studied during the Apollo mission (Saturn V/S-IVB). Although it was concluded that nonventing orbital storage using 10 deg of subcooling would result in a 544.3-kg (1200-lb) payload advantage, the insufficient state of technology development and the prelaunch complexity of the Apollo mission eliminated the use of subcooled hydrogen from consideration [5]. It has also been shown [1] that an approximately 5896.7-kg (13 000-lb) payload increase is possible for a manned Mars fly-by vehicle by using 50-percent solid and 50-percent liquid hydrogen initially. Reliability is increased by reducing the mass vented and by eliminating the complex vent program. Studies for nuclear, manned Mars missions have established that for a payload of 114 000 kg (250 000 lb), efficient hydrogen storage is necessary for periods in

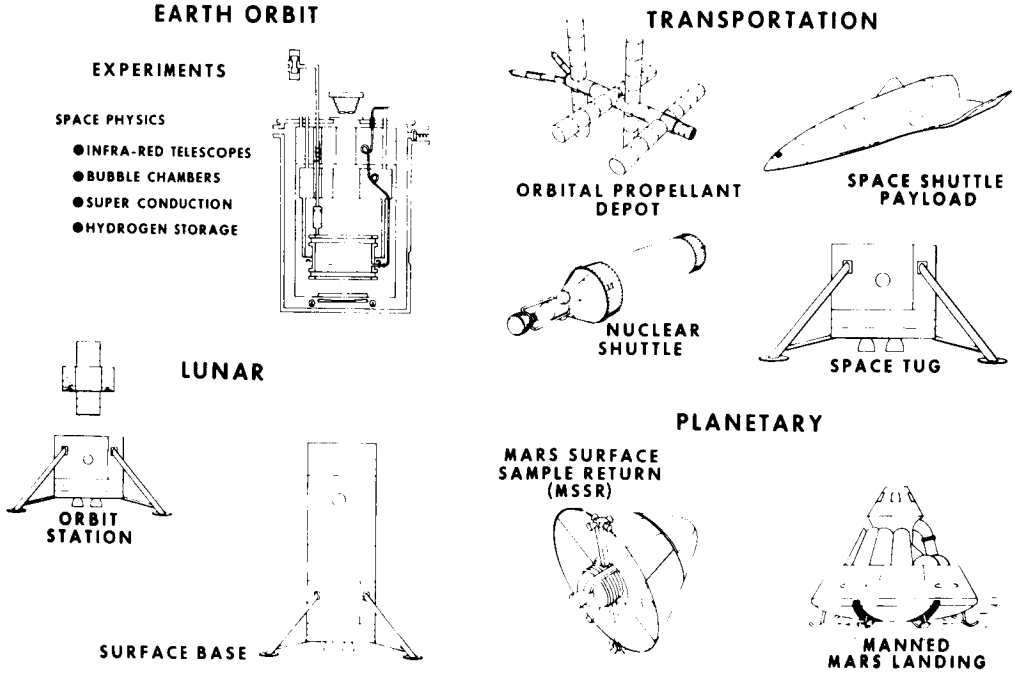

Figure 1. Potential users of slush technology, 1972-1988.

excess of 200 days [6]. Optimization of a propellant storage system for such periods requires careful selection of high performance insulation (HPI), tank design, pressure, initial propellant state, heat transfer, and venting. Inefficient storage systems can result in large penalties to the vehicle mass that is required in earth orbit [5]. For a 1-atm hydrogen storage system for a typical Mars manned mission, the launch weight penalty can be reduced 16 percent by using 50-percent slush hydrogen [5, 7], which is a weight reduction of 120 000 kg (270 000 lb) of hydrogen in earth orbit.

Studies have not been limited to hydrogen, however. Comparison of oxygen storage at supercritical, subcritical, triple-point, and 100-percent solid initial conditions have been made. While solid oxygen adds little to storage duration, cooling below the normal boiling point (1-atm ullage pressure) more than doubles the time of storage over that for supercritical storage at any usable ratios above 0.12. Any further extension of storage duration will require advancements in subcritical storage concepts, high performance insulation, reliquefaction, storage container technology, and gels [8]. It is reported that a liquid in gelled form evaporates about half as fast as do pure liquids [9].

Many of these subcooling studies and slush studies have been pursued independently, often closely connected with a certain piece of hardware. This procedure may or may not have resulted in the most optimum solution, which a systematic technology approach or present technique and hindsight could have achieved.

The production techniques for manufacturing slush cryogens that have been evaluated [5] are helium refrigeration, helium bubbling, straight vacuum pumping, the Joule-Thompson cooling process, and intermittent vacuum pumping. The most promising is the intermittent method, or freeze-thaw process, which has been investigated from laboratory scale to 0.45 m^3 (16 ft^3) by NBS using dewar containers, and to 0.28 m^3 (10 ft^3) by McDonnell-Douglas. Lockheed has operated a slush system up to a production rate of 42.64 kg/hr (94 lb/hr). This compares to an estimated rate of 226.8 kg/hr (500 lb/hr) for the planned MSFC facility.

The helium refrigeration process of cooling on external or internal surfaces is impractical, unless a method can be developed to remove the solid from the heat transfer surfaces. The helium bubbling process is prohibitively costly for large scale slush production but may be useful in upgrading the quality of slush in storage. The Joule-Thompson cooling process using precooled mixtures of hydrogen and helium has a high power requirement, but is of interest from a safety aspect since most of the equipment has a positive pressure [10, 11]. In the Joule-Thompson method, utilization is made of the heat capacity of the boiloff hydrogen, but the helium recirculation requires large volume equipment. A steam ejector pumping process has been studied for vacuum pumping and found prohibitively costly in a two-stage application. The recirculation of warm hydrogen from the blower (pump) outlet through a jet pump upstream of the blower has not been considered in the literature.

Another production process that has been proposed but discounted is the cascade vacuum pumping method. This process has the advantage of being continuous, but is less efficient than the straight vacuum pumping method and requires a large physical plant for production [10]. One detail that seems to have been overlooked in the proposed cascade concept is the possibility of recycling the vapor to cool the previous cascade. The vaporizing gas temperature varies between 20.28°K and 13.8°K depending on the stage pressure, and the gas has a significant heat capacity (4.968 cal/mol deg). Therefore, this possibility seems feasible.

Other methods related to heat transfer that might show promise on more detailed study are the fluidized bed and isentropic demagnetization methods. In the fluidized bed method, a mixture of helium and hydrogen precooled to below the triple-point temperature is introduced into a bed of previously formed solid hydrogen such that the bed is fluidized by the gas. The solid particles grow in the equilibrium mixture much as hailstones are formed. At the proper size and position within the bed, the larger particles are continuously removed and the "dry" helium is recycled, cooled, and replenished with hydrogen. The second cooling technique, which has previously been used at liquid helium temperature in cryostats [12], is isentropic demagnetization of a paramagnetic salt. In this case, it is proposed to build layers of solid hydrogen to the desired radius on a crystal of paramagnetic salt by intermittently demagnetizing in triple-point liquid. The heat of fusion is thus removed internally and the particles remain free of any surface. The particles having magnetic centers can be positioned in fields for uses that will be discussed later.

The intermittent vacuum pumping concept, known as the freeze-thaw process, is the most promising method of manufacturing. This concept consists of alternating the pressure above and below the triple point. Solid particles of fresh slush produced by the freeze-thaw process are 0.5 mm to 7 mm in diameter initially and are oddly shaped. They become more rounded with age, most being 3 mm or less in size. Tests show that the solid fraction increases as a result of density changes from approximately 30 percent to a maximum of 60 percent during the aging process [5]. If one assumes that slush forms as cubic-packed spheres of uniform radius r, the least dense of regular modes of packing, then the solid would only reach a theoretical packing factor of 52 percent [13]. Body-centered packing has a theoretical value of 68 percent and face-centered unit cells, the most dense of uniform packed spheres, will theoretically be 75-percent solid. The packing factor is defined as given in the following equation:

$$\text{P.F.} = \frac{\text{volume of spheres}}{\text{volume of unit cell}} = \frac{4r^3/3}{(2r)^3} = 0.52 \quad . \tag{1}$$

If higher density slush fractions are desired, they may be obtained by mixing particles of the correct ratio so that the small particles fit between the large ones. The correct ratio of radii is governed by geometric rules, and the coordination number, or number of touching particles, gives the minimum ratio as shown below:

Coordination Number	Minimum Ratio
3	0.155
4	0.225
6	0.414
8	0.732
12	1.000

For a mixture of any two particle sizes, the packing factors are given by equation (2) (assuming face-centered cubic, the most dense, and assuming that the larger particles are being held slightly apart by the smaller ones).

$$\text{P.F.} = \frac{4(4r^3/3) + 4(4R^3/3)}{(2r + 2R)^3} \tag{2}$$

The particles supplied in tailor-made size and correctly aged could be mixed to increase the density. Since particles of different size settle at different rates in a gravity field, mixing would be necessary to prevent stratification.

Mission studies have established that development of slush and subcooled cryogen technology can extend the capabilities of current vehicles to undertake post-Apollo missions [5]. The feasibility of manufacturing and handling subcooled/slush cryogens has been established. Larger facilities are needed to verify scaling parameters and production and upgrading techniques, and to evaluate instrumentation [5].

The test efforts on the utilization of slush should be expanded to include the effects of the expected flight environment. Flight experiments have also been proposed [1, 5]. Recirculation of triple-point liquid or slush hydrogen from ground supply dewars to flight tankage is the recommended method of controlling quality during ground operations [1]. Maintaining helium pressure in the ullage space is the best technique available for preventing tank implosion during launch operations. For vehicles requiring long term storage and/or later firings, it is best to vent ground pressurizing helium during ascent.

Higher penalties are incurred for a given instrumentation inaccuracy in measuring slush hydrogen quantity than the same inaccuracy in measuring its quality. For example, a 1-percent error in measuring loaded hydrogen quantity results in a loss of 97.1 kg (214 lb) of payload (Saturn V/S-IVB lunar mission), but an equal percentage error in measuring loaded quality results in a loss of only 6.6 kg (14.6 lb) of payload.

An analysis of insulation systems indicates that space-heating of triple-point hydrogen is 3 to 6 percent higher than for saturated liquids because of the increased temperature difference between the tank and the environment [1]. At the low rate of transfer, this increase is relatively small. The optimum thickness of the insulation becomes thinner as the degree of subcooling is increased. Pressurization and venting system studies indicate that a mixer system located in the hydrogen tank is desirable when subcooling is employed. When a cyclic-venting mode or a no-vent mode is required, the mixer ensures uniform saturation [1]. An axial jet pump submerged in the cryogen and using fluid power (10 W or less) from conventional pumps

driven by a dc motor is said to be optimum [14, 15]. In one study [1], venting was not required for an optimum vehicle designed for a 21-day mission when either triple-point liquid or 50-percent slush was used. The no-vent mode permits operational simplicity and increased reliability which approaches that for vehicles using earth-storables, and the cryogenic propellant specific impulse is higher than that of vehicles using earth-storables. Better performance can be achieved with subcooled hydrogen when a non-ideal or less effective insulation system is used to compare saturated hydrogen with slush or subcooled hydrogen. For example, suppose one wished to fly a vehicle with the insulation optimized for saturated liquid hydrogen at 1 atm and a short storage period on a long duration mission. Without changes in the insulation, some degree of subcooling and/or percent of slush would provide optimum performance for the increased mission duration. This is not meant to infer that an even larger payload cannot be placed into orbit. With the correct tradeoff between thickness, percent of slush, and duration, a given vehicle can perform longer missions than were originally conceived. The amount of slush can be tailored for a given mission after the vehicle insulation has been installed. When compared with 1.17×10^5 N/m^2 (17 psia) saturated liquid [1], an increase of 10 750 kg (23 700 lb) of delivered hydrogen was obtained when the triple-point liquid was loaded initially. An additional 680 kg (1500 lb) is gained by loading 50-percent slush hydrogen instead of triple-point hydrogen.

One important advantage of slush can be seen from Figure 2. By subcooling liquid hydrogen to the triple point, the maximum no-vent pressure is reduced by 2.07×10^5 N/m^2 (30 psia). Using 50-percent (by weight) slush, the maximum no-vent

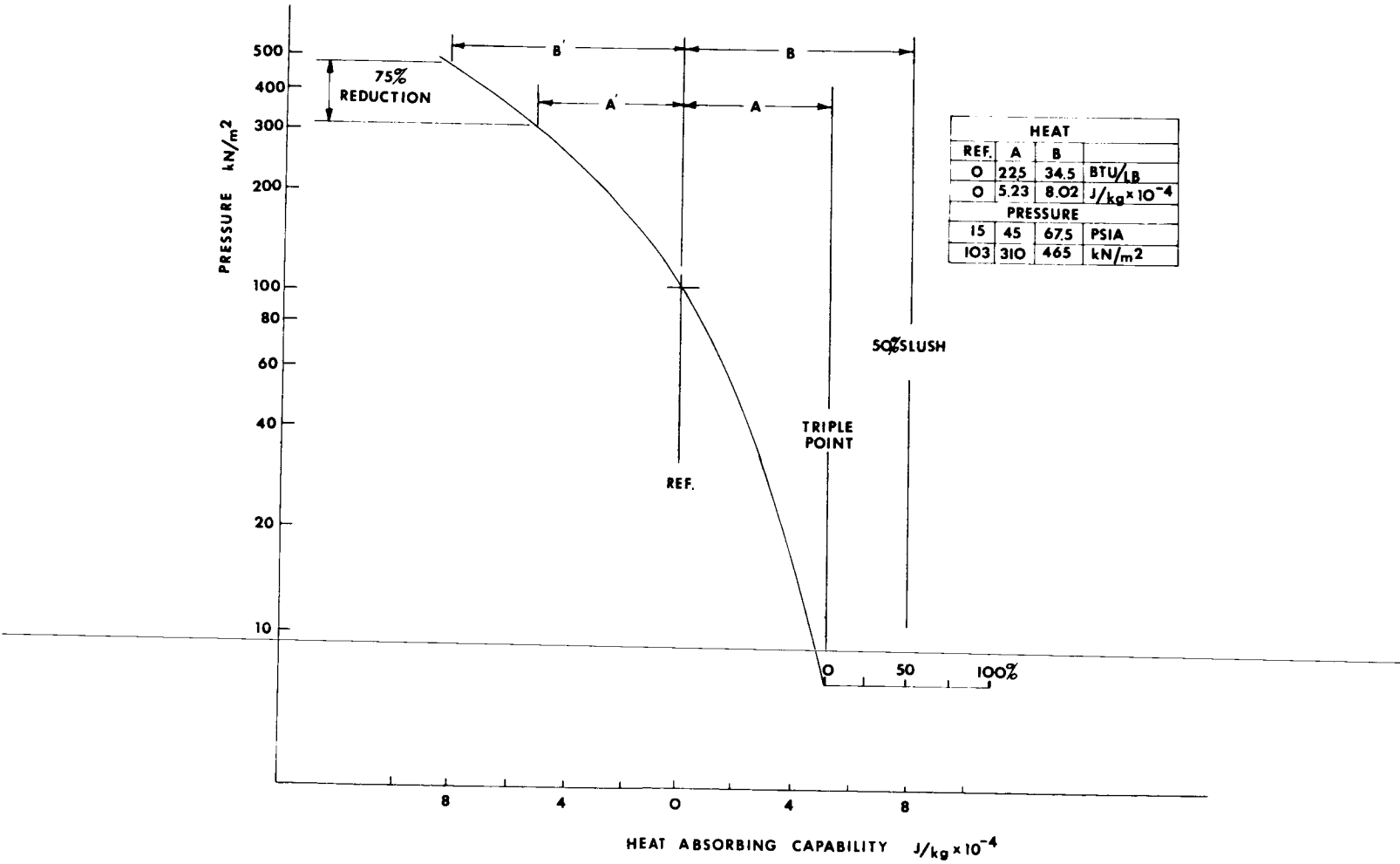

Figure 2. No-vent tank pressure versus heat absorbing capability.

pressure is reduced by 3.62×10^5 N/m^2 (52.5 psia) This represents a 75-percent improvement in vent pressure for 50-percent slush over triple-point hydrogen for the same heat input. Since both tank weight and gaseous pressurant are functions of internal pressure, the potential weight savings is significant.

Calculations of the thermal optimization of tank insulation and the net weight gain and increased storage time using 50-percent slush hydrogen are given in the Appendix; the results are shown in Figures 3 and 4 and Table A-1.

TESTING

During the testing program, the freeze-thaw process of manufacturing slush hydrogen was thoroughly tested [2,3]. A total of 18.93 m^3 (5000 gal) [145 batches, 0.13 m^3 (35 gal) each] were manufactured and transferred by technicians with no prior specialized training on a nonlaboratory basis. Approximately 2.88 m^3 (760 gal) of slush were accumulated and stored in a facility dewar. During the transfer operation, severe fluid and thermal oscillations occurred at transfer line bayonet fittings and valves. A significant quantity (19 percent) of the solid being transferred was melted by the increased heat load resulting from the oscillations. This problem is the result of vapor pockets being formed and recondensation occurring because of the solid and subcooling. Dead-end pockets should be avoided, and proper size openings around the valve stem should be provided. Up to 21.3-percent slush was measured. The slush was stored without venting or excess pressure buildup. Mixing proved to be an effective technique for controlling tank pressure. At the test conclusion, good drainage was demonstrated only after adequate prechilling of the drain line.

Flow tests with slush flowing through restrictions, a globe valve, an orifice, and a venturi were performed and documented [3]. It was shown that mass fractions up to 0.5 will flow through openings as small as 0.635 cm (0.25 in.) as readily as a triple-point liquid will. Pressure losses are essentially the same as or slightly less than that of a triple-point liquid. When plotted as a function of Reynolds number, friction factor, and percent solid and compared to a normal Newtonian fluid, the results are as shown in Figure 5. At high Reynolds numbers, the friction factor is less for such mixtures than for the liquid using triple-point viscosity for the slush values. The pumping characteristics using a centrifugal-type, liquid hydrogen pump in which the slush fraction varied from 0.19 to 0.55

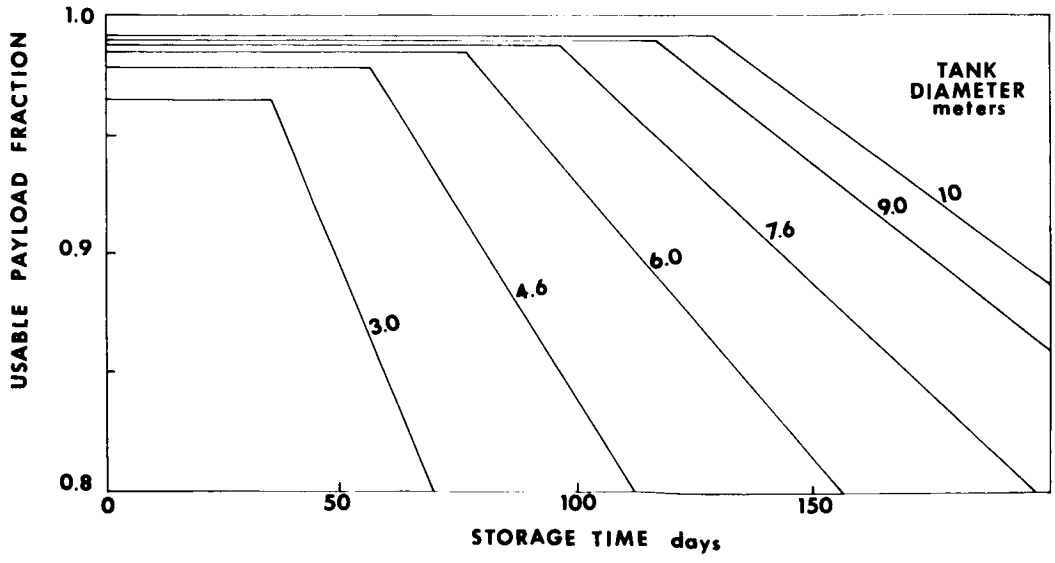

Figure 3. Fraction of usable payload versus storage time.

has a developed head that is the same as that of a triple-point liquid (Fig. 6), considering density differences. The total operating time for the pump with slush was 79 minutes. No wear over that expected from liquid operation was observed.

Experiments on aging and upgrading [16] indicate that the solid fraction of slush hydrogen can be increased by transferring liquid hydrogen and retaining the solids on a screen that has 0.6-mm (0.023-in.) openings. The maximum solid fraction of slush that remains fluid enough to mix and transfer is 0.54 when the mixture has been prepared less than 2 hours. With 6 hours of aging, solid fractions up to 0.64 can be mixed and transferred. Mixing degraded the solid fraction attainable in any given time. A high probability exists that the ullage will collapse if the vessel is precooled, unless helium is used as a pressurant. To replenish fuel, a slush of uniform solid fraction is required, which makes total mixing necessary. Two basic types of mixers were tested. One, which was commercially available and suitable for storage vessels, had an open propeller. The propeller was set off-center to prevent swirl and solid centrifugation. Mixing of slush at 0.25 solid fraction was effective. However, no mixing was observed at 0.45 fraction using a small three-blade, 20.3-cm (8-in.) diameter propeller operating at 47.1 rad/sec (450 rpm). A larger, four-unit, two-blade propeller 40.6 cm (16 in.) in diameter was used to stir batches of slush hydrogen with solid fractions in excess of 0.5. The flight hardware, or ducted propeller mixer, was tested to determine if a high volume, low head pump could be used. Slush fractions up to 0.45 were mixed. The pneumatic motor was replaced with a high speed electric motor, 128 rad/sec (1700 rpm), which mixed solid fractions up to 0.55 very well. Four

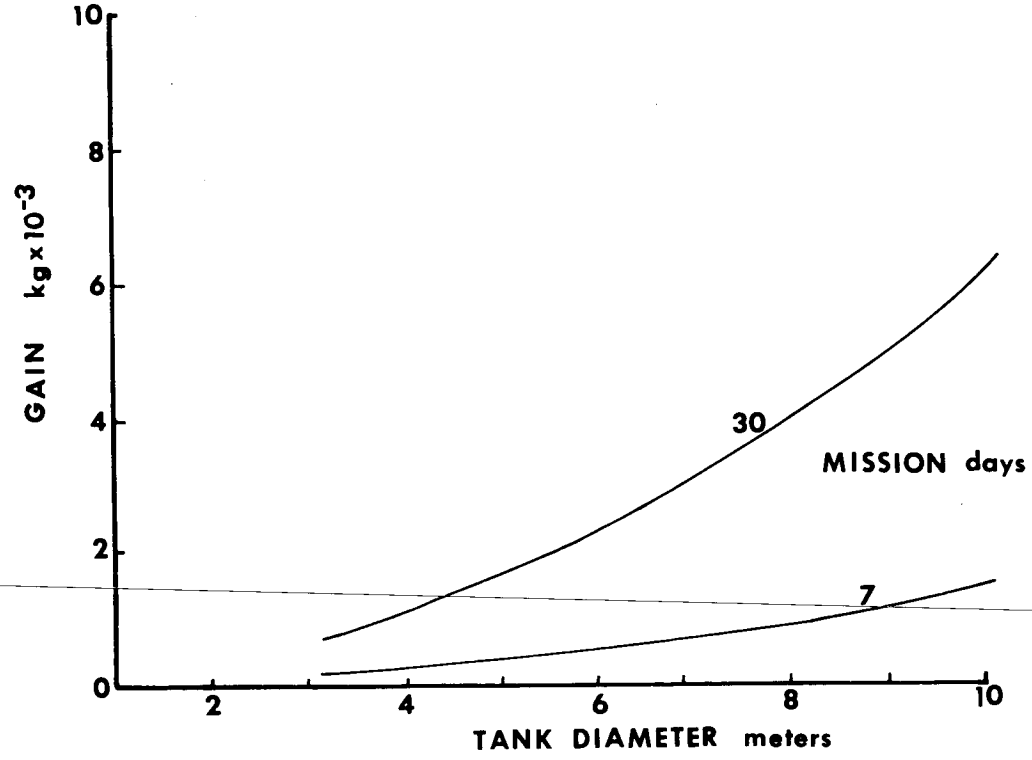

Figure 4. Payload gain versus tank diameter.

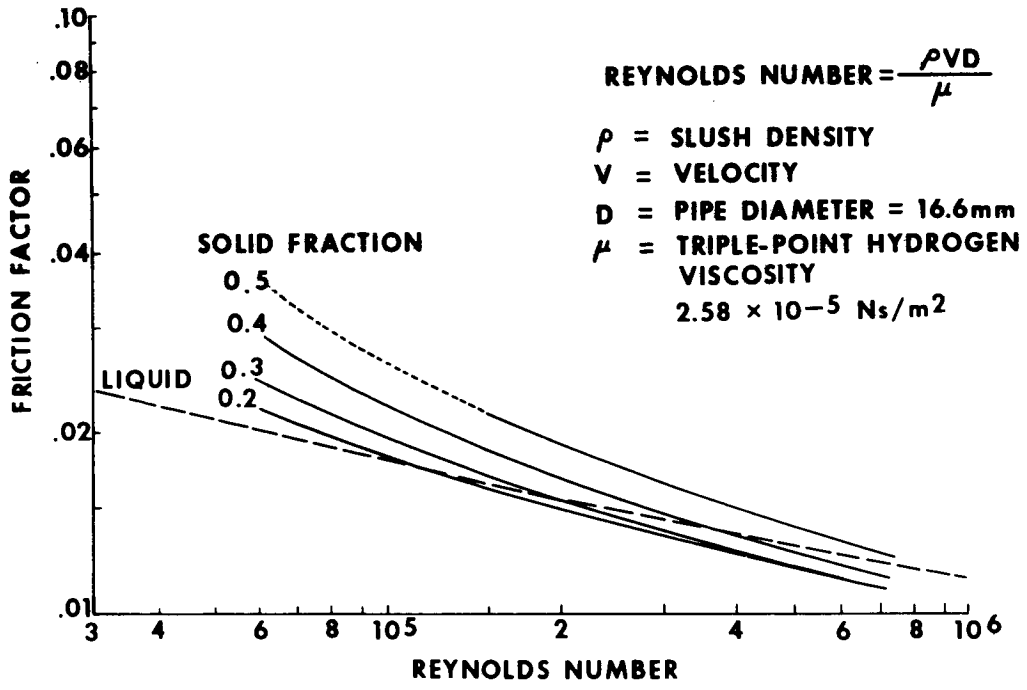

Figure 5. Flow characteristics of liquid/slush hydrogen.

conclusions were reached in the mixing studies: (1) aged slush to 0.64 solid fraction can be mixed if it is not exposed to the ullage gas; (2) the stirring requirements for homogeneous mixing increase above 0.45 solid fraction, but by using fluid discharges, a properly placed fraction of 0.55 can be homogenized; (3) mixing in excess of 0.5 with an open-blade propeller can be accomplished if the tip velocity is high and the blades are properly spaced; and (4) the mixing center should be offset 1/6 of the tank diameter to prevent vortexing and centrifuging of solids.

Contractors and government agencies other than MSFC have been responsible for actual experimental achievements in the slush field to date. MSFC has completed the design of a slush facility, which is a scaled-up version of equipment used by NBS in an earlier slush program (Fig. 7). Tanks and other equipment are on hand and this facility is under construction. The objective of the in-house program is to develop the capability to produce, store, and utilize triple-point slush and gelled liquids. MSFC is planning the following test programs:

1. Scale effects of operations with slush hydrogen using practical-scale equipment for slush hydrogen manufacturing.

2. Development of a measurement and calibration test stand for cryogenic equipment evaluation.

3. Comparison of manufacturing techniques as to rate and minimum energy, including continuous production.

4. Supply slush hydrogen for small scale tests, such as drop tower zero-gravity tests, insulation testing, and tank penetration tests at slush temperature.

5. Experimental verification of storage analysis, transportation, and ground handling.

6. Instrumentation development in the areas of flow, density, temperature, pressure, phase, and level.

7. Production of gels and investigation of their potential advantages.

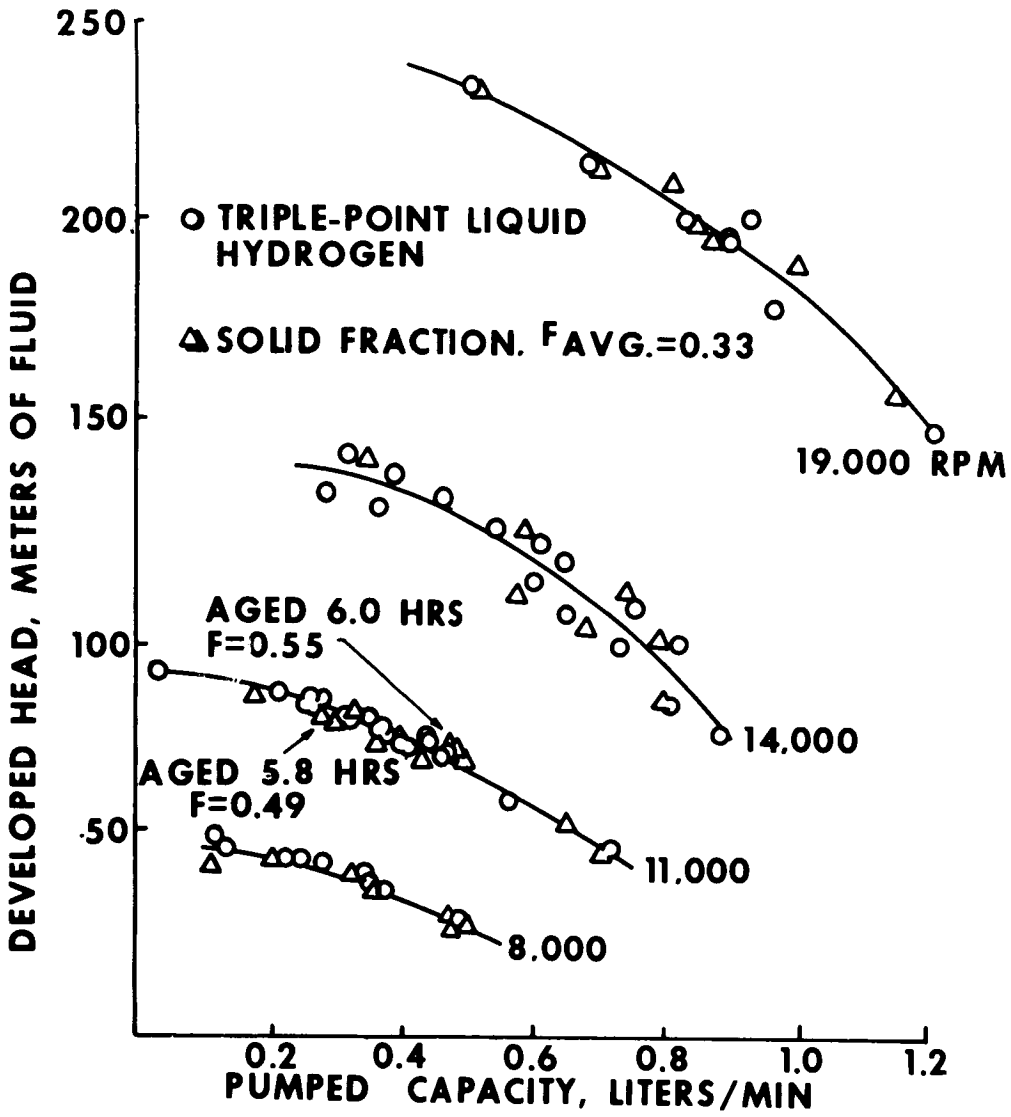

Figure 6. Pump performance for triple-point liquid and slush.

Scale-up, metrology, and slush stratification tests need to be performed first; these can be carried out simultaneously. The next priority should be tests of the fluid handling properties. Flow test data need to be obtained and correlated for various pipe sizes. A knowledge of the solid bridging and vortex near the tank drain is needed to estimate net positive suction head and to arrive at a proper design. No experiment work has been noted that addresses itself to three-phase flow and heat transfer. Since slush flows with slightly less pressure drop at high Reynolds numbers than does triple-point liquid, the regime of three-phase flow with heat input would be of basic interest, especially in connection with gels and penetrating radiation effects. Also of interest is the fluid behavior during venting and draining operations in zero-gravity and during upgrading, mixing, and slosh operations. Testing these effects will require model studies. Investigation of continuous production techniques of both slush and gels will be required to keep pace with the state-of-the-art. Transportation and handling techniques will be an outgrowth of other testing.

GELS

The same desirable properties noted for slush also apply to gelled liquid hydrogen. The increased heat capacity and density allow longer storage of propellant and reduced venting losses. The finite yield strength of gels minimizes sloshing. Evaporation losses using gels have been reported to be reduced by a factor of two or more [9]. The gelled liquid can be retained by screens. A gelled liquid in

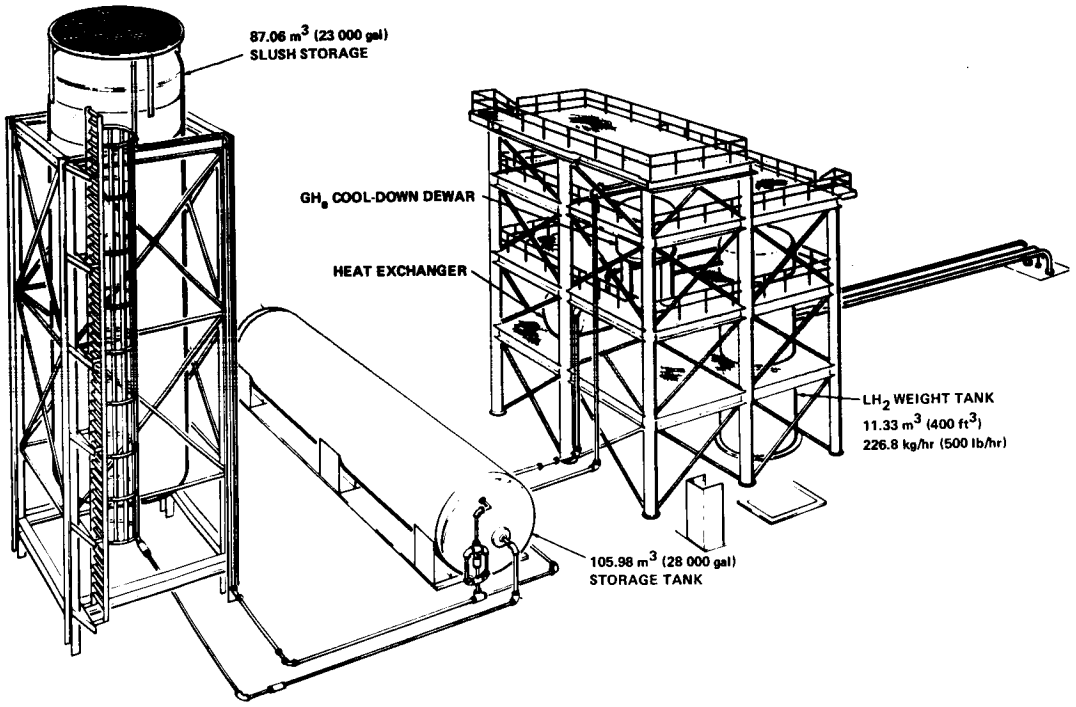

Figure 7. MSFC slush hydrogen facility.

a punctured pipe may stop flowing if the head pressure is relieved. Increased surface tension will aid in passively moving the propellant in a zero-gravity environment, and the gel can be positioned away from a surface that is transferring heat.

The characteristics that a gel possesses at rest are those of a coherent solid. Until a shear force is applied, the material maintains its positional stability. This property eliminates the need for a positive expulsion device, with its associated complexity and material problems, to ensure propellant delivery to the engine. It is known that the resonant frequency is higher for gels than liquids; the motion decay occurs in 2 cycles or less, as compared to 30 to 40 cycles for liquids.

Hydrogen gels, unlike water gelatines that are characterized by partially soluble long chain molecules, must be gelled by surface interaction with a large number of finely divided particles. The number of particles needed per unit volume is a constant. The finer the particles are, the lower the weight is of the gellant needed to gel the liquid. By increasing the amount of solid slush in a mixture of solid slush and liquid hydrogen, the amount of gelling agent needed is reduced. In gelling slush, the solid hydrogen particles are formed before the gelling agent is added; thus, only the liquid part needs to be gelled. The required weight of gelling agent is given by equation (3):

$$Y_s = \frac{Y_1(1 - X)}{\frac{1t}{1b}(1 - Y_1) + Y_1(1 - X)} , \qquad (3)$$

where

Y_1 = weight fraction of the gelling agent in liquid,

X = weight fraction of solid hydrogen or nitrogen,

$1b$ = saturated liquid density,

and

$1t$ = triple-point liquid density.

The gelling agent should have a high heat of combustion per unit weight and have low molecular

weight combustion products. In tests to date Cab-O-Sil, a pyrogenic silica of 0.005 to 0.01 particle size, has been used because of its availability and because of previous investigations. Any agent of small size that is not soluble and is nonactive is of potential use. Testing can often be conducted with inert simulants substituted for the propellants, which greatly reduces the hazard and expense. Both nitrogen and hydrogen gels have been prepared. The weight bearing capacity of each has been measured with plumb bob weights. Hydrogen requires six times the amount of Cab-O-Sil(R) needed for nitrogen.

A primary disadvantage of some of the particular gelants is their reactivity. For example, organics cannot be used with OF_2. Since the liquids become gelled as a result of surface properties, the particles must be small. The major problem is to develop techniques to prepare these fine particles. Some of the inorganics possess no propellant value and significantly degrade performance. In some uses they are not volatile and leave residue in the liner, manifold, and injector and this impaires restart. A literature survey was made [17] of cryogenic propellants and storable oxidizers, etc., and a number of interesting results were reviewed. Gels were produced in situ by condensation of gases into the cryogenic liquids. The feasibility of in situ gelling of liquid hydrogen using particles of other fuel was investigated. Using liquid nitrogen as a similar but safer liquid, n-pentane was introduced into the liquid bubbling. Fine crystals were formed, and a thickening of the liquid was observed. However condensation caused clogging of the feedline. The experiment was repeated using propane, and small amounts (nucleation sites) of pyrogenic silica or acetylene black were added. The propane coagulated with the silica and a gel formed with the acetylene black. Attempts were made to crystalize methane in liquid nitrogen, but these failed because methane is soluble. In another experiment fine crystals of ammonia, whose particle size appeared to be less than 0.1, were prepared, but no gels were formed. Attempts to gel liquid hydrogen with methane by dilution with helium and by bubbling resulted in plugging the inlet tube. A second attempt may have formed submicron particles but no gel. Another attempt at Los Alamos resulted in a suspension that agglomerated and settled. Recent results [18] indicate that liquid hydrogen may be gelled with ethane where ethane is less than 5 percent (by weight) of the total mixture. Other hydrocarbons are being investigated also.

A number of methods have been proposed to control fluids in a zero-gravity environment. These include propulsive acceleration, surface tension, dielectrophoretic, positive expulsion, etc. Each method has its disadvantage; excessive weight, complex structure, excessive power needs, and material incompatibility, respectively. A promising method of effectively controlling propellant in tank expulsion, etc., is to use finely divided material that is magnetic and compatible with the particular propellant (iron powder in the case of slush hydrogen, Fe_3O_4 in the case of slush oxygen, or chromium potassium alum in either case). The propellant can then be moved with the aid of permanent magnets located at the fluid exit and in the pumps. The use of electric magnets would allow, at small power levels, active positioning of the propellant away from high heat transfer areas or would move the propellant during re-ignition even against unfavorable accelerations.

CONCLUSIONS

- Triple-point cryogenics and slush can be used advantageously to increase payload and storage capabilities and reduce or eliminate tank venting.

- A recirculation technique for loading slush into flight-weight tanks during groundhold is the preferred slush upgrading method.

- Flow characteristics and properties such as mass, quality, flow rate temperature, and pressure are measurable and predictable.

- Helium should be used to stabilize flight-weight tanks containing triple-point hydrogen, slush, or gel.

- Gels offer improvements in the performance of rocket systems because of positional stability, reduced sloshing, and vaporization and active positioning in a zero-gravity environment.

- Significant stratification can exist in flight tanks containing slush when subjected to earth gravity and high heat loads. Gels may aid in preventing stratification.

- Future studies should be expanded to include promising slush propellants or slush-gel mixtures. A mature slush-gel technology appears to be a practical, desirable, and useful approach to solving difficult propellant management problems for future space missions.

APPENDIX

CALCULATION OF OPTIMUM INSULATION THICKNESS AND BOILOFF LOSS AS A FUNCTION OF TANK DIAMETER

Introduction

The intent of these calculations is to show the possible benefits, such as increasing the mission time, of mixtures of solid hydrogen and liquid hydrogen using the same hardware that has been optimized, in relation to insulation thickness, for use with liquid hydrogen at 1.03×10^5 N/m^2 (15 psia). The following assumptions have been used:

$k = 1.464 \times 10^{-4}$ J/sec m°K (8×10^{-5} Btu/hr ft°R),

T = 267°K (480°R),

$Q_{pent.} = 1.758$ J/sec (60 Btu/hr),

$\rho_{insulation} = 48.06$ kg/m^3 (3 lb/ft^3),

$LH_2 = 70.8$ kg/m^3 (4.42 lb/ft^3),

$\Delta H_{vapor} = 4.465 \times 10^4$ J/gm (192 Btu/lb) at 1.03×10^5 N/m^2 (15 psia),

$\Delta H_{fusion} = 5.81 \times 10^3$ J/gm (25 Btu/lb) at triple point,

and

Initial mission duration = 7 days (168 hours)

Sample Calculations

$$V_{C+S} = \frac{\pi D^2 L}{4} + \frac{4}{3}\pi R^3 \quad .$$

If L/D = 2,

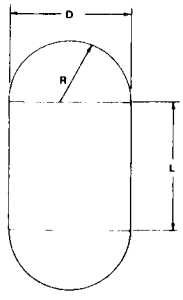

$$V_{C+S} = \frac{\pi D^2 (2D)}{4} + \frac{4}{3}\frac{\pi}{8}D^3$$

$$= \frac{\pi D^3}{2} + \frac{\pi D^3}{6}$$

$$= \frac{3\pi D^3 + \pi D^3}{6}$$

$$= \frac{2}{3}\pi D^3$$

$$= \frac{2}{3}\pi 8R^3$$

$$= \frac{16}{3}\pi R^3$$

$$\therefore D = \left(\frac{3V}{2\pi}\right)^{1/3}$$

Where the payload mass is 2.27×10^4 kg (5×10^4 lb) and since $V = M/\rho$ when $\rho = 70.8$ kg/m^3 (4.42 lb/ft^3), the tank diameter for L/D = 2 is as follows:

$$D = \sqrt[3]{\frac{(5 \times 10^4)}{2\pi\ 4.42}} = 17.4 \text{ ft; } 5.3 \text{ m}$$

$$A_{C+S} = \frac{2\pi D(2D)}{2} + \pi D^2 = 3\pi D^2 = 3(3.14)(17.4)^2$$

$$A_{C+S} = 2851 \text{ ft}^2; 264.8 \text{ m}^2$$

The minimum weight, all other factors being equal, occurs at the tradeoff point of equal boiloff and insulation weight:

Weight boiloff = Weight insulation

$$\text{Weight boiloff} = \frac{kA\,\Delta T\,\theta}{\Delta H_V\,(\Delta X)} + \frac{Q_\rho \theta}{\Delta H_V}$$

$$= M = \rho_i A \Delta X$$

$$\rho_i A \Delta X = \frac{kA\Delta T_i\,\theta}{\Delta H_V\,(\Delta X)} + \frac{Q_\rho \theta}{\Delta H_V}$$

$$\left(\rho_i A\Delta X - \frac{Q_\rho \theta}{\Delta H_V}\right)\Delta X = \frac{kA\Delta T\theta}{\Delta H_V}$$

$$\rho_i A\Delta X^2 - \frac{Q_\rho \theta\,\Delta X}{\Delta H_V} - \frac{kA\Delta T_i \theta}{\Delta H_V} = 0 \quad .$$

The quadratic equation and solution is

$$AX^2 + BX + C = 0$$

$$X = \frac{-b \pm \sqrt{b^2 - 4ac}}{2a}$$

Substituting ΔX for X gives

$$\Delta X = \frac{-\left(\frac{Q_\rho \theta}{\Delta H_V}\right) \pm \sqrt{\left(\frac{Q_\rho \theta}{\Delta H_V}\right)^2 - 4\rho_i A\left(\frac{-kA\Delta T_i \theta}{\Delta H_V}\right)}}{2\rho_i A}$$

The optimum insulation thickness is as follows:

$$\Delta X = \frac{\frac{60(168)}{192} \pm \sqrt{\left(\frac{60 \cdot 168}{192}\right)^2 - 4\,(3)\,2851\left[\frac{-8\times 10^{-5}(2851)480(168)}{192}\right]}}{2\,(3)\,2851}$$

$$= \frac{52.5 \pm \sqrt{2756 - 34212\,(-95.8)}}{17.106}$$

$$= \frac{52.5 \pm \sqrt{2756 + 3.277 \times 10^6}}{1.7106 \times 10^4}$$

$$= \frac{52.5 \pm 1.81 \times 10^3}{1.7106 \times 10^4}$$

$$= 0.1092 \text{ ft } (1.310 \text{ in.}) ; 0.03328 \text{ m}$$

$$M = \rho A \Delta X$$

$$= 3(2851)\,0.1092$$

$$= 933.9 \text{ lb of insulation; } 205.9 \text{ kg of insulation,}$$

where

Payload = 2.268×10^4 kg (5×10^4 lb),

V = 319.9 m^3 (1.13×10^4 ft^3) is required for 70.8 kg/m^3 (4.42 lb/ft^3) for LH_2 ,

A = 265 m^2 (2851 ft^2) for a cylinder tank with spherical head (L/D = 2) ,

and

the mission is a 7-day mission (168 hr) .

This is also the weight of boiloff for 7 days. The heat capacity that may be utilized to reduce the boiloff and extend the mission duration by use of a solid and liquid mixture is related to the mission, θ, as follows:

Heat Loss — Heat Storage Capacity

$$\frac{k\Delta T_i A\theta}{\Delta X} + Q_\rho\,\theta = X_f M\Delta H_f + M\overline{C}_p(T_{BP} - T_{TP}) \quad ,$$

where

X_f = weight fraction of solid hydrogen (0.5) ,

M = mass of hydrogen (tank volume · density of hydrogen), 22 680 kg (50 000 lb),

T_{TP} = 13.9°K (25°R) ,

T_{BP} = 20.0°K (36°R) ,

and

$\overline{C}_p$ = 8.41×10^3 J/gm (2.01 Btu/lb°R) .

Therefore,

$$\frac{8 \times 10^{-5}\,(480)\;2851\,\theta}{0.1092} + 60\,\theta = 0.5\,(50\,000)\;25.2$$

$$+ 50\,000\,(2.01)(36-25)$$

$$1002\theta + 60\theta = 1.735 \times 10^6$$

$$1062\theta = 1.735 \times 10^6$$

θ = 1633 hr (68.0 days) .

The density of triple-point hydrogen is approximately 76.9 kg/m^3 (4.8 lb/ft^3), leaving a void volume in a tank filled to a given payload weight. In this case the volume unfilled is 13.2 m^3 (466 ft^3). This volume may be used to store boiloff until a convenient time for venting occurs, such as auxiliary

propulsion, etc. This volume flexibility can also provide and accommodate a varying payload up to 934.4 kg (2060 lb) for the 5.3-m (17.4-ft) (L/D = 2) tank.

It is known that strong stratification occurs in a slush hydrogen tank between the solid fraction and liquid. It is suspected that heat input may transfer into the liquid phase and result in nonequilibrium boiloff. Calculations presented in this appendix are for various tank volumes and give results for the theoretical weight saving and/or mission duration extension.

TABLE A-1. CALCULATION SUMMARY (CYLINDER TANK WITH SPHERICAL HEADS, L/D = 2)

D, m	V, m^3	A, m^2	M, kg × 10^{-3}	ΔH^a, J × 10^{-6}	Optimum ΔX^b, cm	Insulation Weight[b] and Boiloff Weight, kg	Boiloff Rate, kg/day
1.52	7.4	21.8	0.523	4.22	4.55	48	6.8
3.05	59.2	87.5	4.20	33.8	3.52	148	21.2
4.57	200	197	14.2	114	3.35	317	45.3
5.3	320	265	22.7	183	3.33	424	60.5
6.1	474	350	33.5	270	3.30	555	79.3
7.6	926	547	65.5	529	3.27	860	122.8
9.1	1600	788	133.0	914	3.26	1233	176.1
10.0	2129	953	150.8	1217	3.25	1490	212.9

θ^c, Days	ΔW_{BO}[d], kg	Insulation, percent	Weight Loss Percent[e]			Slush Void, m^3	Slush Payload Variable, kg
			7 Days	28 Days	35 Days		
13.9	94.8	9.13	18.3	45.6	54.8	0.34	24
36.1	635	3.53	7.1	17.6	21.2	0.79	56
56.9	1360	2.24	4.5	11.2	13.4	8.27	585
68.0	1815	1.87	3.7	9.4	11.2	13.2	907
77.3	2380	1.65	3.3	8.2	9.9	18.9	1341
97.3	3685	1.31	2.6	6.6	7.9	38.4	2717
117.3	5284	1.09	2.2	5.4	6.5	65.8	4658
129.4	6387	0.99	2.0	5.0	5.9	87.6	6205

a. Assume heat of penetration — 1.758 J/sec (60 Btu/hr)
b. 7-day mission LH_2 optimum
c. Increase mission duration
d. ΔW gain for slush versus LH_2, 7 days × boiloff rate for 7-day mission (same as insulation weight)
   ΔW gain for slush versus LH_2, 30 days × boiloff rate; $(30-\theta)$ boiloff rate for 30-day mission
e. $(W_I + W_{BO}/M)$ 100 is weight loss percent in tanks optimized for 7-day mission

REFERENCES

1. Keller, C. W., ed.: A Study of Hydrogen Slush and/or Hydrogen Gel Utilization. Vol. II, Fourth Quarterly Progress Report, K-11-68-ID, Lockheed Missiles and Space Company, Sunnyvale, Calif., March 11, 1967.

2. Keller, C. W., ed.: A Study of Hydrogen Slush and/or Hydrogen Gel Utilization. Vol. II, Supplemental Test Program, Lockheed Missiles and Space Company, Sunnyvale, Calif., October 31, 1968.

3. Sindt, C. F.; Ludtke, P. R.; and Daney, D. E.: Slush Hydrogen Fluid Characterization and Instrumentation. National Bureau of Standards TN 377, U. S. Government Printing Office, Washington, D. C., February, 1969.

4. Rapial, A. S.; and Daney, D. E.: Preparation and Characterization of Slush Hydrogen and Nitrogen Gels. National Bureau of Standards TN 378, U. S. Government Printing Office, Washington, D. C., May 1968.

5. Vaniman, J. L.; Worlund, A. L.; and Winstead, T. W.: Slush and Subcooled Propellants for Lunar Interplanetary Missions. Paper A-1 for XIV Cryogenic Engineering Conference, August 1968.

6. Modular Nuclear Vehicle. Study Phase II, LMSC A830244, Lockheed Missiles and Space Company, Sunnyvale, Calif., February 1968.

7. Barry, B. G.: An Analytical Study of Storage of Liquid Hydrogen Propellant for Nuclear Interplanetary Spacecraft. Third Quarterly Progress Report, FPR-046, General Dynamics Fort Worth Division, March 1968.

8. Gerth, B.; and Lundeen, R.: Development of Supercritical Pressure Cryogenic Storage and Supply System Incorporating the Radial Bumper – Discrete Shield Design. Report No. 3873-67 LER 56, Bendix Corporation, April 1968.

9. Kartluke, H.; McKinney, C. D.; Pheasant, R.; and Tarpley, W. B.: Gelling Liquid Hydrogen. NASA CR 54055 RR 64-47, 1964.

10. Slush Hydrogen Production, Storage and Distribution Study Program. Report No. N67-15455, Union Carbide, May 1966.

11. Ventre, A. J.: The Ground Handling of Slush Hydrogen. Report No. ASD-ASTN-1153, Teledyne-Brown Engineering Co., Huntsville, Ala., Contract No. NAS8-20073, May 1970.

12. Scott, R. B.: Cryogenic Engineering. D. Van Nostrand Co., Princeton, N. J., 1959, p. 100.

13. Van Vlack, L. H.: Elements of Materials Science. Second Edition, Addison-Wesly Publishing Company Inc., Reading, Mass., 1967, pp. 42, 57-60.

14. Poth, L. J.: Study of Cryogenic Propellant Stratification Reduction Techniques. Report No. FZA-419-1, General Dynamics Fort Worth Division, September 1967.

15. Stark, J. A.; and Blatt, M. H.: Cryogenic Zero-Gravity Prototype Vent System. Report No. GDC-DDB67-006, General Dynamics Convair Division, October 1967.

16. Sindt, C. F.; and Ludtke, P. R.: Slush Hydrogen Fluid Characterization and Instrumentation. National Bureau of Standards Report No. 9745, U. S. Government Printing Office, Washington, D. C., November 6, 1969.

REFERENCES (Concluded)

17. System Analysis of Gelled Space-Storable Propellants. Summary Report 1038-S, Aerojet-General Corporation, Contract NAS7-473-SA-2, July 1969.

18. Carbon Compounds/Liquid Hydrogen Fuels. Monthly Progress Reports December 1969 through June 1970, Project 396, Aerojet-General Corporation, Contract SNP-1.

BIBLIOGRAPHY

Technology Requirements Document. Report No. Misc-PD-PP-70-1, Program Development Directorate, Marshall Space Flight Center, Huntsville, Ala., April 2, 1970.

Mann, D. B.; Dean, J. W.; Brennan, J. A.; and Kneebone, C. H.: Cryogenic Flow Research Facility. National Bureau of Standards Report No. 9749, U. S. Government Printing Office, Washington, D. C., January 1, 1970.

Ludtke, P. R.: Slush Hydrogen Flow Facility. National Bureau of Standards Report No. 9752, U. S. Government Printing Office, Washington, D. C., March 1, 1970.

System Analysis of Gelled Space-Storable Propellants. Summary Report 1038-02S, Aerojet-General Corporation, Contract NAS7-473-SA-1, July 1969.

Roder, H. M.; and Goodwin, R. D.: Provisional Thermodynamics Functions for Para-Hydrogen. National Bureau of Standards Note 130, U. S. Government Printing Office, Washington, D. C., December 1961.

PROPELLANT THERMAL STRATIFICATION

By

T. W. Winstead

SUMMARY

Large deviations from equilibrium heat distribution are characteristic of cryogen propellant storage tanks. The result of heating nonvented cryogenic tanks in a gravity environment is the development of well-ordered density gradients; the associated temperature gradients were originally characterized as being approximately represented as temperature strata. While the process of distributing heat within cryogens is highly dependent upon environmental influences such as the incident heat flux and acceleration, the basic terminology is generally not associated with the physical environment. Thus, the term "thermal stratification" is used to express nonuniform heat distribution within the bulk propellant.

The nonuniform distribution of heat results in significant temperature variations in booster propulsion propellants and causes an undesirable increase in the self-pressurization rate of cryogen storage systems. A semiempirical prediction method has been developed for high-gravity environments and is adequate for design purposes; model accuracy is somewhat limited to similarity in tank geometries, and additional work is needed to extend the correlation range. Several low-gravity environment models that cover a broad range of predicted results have been developed under NASA contract. Unfortunately, there are no applicable data by which any of these models may be selected in preference over the others.

INTRODUCTION

Accurate predictions of propellant temperature are needed to establish a suitable propulsion system design. The net positive suction pressure (NPSP) required by a rocket engine influences the tank pressure needed to provide adequately subcooled liquid. The influence of propellant temperature is due to the corresponding vapor pressure (P_v) in the equation,

$$NPSP = P_{tank} + \Delta P_h - \Delta P_{friction} - P_v .$$

The hydrostatic head pressure (ΔP_h) is frequently sufficient to provide adequate NPSP for lox systems, except during terminal draining of the propellant system. For LH_2 systems, this term is generally insignificant, and the NPSP is provided almost entirely by tank pressure. The influence of thermal stratification on NPSP is most important for LH_2 applications because of the strong dependency of vapor pressure on temperature and the large increase in structural weight associated with increasing tank pressure. Propellant temperatures can be minimized by adding thermal insulation to the tank, but there is an associated weight penalty. Thus, it is important that propellant temperatures be accurately predicted so that insulation and tank weight can be optimized. The penalty for conservatism in propellant temperature predictions is reduced propulsion performance capability. For example, the payload of a typical upper stage is penalized 400 kg to accommodate a 1°K conservative prediction of LH_2 temperature increase. Propellant temperatures and corresponding density are important to mass gaging systems and may present quantity errors of as much as 0.2 percent. While this value is quite low, it may be a significant contributor to uncertainty in propulsion capability because of the contribution to lift-off weight, flight performance reserves, etc.

The influence of thermal stratification on the venting of storage tanks in a reduced-gravity environment has been studied extensively [1,2]. While various methods have been devised to predict thermal stratification in a low-gravity environment, none are supported by applicable experimental data. The range of corresponding tank self-pressurization rates covers several orders of magnitude. The principal impact is the order-of-magnitude uncertainty in the duty cycle requirements for propellant tank venting systems. This does not present severe difficulties for medium-duration missions (less than 30 days) but does impact feasibility studies for long-duration missions.

PREDICTION METHODS

High-Gravity Environment

Several techniques have been developed for predicting propellant thermal stratification in the high-gravity environment of ground tests and booster flight vehicles. The most successful model employed at the Marshall Space Flight Center (MSFC) is a semiempirical method that was developed for application to the LH_2 tanks of the Saturn booster stages. Limited correlations have been made with lox and LH_2 data accumulated through research and development programs. This model is based on the assumption of log linearity of ΔT and $\Delta V/V$ as illustrated by the typical data in Figure 1, where ΔT is the increase in temperature above initial tank temperature at a given time and at $\Delta V/V$, which is the volume fraction measured from the liquid-gas interface. By this definition, V is the existing liquid volume at any time and ΔV is a fraction of the liquid at which one desires to compute the fluid temperature. The mathematical foundation for this model is a simplified dimensional analysis considering the characteristic parameters of propellant mass (M), tank diameter (D), tank length (L), propellant density, specific heat, and viscosity (C_p, ρ, μ), propellant heating rate (Q), propellant heating (ΔT) above an initial condition, and time (θ). The selected form of the dimensional analysis is

$$(\Delta T)_{\Delta V,\theta} = f\left(\frac{Q}{MC_p}\right)\left(N_{PR}\right)^m\left(\frac{\Delta V}{V}\right)^n \quad . \quad (1)$$

To assess the applicability of this format, a semiempirical model has been developed using data from ground test and flight vehicles.

The temperature profile shown in Figure 1 is of the form

$$\Delta T = K\left(\frac{\Delta V}{V}\right)^n \quad , \quad (2)$$

where ΔT is the temperature increase at the volume fraction ($\Delta V/V$), and K and n are determined as follows. Since the temperature profile equation [equation (2)] is analytically cumbersome, artificial constraints must be employed so that the temperature at the quasi-surface does not exceed the saturation temperature. This is accomplished by integrating the heat load between the bottom of the tank ($\Delta V/V = 1$) and the saturated "surface" temperature. The ΔT at the surface is defined by ΔT_{sat} at the corresponding $\Delta V/V$ at saturation, and the term $\ln (\Delta V/V)_{sat}$ is then employed as a correlation parameter. The resulting equation is

$$\ln K + K\left(\frac{MC_p}{Q}\right)\ln\left(\frac{\Delta V}{V}\right)_{sat} = \ln (\Delta T)_{sat} + \ln\left(\frac{\Delta V}{V}\right)_{sat} \quad . \quad (3)$$

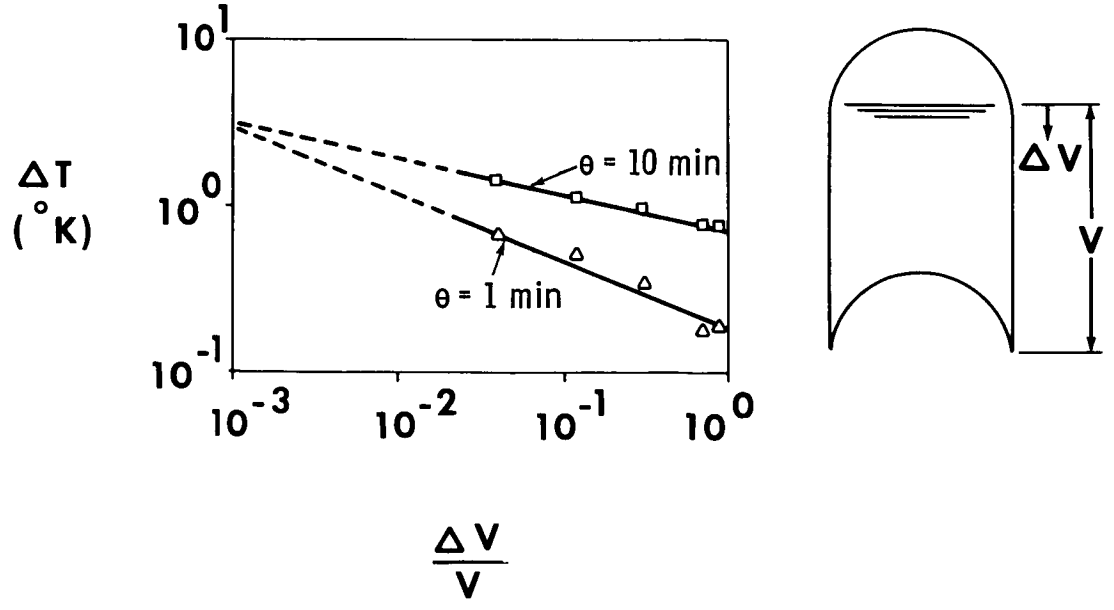

Figure 1. Typical propellant stratification data.

This equation is solved for K , where

$$\frac{-Q}{MC_p\left[\ln\left(\frac{\Delta V}{V}\right)_{sat}\right]} < K < MC_p/Q \quad ,$$

and the exponent n may then be found by

$$n = \left(\frac{MC_p}{Q}\right) K - 1 \quad . \qquad (4)$$

The applicability of this semiempirical method is based on the observations of quasi-steady temperature profiles within several well-instrumented tanks and an experimental implementation of a model that has indicated acceptable agreement with data.

Comparison of Results

The model described in the previous paragraphs has been used extensively in analyses of the liquid hydrogen tanks of the Saturn stages. Recently, an investigation was conducted to assess the use of the model for the Saturn lox tanks, which resulted in order-of-magnitude agreement.

In the liquid hydrogen analyses, the bulk temperature is assumed equal to saturation temperature at the tank ullage pressure just prior to tank prepressurization. Tank ullage pressures are generally stabilized 30 min or more before tank prepressurization during the 2-min period prior to launching the vehicle, and the assumption of a well-mixed, uniform temperature within the tank does not appear to impose any analytical or other difficulties upon the system. However, this assumption is not valid for the lox systems, since inverse stratification has been observed in all the Saturn lox tanks. The analysis and data presented in Reference 3 provide an adequate first-order approximation for estimating lox bulk temperature during this period. Because of the inverse stratification, temperature predictions by the described analytical model cannot be precise, and reasonably small differences between the analysis and data, which will be illustrated later, result. This does not appear to be of significant consequence to the propulsion system, since NPSP for all the Saturn lox systems is more than adequately provided by accelerated head pressure, except during start transient of the upper stages and during terminal draining of the tanks and/or feed systems.

Several features implied by analysis of the stratification problem have not been taken into consideration by this model. These omissions include tank sidewall-to-bottom heating ratios, the influence of baffles, and overall tank geometry considerations (such as tank bottom shape, length, diameter, etc.). It is likely that the selected correlation parameter, $\ln (\Delta V/V)_{sat}$, might be improved as a time, geometry-dependent consideration that considers more carefully the omissions listed above. The use of this parameter as a constant may result in some analytical inconsistencies, but as illustrated in the following paragraphs, it provides a reasonable estimate of the stratification problem.

Propellant tanks are located in the Saturn V vehicle as illustrated in Figure 2.

The following data were selected from several launch vehicles as being either typical or representative of the stage operation or for comparison with the previously described model.

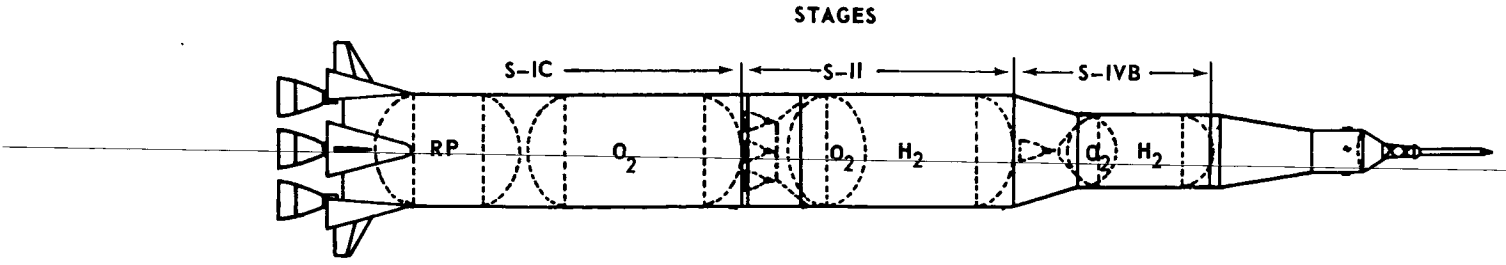

Figure 2. Saturn V propellant tankage.

S-IC STAGE

The S-IC lox flight data parameters essential to a thermal analysis are presented in Figure 3, which shows the heat load, propellant mass, and tank pressure during flight and an approximate geometric description of the tank. The related flight data and results of the stratification analysis are compared in Figure 4.

The discrepancy introduced by prelaunch inverse stratification is most predominant for the S-IC tank. The selection of $\ln (\Delta V/V)_{sat}$ for comparison with data was arbitrary.

S-II STAGE

A comparison of the data and model for the S-II lox tank is shown in Figure 5 for the associated tank pressure, heat load, propellant mass, and tank geometry illustrated in Figure 6. The major portion of the propellant heating occurs prior to the start of draining, with a significant fraction of heating occurring during the prelaunch period. This introduces some difficulties, but the analysis is still adequate for design purposes.

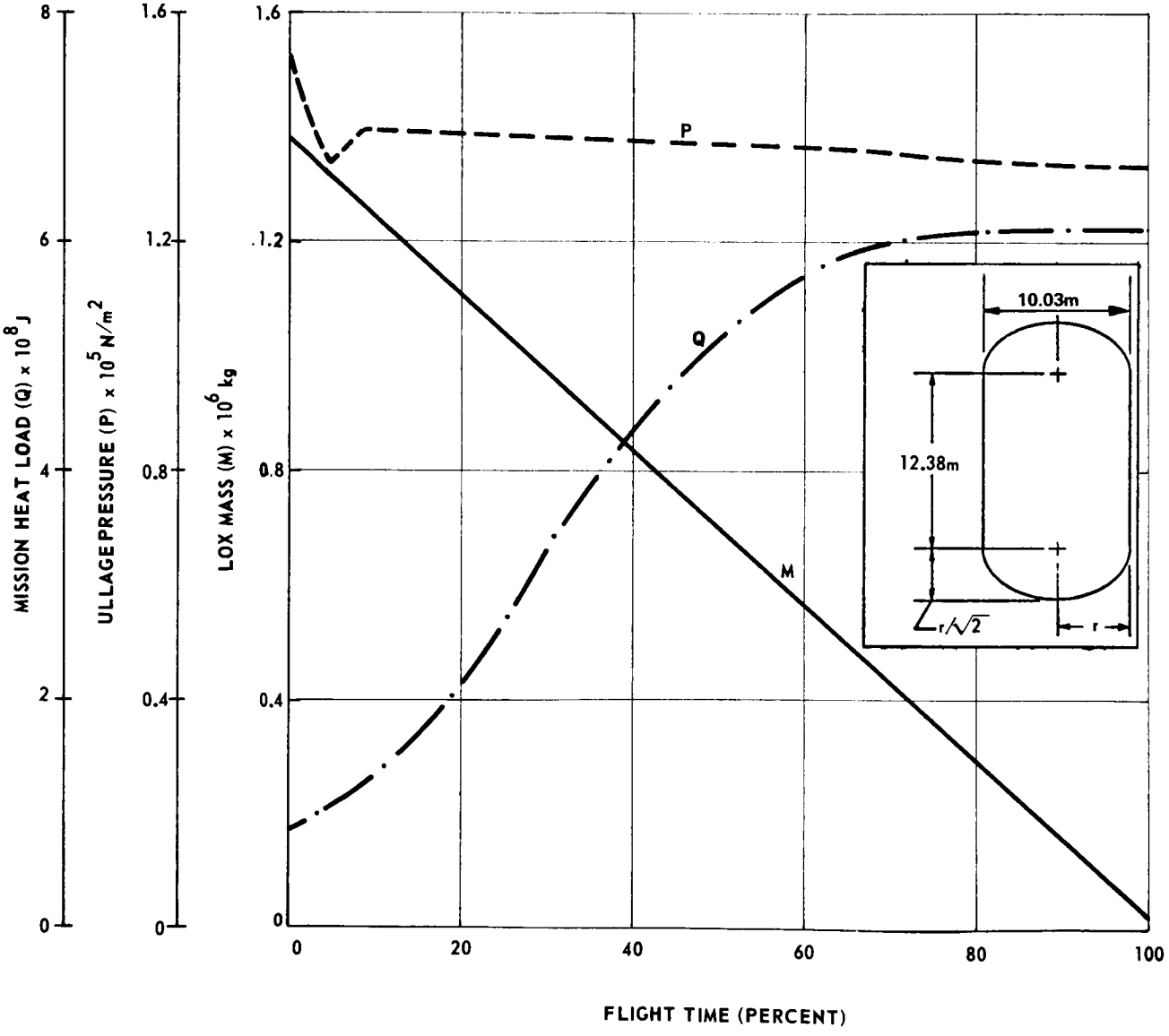

Figure 3. S-IC lox tank flight parameters.

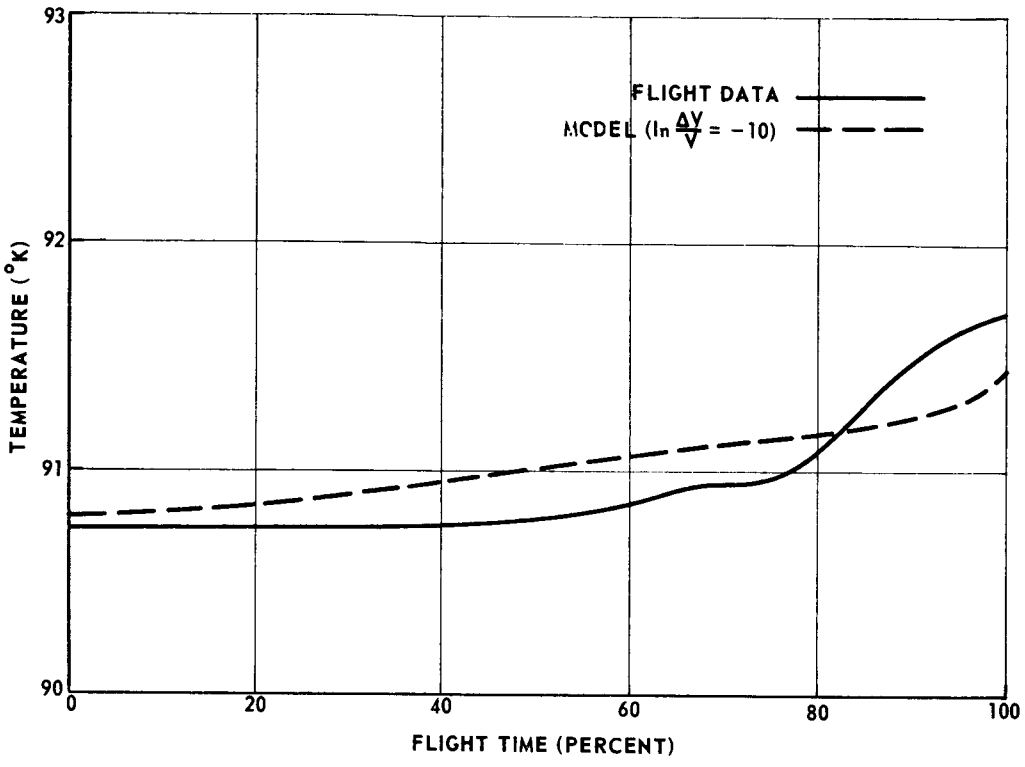

Figure 4. S-IC lox tank drain temperature.

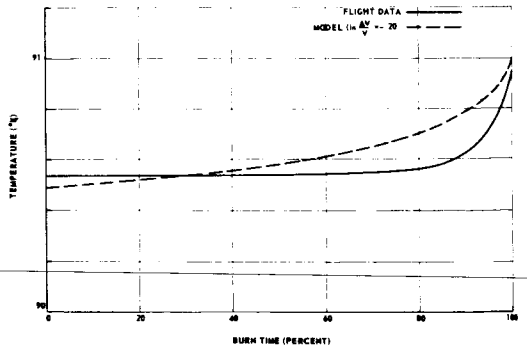

Figure 5. S-II lox tank drain temperature.

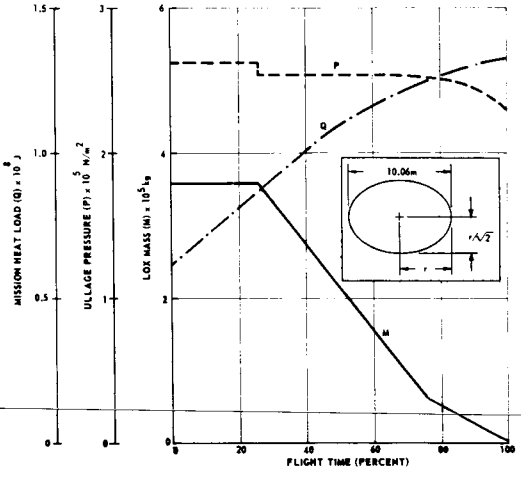

Figure 6. S-II lox tank flight parameters.

Fuel tank stratification data for the S-II stage are compared with the prediction model in Figure 7 for the tank heating, pressure, and propellant mass histories shown in Figure 8. Predictions based on the model show good agreement with both ground and flight test data.

S-IVB STAGE

Flight data for the S-IVB stage propellant systems are from the AS-204 launch. (Propellant tank configurations are essentially identical for the Saturn IB and Saturn V.) Figure 9 is a comparison of tank drain (pump inlet) temperatures for the S-IVB lox tank, and corresponding data on tank pressure, etc., are shown in Figure 10.

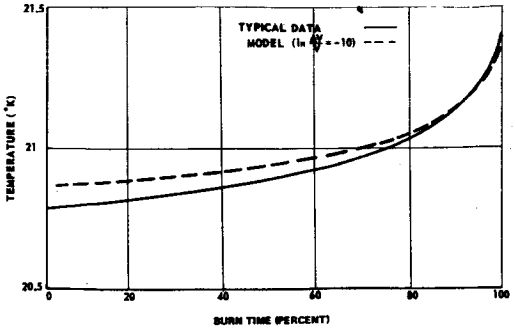

Figure 7. S-II LH_2 tank drain temperature.

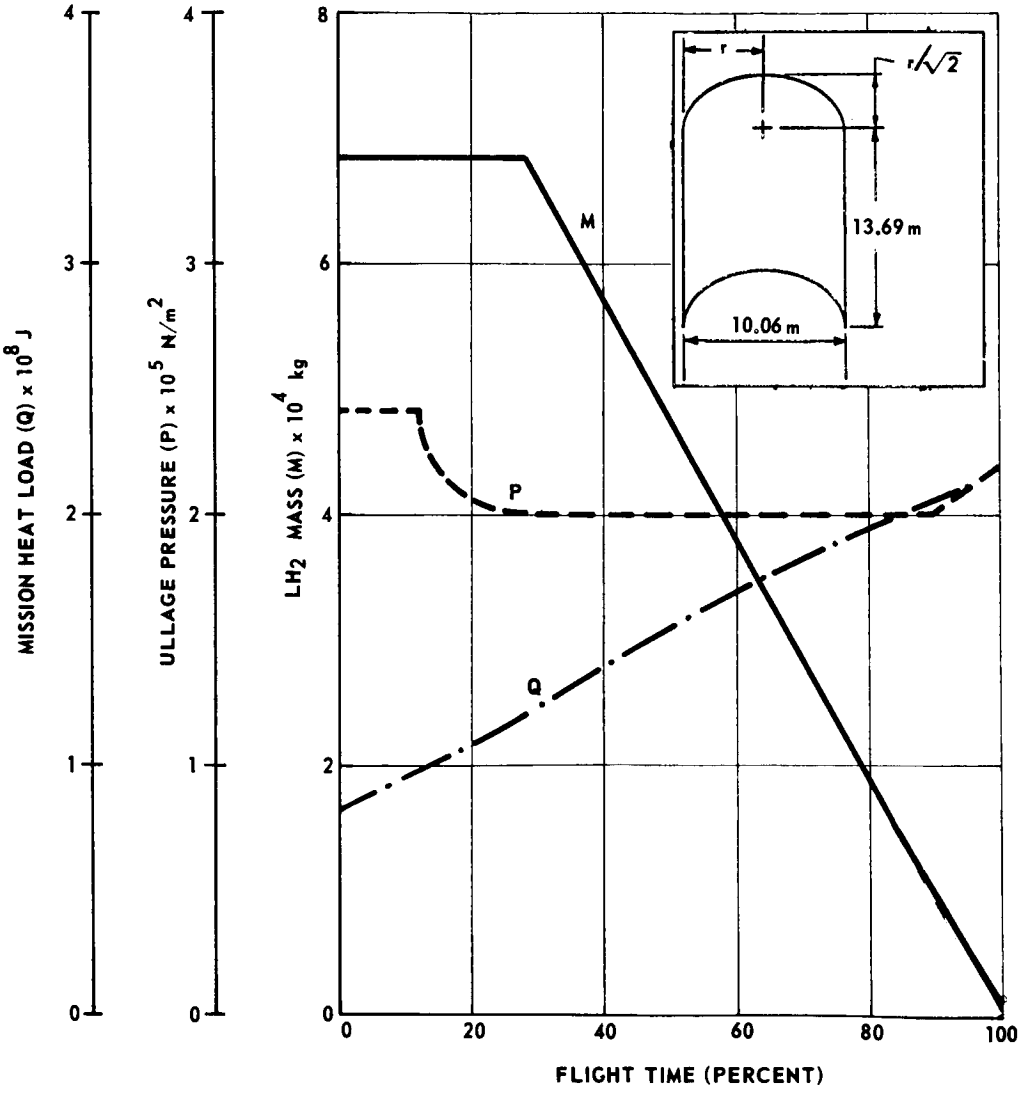

Figure 8. S-II LH_2 tank flight parameters.

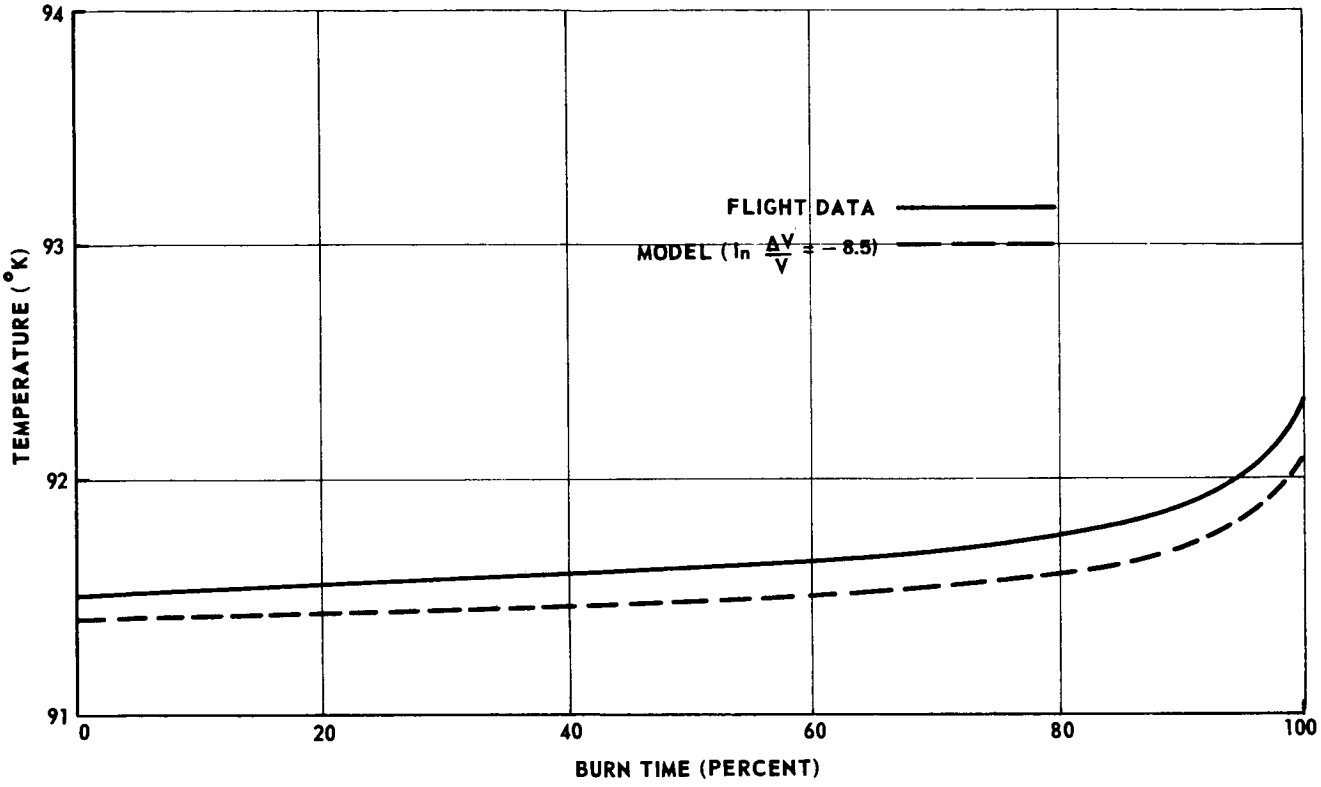

Figure 9. S-IVB lox tank drain temperature.

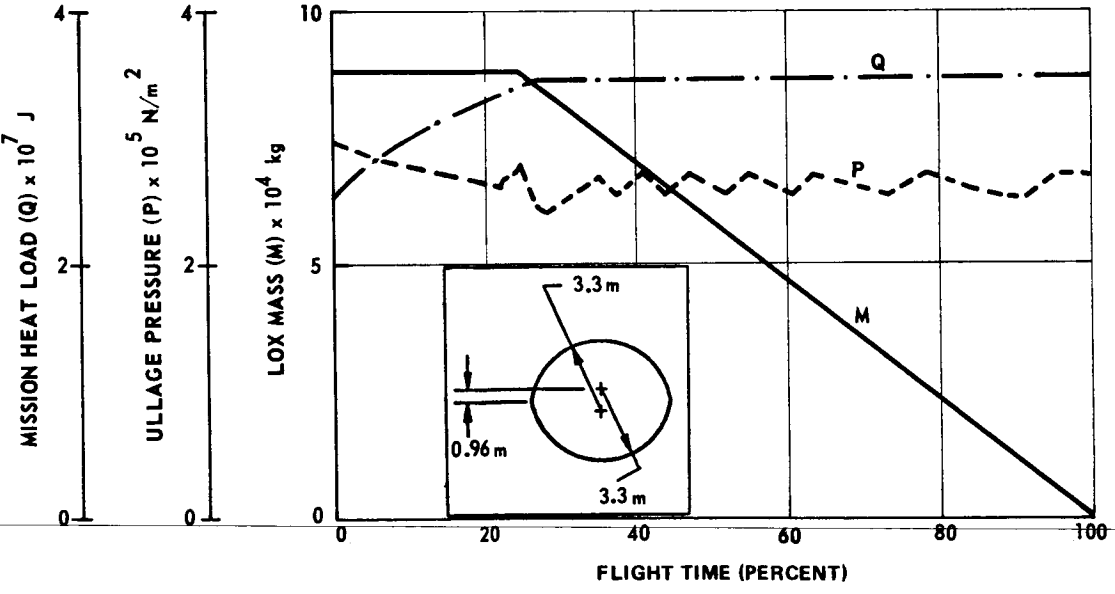

Figure 10. S-IVB lox tank flight parameters.

The comparison of S-IVB fuel tank data to the prediction model results in Figure 11 shows good agreement. The associated input data are presented in Figure 12. Data from the Saturn I, S-IV stage and the Saturn IB, S-IVB stage were used as the basis for developing the analytical model. Data from the S-IV stage are presented in Reference 4.

Several obvious deficiencies are indicated in the previous data presentation. However, the model results generally are adequate from a design perspective, and they represent the only model known to the author that can accommodate various propellants and tank shapes with a reasonable expectation of acceptable predictions. Additional work needs to be done to extend the data correlation using existing data; normalizing the data to determine influences of tank size, geometry, heating rates, fluid, etc., is also indicated.

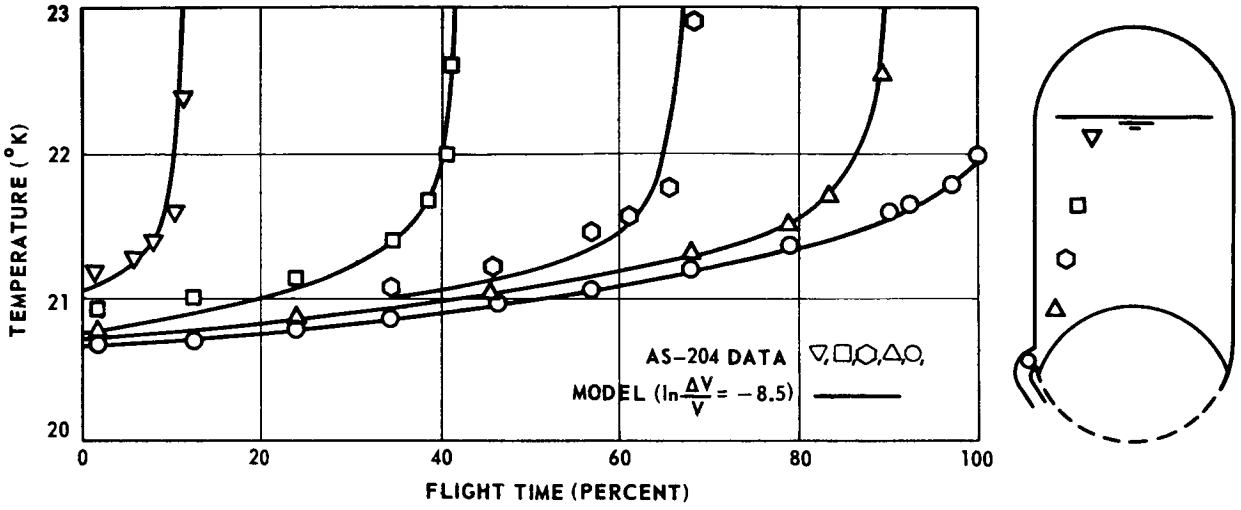

Figure 11. S-IVB LH_2 tank temperatures during flight.

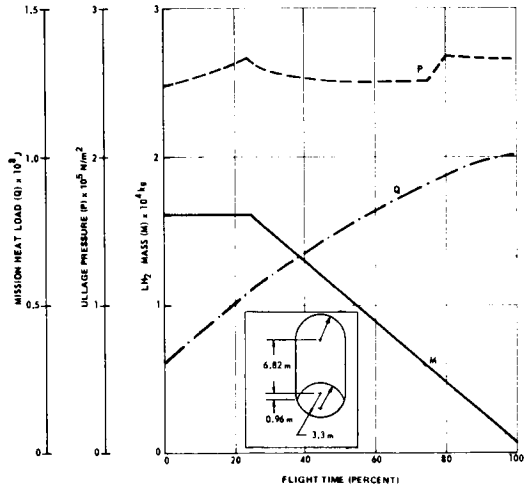

Figure 12. S-IVB LH_2 tank flight parameters.

Low-Gravity Environment

Several methods have been developed under contract to evaluate propellant thermal stratification in low-gravity applications [1,2,5]. A comparison of the results of several prediction techniques is shown in Figure 13, which indicates the wide range of results possible from the several techniques. The principal considerations for these techniques are[1]:

1. Boiling (at heat shorts)
2. Ullage heating
3. Conduction
4. Boundary layer modeling
5. Navier Stokes matrix solution

The data are presented as pseudo-Nusselt numbers, as suggested by Poth in Reference 6, so that the

1. The numbers on Figures 13 and 14 refer to this listing.

maximum stratification ΔT can be compared for a given system. These data are illustrated as tank pressure rise rates in Figure 14; the rates are shown without units since rates are highly dependent on initial vapor pressure and since the results are somewhat dependent on the method employed to control tank pressure and on controller operating range. As illustrated, the prediction techniques may yield results that differ by several orders of magnitude.

Execution of analytical models is generally cumbersome, and large amounts of computer time may be expended. However, since there are no applicable data by which any model could be selected, it hardly appears justified to expend efforts to streamline any specific technique. Currently, planning is underway to accumulate appropriate experimental data during early space shuttle flights, and it is expected that this will provide a basis for selection and improvement of the analytical techniques deemed appropriate at that time.

The principal impact of these stratification predictions is that the corresponding tank pressure increase requires operation of a zero-gravity vent system and/or mixer system to control tank pressure. For short-duration missions of 30 days or less, there appears to be a negligible impact on vent/mixer system design. There is some uncertainty concerning the electrical power required to operate the system, but the effect of power dissipated to the propellant is highly dependent on the duration of the mission. The uncertainty in the stratification predictions may result in a considerable weight penalty to the tank vent system for extremely long (1 year) missions. A current discussion of zero-gravity vent systems was presented previously in this report.

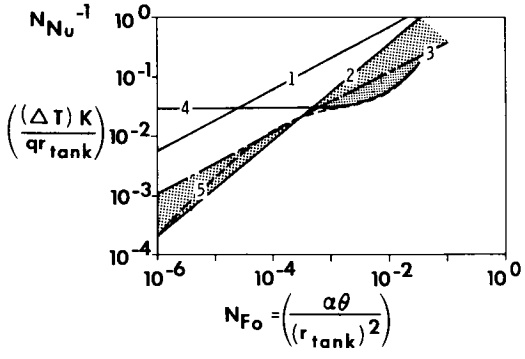

Figure 13. Comparison of low-gravity stratification model results.

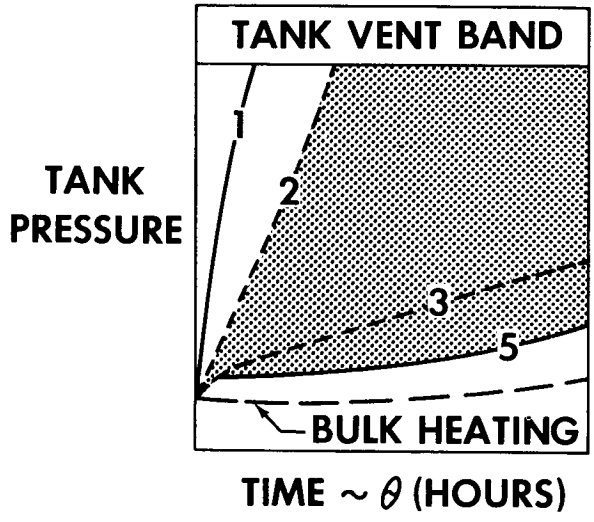

Figure 14. Effect of prediction technique on tank pressurization rates.

REFERENCES

1. Poth, L. J.; et al.: Study of Cryogenic Propellant Stratification Reduction Techniques. Annual Report, Contract NAS8-20330, General Dynamics Fort Worth Division, Report No. FZA-419-1, September 15, 1967.

2. Van Hook, J. R.: Study of Cryogenic Fluid Mixing Techniques. Final Report, Contract NAS8-24882, General Dynamics Fort Worth Division, Report No. FZA-450-2, September 15, 1970.

3. Arnett, R. W.; and Millhiser, D. R.: Experimental Determination and Analytical Prediction of the Bulk Density of Boiling Liquid Oxygen. Final Summary Report, National Bureau of Standards, Boulder, Colorado, NASA Order Nos. H-12350 and H-41963, March 27, 1963.

4. Barnett, D. O.; Winstead, T. W.; and McReynolds, L. S.: An Investigation of LH_2 Stratification in a Large Cylindrical Tank of the Saturn Configuration. Cryogenic Engineering Conference, Marshall Space Flight Center, Alabama, 1964.

5. Modular Nuclear Vehicle Study. LMSC-A794907, Volume IV, Asymmetric Propellant Heating Computer Program, Final Report, Contract NAS8-20007, Lockheed Missiles and Space Co., Sunnyvale, California, March 3, 1966.

6. Poth, L. J.; et al.: A study of Cryogenic Propellant Mixing Techniques. Final Report, Contract NAS8-20330, General Dynamics Fort Worth Division, Report No. FZA-439-1, November 1, 1968.

MATERIALS FOR FOAM TYPE INSULATION

By

W. E. Hill

SUMMARY

The internal cryogenic insulation used on the S-IVB hydrogen tanks established the precedent for using internal foam insulation systems in the hydrogen tanks of the shuttle vehicle. The three-dimensional polyurethane used on the S-IVB tanks failed to meet the higher temperature requirements of the shuttle vehicle, however, and other foams under consideration include polyisocyanurates, polyphenylene oxides, polyimides, and polybenzimidazoles. Improved adhesive systems for attaching the foams to the interior tank wall are under study.

INTRODUCTION

An internal foam fabrication is one of the concepts being considered for cryogenic insulation on the hydrogen tanks of the shuttle vehicle. Figure 1 represents the internal cryogenic insulation for the S-IVB hydrogen tanks, which is briefly reviewed here because this concept is the basis for advanced internal systems intended for potential shuttle application.

Next to the waffle patterns of the tank wall is the major insulation component of the system, a layer of polyurethane foam bonded to the aluminum tank wall with an epoxy adhesive. The interior surface of the foam is faced with a liner that protects the foam and minimizes the diffusion of hydrogen gas into the foam, which would, of course, degrade the insulation function. The third component, which actually may be regarded as part of the liner, is a seal coat that reinforces the diffusion barrier.

The foam component is a 48.06 kg/m^3 (3 lb/ft^3) polyurethane that is orthogonally reinforced with a three-dimensional grid of glass fibers; it is commonly called 3D foam. The liner is one ply of fiberglass cloth impregnated with polyurethane resin, while the sealer consists of one wiped-on coat of the same polyurethane resin.

DISCUSSION

For shuttle application, the S-IVB tank insulation must be modified to achieve these objectives:

1. Extended service temperature
   a. Primary goal — 150°C (300°F)
   b. Secondary goal — 315°C (600°F)
2. Reliability — 100 flights with minimum refurbishment
3. Reduced weight

Elevated temperature requirements were not imposed upon the internal insulation of the S-IVB and the S-IVB tanks, but because of the flight objectives of the shuttle vehicle, there is a real possibility that a design temperature of 150°C, in keeping with an aluminum structure, might be set for thermal stability of the insulation. There is an additional possibility that if titanium or other metals are selected for the hydrogen tank walls, the commensurate design temperature for internal insulation should range to 315°C.

The reliability of the system should assure a service life of 100 flights with a minimum of reworking. Although preservation of some percentage of the inherent insulating properties of the pure foam will be an engineering objective, the design allowables will be based upon the K-value expected at the end of 100 flights, thus eliminating a risky dependence upon very low gas permeation criteria.

Although the goals for weight reduction are not specific at the present time, this will be a major objective. The foam constitutes 50 to 60 percent of the weight of the insulation system, therefore substitution of a lighter weight foam would make the greatest contribution toward weight saving. The second most productive area for weight reduction is

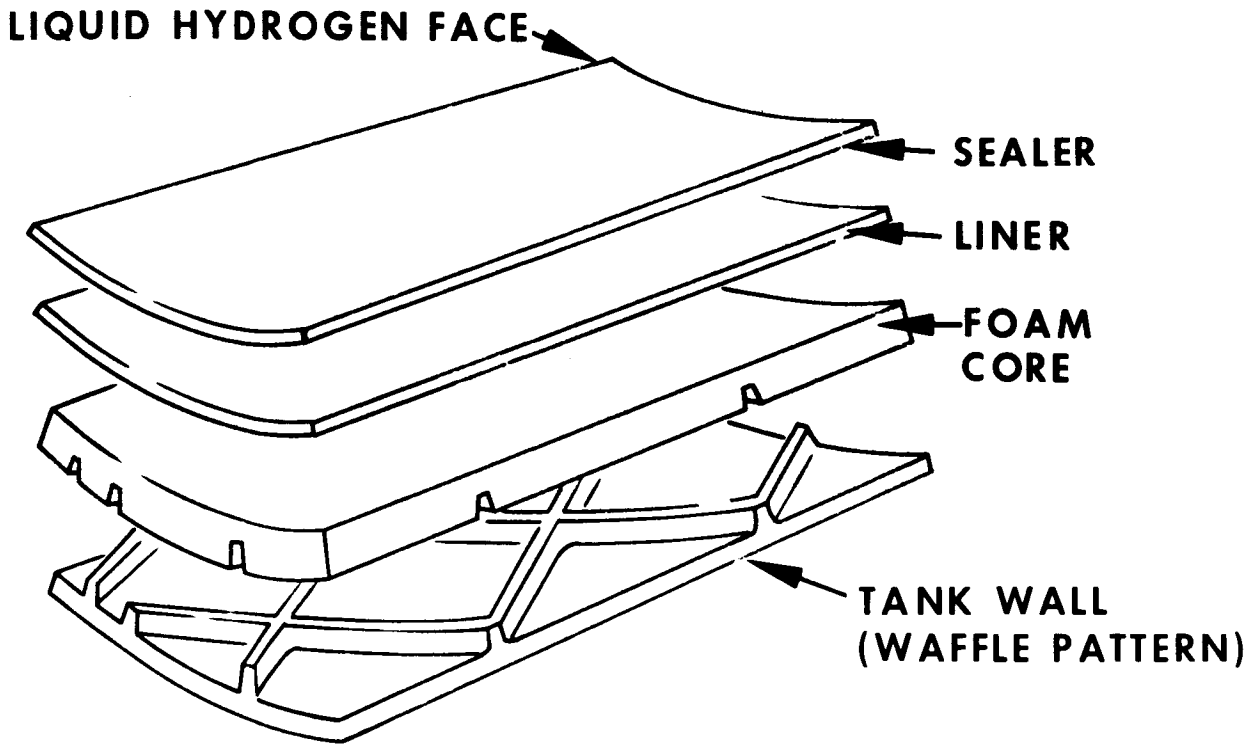

Figure 1. S-IVB internal insulation.

the adhesive used to bond the foam to the tank wall; a polyurethane system, for example, would weigh only one-half as much as the epoxy now in use.

Figure 2 shows two of the foam materials considered for 150° C service. The first of these, the polyurethane 3D foam, is the S-IVB insulation, which is now being evaluated at higher temperatures. The thermally susceptible linkage in a polyurethane polymer is indicated by the dotted line. The second structure is a polyisocyanurate, which is an isocyanate derivative as is the polyurethane. The polyisocyanurate, however, lacks the urethane linkage, and therefore is inherently more thermally stable.

Figure 3 shows some of the foam materials that possibly may be considered for 315° C service. The first of these is polyphenylene oxide, a linear aromatic ether. Some preliminary thermal testing has been initiated on this material. The next two polymers, polyimide and polybenzimidazole, are aromatic-heterocyclic derivatives, a structural class that includes most of the high temperature polymers under development today. Testing is planned but has not yet begun under this program for these two materials. The concept of three-dimensional reinforcement may be difficult to apply with any of these three materials because of the specialized fabrication techniques required to make foams from polymers of these types.

Isothermal weight loss over comparable time periods for three of the foams listed previously is shown in Table 1. At 150° C, the 3D polyurethane loses 7 percent of its original weight; furthermore, differential thermal analysis has diagnosed an endothermic decomposition reaction beginning at 150° C. These findings alone effectively eliminate this particular polyurethane from serious contention. The polyisocyanurate has a density of 28.8 kg/m^3 (1.8 lb/ft^3) as compared to 48.06 kg/m^3 (3 lb/ft^3) for the polyurethane; this represents a considerable weight saving bonus. The weight loss of 5 percent at 160° C is not as low as would be hoped, however,

TABLE 1. ISOTHERMAL WEIGHT LOSS

	150° C	288° C	360° C	385° C
Polyurethane D = 48.06 kg/m^3 (3 lb/ft^3)	7%			
Polyisocyanurate D = 28.8 kg/m^3 (1.8 lb/ft^3)	5% (160° C)			
Polyphenylene Oxide D = 40.05 kg/m^3 (2.5 lb/ft^3)	~1%	2.2%	4.0%	5.0%

1. POLYURETHANE (3D)

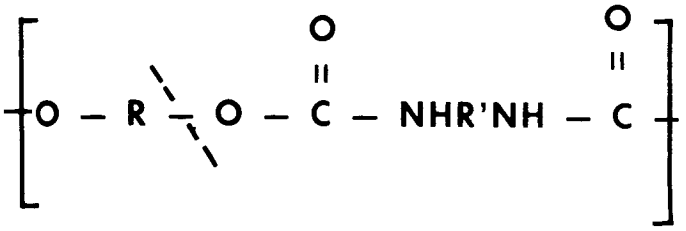

2. POLYISOCYANURATE

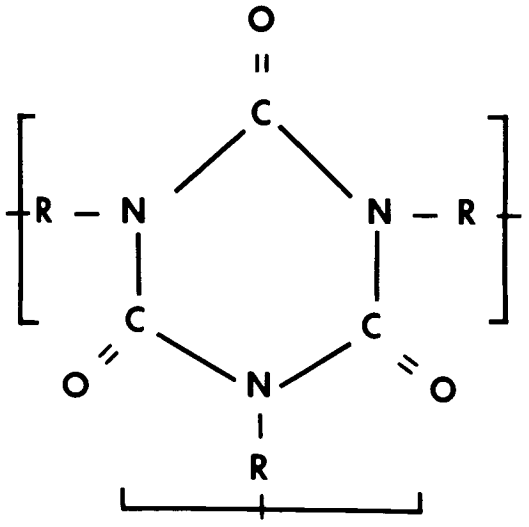

Figure 2. Materials evaluated for 150° C service.

1. POLYPHENYLENE OXIDE (PPO)

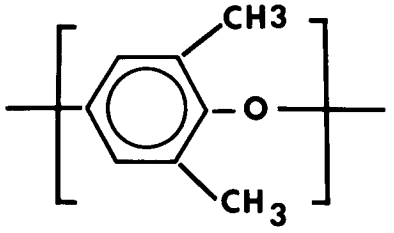

2. POLYIMIDE (PI)

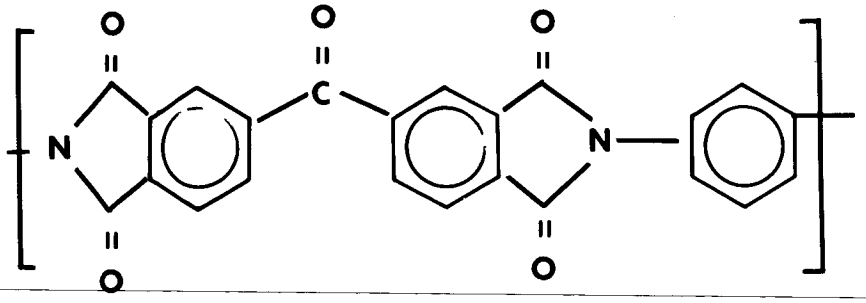

3. POLYBENZIMIDAZOLE (PBI)

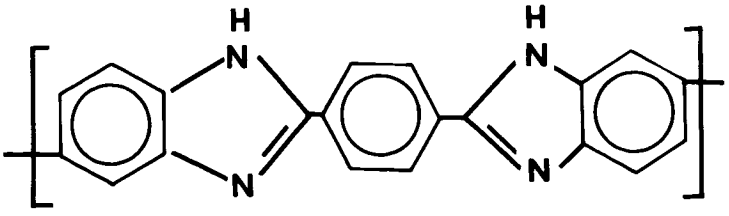

Figure 3. Materials considered for 315° C service.

and some dimensional instability occurs over a period of several days at 150° C. The density of 40.05 kg/m^3 (2.5 lb/ft^3) for polyphenylene oxide represents some weight saving, and the isothermal weight losses of approximately 1 percent at 150° C and of 2.2 percent at 288° C warrant further evaluation of this material for potential high temperature application.

Table 2 presents a quantitative indication of a critical mechanical property of structural foams, the flatwise tensile strength, measured in newtons per square meter and pounds per square inch. The 3D polyurethane sample is strong in the cryogenic region, but much weaker at higher temperatures. These sharply reduced strength values are consistent with an earlier observation that when the 3D foam is bonded to an aluminum plate subjected to controlled heat, cracks develop in the foam near the bondline at 150° C. These tests, together with previous results indicate that the external temperature of tanks insulated with the present 3D foam should not be allowed to exceed 120° C. The same polyurethane foam without reinforcement gives much lower strengths in tests conducted up through 70° C.

The polyisocyanurate has a remarkably constant strength throughout the tested temperature range; this strength would presumably improve with reinforcement. Even without reinforcement, the high temperature strength equals or exceeds that of the 3D polyurethane. Polyisocyanurate foams from different sources will be evaluated as this program continues.

In consideration of adhesives for attaching the proposed insulation to the tank wall, Table 3 compares the S-IVB adhesive with three polyurethane formulations. Focusing on aluminum lap shear tensile values at 150° C, the presently used epoxy adhesive shows a strength of 24.13 × 10^5 N/m^2 (350 psi), while Narmco 7343 polyurethane exhibits only 6.89 × 10^5 N/m^2 (100 psi) at the same temperature. Modification of Narmco 7343 adhesive by the simple addition of 1.0 percent by weight of Z-6040 silane coupling agent raises this value to 62.05 × 10^5 N/m^2 (900 psi). The fourth formulation shown is a blend of two polyurethanes, once again with a coupling agent added to yield a value of 82.74 N/m^2 (1200 psi) at 150° C, while maintaining the high cryogenic strength typical of polyurethanes. Either of the last two polyurethane formulations has the required strength, and either would represent a considerable weight saving.

CONCLUSIONS

1. The 3D polyurethane foam is unacceptable for service at 150° C.

2. Polyisocynaurate foams exhibit some weaknesses but may ultimately be acceptable for 150° C service.

3. Polyphenylene oxides, polyimides, and polybenzimidazoles have inherent thermal stability, but characterization of their foams under this program has just begun.

4. Modified and blended polyurethane adhesive formulations have been developed for lighter weight and higher strength at 150° C.

TABLE 2. FLATWISE TENSILE STRENGTH

Foam Sample	-185° C	25° C	70° C	150° C	175° C
1. Polyurethane 3D Reinforced	15.17 × 10^5 N/m^2 (220 psi)	17.24 × 10^5 N/m^2 (250 psi)		2.76 × 10^5 N/m^2 (40 psi)	0.83 × 10^5 N/m^2 (12 psi)
2. Polyurethane Not Reinforced	3.10 × 10^5 N/m^2 (45 psi)	6.89 × 10^5 N/m^2 (100 psi)	5.52 × 10^5 N/m^2 (80 psi)		
3. Polyisocyanurate Not Reinforced	2.48 × 10^5 N/m^2 (36 psi)	3.86 × 10^5 N/m^2 (56 psi)		2.41 × 10^5 N/m^2 (35 psi)	2.69 × 10^5 N/m^2 (39 psi)

TABLE 3. ADHESIVE EVALUATION, LAP SHEAR TENSILE VALUES

Adhesive	-185°C	25°C	93°C	150°C
1. Lefkoweld 109/LM-52 (Epoxy)	158.58 × 10^5 N/m^2 (2300 psi)	310.26 × 10^5 N/m^2 (4500 psi)	44.82 × 10^5 N/m^2 (650 psi)	24.13 × 10^5 N/m^2 (350 psi)
2. Narmco 7343/7139 (Polyurethane)	448.16 × 10^5 N/m^2 (6500 psi)	110.32 × 10^5 N/m^2 (1600 psi)	31.03 × 10^5 N/m^2 (450 psi)	6.89 × 10^5 N/m^2 (100 psi)
3. Narmco 7343/7139/Z-6040 (Modified Polyurethane)	655 × 10^5 N/m^2 (9500 psi)	206.84 × 10^5 N/m^2 (3000 psi)	82.74 × 10^5 N/m^2 (1200 psi)	62.05 × 10^5 N/m^2 (900 psi)
4. Narmco 7343 / Dupont L-315 7139/Z-6040 (Blended Polyurethane)	496.42 × 10^5 N/m^2 (7200 psi)	248.21 × 10^5 N/m^2 (3600 psi)	248.21 × 10^5 N/m^2 (1800 psi)	82.74 × 10^5 N/m^2 (1200 psi)

APPROVAL

RESEARCH ACHIEVEMENTS REVIEW
VOLUME IV REPORT NO. 2

The information in these reports has been reviewed for security classification. Review of any information concerning Department of Defense or Atomic Energy Commission programs has been made by the MSFC Security Classification Officer. These reports, in their entirety, have been determined to be unclassified.

These reports have also been reviewed and approved for technical accuracy.

Karl L. Heimburg

KARL L. HEIMBURG
Director, Astronautics Laboratory

1. Report No.	2. Government Accession No.	3. Recipient's Catalog No.
TM X-64561		

4. Title and Subtitle	5. Report Date
RESEARCH ACHIEVEMENTS REVIEW, VOL. IV, REPORT NO. 2 Cryogenic Research at MSFC	November 1971
	6. Performing Organization Code

7. Author(s)	8. Performing Organization Report No.
J. E. Kingsbury, D. J. Miller, E. H. Hyde, J. M. Walters, I. C. Yates, J. M. Stucky, E. W. Urban, L. J. Hastings, R. E. Stonemetz, J. H. Pratt, T. W. Winstead, J. Z. Adamson, and W. E. Hill	
9. Performing Organization Name and Address	10. Work Unit No.
George C. Marshall Space Flight Center Marshall Space Flight Center, Alabama 35812	11. Contract or Grant No.
	13. Type of Report and Period Covered
12. Sponsoring Agency Name and Address	Technical Memorandum
National Aeronautics and Space Administration Washington, D. C. 20546	14. Sponsoring Agency Code

15. Supplementary Notes

Prepared by Astronautics Laboratory, Science and Engineering

16. Abstract

Achievements in cryogenic research applicable to new programs such as the skylab, space station, and space shuttle are presented. A brief description of the contents of each of the 11 papers follows.

1. A perspective on cryogenic technology as it relates to new programs and systems is presented.
2. Results of thermal tests on various types of evacuating multilayered insulations are correlated, and applications to space cryogenic storage systems are shown.
3. Practical design and testing procedures for solving structural design problems in the use of evacuating, high performance insulation for large cryogenic tanks are discussed.
4. Recent developments are described for manufacture and assembly techniques to be used in the application of evacuating, multilayered, thermal insulation pads to large, space-vehicle cryogen tank assemblies.
5. Procedures and techniques for evaluating materials for use in high-performance insulation systems are discussed.
6. Potential applications in space for improved superconducting magnet systems are discussed.
7. A review of pertinent heat transfer and fluid machanics research is presented along with promising subsystems for collecting the cryogenic fluid fraction from an amorphous vapor mix which occurs under zero-g conditions during propellant tanking operations and engine restart in orbit.
8. Considerations for system integration and optimization of subsystems applicable to cryogen management and control are described.
9. Mixtures of solid and liquid hydrogen and gelling agents hold promise in increased propellant effectiveness resulting from increased density and heat capacity and reduced fluidity. Space systems design influences are analyzed.

Continued

17. Key Words (Suggested by Author(s))		18. Distribution Statement
Multilayered insulation	Heat transfer	Unclassified—Unlimited
Cryogenic tanks	Fluid mechanics	
High performance insulation	Gelling	See Document Release Form
Structural design	Thermal stratification	
Superconducting magnet systems	Polymeric foams	

19. Security Classif. (of this report)	20. Security Classif. (of this page)	21. No. of Pages	22. Price*
Unclassified	Unclassified	203	$3.00

*For sale by the Clearinghouse for Federal Scientific and Technical Information
Springfield, Virginia 22151

10. Thermal stratification of cryogenic liquids in near-zero gravity causes large variations in booster propulsion propellants. Semiempirical methods for predicting these phenomena have been devised and are compared with flight data.

11. Low-temperature integrity limits and methods of adhesion to metallic structure are discussed for several promising foam materials.

☆U. S. GOVERNMENT PRINTING OFFICE: 1972—745-381/4038—Region 4

CALENDAR OF REVIEWS

FIRST SERIES (VOLUME I)

REVIEW	DATE	RESEARCH AREA
1	2/25/65	RADIATION PHYSICS
2	2/25/65	THERMOPHYSICS
3	3/25/65	CRYOGENIC TECHNOLOGY
4*	3/25/65	CHEMICAL PROPULSION
5	4/29/65	ELECTRONICS
6	4/29/65	CONTROL SYSTEMS
7	5/27/65	MATERIALS
8	5/27/65	MANUFACTURING
9	6/24/65	GROUND TESTING
10	6/24/65	QUALITY ASSURANCE AND CHECKOUT
11	9/16/65	TERRESTRIAL AND SPACE ENVIRONMENT
12	9/16/65	AERODYNAMICS
13	9/30/65	INSTRUMENTATION
14	9/30/65	POWER SYSTEMS
15	10/28/65	GUIDANCE CONCEPTS
16	10/28/65	ASTRODYNAMICS
17	1/27/66	ADVANCED TRACKING SYSTEMS
18	1/27/66	COMMUNICATIONS SYSTEMS
19	1/6/66	STRUCTURES
20	1/6/66	MATHEMATICS AND COMPUTATION
21	2/24/66	ADVANCED PROPULSION
22	2/24/66	LUNAR AND METEOROID PHYSICS

SECOND SERIES (VOLUME II)

REVIEW	DATE	RESEARCH AREA
1	3/31/66	RADIATION PHYSICS
2	3/31/66	THERMOPHYSICS
3	5/26/66	ELECTRONICS
4	7/28/66	MATERIALS
5	9/29/66	QUALITY AND RELIABILITY ASSURANCE
6	1/26/67	CHEMICAL PROPULSION
7	3/30/67	CRYOGENIC TECHNOLOGY
8**	5/25/67	COMPUTATION
9	7/27/67	POWER SYSTEMS
10	9/28/67	TERRESTRIAL AND SPACE ENVIRONMENT
11	11/30/67	MANUFACTURING
12	1/25/68	INSTRUMENTATION RESEARCH FOR GROUND TESTING

THIRD SERIES (VOLUME III)

REVIEW	DATE	RESEARCH AREA
1	3/28/68	AIRBORNE INSTRUMENTATION AND DATA TRANSMISSION
2	5/22/68	ASTRODYNAMICS, GUIDANCE AND OPTIMIZATION
3	7/25/68	CONTROL SYSTEMS
4	9/26/68	AEROPHYSICS
5	11/21/68	COMMUNICATION AND TRACKING
6	1/30/69	THERMOPHYSICS
7	3/27/69	RADIATION PHYSICS
8	6/26/69	METEOROID PHYSICS
9	9/25/69	COMPUTATION RESEARCH (PART I)
10	12/18/69	MATERIALS RESEARCH FOR SHUTTLE AND SPACE STATION
11	1/29/70	MICROELECTRONICS RESEARCH FOR SHUTTLE AND SPACE STATION
12	3/26/70	COMPUTATION RESEARCH (PART II)

FOURTH SERIES (VOLUME IV)

REVIEW	DATE	RESEARCH AREA
1	5/28/70	STRUCTURES
2	10/29/70	CRYOGENICS
3	11/19/70	INSTRUMENTATION
4	3/25/71	ELECTRICAL POWER SYSTEMS
5	5/27/71	QUALITY AND RELIABILITY ASSURANCE

*Classified. Proceedings not published.
**Proceedings summarized only.

Correspondence concerning the Research Achievements Review Series should be addressed to:
Research Planning Office, S&E-R, Marshall Space Flight Center, Alabama 35812